NOVEL MULTILATERAL TELEOPERATION AND COOPERATIVE CONTROL APPROACHES FOR MULTIPLE MANIPULATORS

by

Usman Ahmad

Submitted in partial fulfillment of the requirements
for the degree of Doctor of Philosophy

at

Dalhousie University
Halifax, Nova Scotia
December, 2018

To those who serve the living kind in every possible way.

Table of Contents

List of Tables . . . . . **vi**

List of Figures . . . . . **vii**

Abstract . . . . . **xi**

List of Abbreviations and Symbols Used . . . . . **xii**

Acknowledgements . . . . . **xxvii**

Chapter 1 Introduction **1**

1.1 Fixed-Base vs Mobile Manipulators 1
1.2 Teleoperation of Manipulators 5
1.3 Bilateral Teleoperation 6
1.4 Multilateral Teleoperation 7
1.5 Research Motivation 9
1.6 Thesis Outline and Contributions 9

Chapter 2 Literature Review **13**

2.1 Multilateral Teleoperation of Fixed-Base Manipulators 13
2.2 Cooperative Control of Mobile Manipulators 21
2.3 Teleoperation of Mobile Manipulators 25
2.4 Preliminaries of Graph Theory 28

Chapter 3 Time Domain Passivity Control of Multilateral Teleoperation Systems **30**

3.1 Time Domain Passivity Control (TDPC) for Teleoperation 30
3.1.1 Introduction 30
3.1.2 Challenges in TDPC 31
3.1.3 Motivation of Research 31
3.2 TDPC for Bilateral Teleoperation 32
3.3 Switching TDPC with Constant Time Delay 33
3.3.1 Simulation Results 39
3.3.1.1 Without Switching Action - Case 0 40
3.3.1.2 With Switching Action - Case 1 40
3.3.1.3 With Switching Action - Case 2 44
3.3.2 Experimental Results 47
3.3.2.1 Set 1: 2 Masters and 2 Slaves with no delay 49
3.3.2.2 Set 2: 2 Masters and 2 Slaves with delay of $0.2s$ 52

3.4 Switching TDPC with Varying Time Delay . . . 55
3.4.1 Simulation Results . . . 59
3.4.1.1 Without Switching Action - Case 0 . . . 60
3.4.1.2 With Switching Action - Case 1 . . . 61
3.4.1.3 With Switching Action - Case 2 . . . 65
3.4.2 Experimental Results . . . 66
3.4.2.1 Without Switching Dissipation . . . 68
3.4.2.2 With Switching Dissipation . . . 68
3.5 Summary . . . 71

Chapter 4 Modeling of Mobile Manipulators . . . 72

4.1 System Description . . . 72
4.2 Kinematics of Mobile Manipulator . . . 72
4.2.1 Holonomic Constraints . . . 73
4.2.2 Nonholonomic Constraints . . . 73
4.2.3 Assumptions on Kinematic Structure . . . 74
4.2.4 Derivation of Kinematics of Mobile Manipulator . . . 74
4.3 Dynamics of Mobile Manipulator . . . 75
4.3.1 Nonholonomic Constraint and Reduced Dynamics . . . 76
4.3.2 Dynamic Properties . . . 79
4.4 Summary . . . 79

Chapter 5 Cooperative Adaptive Backstepping Control of Two Mobile Manipulators . . . 80

5.1 System Description . . . 80
5.1.1 Object Model . . . 82
5.2 Coordinated Control Design . . . 82
5.2.1 Control Objective . . . 83
5.2.2 Assumptions . . . 84
5.2.3 Velocity Tracking Problem . . . 85
5.2.3.1 Kinematic Controller . . . 85
5.2.4 Cooperative Torque Control Problem . . . 87
5.2.4.1 Adaptive Torque Control . . . 87
5.3 Simulation Results . . . 90
5.4 Summary . . . 94

Chapter 6 Cooperative Control of Networked Mobile Manipulators . . . 95

6.1 System Description . . . 96
6.2 Coordination Control Design . . . 102
6.3 Cooperation Control Design . . . 104
6.3.1 Decoupling of Null and Operational Space . . . 105
6.3.2 Null Space Control . . . 107

6.3.3 Operational Space Control . . . 108
6.4 Simulation Results . . . 112
6.4.1 Simulation Scenario 1 . . . 113
6.4.2 Simulation Scenario 2 . . . 117
6.5 Summary . . . 120

Chapter 7 Adaptive Robust Control of Multilateral Teleoperation Systems . 122

7.1 System Description . . . 123
7.1.1 Master System . . . 124
7.1.2 Object and Environment . . . 124
7.1.3 Slave System . . . 125
7.2 Control Architecture . . . 131
7.2.1 Parameter Estimation . . . 131
7.2.2 Controller Design for the Master Side . . . 133
7.2.3 Controller Design for the Slave Side . . . 135
7.2.3.1 ARC for Slaves . . . 135
7.3 Simulation Results . . . 138
7.3.1 Simulation Scenario: . . . 138
7.4 Summary . . . 144

Chapter 8 Conclusions and Future Work . . . 145

8.1 Conclusions . . . 145
8.2 Future Work . . . 147

Bibliography . . . 148

Appendix A Mathematical Equations . . . 162

A.1 The Jacobian . . . 162
A.2 The Dynamic Model . . . 164
A.3 Regressor Matrix . . . 167
A.3.1 Regressor Matrix in Terms of Linear and Angular Velocities . . . 170

Appendix B Author's Publications . . . 172

List of Tables

3.1 Simulation Parameters 40

3.2 Summary of Simulation Results 48

3.3 Simulation Parameters 59

3.4 Summary of Simulation Results 68

5.1 Simulation Parameters 90

6.1 Simulation Parameters 113

List of Figures

1.1 (a) A robotic demining mobile manipulator, (b) Gryphon experimental mobile manipulator, (c) A D&D fixed-base manipulator, (d) A mobile excavator 2

1.2 (a) A fixed-base assembly manipulator, (b) PUMA fixed-base manipulator, (c) A cleaning mobile manipulator, (d) Fixed-base welding manipulators 3

1.3 (a) A cut-to-length mobile manipulator, (b) A mobile tree harvester . 3

1.4 (a) A mobile manipulator used at Sago Mine disaster in 2006, (b) A home searching mobile manipulator, (c) A mobile manipulator for disaster management, (d) Testing of a manipulator for rescue missions 4

1.5 (a) Ranger, the space manipulator, (b) A space shuttle remote manipulator system, (c) A Mars exploration rover equipped with a manipulator arm, (d) A conceptual drawing for robotic rescue of Hubble space telescope 5

1.6 Bilateral Teleoperation 7

1.7 Multilateral Teleoperation 8

2.1 A general representation of bilateral teleoperation system 13

2.2 A general representation of cooperative multilateral teleoperation system 14

2.3 Wave variables approach 17

2.4 Wave variable approach input and output 18

2.5 Wave variable based teleoperation 18

2.6 A general teleoperation system 20

2.7 Teleoperation with master and slave 20

2.8 TDPC based Teleoperation 20

2.9 Teleoperation of multiple mobile manipulators 26

3.1 A bilateral teleoperator with TDPC 33

3.2 Multilateral teleoperation system with switching TDPC 34

3.3 Multilateral teleoperation communication channel 37
3.4 Multilateral teleoperation structure with two masters and two slaves 39
3.5 M/S: Positions, forces, contact force and energy 41
3.6 M/S: Positions, forces, contact force and energy 41
3.7 Case 1 - M/S: positions and velocities with $\alpha_i = 0.5$ 42
3.8 Case 1 - Masters side PO and dissipation values with $\alpha_i = 0.5$ 43
3.9 Case 1 - Slaves side PO and dissipation values with $\alpha_i = 0.5$ 43
3.10 Case 1 - M/S: Forces and contact force values with $\alpha_i = 0.5$ 44
3.11 Case 1: Total energy with $\alpha_i = 0.5$ 44
3.12 Case 2: M/S positions and contact forces with delay of $1s$ 45
3.13 Case 2: Masters side PO and dissipation values with delay of $1s$ . . . 46
3.14 Case 2: Salves side PO and dissipation values with delay of $1s$ . . . 46
3.15 Case 2: Force and velocity signals with delay of $1s$ 47
3.16 Case 2: Total energy with delay of $1s$ and different α_i 47
3.17 Experimental setup 48
3.18 Direct contact with the foam 49
3.19 Set 1: M/S positions and forces with $\alpha_i = 0.5$ 50
3.20 Set 1: Passivity observer and dissipation values for the masters with $\alpha_i = 0.5$ 50
3.21 Set 1: Passivity observer and dissipation values for the slaves with $\alpha_i = 0.5$ 51
3.22 Set 1: Environment force and total energy with $\alpha_i = 0.5$ 51
3.23 Direct contact with the Aluminum plate 52
3.24 Set 2: M/S positions and forces with different α_i 53
3.25 Set 2: PO and dissipation values for the masters with different α_i . . 53
3.26 Set 2: PO and dissipation values for the slaves with different α_i . . . 54
3.27 Set 2: Environment forces with different α_i 54
3.28 Set 2: Total energy with different α_i 55

3.29 $T_{mij}(t)$, $T_{sij}(t)$ and their rates of change 60
3.30 M/S Positions and contact forces 61
3.31 Total energy 61
3.32 Case 1: M/S positions and velocities with $\alpha_i = 0.5$ 62
3.33 Case 1: M/S PO and dissipation values with $\alpha_i = 0.5$ 63
3.34 Case 1: M/S PO and dissipation values with $\alpha_i = 0.5$ 63
3.35 Case 1 - Force feedback and contact force with $\alpha_i = 0.5$ 64
3.36 Case 1 - Total energy with $\alpha_i = 0.5$ 64
3.37 Case 2: M/S positions,velocities, contact forces, energy, masters and slaves forces with different α_i 66
3.38 Case 2: PO and dissipation values for slaves, PO and dissipation values for masters, forces of masters and slaves with different α_i . . 67
3.39 M/S positions 68
3.40 M/S positions and forces 69
3.41 PO and dissipation values for the masters 70
3.42 PO and dissipation values for the slaves 70
3.43 Environmental contact forces 71

4.1 $n+m$ DOF mobile manipulator 73

5.1 Two $n+m$ DOF mobile manipulators 81
5.2 End-effector positions and errors 91
5.3 Velocity of mobile base in x and y direction 92
5.4 Joint angles, object trajectory and internal force 92
5.5 Actual velocities, controlled velocities and error 93

6.1 A nonholonomic mobile manipulator 98
6.2 The coordinate system 109
6.3 A general scenario of the mobile manipulators holding an object . . 112
6.4 Graph topology $\mathcal{G}_1$. 113

6.5 End-effector errors and actuator torques 114
6.6 Mobile platform position and sliding vector errors 115
6.7 Sliding vector and object tracking errors 116
6.8 End-effector positions (m) of agents at 4 s 116
6.9 End-effector positions (m) of agents at 12 s 116
6.10 End-effector errors and actuator torques 117
6.11 Mobile platform position and sliding vector errors 118
6.12 Sliding vector and object tracking errors 119
6.13 End-effector positions (m) of agents at 4 s 119
6.14 End-effector positions (m) of agents at 12 s 120

7.1 Control architecture of SMMS teleoperation system. 132
7.2 The human inputs 139
7.3 Master trajectories: desired, actual and their error 139
7.4 The contact force F_e and its prediction $\hat{F}_e$ 140
7.5 The estimates of environmental parameters $\hat{\theta}_e$ 141
7.6 The forces exerted on the object 142
7.7 The desired object trajectory x_{od} and its tracking error 143
7.8 Mobile platform position errors 143

Abstract

Teleoperation of robotic manipulators has been one of the popular research areas in the robotics research community for last couple of decades. A variety of control methods have been proposed for bilateral and multilateral teleoperation of robotic manipulators. Although a lot of research has been carried out on teleoperation control, some of the aspects of these systems are still unexplored. For example, most of the control schemes for teleoperation systems focus only on the compensation of time delays while there exist other performance metrics for these systems such as better transparency, optimal force distribution and authority adjustment in cooperative applications. Additionally, some of the control schemes lack to provide the guaranteed stability of the teleoperation system. This research works aims to propose novel teleoperation and cooperative control schemes for fixed-base and mobile manipulators. This research work can be divided into two main parts. The first part of this thesis is focused on the development of a Time Domain Passivity Control (TDPC) scheme which ensures the stability of the multilateral teleoperation system under constant and varying time delays. The proposed control framework not only avoids the zero division problem of the control laws of traditional TDPC but also provides a novel communication channel architecture to assign weights to master and slave robots to cooperatively execute the task. Simulation and experimental results validate the efficacy of the proposed TDPC scheme for the multilateral teleoperation of fixed-base robotic manipulators. The second part is focused on the cooperative and teleoperation control of mobile manipulators. A couple of novel cooperative control schemes have been proposed for the cooperative control of mobile manipulators to manipulate a common object attached to the end-effectors. An adaptive robust teleoperation control scheme has also been proposed with the control objectives of guaranteed stability, synchronization and internal force distribution. Simulation results validate the efficacy of the proposed schemes for the cooperative control and teleoperation of mobile manipulators.

List of Abbreviations and Symbols Used

Chapter 1

NCS	Networked control system
TDPC	Time domain passivity control
SMMS	Single master multiple slaves
D&D	Deactivation & decommissioning
MAS	Multiagent systems
UAVs	Unmanned aerial vehicles

Chapter 2

LTI	Linear time invariant
PD	Proportional derivative
VF	Virtual fixture
GVF	Guided virtual fixture
PBC	Passivity based control
PID	Proportional integral derivative
TDPC	Time domain passivity control
MM/SS	Multiple master single slave
SM/SS	Single master single slave
LMIs	Linear matrix inequalities
ANTS	Amplifying N-robot transport system
MPC	Model predictive control
NMPC	Nonlinear model predictive control
GUI	Graphical user interface
NDO	Neural dynamic optimization
QP	Quadratic programming
PDNN	Primal dual neural network
GPNN	General projection neural network
EEG	Electroencephalogram

BCI	Brain computer interface
HMI	Human machine interface
sEMG	Surface electromyography
DOF	Degrees of freedom
RCLF	Robust control Lyapunov functions
LMI	Linear matrix inequality
TDPA	Time domain passivity approach

α	Dominance factor
$H(s)$	Scattering matrix
f	Force
$\dot{x}$	Velocity
P	Power flow
b	Wave impedance constant
$\mathcal{G}$	A communication graph
$\mathcal{V}(\mathcal{G})$	Vertices or nodes of $\mathcal{G}$
$\mathcal{E}(\mathcal{G})$	Edges of $\mathcal{G}$
d_i	The in-degree of a vertex
$\mathcal{G}_w$	A weighted graph
$\mathcal{W}$	Weights of a weighted graph
w_{ij}	Weight of an edge
$\mathcal{N}$	Finite set of robots
$\mathcal{A}$	Adjacency or connectivity matrix
$\mathcal{D}$	Diagonal in-degree matrix
$\mathcal{L}$	Laplacian matrix of a graph
$\mathcal{L}_w$	Weighted Laplacian of a directed graph

Chapter 3

TDPC	Time domain passivity control
ETDPC	Energy based time domain passivity control
PTDPC	Power based time domain passivity control

PO	Passivity observer
PD	Proportional derivative
PC	Passivity controller
QUARC	Quanser Real Time Control
TCP/IP	Transmission control protocol/Internet protocol

P	Power flow
E	Energy
f	Force
v	Velocity
P_{diss}	Dissipated power
b_i	Damping parameter
B	Proportional gain
K	Derivative gain
m	Endpoint mass
f_h	Human operator force
f_{si}	Forces of slave controllers
v_{mi}	Velocities of masters
f_e	Environmental contact force
T_{mij}	Forward delays from jth master to ith slave
T_{sij}	Backward delays from jth slave to ith master
$\dot{T}_{mij}$	Rate of change of T_{mij}
$\dot{T}_{sij}$	Rate of change of T_{sij}
$\alpha_{vij}, \alpha_{fij}$	Weighting coefficients of masters and slaves
n	Number of masters or slaves
n_m	Number of masters
n_s	Number of slaves
P_{obsv}^{mi}	Passivity observers for masters
P_{obsv}^{si}	Passivity observers for slaves
PC_{mi}	Passivity controllers for masters
PC_{si}	Passivity controllers for slaves

f_{pci} or f_d	Dissipation of masters
v_{pci} or v_d	Dissipation of slaves
P^*	Power flow with switching time domain passivity control
ε	Upper bound on delays
$F_{mc}(S)$	Laplace transform of f_{mc}
$F_s(S)$	Laplace transform of f_s
$V_m(S)$	Laplace transform of v_m
$V_{sc}(S)$	Laplace transform of v_{sc}
K_1	Wall stiffness
x	Wall distance
x_{si}	Position of slaves

Chapter 4

DOF	Degrees of freedom
EL	Euler Langrange

n	Degrees of freedom of the manipulator arm
m	Degrees of freedom of the mobile base
l_1, l_2	Lengths of the links
θ_1, θ_2	Angles of the joints
θ_b	Orientation of the mobile base
$\mathcal{L}$	Langrangian
K	Kinetic energy
P	Potential energy
M	Inertia matrix
C	Centripetal and coriolis matrix
G	Gravitational force vector
f	Generalized constraint force
f_n	Generalized constraint force of nonholonomic constraint
f_h	Generalized constraint force of holonomic constraint
λ	Langrangian multiplier

λ_n	Langrangian multiplier of nonholonomic constraint
λ_h	Langrangian multiplier of holonomic constraint
A	Kinematic constraint matrix
B	Input transformation matrix
τ	Control input
q	Generalized coordinates
q_b	Generalized coordinates of the mobile base
q_a	Generalized coordinates of the manipulator arm
M_b	Inertia matrix of the mobile base
M_a	Inertia matrix of the manipulator arm
M_{ba} and M_{ab}	Coupling inertia matrices of the base and arm
C_b	Centripetal and coriolis matrix of the mobile base
C_a	Centripetal and coriolis matrix of the manipulator arm
C_{ba} and C_{ab}	Coupling centripetal and coriolis matrices of the base and arm
G_b	Gravitational force of the mobile base
G_a	Gravitational force of the manipulator arm
B_b	Input transformation matrix of the mobile base
B_a	Input transformation matrix of the arm
τ_b	Control input of the mobile base
τ_a	Control input of the manipulator arm
x, y	Coordinates of center of the mobile base
θ_b	Heading angle of the mobile base
H	Rank m matrix
α	Steering velocity of the mobile base
v, ω	Linear and angular velocities of the mobile base
θ_R, θ_L	Left and right wheel velocities of the mobile base
R	Radius of the wheels
D	Distance of two wheels
η	A vector
$\bar{M}$	Inertia matrix of reduced dynamic model
$\bar{C}$	Centripetal and coriolis matrix of reduced dynamic model

$\bar{G}$	Gravitational force vector of reduced dynamic model
$\bar{\tau}$	Control input of reduced dynamic model

Chapter 5

DLS	Damped least squares

n	Degrees of freedom of the manipulator arm
m	Degrees of freedom of the mobile base
M_i	Inertia matrix
C_i	Centripetal and coriolis matrix
G_i	Gravitational force vector
f_i	Generalized constraint force
f_{in}	Generalized constraint force of nonholonomic constraint
f_{ih}	Generalized constraint force of holonomic constraint
λ_i	Langrangian multiplier
λ_{in}	Langrangian multiplier of nonholonomic constraint
λ_{ih}	Langrangian multiplier of holonomic constraint
A_i	Kinematic constraint matrix
B_i	Input transformation matrix
τ_i	Control input
q_i	Generalized coordinates
q_{ib}	Generalized coordinates of the mobile base
q_{ia}	Generalized coordinates of the manipulator arm
$\bar{M}_i$	Inertia matrix of reduced dynamic model
$\bar{C}_i$	Centripetal and coriolis matrix of reduced dynamic model
$\bar{G}_i$	Gravitational force vector of reduced dynamic model
$\bar{\tau}_i$	Control input of reduced dynamic model
M_o	Inertia matrix of the object
C_o	Centripetal and coriolis matrix of the object
G_o	Gravitational force vector of the object
F_i	Force exerted on the object by the ith manipulator

x_o	Position of the object
L_i	Nonsingular transformation matrix
Φ_{di}	Desired trajectory of the mobile base
Ψ_{di}	Desired trajectory of the end-effector
L_s	s norm of a function
L_∞	∞ norm of a function
$e_i(t)$	Tracking error of the desired trajectory
$\Psi_i(t)$	Configuration of the mobile base velocity and pose of end-effector
Δ_i	Extended Jacobian matrix
η_{ci}	Virtual velocity control
V	Lyapunov function
K_i	Positive constant control gain
k	Damping factor
$\eta_{ei}(t)$	Joint velocity error
K_{1i}	Positive definite matrix
$\hat{p}_i$	Estimation of unknown parameters
Γ_i	Symmetric positive definite matrix

Chapter 6

EL	Euler Lagrange
n	Degrees of freedom of the manipulator arm
m	Degrees of freedom of the mobile base
M_i	Inertia matrix
C_i	Centripetal and coriolis matrix
G_i	Gravitational force vector
f_i	Generalized constraint force
f_{in}	Generalized constraint force of nonholonomic constraint
f_{ih}	Generalized constraint force of holonomic constraint
λ_i	Langrangian multiplier

λ_{in}	Langrangian multiplier of nonholonomic constraint
λ_{ih}	Langrangian multiplier of holonomic constraint
A_i	Kinematic constraint matrix
B_i	Input transformation matrix
τ_i	Control input
q_i	Generalized coordinates
q_{ip}	Generalized coordinates of the mobile base
q_{ia}	Generalized coordinates of the manipulator arm
M_{ip}	Inertia matrix of the mobile base
M_{ia}	Inertia matrix of the manipulator arm
M_{ipa} and M_{iap}	Coupling inertia matrices of the base and arm
C_{ip}	Centripetal and coriolis matrix of the mobile base
C_{ia}	Centripetal and coriolis matrix of the manipulator arm
C_{ipa} and C_{iap}	Coupling centripetal and coriolis matrices of the base and arm
G_{ip}	Gravitational force of the mobile base
G_{ia}	Gravitational force of the manipulator arm
B_{ip}	Input transformation matrix of the mobile base
B_{ia}	Input transformation matrix of the arm
τ_{ip}	Control input of the mobile base
τ_{ia}	Control input of the manipulator arm
x_i, y_i	Coordinates of center of the mobile base
θ_{ip}	Heading angle of the mobile base
H_i	Rank m matrix
α_i	Steering velocity of the mobile base
v_i, ω_i	Linear and angular velocities of the mobile base
θ_{iR}, θ_{iL}	Left and right wheel velocities of mobile base
R	Radius of the wheels
D	Distance of two wheels
η_i	A vector
$M_{\eta i}$	Inertia matrix of reduced dynamic model
$C_{\eta i}$	Centripetal and coriolis matrix of reduced dynamic model

$G_{\eta i}$	Gravitational force vector of reduced dynamic model
$\tau_{\eta i}$	Control input of reduced dynamic model
X_i	Variables defining the task of the mobile manipulator
X_{ma}	End-effector pose
$f_i(\eta_i)$	A nonlinear transformation
J_{ma}	Jacobian of the end-effector
X_{mp}	Motion of the mobile base
$g_i(\eta_i)$	A nonlinear transformation
J_{mp}	Jacobian of the mobile base
$J(\eta_i)$	Extended square Jacobian matrix
M_{xi}	Operational space inertia matrix
C_{xi}	Operational space centripetal and coriolis matrix
G_{xi}	Operational space gravitational force
τ_{xi}	Operational space control input
λ_{Mi} and $\bar{\lambda}_{Mi}$	Positive constants
I_n	$n \times n$ identity matrix
ξ	A differentiable vector
Θ_i	Vector of unknown parameters
Y_i	Regressor matrix
X_d	Desired trajectory of the mobile manipulator
X_{da}	Desired trajectory of the manipulator arm
X_{dp}	Desired trajectory of the mobile base
$\mathcal{L}_\infty$	∞ norm of a function
X_{dr}	A reference trajectory
σ_i	A constant formation vector
$\dot{X}_{ri}$	Reference velocity
e_{xi}	Sliding vector in operational space
$\hat{M}_{xi}$	Estimate of M_{xi}
$\hat{C}_{xi}$	Estimate of C_{xi}
$\hat{G}_{xi}$	Estimate of G_{xi}
K_i	Positive constant gain

τ_{sm}	Control input for the synchronous motion
$\tilde{\Theta}_i$	Error of the dynamic parameter estimation
Γ_i	constant positive definite matrix
T_d	Positive bounded time delay
$\mathcal{N}_i$	A set of all the agents
N_j, N_n	Sets of connected and disconnected agents
$\mathcal{L}_2$	Euclidean norm
J^*	Pseudo inverse of $J(\eta_i)$
N_i	Null space of the mobile manipulator
J°	Weighted pseudo inverse of $J(\eta_i)$
f_{io}	Operational space force
τ_{j_i}	Vector of joint torques
f_{ei}	External forces acting on the mobile manipulator
u_{Oi}, u_{Ni}	Operational and null space control inputs
u_{pi}	Formation control input of the mobile base where $u_{pi} = u_{pi_v}$
M_o	Inertia matrix of the object
C_o	Centripetal and coriolis matrix of the object
h_o	Resultant wrench from the end-effector
X_o	Position of the object
m_o	Mass of the object
I_o	Inertia of the object
I_3	Identity matrix of dimension 3×3
$\ddot{X}_o^d$	Desired acceleration of the object
h_{env}	Environmental or external wrench
a_d, b_d, c_d	Constant positive gains
G	Grasp or grip transformation matrix
G^*	Generalized inverse of G
$\dot{\nu}_{ri}$	Operational space reference velocity
k_a, k_b	Positive constants
h_i^d	Desired wrench to be exerted by the end-effector
δ_i	Operational space sliding vector

Chapter 7

EL	Euler Lagrange
SMMS	Single master multiple slaves
ARC	Adaptive robust controller
DOF	Degrees of freedom

M	Inertia matrix of the master manipulator
C	Centripetal and coriolis matrix of the master manipulator
G	Gravitational force vector of the master manipulator
u_m	Control input to the master manipulator
J_m	Jacobian matrix
F_h	Force applied by the human operator
x_m	Position and angle of the end-effector
M_c	Inertia matrix in Cartesian space
C_c	Centripetal and coriolis matrix in Cartesian space
G_c	Gravitational force vector in Cartesian space
u_{m_c}	Control input in Cartesian space
F_{h_c}	Force applied by the human operator in Cartesian space
M_o	Inertia matrix of the object
C_o	Centripetal and coriolis matrix of the object
G_o	Gravitational force vector of the object
F_i	Force exerted on the object by the ith manipulator
F_e	Environment reaction force
B_e, C_e, K_e	Unknown parameters of environment reaction force
φ_e	Regressor signal of the object
x_o	Position of the object
L_i	Nonsingular transformation matrix
n	Degrees of freedom of the manipulator arm
m	Degrees of freedom of the mobile base
M_{si}	Inertia matrix of the slave

C_{si}	Centripetal and coriolis matrix of the slave
G_{si}	Gravitational force vector of the slave
f_i	Generalized constraint force or torque
f_{in}	Generalized constraint force of nonholonomic constraint
f_{ih}	Generalized constraint force of holonomic constraint
λ_i	Langrangian multiplier
λ_{in}	Langrangian multiplier of nonholonomic constraint
λ_{ih}	Langrangian multiplier of holonomic constraint
A_i	Kinematic constraint matrix
B_i	Input transformation matrix
τ_i	Control input
q_{si}	Generalized coordinates of the slave
q_{ip}	Generalized coordinates of the mobile base
q_{ia}	Generalized coordinates of the manipulator arm
M_{ip}	Inertia matrix of the mobile base
M_{ia}	Inertia matrix of the manipulator arm
M_{ipa} and M_{iap}	Coupling inertia matrices of the base and arm
C_{ip}	Centripetal and coriolis matrix of the mobile base
C_{ia}	Centripetal and coriolis matrix of the manipulator arm
C_{ipa} and C_{iap}	Coupling centripetal and coriolis matrices of the base and arm
G_{ip}	Gravitational force of the mobile base
G_{ia}	Gravitational force of the manipulator arm
B_{ip}	Input transformation matrix of the mobile base
B_{ia}	Input transformation matrix of the arm
τ_{ip}	Control input of the mobile base
τ_{ia}	Control input of the manipulator arm
x_i, y_i	Coordinates of center of the mobile base
θ_{ip}	Heading angle of the mobile base
H_i	Rank m matrix
α_i	Steering velocity of the mobile base
v_i, ω_i	Linear and angular velocities of the mobile base

θ_{iR}, θ_{iL}	Left and right wheel velocities of the mobile base
R	Radius of the wheels
D	Distance of two wheels
η_i	A vector
$M_{\eta i}$	Inertia matrix of reduced dynamic model
$C_{\eta i}$	Centripetal and coriolis matrix of reduced dynamic model
$G_{\eta i}$	Gravitational force vector of reduced dynamic model
$\tau_{\eta i}$	Control input of reduced dynamic model
X_i	Variables defining the task of the mobile manipulator
X_{ma}	End-effector pose
$f_i(\eta_i)$	A nonlinear transformation
J_{ma}	Jacobian of the end-effector
X_{mp}	Motion of the mobile base
$g_i(\eta_i)$	A nonlinear transformation
J_{mp}	Jacobian of the mobile base
$J(\eta_i)$	Extended square Jacobian matrix
M_{xi}	Operational space inertia matrix
C_{xi}	Operational space centripetal and coriolis matrix
G_{xi}	Operational space gravitational force
τ_{xi}	Operational space control input
$\mu_{m1,m2}$ and $\mu_{o1,o2}$	Positive constants
I	Identity matrix
θ_m	Vector of unknown parameters of the master manipulator
θ_o	Vector of unknown parameters of the object
θ_e	Vector of unknown parameters of the environment
φ_m	Regressor matrix of the master manipulator
φ_o	Regressor matrix of the object
$\dot{x}_{m,r}, \ddot{x}_{m,r}, \dot{x}_{o,r}, \ddot{x}_{o,r}$	Reference velocities and accelerations
$\hat{\theta}$	Estimate of the parameters
$\tilde{\theta}$	Estimation error of the parameters
Ω_θ	Known bounded set

$\theta_{min}, \theta_{max}$	Known constant vectors or scalars
$\hat{F}_e$	Predicted environment reaction force
x_{od}	Desired object trajectory
Γ	Positive definite matrix
γ	Adaptation parameter
$n_{\hat{\theta}}$	Unit normal vector at $\hat{\theta}$
$\mathring{\Omega}$	Interior of Ω_θ
$\delta\Omega_\theta$	Boundary of Ω_θ
$\bar{\Omega}_\theta$	Known bounded set
$H_f(s)$	A stable filter
F_{ef}	Filtered value of F_e
φ_{ef}	Filtered value of φ_e
$\hat{F}_{ef}$	Prediction output
ε	Prediction error
α	Forgetting factor
ν	A positive constant
ζ_M	Bound on $\|\|\Gamma_e(t)\|\|$
k_m	A positive constant
$x_{m_{dt}}$	Desired master trajectory
k_f	A positive force scaling factor
θ_d	Target parameter vector of impedance behavior
s_m	A switching like quantity
k_{m1}	A positive diagonal matrix
K_p	A symmetric positive definite matrix
u_f	Robust control term
σ_m	A small design parameter
σ_{min}	Minimum eigenvalue of a matrix
$H_r(s)$	A stable filter
s_s	A switching like quantity
k_{s1}	A positive diagonal matrix
K_d	A symmetric positive definite matrix

u_r	Robust control term
σ_s	A small design parameter
u_{si}	Input to the slaves
F_{int}	The internal force
Q	A weighting matrix
f_d	An arbitrary force vector

Acknowledgements

First and foremost, I would like to acknowledge the invaluable support and guidance of my supervisor, Dr. Ya-Jun Pan. Her constructive criticism and timely support not only enabled me to improve the content of this thesis but aided in the development of my perspective in my research area. I deeply appreciate all her contributions of time and financial support over these years. It has been a privilege to be her student. Without her support and encouragement, it would not have been possible for me to call this beautiful country home. I thank her for providing me an opportunity to permanently settle in Canada.

I am grateful to my supervisory committee member, Dr. Mohamed E. El-Hawary, for his deep insights on my research topic. He has taught me to see things from different perspectives. His enthusiasm for research has motivated me to come this far. He has been a huge support right from the beginning of this journey.

I would also like to thank Dr. Marek Kujath for his role on my supervisory committee and for his support in graduate seminars. A special acknowledgement of support to Dr. Andrew Warkentin for kindly agreeing to be on my supervisory committee after the retirement of Dr. Marek Kujath.

I am grateful to Jascinth Butterfield, Selina Cajolais, Kate Hide, Donna Laffin, Peter Jones and Jonathan MacDonald for their support in facilitating my research work.

Special thanks to the current and past members of Advanced Control and Mechatronics (ACM) Lab for all their support and contributions.

I am grateful to Dr. Rickey Dubay for his availability and kindly agreeing to be the external examiner for my thesis defence. His comments have significantly improved the content of this thesis.

Finally, I would like to acknowledge the support of my wife, Abeera Fatima, during this work. Her endless encouragement made me survive all the ups and downs of this journey.

Chapter 1

Introduction

In robotics, a robotic manipulator is normally considered to be a device or a mechanism which is used to manipulate things without a direct contact of the human. A robotic manipulator consists of multiple links attached to each other by different types of joints. Applications of robotic manipulators have a wide variety that is why a lot of research has been carried out on robotic manipulators in last two decades. The applications of robotic manipulation can be found in hazardous material handling, manufacturing, logistics and transportation, agriculture, rescue missions, space and planetary explorations, underwater explorations, fire fighting, surgical operations and disaster management [1–6]. The robotic manipulators can be divided into two main categories based on the mobility of the systems.

1.1 Fixed-Base vs Mobile Manipulators

Fixed-base manipulators, as the name suggests, are the robotic manipulators which are fixed on a static base having zero mobility in the workspace. This means that the only available workspace or reachability of such manipulators depends on the movements of the links or the joint motions. Increasing the number of links may increase the workspace of a fixed-base robotic manipulator however as the base is fixed, the manipulator itself can not move in the workspace for the execution of a task. Although such manipulators have disadvantage of limited workspace, but their control is relatively easy as the system only consists of links and joints.

In contrast to the fixed-base manipulators, mobile manipulators are defined as the robotic manipulators equipped with legs, tracks or wheels. A special class of mobile manipulators is aerial manipulators. Mobile manipulators have the ability to move from one point to another depending on the task requirements thus having an increased workspace as compared to the fixed-base manipulators. Although we get the obvious advantage of increased workspace of mobile manipulators, their control and motion planning is difficult as in addition to the links and joints the system now includes a mobile base or platform. The

control design of such systems must take into account the movement of the legs or wheels for motion planning or obstacle avoidance. A number of control methods have appeared in the literature for various applications of the fixed-base and mobile robotic manipulators.

- **Hazardous Applications:** Fixed-base or mobile manipulators have been used in hazardous environments where a human is unable to work. Hazardous material handling is one of the famous area of such applications specifically in nuclear plants where radioactive materials are used. Other applications include landmine eradication, land excavation, deactivation and decommissioning (D&D), hazardous site cleaning and biological experimentation [2]. A few examples of robotic manipulators in hazardous applications are shown in Fig.1.1.

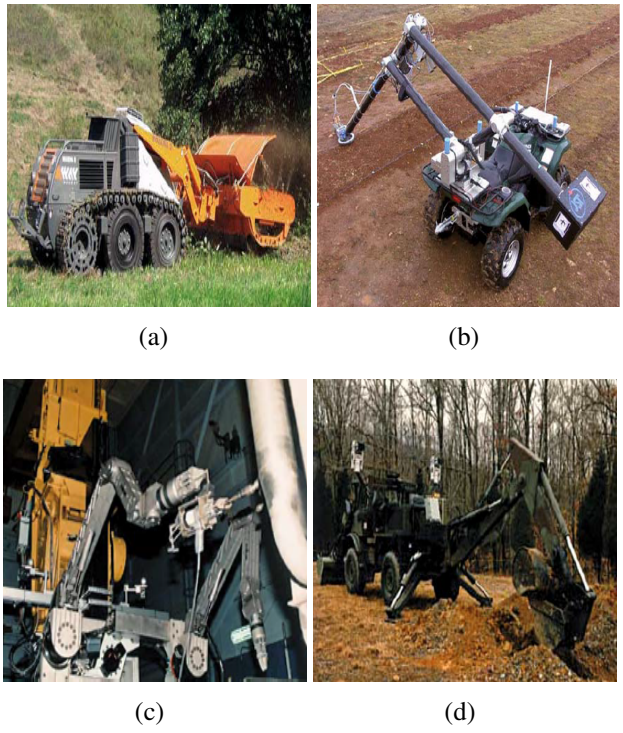

(a) (b)

(c) (d)

Figure 1.1: (a) A robotic demining mobile manipulator, (b) Gryphon experimental mobile manipulator, (c) A D&D fixed-base manipulator, (d) A mobile excavator [2]

- **Industrial Applications:** A variety of applications of fixed-base and mobile manipulators can be found in industry these days. These applications vary from manufacturing, logistics, food to electronics and solar cells [2]. A few examples of robotic manipulators in industry are shown in Fig.1.2.

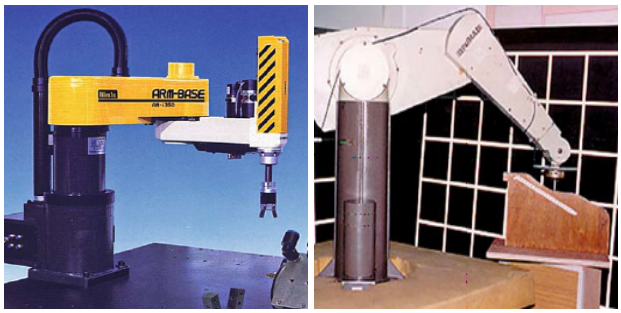

(a) (b)

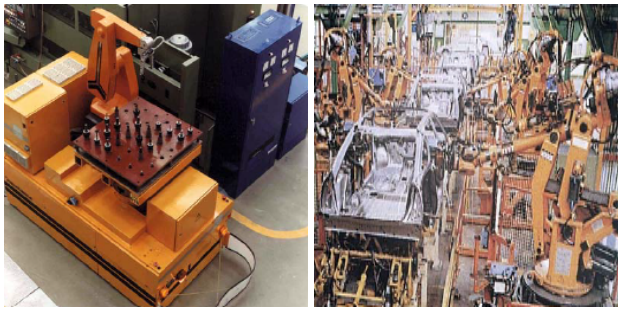

(c) (d)

Figure 1.2: (a) A fixed-base assembly manipulator, (b) PUMA fixed-base manipulator, (c) A cleaning mobile manipulator, (d) Fixed-base welding manipulators [2]

- **Agricultural Applications** Mobile manipulators have been widely used in the harvestation of crops and cutting tress. The accuracy and efficiency of these manipulators is much more than humans so they are used in large agricultural areas. A couple of examples of such manipulators are shown below in Fig.1.3 [2].

(a) (b)

Figure 1.3: (a) A cut-to-length mobile manipulator, (b) A mobile tree harvester [2]

- **Search and Rescue Applications** Another area of research and applications of robotic manipulators is in search and rescue operations. Disaster management with the help

of robots have proved to be extremely invaluable especially in situations where the human presence is dangerous for rescue missions. Earthquakes and other natural disasters are unavoidable however the loss from such events can be reduced significantly with the help of well executed plans when platoons of robotic manipulators operate in tough conditions [2]. A few examples of robotic manipulators in search and rescue operations are shown in Fig.1.4.

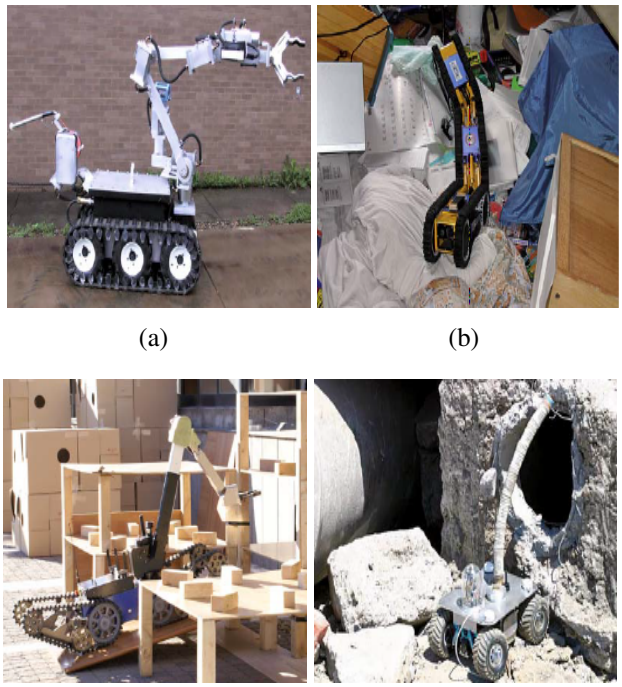

(a) (b)

(c) (d)

Figure 1.4: (a) A mobile manipulator used at Sago Mine disaster in 2006, (b) A home searching mobile manipulator, (c) A mobile manipulator for disaster management, (d) Testing of a manipulator for rescue missions [2]

- **Space Applications** Robotic manipulators in space applications serve as the assistants of the astronauts for facilitating the tasks of manipulation, servicing and assembly. Space applications not only involve the on-site robotic manipulators in the presence of humans but their teleoperation is equally popular in the space community. In fact, the teleoperation of robotic manipulators in space is considered to be much more useful as in that case the human does not have to be present at the remote site. A widely accepted application of space manipulators is the servicing of a malfunctioning space craft [2]. A few examples of robotic manipulators in space are

shown in Fig.1.5.

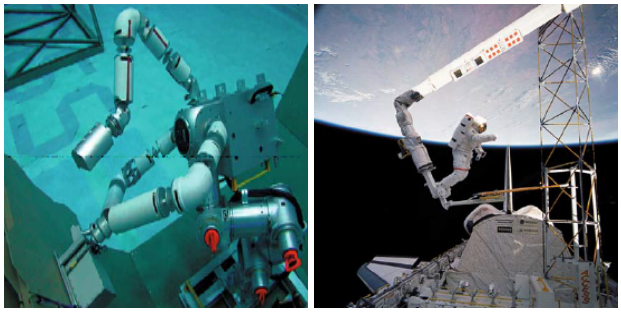

(a) (b)

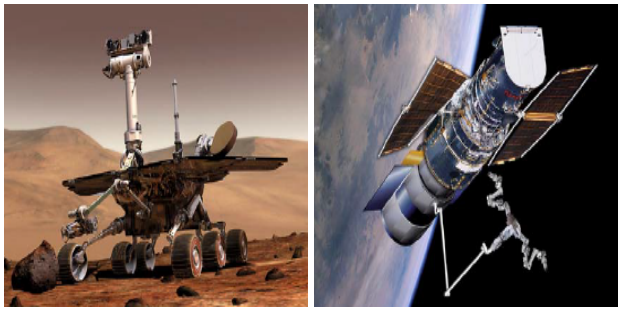

(c) (d)

Figure 1.5: (a) Ranger, the space manipulator, (b) A space shuttle remote manipulator system, (c) A Mars exploration rover equipped with a manipulator arm, (d) A conceptual drawing for robotic rescue of Hubble space telescope [2]

1.2 Teleoperation of Manipulators

Robotic applications such as rescue and surveillance, heavy object manipulation, manufacturing, fire fighting, agriculture management, logistics and disaster management normally require multiple fixed-base manipulators or mobile manipulators due to their increased capacity of cooperative and coordinated handling. A single robotic manipulator is not enough to handle complex tasks especially in industrial applications so there comes a dire need to replace such a manipulator with multiple robotic manipulators. Many tasks which are not feasible or impossible to be carried out by a single manipulator become suitable when we employ multiple manipulators to cooperatively execute the task. Over the past decade, there has been an increased interest of researchers in investigating new control methods for multiple robotic manipulators. Cooperative nature of control strategies for robotic manipulators makes it more suitable for researchers to develop models which can be applied to

any application without the loss of generality. Another key advantage of multiple robotic manipulators applications is the involvement of the human operator as required by the task completion. The human operator can stay in the loop to supervise the task performance even though the centralized or decentralized control schemes are robust enough to take care of the disturbances and exogenous inputs in the system. A team of robots operating under the supervision of a human operator or multiple human operators is obviously much more efficient and reliable than a single robot performing a task.

The collaborative and cooperative nature of control for robot teams has emerged as a decent solution to the applications where a single robot is not capable of handling complex tasks and that is the reason that these systems have found applications in diverse areas as mentioned above. This applicability and feasibility of multiple robots in various applications is motivating the researchers to carry out research in this area. Over the last few years, a number of control methods have appeared in the literature for cooperative and coordinated control of multiple robots. Although, the generalization of applicability of control schemes for robot teams is considered appropriate however, as the dynamics of robotic manipulators differ from conventional multiagent systems so the nature of control changes accordingly. The nature of control becomes even more complex when the multiple robotic manipulators, fixed-base or mobile, handle an object for the transportation from one point to another and the main reason of this complexity is the coupling of these interconnected systems. The task achievement heavily depends on the understanding of these coupling interactions and appropriate motion and force control schemes. This research work is focused on different control methods for the applications of teleoperation and cooperative/coordinated control of robotic manipulators. The following sections provide an introduction of teleoperation systems, bilateral and multilateral, for the research work that will be used in the subsequent chapters.

1.3 Bilateral Teleoperation

Teleoperation, as the name depicts, is a branch of robotics in which a robotic operation is completed maintaining a distance between the user and the environment. More specifically, teleoperation is a loop of actions in which a user operates a master device which in turns sends the position or velocity commands to the slave and the slave tracks the trajectory of the master to interact with the environment. The interaction forces are sent back to the

master side for the human operator to feel. These commands are sent over a communication network. A bilateral teleoperation system usually consists of a single master and a single slave robot. A general bilateral teleoperation system looks like the one shown in Fig.1.6 [3]. The involvement of a human operator in teleoperation systems makes it interesting and that

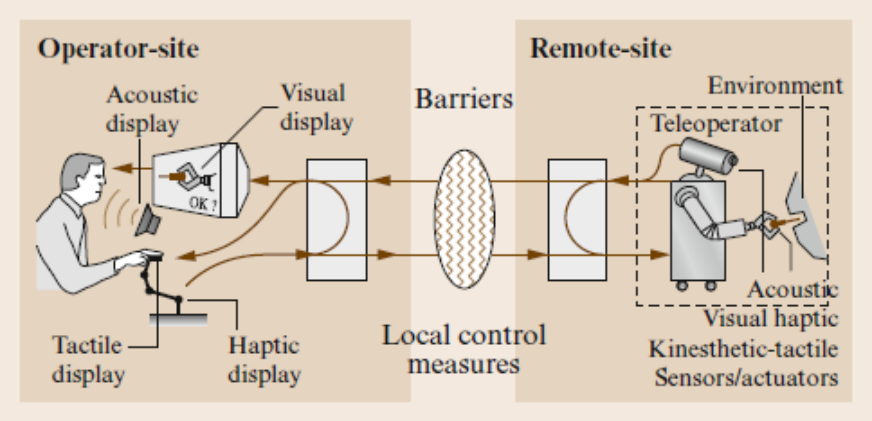

Figure 1.6: Bilateral Teleoperation [3]

results in numerous applications that are not limited to space, underwater, rescue situations, hazardous environments, rehabilitation and medical systems [3].

1.4 Multilateral Teleoperation

A substantial increase in the requirements of coordinated manipulations in industry or in other environments, demands the conventional bilateral teleoperation systems to be extended to multilateral teleoperation systems where a human operates n master manipulators to control n slave manipulators in a remote environment to perform a coordinated task such as hazardous material handling, underwater and outer space exploration, surgical operations, mining, education, multi-user online gaming and etc [7–11]. This extension of bilateral teleoperation systems to multilateral teleoperation systems increases the overall complexity and control as more signals are transmitted over the communication network. A typical multilateral teleoperation system is shown in Fig.1.7 [11].

The main challenging issues faced in multilateral teleoperation systems are, 1) time delay in signal transmission between the masters and slaves; 2) transparency, giving the human the real feel of handling the objects in a remote environment; 3) the nonlinear dynamics of manipulators, modeling errors, parametric uncertainties and exogenous inputs; 4)

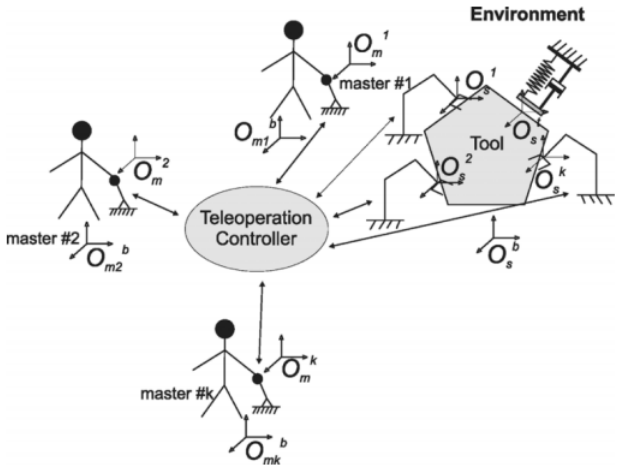

Figure 1.7: Multilateral Teleoperation [11]

the distribution of internal force in multiple slaves cooperatively manipulating a tool or object [1, 12–14]. As a lot of research has already been done on bilateral teleoperation systems, in some cases we can borrow the same ideas of control methods to meet the requirements of multilateral teleoperation systems control as the main focus of such control schemes would normally be the communication delay [15–17].

The use of communication channels to make it possible for humans to link various plants together to perform specified tasks is giving a substantial rise to develop more robust control structures. Distributed control systems are increasing day by day. Communication between different nodes in a networked control system (NCS) is a vital aspect of distributed control systems. Ease of maintenance, low cost, flexibility and ease of installation of an NCS are the main benefits that are making NCS more desirable for control engineers to use in teleoperation applications. But before we get all these advantages, there are some issues that need to be resolved first and the most important issue that is of more importance is to reduce the delay in communication between separate nodes, controllers or agents. The constraints of an NCS can be roughly described as below [18–25].

- Packet drpouts due to unreliability of network
- Quantization errors
- Variable sampling/transmission intervals
- Variable communication delay

- Constraints caused by the sharing of network by multiple nodes

As we consider the communication delay as the most disadvantageous factor of an NCS, we always want to have a minimum communication delay in our control systems. The reason of delay can be limited bandwidth and overhead in the nodes and network [26]. Numerous efforts have been made to reduce the latency or network delay to make control architectures more sophisticated and reliable. In recent years, different strategies have been developed and many more are in the development process which truly clarify the importance of network delay in a control system.

1.5 Research Motivation

Teleoperation or cooperative/coordinated control of robotic manipulators can be challenging as it involves multiple human operators, multiple master and slave manipulators and increased number of signal transmission over a communication channel or a graph topology. A lot of research has been carried out focusing the teleoperation and cooperative control of robotic manipulators for number of applications however some certain constraints, cooperative/coordinated nature of control or time delays, of these systems are not considered in control design. For example, the teleoperation systems encounter a general constraint of time delays and some of the control methods rely on assumptions that the time delay is constant however in reality it can be time varying. There can be room for improvement in the existing control methods so the research to improve the existing methods as well as the development of novel control designs is important to increase the robustness and applicability of these systems.

1.6 Thesis Outline and Contributions

This thesis is focused on the development of new control schemes for fixed-base and mobile manipulators. More specifically, this works intends to propose control schemes for the teleoperation and cooperative/coordinated control of multiple manipulators. The organization of this thesis is focused on the teleoperation control of fixed-base robotic manipulators and modeling, control and teleoperation of multiple mobile manipulators. Chapter 1 presents the background information on fixed-base manipulators, mobile manipulators, and teleoperation of manipulators followed by the contributions of the thesis. Chapter 2 presents the

literature review of the existing control schemes on the multilateral teleoperation of fixed-base and mobile manipulators with coooperative control schemes of mobile manipulators. Chapter 3 is focused on the Time Domain Passivity Control (TDPC) for multilateral teleoperation of fixed-base manipulators. Chapter 4 is on the modeling of the mobile manipulators and Chapter 5 and 6 present novel control methods on cooperative and coordinated control for object manipulation. Chapter 7 is focused on the adaptive robust control for the teleoperation of mobile manipulators followed by the conclusions and future work in Chapter 8. The contributions of this research work can be divided into three main parts:

1. Teleoperation of fixed-base manipulators: This part is focused on the development of a novel TDPC scheme for multilateral teleoperation of fixed-base robotic manipulators under constant and varying time delays. This part of the research work has been published in the following articles.

- **Ahmad, U.**, and Pan, Y. J. (2018). A Time Domain Passivity Approach for Asymmetric Multilateral Teleoperation System. *IEEE Access, 6, 519-531.*
- **Ahmad, U.**, Pan, Y. J. (2016, December). Switching Time Domain Passivity Control for Multilateral Teleoperation Systems under Time Varying Delays, In *Decision and Control (CDC), 2016 IEEE 55th Conference on (pp. 1429-1434). IEEE.*
- **Ahmad, U.**, Pan, Y. J., ul Husnain, A. (2016, November). Switching Time Domain Passivity Control for Multilateral Teleoperation Systems, In *Robotics and Artificial Intelligence (ICRAI), 2016 2nd International Conference on (pp. 69-74). IEEE.*

2. Cooperative control of mobile manipulators: This part presents the development of novel cooperative/coordinated control of multiple mobile manipulators for manipulation tasks. A part of this research work has been published or in-preparation in the following articles.

- **Ahmad, U.**, Pan, Y. J., Shen, H., Liu, S., Cooperative Control of Mobile Manipulators Transporting an Object based on an Adaptive Backstepping Approach, In *2018 IEEE 14th International Conference on Control and Automation (ICCA) (pp. 198-203), IEEE.*
- **Ahmad, U.**, Pan, Y. J., Shen, H., Null Space and Operational Space Control of Mobile Manipulators for Object Transportation, *International Journal of Robust and*

Nonlinear Control, November 2018 (In-preparation).

3. Teleoperation of mobile manipulators: This part provides the development of a novel multilateral teleoperation control scheme for single master multiple slave system. This research work is in-preparation in the following article.

- **Ahmad, U.,** Pan, Y. J., Shen, H., Adaptive Robust Control for Teleoperation of Single Master Multiple Slave Manipulators under Time Delays, *IET Control Theory and Applications, November 2018* (In-preparation).

The contributions of the individual chapters of this thesis are as follows. Chapter 3 is focused on the development of a novel TDPC scheme for the multilateral teleoperation of fixed-base manipulators where the constant and varying time delays have been considered in control design. The existing framework of TDPC control design inherits the possibility of singularity points in velocity and force signals of the master and slave. The occurrence of these singularity points is unwanted and is the main motivation of this work. This work proposes an improved TDPC scheme where the singularity points are avoided in the control design thus guaranteeing the stability of the whole system. A novel passivity controller design is proposed to overcome the zero division problem of the traditional TDPC. A novel communication channel architecture is implemented for the transmission of signals in forward and backward directions. Chapter 5 and 6 develop novel cooperative control schemes based on the adaptive backstepping control and null and operational space control of the mobile manipulators handling a common object. In Chapter 5, the main contribution is to propose an approach to simultaneously control the mobile platform and the robotic arm for proper trajectory tracking of the end-effectors for motion coordination. In Chapter 6, an adaptive control design is developed to deal with the uncertain parameters of the system. A synchronizing controller is used to achieve the synchronization of the mobile manipulators communicating over a strongly connected graph while dealing with the time delays. Decoupling of null and operational space provides the decentralized control of the mobile platform and the manipulator arm. A predefined object trajectory is provided to the agents to control the mobile platforms to achieve the main objective of the transportation of the object. The teleoperation control of single master multiple slaves (SMMS) is presented in Chapter 7 where the master system is a fixed-base robotic manipulator and the slaves are multiple mobile manipulators. An adaptive robust control design is proposed for the SMMS

teleoperation system which not only guarantees the stability of the system but also meets the control objectives of synchronization and internal force distribution.

Chapter 2

Literature Review

The substantial increase of the advancement in the field of robotics has resulted in the development of various autonomous systems operating in different environments. However, all the robotic systems which are being employed in industry or in other environments are associated with different performance metrics depending upon the task requirements. The importance of these performance metrics is so vital that in some of the applications the involvement of human operators is highly demanding. One of the class of such robotic operations is teleoperation where the human operator remains in the loop to supervise the whole robotic operation. This chapter presents the literature review of the control methods for multilateral teleoperation systems.

2.1 Multilateral Teleoperation of Fixed-Base Manipulators

Multilateral teleoperation systems are considered to be an extended class of bilateral teleoperation systems where multiple humans, and robotic systems can be the part of a single teleoperation system. A bilateral teleoperation usually consists of a human, a master robot, a communication channel for forward and backward signal transmission, a slave robot and the environment as shown in Fig.2.1 [27].

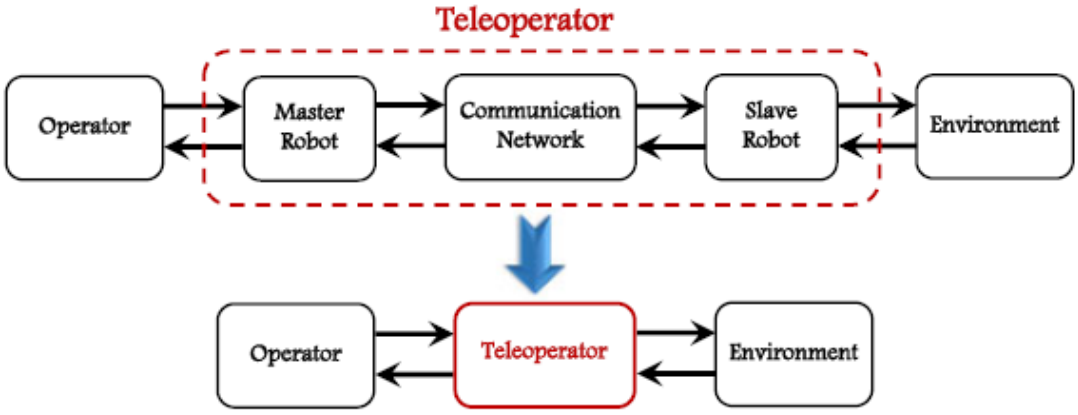

Figure 2.1: A general representation of bilateral teleoperation system [27]

A multilateral teleoperation system can have more than 2 robotic agents (master and slave robots) involved in the operation. Another class of teleoperation systems is trilateral teleoperation where the number of robotic agents is 3, however, in this work we will be considering the trilateral teleoperation systems as a general case of multilateral teleoperation systems. A general representation of cooperative multilateral teleoperation is depicted in Fig.2.2 [27]. For any teleoperation system, the control objectives include guaranteed stability, synchronization, better transparency or realism and in some cases optimal force distribution. The subsequent content of this chapter discusses the control schemes for multilateral teleoperation systems.

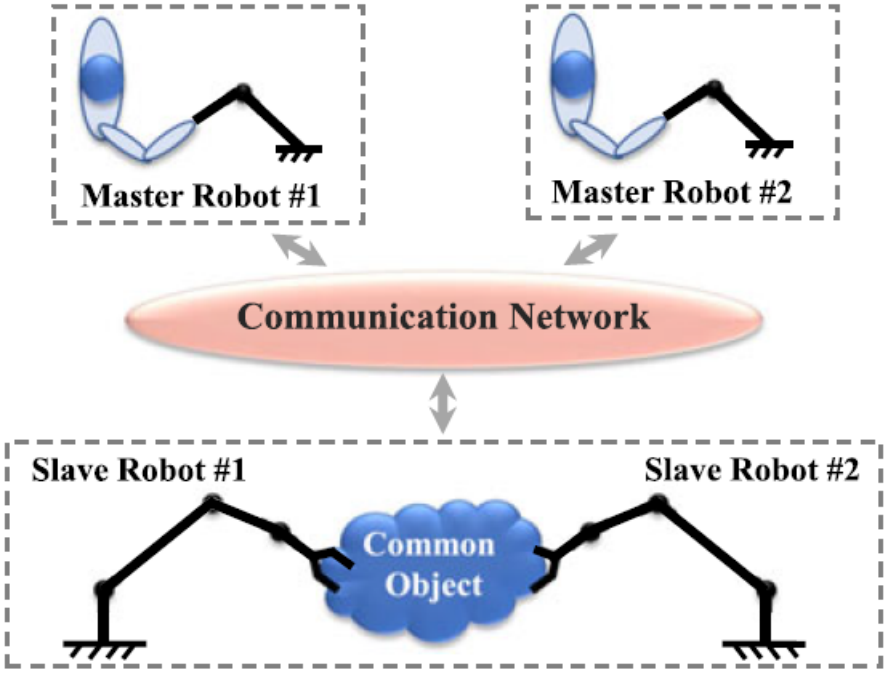

Figure 2.2: A general representation of cooperative multilateral teleoperation system [27]

Model based control of teleoperation systems some time face the challenges of modeling errors and uncertainties. Precise measurement of parameters of robots used in teleoperation systems is hard and there can be a situation where nonlinear dynamics of the robots are not available. Adpative control schemes are proposed for such situations where robot parameters are estimated online or offline. Adaptive and robust techniques have been widely used for the control of multilateral teleoperation systems. In [28], an adaptive robust

control framework was proposed for cooperative teleoperation. The framework allowed the exchange of information, position force signals, between all the agents. A μ-synthesis based scheme was implemented to handle the cooperative nature of the task while achieving the robust stability of the system. An adaptive motion force cooperative control scheme was presented in [29] where the projected force mappings were utilised to define the task subspaces of the agents. The division of task subspaces of the master and slave robots allowed to achieve the transparency objectives of the task. A couple of other adaptive control schemes for multilateral teleoperation appeared in [30, 31].

As most of the control schemes for teleoperation systems focus on the guaranteed stability without taking into account the uncertainties and external disturbances, there is a need of having a control design that guarantees the stability of the system in presence of exogenous inputs. This type of control is considered as robust control which actually makes the system less sensitive to the disturbances. [32] proposed a robust control scheme for bilateral teleoperation system where the slave was not equipped with a force sensor to measure the environment interaction forces. This scheme used a linearize model for the design of robust controller. Normally, in robust control design methods time delay is treated as a perturbation which makes sense but this approach was not valid if the time delay was large. In [33], the authors presented a novel adaptive robust control algorithm which not only guaranteed the stability of the multilateral teleoperation system but also provided excellent tracking performance, transparency and optimized internal force distribution in the presence of time delays, modeling errors and disturbances. [34] presented a new force position control architecture for multilateral teleoperation systems based on the small gain theorem and H_∞ robust control. The dynamics of the operators and the environment were modeled as linear time invariant (LTI) one port networks and the masters and slaves were controlled by local PD controllers. Then, an H_∞ robust controller was derived for the slave side to cater the uncertainties and it provided satisfactory tracking performance. The controller gains were tuned using the small gain theorem and H_∞ control theory. In [35], the authors presented the idea of incorporating the virtual fixtures (VF) to allow an expert and a novice perform a surgical procedure concurrently. The motion generated by the expert who is performing the procedure was used to create an adaptive VF in the workspace of the novice. Different performance metrics were proposed and the same impedance control methodology was

adopted as in [36]. The main objective of the proposed medical training system was to have a slave robot following an α-based combination of the masters positions. The parameter α was the dominance factor of the task and the adaptation law for this dominance factor was defined on four performance metrics, 1) total path length; 2) response orientation; 3) motion smoothness and 4) VF force effect. Adaptive guidance virtual fixture (GVF) was designed with the impedance control methodology to satisfy the desired objectives and the small gain theorem was used for the stability analysis.

Passivity based control (PBC) can be considered as one of the pioneer form of control methods for teleoperation systems. PBC initially emerged as a decent solution to maintain the stability of the bilateral teleoperation systems which was then extended to multilateral teleoperation. Over the last decade, it has been proved that the PBC schemes perform equally well under constraints of time delays. Passivity theory is considered an input-output property of a system and has its roots in network systems and it describes the transfer of energy in connected systems. Considering the interconnections of systems, we can prove that interconnection of two passive systems will be a passive system. As teleoperation systems are interconnection of subsystems, human operator, teleoperator and environment, so by proving the passivity of the whole system we can reasonably discuss the stability. In teleoperation systems, it is sometime assumed that the models of the human operator and the environment are passive so if we can prove that the teleoperator is passive then the stability of the closed loop system can be achieved.

In PBC control, scattering approach is one of the fundamental control methods for the teleoperation systems which again considers the teleoperation systems as interconnection of subsystems. Considering the subsystems of a teleoperation system as one port or two port networks, one can see the exchange of effort-flow (force-velocity) signals between them. The relationship of the forces and velocities can be expressed in terms of a hybrid or scattering matrix $H(s)$ as given below [37]. This scattering matrix can be used to prove the stability of the system.

$$\begin{pmatrix} f_1(s) \\ -\dot{x}_2(s) \end{pmatrix} = H(s) \begin{pmatrix} \dot{x}_1(s) \\ f_2(s) \end{pmatrix}$$

Wave variables approach was proposed in [38]. A lot of research hase been carried out using the same approach of wave variables for teleoperation [39]. As the teleoperation systems frequently experience the time delays so to avoid that a new control approach was required. Wave variable approach is closely related to scattering approach of [40]. The

whole concept of wave variable approach comes under the umbrella of passivity and wave variable transformation ensures that the passivity is preserved under this scheme. Power flow can be defined as,

$$P = \dot{x}^T F = \frac{1}{2} u^T u - \frac{1}{2} v^T v$$

Here, $\frac{1}{2} u^T u$ is the power flowing along the main direction considering a positive sign and $\frac{1}{2} v^T v$ is the power flowing against the main direction so having a negative sign. In this approach, (u, v) can be calculated from $(\dot{x}, F)$ as follows,

$$u = \frac{b\dot{x} + F}{\sqrt{2b}}, \qquad v = \frac{b\dot{x} - F}{\sqrt{2b}}$$

Here, b is the wave impedance constant. This transformation is one to one and always remains unique. All the information is preserved in this transformation. A simple illustration of wave variables is given in Fig.2.3 [38]. Power variables can be computed as follows,

$$b\dot{x} = \sqrt{\frac{b}{2}}(u + v)$$

$$F = \sqrt{\frac{b}{2}}(u - v)$$

We can write,

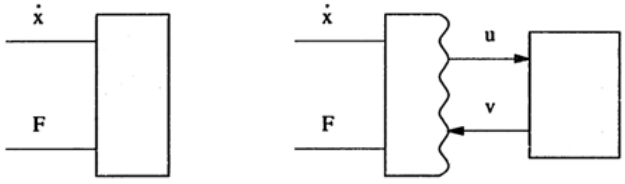

Figure 2.3: Wave variables approach [38]

$$F = b\dot{x} - \sqrt{2b}v$$

$$u = -v + \sqrt{2b}\dot{x}$$

In the wave variable approach, the impedance constant is the parameter that is used for tuning the system and is related to motion and force levels. If the value of impedance constant is increased, it will reduce the motion and causes an increase in the force levels and system appears as more damped. In contrast, if its value is decreased, the motion is increased and the force levels are reduced so the system appears less damped. Wave based

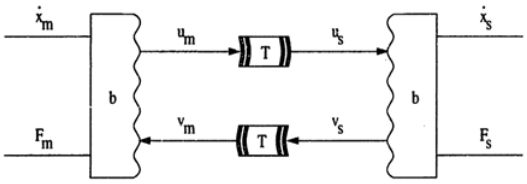

Figure 2.4: Wave variable approach input and output [38]

communication in terms of input and output variables can be shown as in Fig.2.4 [38]. The governing equations for the transmission are,

$$u_s(t) = u_m(t-\tau)$$

$$v_m(t) = v_m(t-\tau)$$

The input is given as,

$$u_m(t) = \frac{b\dot{x}_m(t) + F_m(t)}{\sqrt{2b}}$$

$$v_s(t) = \frac{b\dot{x}_s(t) - F_s(t)}{\sqrt{2b}}$$

And output equations are,

$$\dot{x}_m(t) = \sqrt{\frac{2}{b}}v_m(t) + \frac{1}{b}F_m(t)$$

$$\dot{x}_s(t) = \sqrt{\frac{2}{b}}v_s(t) - \frac{1}{b}F_s(t)$$

This approach is now widely used in the teleoperation systems and has produced stable results. A wave variable based complete teleoperation scheme is shown below in Fig.2.5 [38].

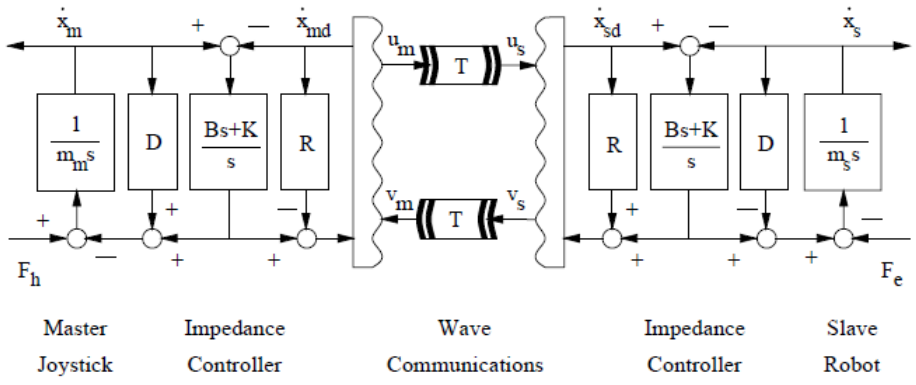

Figure 2.5: Wave variable based teleoperation [38]

This wave variable approach can be easily extended to multilateral teleoperation systems. A modified wave variable control design was proposed in [41] to not only attain the synchronization of the slaves but the force tracking too. The modified control scheme reduced the reflections in the wave based structure while guaranteeing the passivity of the channels. Another improved verison of wave variable method for multilateral teleoperation appeared in [9] where a wave node was created to connect multiple wave variable based transmission lines. Under constant time delays, passivity of the system was achieved and the position drift was compensated by the wave integral error feedback. A conflict resolution type of control scheme for multiuser teleoperation was presented in [42] which used virtual nonlinear springs between the end of the transmission line and the master arm. A force threshold enabled the users to apply appropriate forces to execute the task and the forces were limited to a certain range in case of wrong inputs from the users. A study of experimental evaluations of multilateral teleoperation using wave filter was presented in [43] which used a proportional integral and derivative (PID) controller to improve the tracking in the teleoperator side. The main idea of that work was to establish the relationship of the stability analysis of wave variables and the PID control. A dual user authority adjustment mechanism was proposed in [44] based on the wave variable approach which provided guaranteed stability in the presence of constant communication delay and time varying authority function. Local impedance based controllers were implemented for each robot and the dominance function was modified with a wave transformation. A wave based control mechanism was presented in [45] for the cooperative manipulation of a virtual object. The users sent the position commands to control the object and received the forces. Using the passivity condition for multirate wave transformations, the stability of cooperative task was analyzed under multirate discrete time state space framework.

In 2002, Hannaford and Ryu put forward their control architecture of teleoperation system based on the passivity observers and controllers [46] and this control strategy ensured the stable teleoperation by making the whole system passive. Passivity is closely related to stability and making a system passive guarantees the stable operation of the system. A general teleoperation structure with passivity is presented in Figs.2.6 and 2.7. The time domain passivity control (TDPC) of teleoperation looks like the one shown in Fig.2.8. Two series passivity controllers were designed for passivity based teleoperation which worked on the principle of observing the passivity of the system by the use of passivity observers

on both sides. Passivity observers are designed such that at every time instant, passivity of the system is monitored. If at any instant, the system goes in an active state the passivity controller starts injecting damping in the system to maintain the passivity of the system by dissipating the extra energy. For detailed reading on passivity based control for bilateral teleoperation systems, the reader is referred to [47–51].

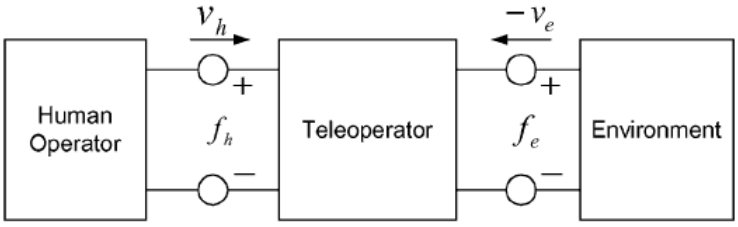

Figure 2.6: A general teleoperation system [47]

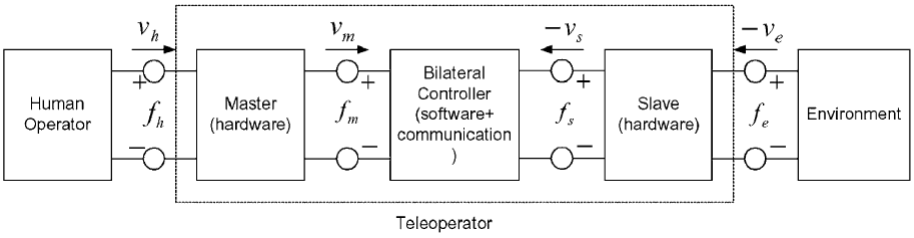

Figure 2.7: Teleoperation with master and slave [47]

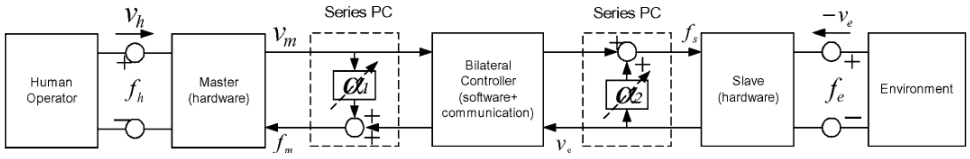

Figure 2.8: TDPC based Teleoperation [47]

Based on TDPC, different control schemes have been proposed for multilateral teleoperation systems. In [52], an improved TDPC scheme was proposed which not only provided the guaranteed stability of the systems but also enhanced the transparency of the system using measured force feedback from the environment. The control design was flexible to be integrated with other passivity based control algorithms. A TDPC architecture was proposed in [53] which not only introduced the idea of using weighting coefficients for velocity and force signals but improved the traditional TDPC controller design in such a way that it

avoided the singularity points. Weighting coefficient selection allowed the user to transfer the authority of operation of the task while maintaining the stability of the system. In [36], a novel cooperative framework for multiple master single slave (MM/SS) teleoperation systems was proposed. The desired objective of the work was to have such a system which could be used to train the trainees for medical procedures using a dominance factor of the operators. To realize such a system, the position of the slave was proposed using α_i as the dominance factor specifying the authority of the operators in the task. In traditional single master single slave (SM/SS) systems, passivity theory can be used to prove the stability of the system. It is observed that the SM/SS systems are passive when the communication delay is negligible. The aforementioned work motivated the use of impedance surfaces to prove the stability as MM/SS systems did not exhibit the passivity property.

A multiuser collaborative teleoperation system was presented in [54] to control a robot arm. Visual feedback was sent to the users to cooperatively control the arm over the internet. A user interface was developed to get inputs from the users which was then converted to a single control stream for the robot arm. The potential application of this work was a multiuser game. Fuzzy system theory and neural networks have also been used to realize the cooperative nature of the multilateral teleoperation systems as in [55–60]. Some of the research work on multilateral teleoperation has been reported in [61–63] related to medical applications.

2.2 Cooperative Control of Mobile Manipulators

Industrial applications like heavy object manipulation require a sophisticated system design in order to perform a task with accuracy and meeting a certain performance criteria. Cooperative mobile manipulators emerged as a decent solution to such industry applications and they not only provide the flexibility in task completion but also improve the applicability of these systems. An obvious advantage of the mobile manipulators over fixed-base manipulators is the increased workspace and dexterity [64–66]. In recent years, this area has attracted a lot of researchers working in robot control [67]. Over the last few years, cooperative task completion has emerged as an important research area especially when applications involve mobile manipulators [68–70]. Two novel control strategies were put forward in [69] to cooperatively manipulate an object by a team of mobile manipulators. One of the controllers was designed to achieve the perfect tracking of the object twist while the second controller

dealt with the stabilization of the twist in the presence of errors in the estimation of the parameters. A multi layer adaptive control was designed in [70] for cooperatively manipulating an object. A two layered coordinated control scheme was addressed in [71] for the object transportation with obstacle avoidance where a centralized-decentralized collision free architecture was implemented for safe manipulation. Similar to [70], a multi layer approach was proposed in [72] for the coordinated control of mobile manipulators where each layer was considered independent in the operation. One layer dealt only with the coordination control and the other layers adaptively updated the parameters of the robots. Obstacle avoidance was achieved by the redundancy of the system.

[73] presented a novel control of mobile manipulators for cooperatively grasping and driving an object rigidly attached to the end-effectors. Velocity commands were used to manipulate the object and the grasp shape was maintained without any fixtures with the formation control for collision avoidance. In [74], the authors proposed a decentralized integral sliding mode controller based on force and position to guarantee the exponential tracking of the mobile manipulators. The control scheme was implemented on omnidirectional mobile manipulators to transport an object. The controller design did not need dynamics or interaction force of the ith mobile manipulator. Omnidirectional base in that system achieved object mobility using passive smooth velocity fields for collision free tracking. A constrained sequential linear quadratic optimal control approach was discussed in [75] where the problem of kinematic trajectory tracking of mobile manipulators was solved and the control was implemented on a 26 degrees of freedom (DOF) system. [76] presented a robust impedance controller with delay compensation for mobile manipulators. A state space model was addressed for electrically driven nonholonomic mobile manipulator. In that work, motor dynamics control provided fast computation as compared to torque control laws. The control law was not dependent on the robot dynamics as the nonlinear dynamics of the system were considered to be an external load.

Multi objective grasping of mobile manipulators was discussed in [77]. A path planning algorithm was proposed to compute the trajectory while increasing the manipulability of the system. The main goal was to find an optimized pose of the end-effector grasping an object. The pose of the object was obtained by a visual system in order to compute the optimized pose of the end-effector. An interesting manipulation scenario was reported in [78]

where the mobile manipulators had to carry an object on a slope following a desired trajectory. The control was divided into two parts: the first part used the extra degrees of freedom of the mobile manipulators to avoid any falling situation of the robots and the second part dealt with the instability in the robot postures by adjusting the forces exerted on the object. The inclined angle of the slope was measured by the extra sensors mounted on the robots which is not desirable in some situations due to extra cost.

With reference to mobile manipulators, backstepping can be used in systems with a specialized structure. It attempts to solve the nonholonomic navigation drawbacks that prevent tracking of a reference trajectory, following a path and point stabilization [79,80]. It utilizes a Lyapunov design based on virtual controls [81]. Robust backstepping leads to quadratic robust control Lyapunov functions (RCLF) in a set of transformed coordinates [82, 83]. This type of RCLF can generate control laws with local gains that are not entirely necessary, leading to excessive control efforts such as high magnitude chattering in the control signal. This property is amplified at every stage in the recursive backstepping design.

A motion planning and control scheme was presented in [84] to manipulate a common object rigidly attached to the manipulators. A leader follower control was proposed in the aforementioned work where the object was considered to be a virtual leader. In [85], the author presented a two step controller design to manipulate an object using mobile robots. The first step used the artificial potential fields to control the motion of the mobile manipulators while avoiding the collisions and the second step involved the grasping of the object. An adaptive robust control scheme was presented in [86, 87] to manipulate a commonly grasped object by the mobile manipulators. The robustness of the control scheme not only managed to deal with the uncertainties in the parameters but with exogenous disturbances too. An adaptive fuzzy control design was addressed in [57] where the linear matrix inequalities (LMIs) were utilized to suppress the effects of uncertainties, perturbations and network delays. An extended impedance based control scheme was presented in [88] where the focus was to eliminate the undesired internal forces. The impact of the disturbances was reduced by means of decoupling in the task space.

In [89], a switched control algorithm was presented for cooperative mobile manipulation of rigid objects. The mobile manipulators accomplished the tasks of grasping the object and following a desired pose. A distributed scheme for the estimation of unknown

parameters of an unknown object was presented in [90]. A two phase, transport and manipulation, control scheme appeared in [91] where in the first phase, the mobile manipulators followed a trajectory by controlling the actuators for the wheels and in the second phase, the object was manipulated by controlling the joints of the arms. A simplified cooperative control approach was presented in [92] where the mobile platforms tracked an off-line designed trajectory and the compliant control was used to suppress the motion errors of the platforms. A Force-Amplifying N-robot Transport System (Force-ANTS) was proposed in [93] to coordinate the transportation of a heavy object in a plane. A hybrid methodology of cluster space control and force control appeared in [94] to effectively and safely manipulate an object with mobile manipulators. The formation of the mobile manipulators was maintained by cluster space control and the explicit force control provided safe application of the required forces to move the object in the desired orientation. A multiple layer control scheme was proposed in [95] for the coordinated and cooperative control of the mobile manipulators to transport a common object. Independent modules were developed for each layer to achieve cooperation and coordination while avoiding the obstacles in the trajectory of the mobile manipulators.

In [96], an optimal algorithm was used to search a graph which satisfied the closure and collision constraints of the mobile manipulators to find a possible shortest path for the cooperative manipulation of a body. Time optimal trajectories were calculated in a sequence to move along the consecutive points of the path. A heuristic approach was then utilized to avoid collisions with the moving objects in the environment. A local motion planning control was prsented in [97] for the collaborative manipulation of the deformable objects. A hybrid approach of distributed and centralized control was used for the collision avoidance and motion planning. A convex optimization problem was developed in a receding horizon planner which considered the shape of the soft object to provide a collision free path. A nonlinear model predictive control (NMPC) design guaranteed the manipulation of an object to a desired pose while navigating through the obstacles of the workspace. NMPC not only ensured the collision free manipulation but also provided the singularity free configurations of the mobile manipulators [98].

A teleoperation control scheme was presented in [99] for mobile robots where the gaze control of the robots was used. The environment of the mobile robot was represented with the help of a graphical user interface (GUI) to help the human operator understanding

the spatial relationships. An MPC control design was presented in [100] for the trajectory tracking of mobile robots with nonholonomic constraints. The MPC control incorporated the neural dynamic optimization (NDO) to track the trajectory. The tracking error kinematics were used in MPC to formulate the system as a quadratic programming (QP) problem which was then solved by primal dual neural network (PDNN). [101] proposed an MPC based technique to deal nonholonomic chained systems as two subsystems. The MPC used a general projection neural network (GPNN) to find the solution of a QP problem. The stability of GPNN was proved using Lyapunov method and the convergence of the optimal solution was guaranteed. As mobile robots fall under the same category of nonholonomic chained system or can be formulated as chained systems, the above mentioned method can be reformulated for the trajectory tracking of mobile robots with nonholonomic constraints. Assumptions regarding smoothness can be made in recursive backstepping models as there is a need to calculate the function derivatives during the creation of control law and Lyapunov function [102].

2.3 Teleoperation of Mobile Manipulators

The ever increasing demand of industrial applications like heavy object manipulation, safe and stable operation and complex task performances require a well designed control system to achieve all these goals. Traditional bilateral teleoperation systems are sometime not suitable for such applications and there comes the need to extend these systems to multilateral teleoperation. Another disadvantage of bilateral teleoperation systems having fixed base manipulators is the limited workspace and dexterity. Teleoperation of mobile manipulators emerges as a decent solution to all these problems and provides enough flexibility of achieving task execution goals with guaranteed stability and safety of operation. Additionally, the mobility of a robotic manipulator not only maximizes the task generality of the system but also provides an increased task space in structured or unstructured environments. This increase in the manipulation task capabilities of the mobile manipulators outclasses the conventional fixed base robotic manipulators however this comes at the cost of additional control design challenges.

Although multilateral teleoperation of mobile manipulators is a solution to the requirements of the industrial applications, the system becomes complicated due to increased number of human operators, master robots, slave robots, the transmission of signals over the

communication channel and the control of mobile base. The multilateral teleoperation control design poses challenges in handling the time delay, dynamics of the master and slave robots, the realism of the teleoperation system and the internal forces of the target object. The control algorithms for the mobile manipulators not only have to achieve a task specific criteria but also have to deal with other issues like redundancy resolution and simultaneous or decoupled control of the robotic arm and the mobile base. As we leverage the increased task space and dexterity of the mobile manipulator system, we face the challenges of high dimensionality and complexity in the control design [2, 64, 103].

Teleoperation control of mobile manipulators has attracted researchers over the past few years and a number of control designs appear in the existing literature. A general scenario of the teleoperation of multiple mobile manipulators is depicted in Fig.2.9 [104]. A formation control design for the teleoperation of nonholonomic mobile manipulators under constant delays was proposed in [105]. A partial feedback linearization approach was applied for the formation control of the mobile manipulators teleoperated by a human. One of the limitations of the research was that the slave mobile manipulators were only controlled in the constrained workspace of the master robot. Additionally, only constant time delay in the communication channel was considered whereas in reality the delay could be time varying. A brain machine interfacing control of the mobile robot teleoperation was developed in [106] which was based on the visual feedback. Given an initial set and a goal set of the images, visual evoked potentials were used to generate the electroencephalogram (EEG) motion commands to make the image set converge to the goal set and the robots were controlled by the brain actuated path as indicated by the Bezier curve between the

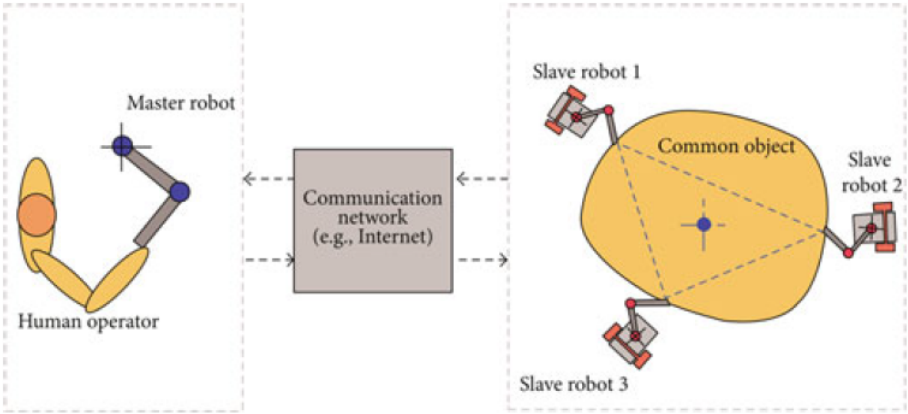

Figure 2.9: Teleoperation of multiple mobile manipulators [104]

initial and the target points. Similar to [106], a brain actuated teleoperation control for a mobile robot was presented in [107] where the trajectory tracking of mobile robot was achieved by Bezier curve methodology. An EEG signal based telepresence control was presented in [108] to teleoperate a mobile robot. The teleoperation control was realized with the help of a brain computer interface (BCI) allowing the user to complete different tasks in the remote environment.

A human machine interface (HMI) was developed in [109] for the teleoperation of a mobile robot. The interface design was based on two separate components where one component received the surface electromyography (sEMG) signal from the human upper limb and the other component received the signals from Microsoft Kinect sensor. The interface allowed to control the movements of a humanoid mobile robot in 3D space using the estimation of the human upper limb movements by sEMG recordings and Microsoft Kinect sensor. In contrast to [109], a speech control method was presented in [110] for the teleoperation of a humanoid mobile robot. An active auditory perception system was implemented to make sure that the robot operated effectively. A voice signal was sent over the communication channel to the robot and the human received the visual feedback over the same communication channel. The event based teleoperation control provided robustness in the system to avoid time delays.

An adaptive controller was proposed in [111] to remotely control a mobile manipulator operating in an unbounded workspace. A velocity command from a joystick was sent over the communication channel to the slave side and the slave local controller made the slave end-effector converge globally and asymptotically to a proportional part of the master pose. A neural adaptive control scheme was developed in [112] for single master multiple slaves teleoperation system of mobile manipulators. The time delays and the dead zone uncertainties were take into account for the controller design of the mobile manipulators cooperatively handling an object. A linear matrix inequality (LMI) based model reference neural control approach was implemented to make the tracking errors converge to zero. The control algorithm was robust in the presence of uncertain parameters, disturbances, dead zone in input and time delays.

A time domain passivity approach (TDPA) was proposed in [46] for the bilateral teleoperation of a mobile manipulator. The human operator controlled the speed of the mobile base via a haptic device and the force feedback was transmitted to the human operator when

the robot interacted with the environment. The passivity observer and passivity controller made sure that the system remained passive during the operation to avoid instability. A switching control mechanism was proposed in [113] where the human operator could either control the position of the end-effector or the speed of the mobile base depending upon the requirement of the task. In [114], the authors proposed a switching control based teleoperation system where the control was classified into two modes. The locomotion mode allowed the user to control the motion of the mobile base of the mobile manipulator and the manipulation mode allowed to control the robotic arm only. The switching of these two modes was achieved by mounting a switch on the haptic device,

A hybrid control approach was presented in [115] where a teleoperation control without sensor feedback was realized by applying the torque observers. In [116], the authors proposed a proportional derivative (PD) like scheme to control the velocity of the end-effector of the mobile manipulator and the dynamics control and secondary control actions were achieved in the operational space. Absolute transparency based control schemes were discussed in [117] where the authors analyzed different control criterion applied to bilateral teleoperation of mobile robots. Absolute transparency, the realism of the teleoperation system, was tested for various control approaches applicable for mobile robot teleoperation. In all of the above mentioned research, the control design either deals with the control of a single mobile manipulator or with the bilateral teleoperation.

2.4 Preliminaries of Graph Theory

Multiagent systems (MAS) are comprised of several agents that are intelligent in nature and communicate over a network. Due to advantageous applications of multiagents systems, they are widely used these days for different purposes [118]. Multiagents systems are designed to perform those specific tasks which are nearly impossible to do by a single agent. However as the number of agents increases in multiagent systems, the level of difficulty to design controllers also gets increased. Multiagent systems work on the principle of consensus, a specific term which is used for the cooperative behavior of the agents working for a common task [119–124]. The control laws are formulated on the basis of a common consensus which is followed by the agents. Algebraic Graph theory is one of the most basic approach to easily understand the consensus and cooperative control of MAS.

The information that is exchanged between the agents is essentially based on graph theory. In a network of multiple agents connected over a communication network, the signal sharing or information exchange can be described by a communication graph. This section presents some basic concepts and definitions of graph theory which will subsequently be used in this thesis.

A graph $\mathcal{G}(\mathcal{V},\mathcal{E})$ can be defined as a finite set $\mathcal{V}(\mathcal{G}) = \{v_i,...,v_n\}$, with elements called nodes or vertices, including a set $\mathcal{E}(\mathcal{G}) \subset \mathcal{V} \times \mathcal{V}$ with elements defined as edges, which is an ordered pair of distinct nodes [125–127]. The in-degree d_i of a vertex $v \in \mathcal{V}(\mathcal{G})$ is the number of edges that have this vertex as a head. An undirected graph is a graph for which all the edges $(v_i,v_j) \in \mathcal{E}(\mathcal{G})$ and $(v_j,v_i) \in \mathcal{E}(\mathcal{G})$ otherwise it is a directed graph. A *strongly connected* graph is a directed graph in which any two vertices in $\mathcal{V}(\mathcal{G})$ can be joined by a path. The robots in a networked system can be represented as the vertices of a graph and the information exchange among them can be defined by a weighted graph as $\mathcal{G}_w = (\mathcal{V},\mathcal{E},\mathcal{W})$ where $\mathcal{W}(\mathcal{G}_w) = \{w_{ij}\}, j \in \mathcal{N}$, where w_{ij} is the weight of the edge from v_j to v_i and $\mathcal{N}$ is the finite set of the robots sharing the information. Given the edge weights w_{ij}, a communication graph can be represented by a connectivity or adjacency matrix $\mathcal{A} = [w_{ij}]$ as,

$$\mathcal{A} = \begin{cases} w_{ij} > 0 & if \quad (v_i,v_j) \in \mathcal{E} \\ w_{ij} = 0 & otherwise \end{cases}$$

The diagonal in-degree matrix $\mathcal{D} = diag[d_i]$ is used to define the Laplacian matrix $\mathcal{L}$ of the graph which is given by $\mathcal{L} = \mathcal{D} - \mathcal{A}$. It is noted that $\mathcal{L}$ has row sum zero. The weights of the edges are not always identical so the weighted Laplacian for the directed graph can be defined as,

$$\mathcal{L}_w = \begin{cases} \sum\limits_{j \in \mathcal{N}} w_{ij} & if \quad i = j \\ -w_{ij} & if \quad j \in \mathcal{N} \\ 0 & otherwise \end{cases}$$

Chapter 3

Time Domain Passivity Control of Multilateral Teleoperation Systems

In this chapter, a novel switching time domain passivity control (TDPC) scheme for multilateral teleoperation of fixed-base manipulators is proposed which not only ensures the stability of the system but also avoids zero division. In contrast to bilateral teleoperation systems, the multilateral teleoperation system is much more complex as it involves increased number of master and slave hardware, multiple operators and transmission of multiple signals over the communication network. A new framework for the communication channel has been proposed which incorporates the use of weighting coefficients to give the masters and slaves authority depending upon the requirements of the operation. As the switching time domain passivity control keeps the system passive all the time, the stability is guaranteed. The proposed control scheme is valid for n masters and n slaves. Simulations and experiments, in the presence of constant and time varying communication delays, are carried out to verify the effectiveness of the proposed scheme.

3.1 Time Domain Passivity Control (TDPC) for Teleoperation

3.1.1 Introduction

A widely used approach for teleoperation systems is the time domain passivity control (TDPC) [128, 129]. This scheme is basically based on varying damping injection which maintains the system passivity. The energy based time domain passivity control (ETDPC) observes overall energy of the system. As teleoperation systems sometime encounter large force signals from the environment so to eliminate this, TDPC with reference energy scheme has already been proposed [130]. [129, 131] proposed a power based time domain passivity control (PTDPC) which was applied to teleoperation system and in [17] with application to haptic control.

Less complex and model free structure of time domain passivity control schemes makes them easier to implement but as mentioned earlier the only drawback of these schemes is

the zero division which should be avoided at any cost for the stability of the teleoperation system and the safety of the human operator. One mechanism that has been put forward in [132] naturally avoids this problem of zero division by removing the noisy behavior due to zero velocity. Another approach to avoid zero division has been presented in [50] which takes the advantage of deactivating the passivity controller and outputs a zero in low force or velocity. However, the deactivation of passivity controller at an instant of time causes the loss of passivity at that instant and the activeness may accumulate leading to instability of the system. Although several schemes for teleoperation systems, especially for multilateral teleoperation systems [133–137], have appeared in literature, but initially the notion of switching time domain passivity control was proposed by [138] to overcome the zero division but it was found that the scheme was not valid where the varying time delays were under consideration. We propose a simple yet practical time domain passivity control based on the same switching idea with application to multilateral teleoperation systems. The main contributions of this chapter are:

- To propose a new switching TDPC scheme for multilateral teleoperation systems with constant and varying time delays which ensures the stability of the system.
- To introduce a novel communication structure incorporating the weighting coefficients for the proper weight selection of the masters and slaves.
- To verify the effectiveness of the proposed scheme with simulation and experimental results.

3.1.2 Challenges in TDPC

Time domain passivity control normally works under the constraint of zero division. Small force or velocity signals can cause the occurrence of zero division which ultimately leads the system to be unstable. This instability in the system can result in undesired situations which include unsafe operation of the system when human operator is in the loop and damage to the hardware due to sudden large inputs.

3.1.3 Motivation of Research

The existing framework of TDPC control design inherits the possibility of singularity points in velocity and force signals of the master and slave. The occurrence of these singularity

points is unwanted and is the main motivation of this work. This work proposes an improved TDPC scheme where the singularity points are avoided in the control design thus guaranteeing the stability of the whole system. A comparison of existing and proposed TDPC control design will be presented in subsequent sections for better understanding of the novelty of this research.

3.2 TDPC for Bilateral Teleoperation

The power P of a system can be expressed as

$$P = fv = \frac{dE}{dt} + P_{diss}, \tag{3.1}$$

where f is the output force, v is the input velocity, E is the low bounded stored energy and the dissipation is P_{diss}. It is well known that if,

$$P_{diss} \geq 0, \tag{3.2}$$

then the system is passive. The integration of (3.1) can be expressed as

$$\int_0^t P(\tau)d\tau \;=\; \int_0^t f(\tau)v(\tau)d\tau = E(t) - E(0) + \int_0^t P_{diss}(\tau)d\tau \geq -E(0) \tag{3.3}$$

$E(0)$ is the initial energy and is typically zero so (3.3) can be reduced to

$$\int_0^t f(\tau)v(\tau)d\tau \geq 0, \tag{3.4}$$

ensuring that for all time the overall energy of the system must be positive. Similarly, the m-port network is passive iff

$$\int_0^t P(\tau)d\tau = \int_0^t (\sum_{i=1}^{m} f_i(\tau)v_i(\tau))d\tau \geq -E(0), \tag{3.5}$$

where $f_i(t)$ and $v_i(t)$ represent the force and velocity for the ith port. The idea of TDPC [128] is derived from the inequality (3.4). A bilateral teleoperator system with switching TDPC is shown in Fig.3.1 in which b is the damping parameter, B and K are the proportional and derivative gains of the slave PD controller. [17] proposed the use of a passivity observer (PO) to calculate the power condition in (3.2). Passivity observers are designed at the master and slave sides to observe the power at every time instant and a combination of a switch and a damper is utilized to assure the stability of the system.

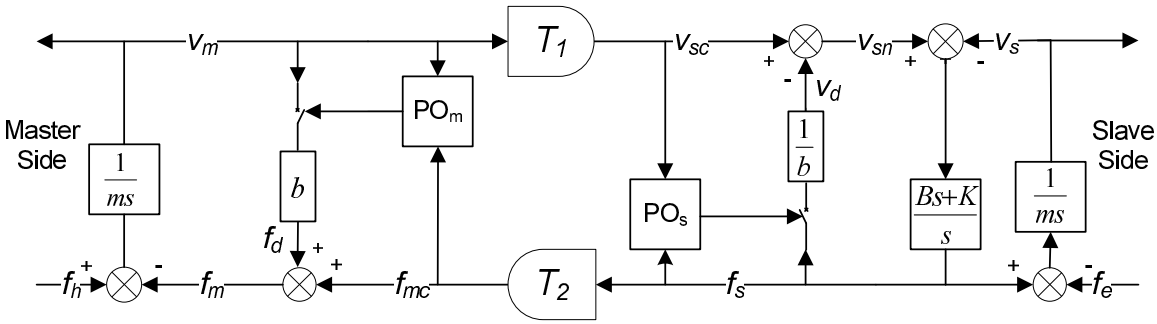

Figure 3.1: A bilateral teleoperator with TDPC [129]

3.3 Switching TDPC with Constant Time Delay

The complete multilateral teleoperation system can be shown as in Fig.3.2. In contrast to bilateral teleoperation, the system for multilateral teleoperation is much more complex as it involves more masters and slaves and multiple operators which increase the number of transmitted signals over the communication network. This work is focused on the development of an improved version of time domain passivity control where the zero division will be avoided in control laws thus guaranteeing the stability of the system.

In Figs.3.1 and 3.2, the masters and slaves are represented by effective masses of m. A human operates the masters with force f_h. The force which is generated by the slave controllers is f_s. The force that an environment exerts on the slaves is f_e. As in Fig.3.2, signals $v_{mi}(t)$ and $f_{si}(t)$ are sent with delays T_{mi} and T_{si}, are governed by

$$v_{sci}(t) = \sum_{j=1}^{n} v_{scij}(t),\ v_{scij}(t) = \alpha_{vij} v_{mj}(t - T_{mij}), \tag{3.6}$$

$$f_{mci}(t) = \sum_{j=1}^{n} f_{mcij}(t),\ f_{mcij}(t) = \alpha_{fij} f_{sj}(t - T_{sij}), \tag{3.7}$$

where α_{vij} and α_{fij} describe the weighted effects of the weighting coefficients on masters and slaves (i=j=1,$\cdots$,n). T_{mij} and T_{sij} represent the delay from the jth master to the ith slave and from the jth slave to the ith master respectively. An example of the weighting coefficients can be found in medical applications where an expert is training a trainee. Initially the expert user holds the maximum authority for the operation and as the trainee gets skills, the expert user reduces his authority of operation to let the trainee perform the task.

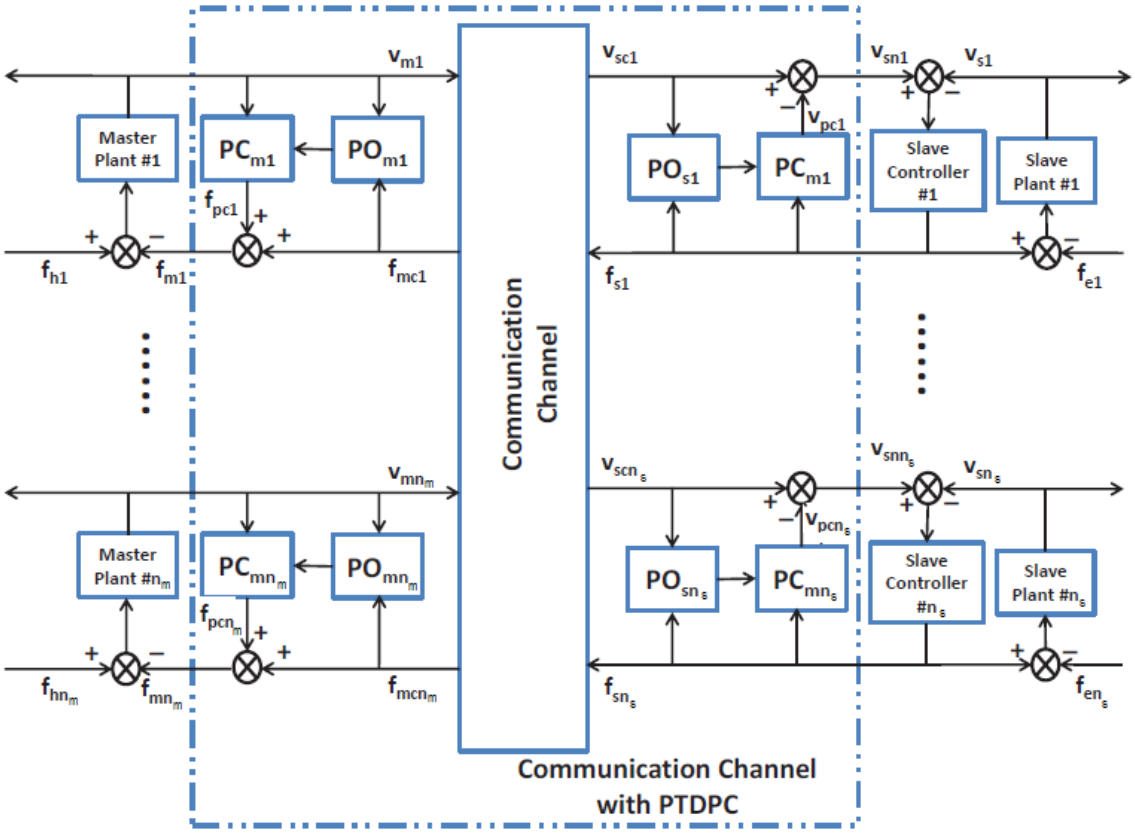

Figure 3.2: Multilateral teleoperation system with switching TDPC

The power flow of the multilateral communication is,

$$P = \sum_{i=1}^{n} [v_{mi}(t) f_{mci}(t) - v_{sci}(t) f_{si}(t)]. \tag{3.8}$$

A positive constant b_i is introduced as in [139], and (3.8) is rewritten as

$$\begin{aligned} P &= \sum_{i=1}^{n} [\frac{1}{2b_i} f_{mci}^2(t) + \frac{b_i}{2} v_{mi}^2(t) - \frac{1}{2b_i}(f_{mci} - b_i v_{mi})^2(t) \\ &\quad + \frac{1}{2b_i} f_{si}^2(t) + \frac{b_i}{2} v_{sci}^2(t) - \frac{1}{2b_i}(f_{si} + b_i v_{sci})^2(t)] \\ &= \sum_{i=1}^{n} [\frac{1}{b_i} f_{mci}^2(t) - \frac{1}{2b_i}(f_{mci} - b_i v_{mi})^2(t) \\ &\quad + b_i v_{sci}^2(t) - \frac{1}{2b_i}(f_{si} + b_i v_{sci})^2(t) + \frac{1}{2b_i} f_{si}^2(t) \\ &\quad - \frac{1}{2b_i} f_{mci}^2(t) + \frac{b_i}{2} v_{mi}^2(t) - \frac{b_i}{2} v_{sci}^2(t)], \end{aligned} \tag{3.9}$$

Using Eqns. (3.6) and (3.7), the last four terms in (3.9) become

$$\begin{aligned}\sum_{i=1}^{n}[\frac{1}{2b_i}f_{si}^2(t)-\frac{1}{2b_i}f_{mci}^2(t)] &= \sum_{i=1}^{n}\frac{1}{2b_i}[f_{si}^2(t)-(\sum_{j=1}^{n}\alpha_{fij}f_{sj}(t-T_{sij}))^2] \\ &\geq \sum_{i=1}^{n}\frac{1}{2b_i}[f_{si}^2(t)-n\sum_{j=1}^{n}\alpha_{fij}^2 f_{sj}^2(t-T_{sij})] \\ &= \sum_{i=1}^{n}[\frac{1}{2b_i}f_{si}^2(t)-n\sum_{j=1}^{n}\frac{1}{2b_j}\alpha_{fji}^2 f_{si}^2(t-T_{sji})], \quad (3.10)\end{aligned}$$

$$\begin{aligned}\sum_{i=1}^{n}[\frac{b_i}{2}v_{mi}^2(t)-\frac{b_i}{2}v_{sci}^2(t)] &= \sum_{i=1}^{n}\frac{b_i}{2}[v_{mi}^2(t)-(\sum_{j=1}^{n}\alpha_{vij}v_{mj}(t-T_{mij}))^2] \\ &\geq \sum_{i=1}^{n}\frac{b_i}{2}[v_{mi}^2(t)-n\sum_{j=1}^{n}\alpha_{vij}^2 v_{mj}^2(t-T_{mij})] \\ &= \sum_{i=1}^{n}[\frac{b_i}{2}v_{mi}^2(t)-n\sum_{j=1}^{n}\frac{b_j}{2}\alpha_{vji}^2 v_{mi}^2(t-T_{mji})], \quad (3.11)\end{aligned}$$

if T_{sji} and T_{mji} are constants. In the proposed framework, the selection of the weighting coefficients in (3.6) and (3.7) is based on a generalized form to satisfy

$$\frac{1}{2b_i}=n\sum_{j=1}^{n}\frac{1}{2b_j}\alpha_{fji}^2, \quad \frac{b_i}{2}=n\sum_{j=1}^{n}\frac{b_j}{2}\alpha_{vji}^2 \quad (3.12)$$

This selection method of weighting coefficients helps us to further simplify (3.12) when all the damping coefficients are equal, we get

$$n\sum_{j=1}^{n}\alpha_{fji}^2=1 \quad and \quad n\sum_{j=1}^{n}\alpha_{vji}^2=1$$

For specific medical applications, the selection of these weights is based on different factors as listed in [35]. The right hand side of the inequalities (3.10) and (3.11) is represented as,

$$\begin{aligned}\frac{dE}{dt} &= \sum_{i=1}^{n}[\frac{1}{2b_i}f_{si}^2(t)-n\sum_{j=1}^{n}\frac{1}{2b_j}\alpha_{fji}^2 f_{si}^2(t-T_{sji})] \\ &\quad +\sum_{i=1}^{n}[\frac{b_i}{2}v_{mi}^2(t)-n\sum_{j=1}^{n}\frac{b_j}{2}\alpha_{vji}^2 v_{mi}^2(t-T_{mji})] \quad (3.13)\end{aligned}$$

$$\begin{aligned}E &= \sum_{i=1}^{n}\sum_{j=1}^{n}[\int_{t-T_{sji}}^{t}\frac{n}{2b_j}\alpha_{fji}^2 f_{si}^2(\tau)d\tau \\ &\quad +\int_{t-T_{mji}}^{t}\frac{nb_j}{2}\alpha_{vji}^2 v_{mi}^2(\tau)d\tau] \quad (3.14)\end{aligned}$$

Substituting (3.10),(3.11) and (3.13) in (3.9), the power flow of the communication channel can be given as,

$$\begin{aligned} P \;\geq\; & \sum_{i=1}^{n}[\frac{1}{b_i}f_{mci}^2(t) - \frac{1}{2b_i}(f_{mci} - b_i v_{mi})^2(t) \\ & + b_i v_{sci}^2(t) - \frac{1}{2b_i}(f_{si} + b_i v_{sci})^2(t)] + \frac{dE}{dt}. \end{aligned} \tag{3.15}$$

The comparison of (3.1) and (3.15) gives us the total power dissipation of multilateral teleoperation with constant time delays as

$$\begin{aligned} P_{diss} \;\geq\; & \frac{1}{b_i}f_{mci}^2(t) - \frac{1}{2b_i}(f_{mci} - b v_{mi})^2(t) + b_i v_{sci}^2(t) \\ & - \frac{1}{2b_i}(f_{si} + b_i v_{sci})^2(t). \end{aligned} \tag{3.16}$$

$P_{diss} < 0$ shows the non-passiveness of the system, an indication that the action of passivity controller is needed. For real-time checking, (3.16)$\geq$0 is divided in two sufficient conditions,

$$\frac{1}{b_i}f_{mci}^2(t) - \frac{1}{2b_i}(f_{mci} - b_i v_{mi})^2(t) \geq 0, \tag{3.17}$$

$$b_i v_{sci}^2(t) - \frac{1}{2b_i}(f_{si} + b_i v_{sci})^2(t) \geq 0. \tag{3.18}$$

The passivity observers for the masters and the slaves are designed the similar way as in [129],

$$P_{obsv}^{mi} = \frac{1}{b_i}f_{mci}^2(t) - \frac{1}{2b_i}(f_{mci} - b_i v_{mi})^2(t), \tag{3.19}$$

$$P_{obsv}^{si} = b_i v_{sci}^2(t) - \frac{1}{2b_i}(f_{si} + b_i v_{sci})^2(t). \tag{3.20}$$

Thus, the power flow of the communication channel (3.15) can be rewritten as

$$P \geq \sum_{i=1}^{n}[P_{obs}^{mi} + P_{obs}^{si}] + \frac{dE}{dt} \tag{3.21}$$

The novel communication channel for different number of masters and slaves is shown in Fig.3.3.

The control laws for PC_{mi} and PC_{si}, (passivity controllers at the master and slave sides), are defined as,

$$f_{pci} = \begin{cases} v_{mi} b_i & P_{obs}^{mi} < 0, \\ 0 & P_{obs}^{mi} \geq 0, \end{cases} \tag{3.22}$$

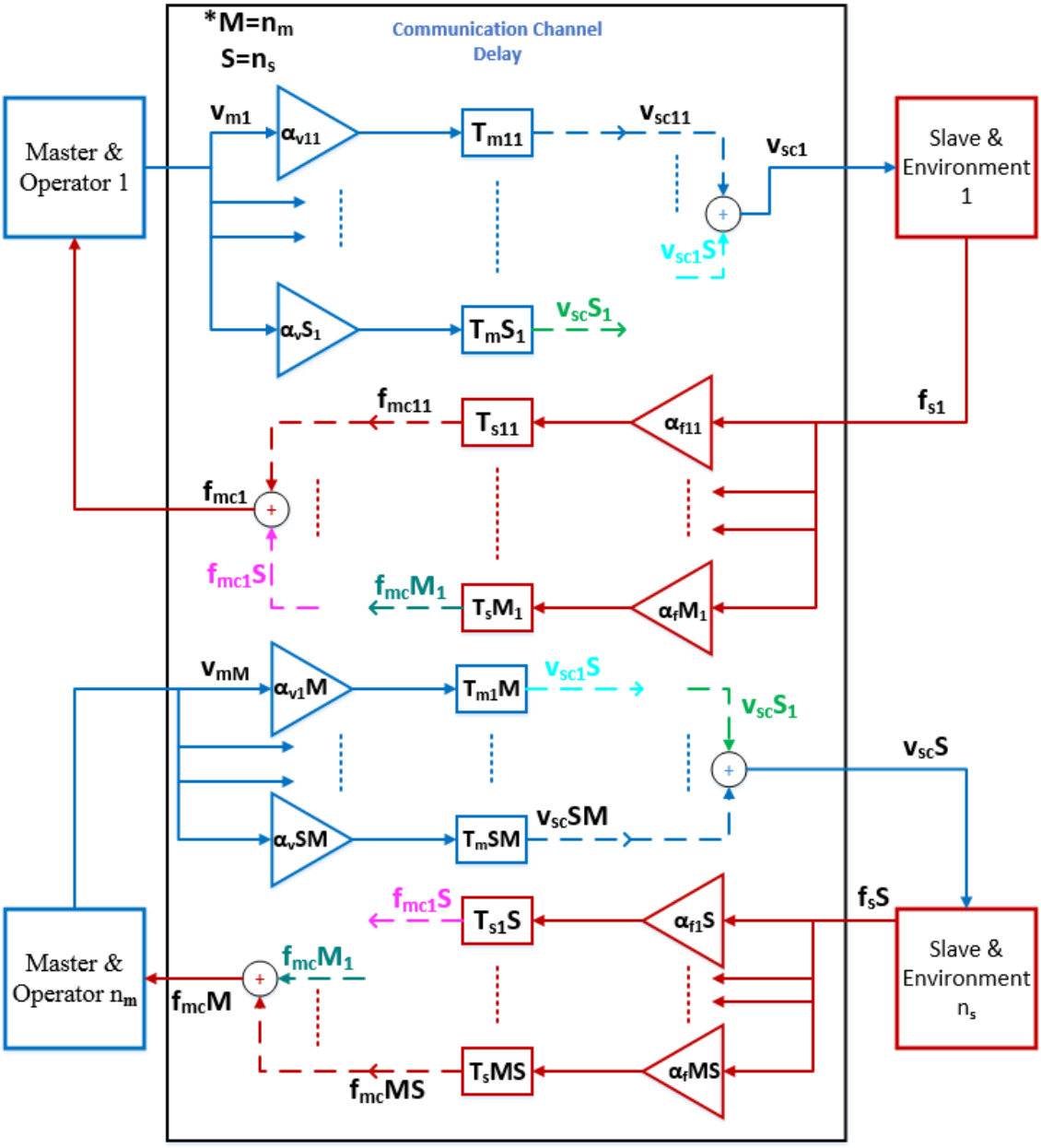

Figure 3.3: Multilateral teleoperation communication channel

and

$$v_{pci} = \begin{cases} \dfrac{f_{si}}{b_i} & P_{obs}^{si} < 0, \\ 0 & P_{obs}^{si} \geq 0. \end{cases} \tag{3.23}$$

It can be noted that these control laws naturally avoid zero division situation and these controllers can be easily implemented by the hardware thus eliminating the software computation. If TDPC [50] and [51, 131] for bilateral teleoperation is used, the passivity controllers (PCs) at each port are

$$f_d(t) = \begin{cases} -\dfrac{P^m_{obsv}(t)}{v_m(t)} & P^m_{obsv} < 0, \\ 0 & P^m_{obsv} \geq 0, \end{cases} \tag{3.24}$$

and

$$v_d(t) = \begin{cases} -\dfrac{P^s_{obsv}(t)}{f_s(t)} & P^s_{obsv} < 0, \\ 0 & P^s_{obsv} \geq 0. \end{cases} \tag{3.25}$$

One can see that control law can crash when $v_m(t)$ or $f_s(t)$ is close to zero. Hence the motivation of the switching TDPC is clear. The proposed switching TDPC approach shown in Fig.3.2 clearly shows that when P^{mi}_{obsv} is negative, the dampers b_i are activated; when P^{mi}_{obsv} is positive, the dampers b_i are deactivated. When P^{si}_{obsv} is negative, the dampers $\frac{1}{b_i}$ are activated; when P^{si}_{obsv} is positive, the dampers $\frac{1}{b_i}$ are deactivated. The benefit that we take from the switching TDPC is not only the stability of the system but it also replaces the passivity controller by the combination of one switch and a damper. The safety of the operation is guaranteed avoiding the zero division.

Theorem 1: The communication channel in Fig.3.2 is passive using the passivity observers and passivity controllers defined in (3.19), (3.20) and (3.22,3.23) respectively.

Proof: The power flow of the communication channel with switching TDPC can be calculated as,

$$\begin{aligned} P^* &= \sum_{i=1}^{n} [v_{mi} f_{mi} - v_{si} f_{si}] \\ &= \sum_{i=1}^{n} [v_{mi}(f_{mci} + f_{pci}) - (v_{sci} - v_{pci}) f_{si}] \\ &= P + \sum_{i=1}^{n} [v_{mi} f_{pci} + v_{pci} f_{si}]. \end{aligned} \tag{3.26}$$

Substitute (3.21) in (3.26) and notice (3.22,3.23), it is obtained,

$$\begin{aligned} P^* &\geq \sum_{i=1}^{n} [P^{mi}_{obs} + P^{si}_{obs}] + \frac{dE}{dt} + \sum_{i=1}^{n} [v_{mi} f_{pci} + v_{pci} f_{si}] \\ &\geq \frac{dE}{dt}. \end{aligned} \tag{3.27}$$

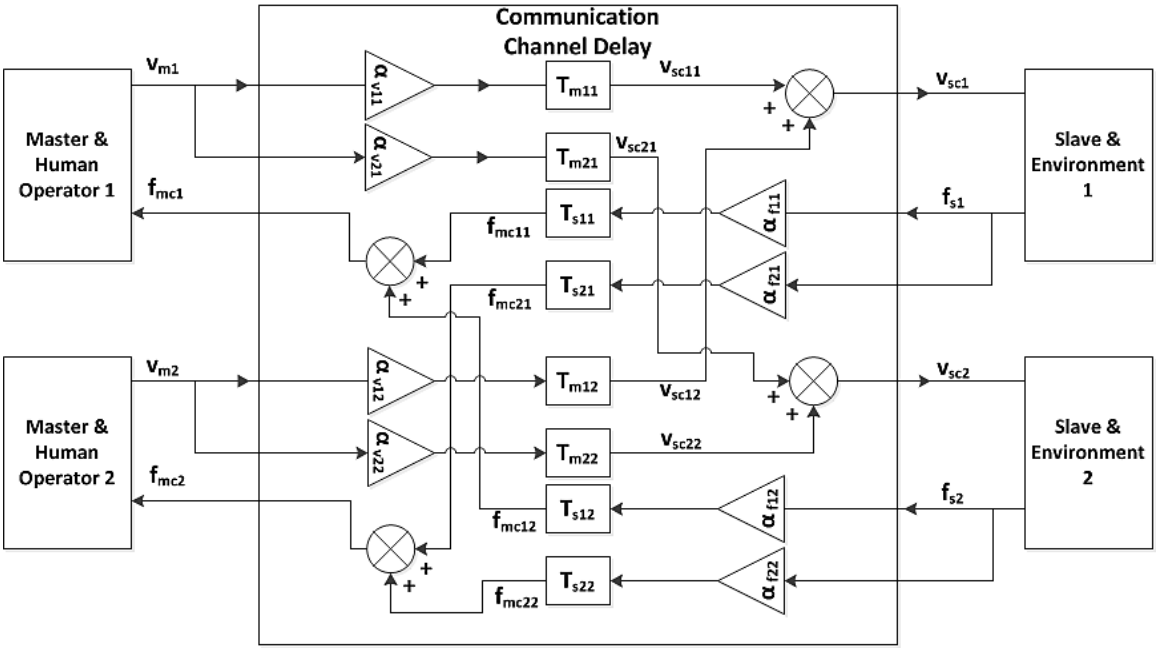

Figure 3.4: Multilateral teleoperation structure with two masters and two slaves

It is obtained that,

$$\int_0^t P^*(\tau)d\tau \geq E(t) - E(0) \geq -E(0). \tag{3.28}$$

From the definition of m-port network (3.5), the communication channel is passive under switching TDPC.

To better show the detailed scheme for a simplified case with $n = 2$, the novel communication channel that is used for the switching TDPC for two masters and two slaves is shown in Fig.3.4.

3.3.1 Simulation Results

The multilateral teleoperation system shown in Fig.3.2 is simulated for 2 masters 2 slaves (2M/2S) with the simulation parameters given in Table 3.1. b_i is the parameter that changes the effect of damping. A higher value of b_i will make the system to be more damped. In contrast, a lower value of b_i makes the system less damped. The selection of this parameter depends on the application. [140] suggest to choose this value equal to the derivative gain of PD controller of the slave (SC_i) side for proper impedance matching. In our simulations, we simply follow the same principle for impedance matching. The human operator model is taken from [141], which is a PD controller (i.e, spring and damper) with gains 75 N/m and

Table 3.1: Simulation Parameters

	Value		Value
Time delays	0.5, 1 s	Endpoint mass m	0.1 Kg
Ratio b_i	2.5 Ns/m	Slave D gain	2.5 Ns/m
Slave P gain	370 N/m	Sampling rate	1 KHz

50 Ns/m respectively. The slaves are required to contact with a hard wall with a stiffness K_1=30 kN/m at $x = 0.5$ m. In simulations, the environment contact force model is simulated to satisfy the given conditions.

$$f_e = \begin{cases} f_e & if \quad x_{si} - 0.5 > 0 \\ 0 & if \quad x_{si} - 0.5 \leq 0. \end{cases} \tag{3.29}$$

Different scenarios of the simulation results are presented next.

3.3.1.1 Without Switching Action - Case 0

The system is unstable without switching actions when a contact is made. Fig.3.5(a) and 3.6(a) clearly show that without the switching action, oscillations are produced in the positions of both the masters and slaves. Force values of the first pair of master and slave are shown in Fig.3.5(b). The contact force of first slave with the environment is shown in Fig.3.5(c). Such higher contact forces are not desirable in teleoperation systems. The energy values are given in Fig.3.5(d) and negative energy values clearly show that the system is unstable without switching dissipation. The simulation results are same for the second master slave pair as shown in Figs.3.6(a), 3.6(b), 3.6(c) and 3.6(d). Stability of the system can be ensured by making the energy value positive.

3.3.1.2 With Switching Action - Case 1

In this case we simulated the system with delay of $0.5s$ and the weighting coefficients as,

$$\alpha_{v11} = \alpha_{v21} = \alpha_{v12} = \alpha_{v22} = 0.5$$

$$\alpha_{f11} = \alpha_{f21} = \alpha_{f12} = \alpha_{f22} = 0.5.$$

With switching dissipation in action and all the weighting coefficients being 0.5, a stable contact with the environment is achieved which is evident from the positions of both the masters and slaves in Figs.3.7(a) and 3.7(b). The slaves stay at the position where the wall

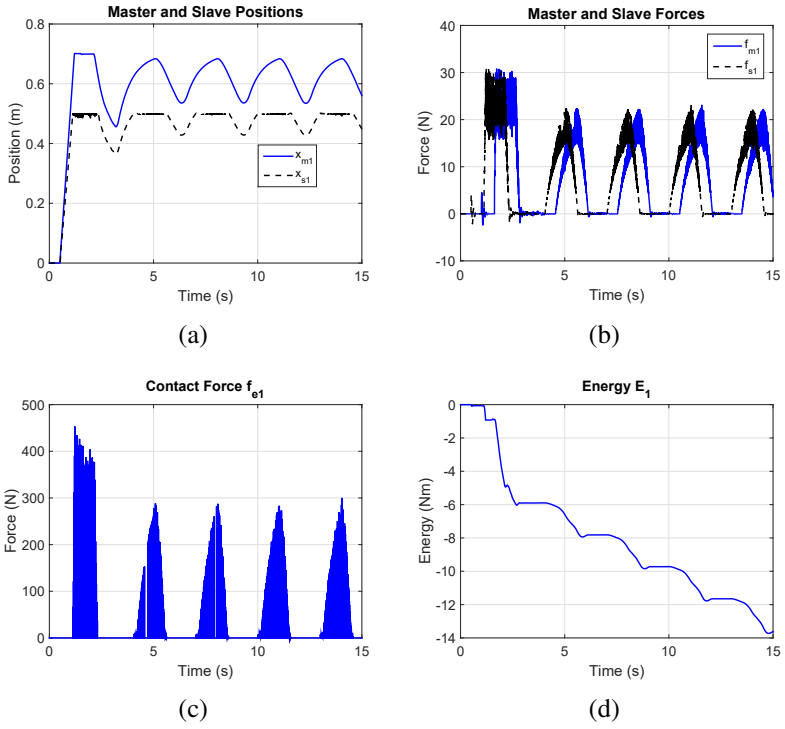

Figure 3.5: M/S: Positions, forces, contact force and energy

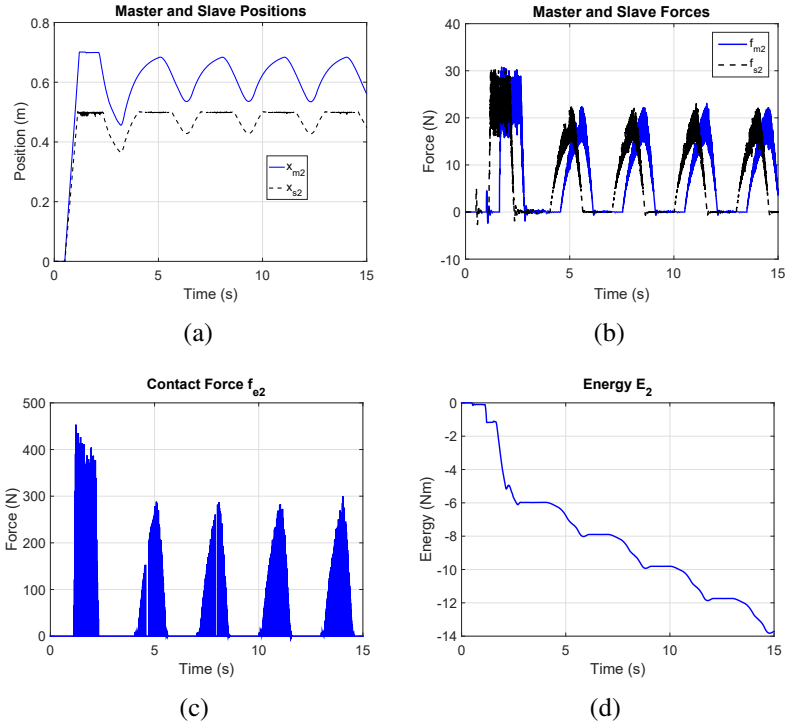

Figure 3.6: M/S: Positions, forces, contact force and energy

is located after the contact happens. Velocity signals for both the masters and slaves side are recorded in Figs.3.7(c) and 3.7(d). Passivity observers values for both the masters and

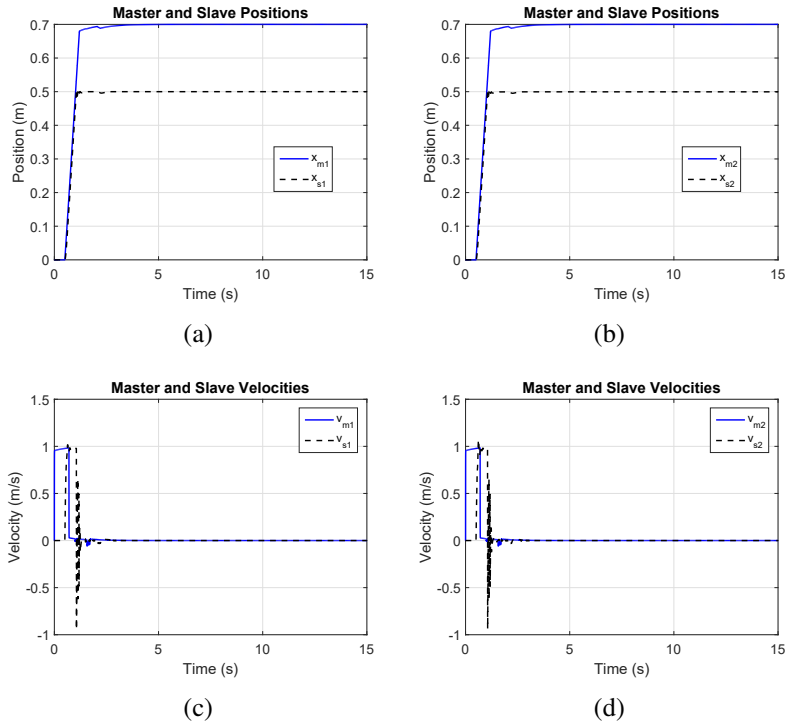

Figure 3.7: Case 1 - M/S: positions and velocities with $\alpha_i = 0.5$

their corresponding dissipation values are shown in Figs.3.8(a), 3.8(b), 3.8(c) and 3.8(d). It can be observed that in the start of the simulation, as the passivity observers at the master side observe the negative power values, the dampers get activated and start injecting damping in the system to maintain the passivity. And as soon as the passivity observers start observing the positive power values, the dampers go in an inactive state as the switching action is no longer needed. Similarly, passivity observer values for both the salves and their corresponding dissipation values are shown in Figs.3.9(a), 3.9(b), 3.9(c) and 3.9(d). It is clear from the results of the passivity observers that damping is injected in the system for a very small interval of time when the system goes in an active state. Switches at the slaves side come into action and by the use of damping injection, passivity is maintained.

The forces for both the masters and slaves side are presented in Figs.3.10(a) and 3.10(b). The environment contact force values for both the slaves are shown in Figs.3.10(c) and 3.10(d). It can be seen that the values of environment contact forces satisfy (3.29) and the force spikes appear exactly the same time as the slaves interact with the wall. The total

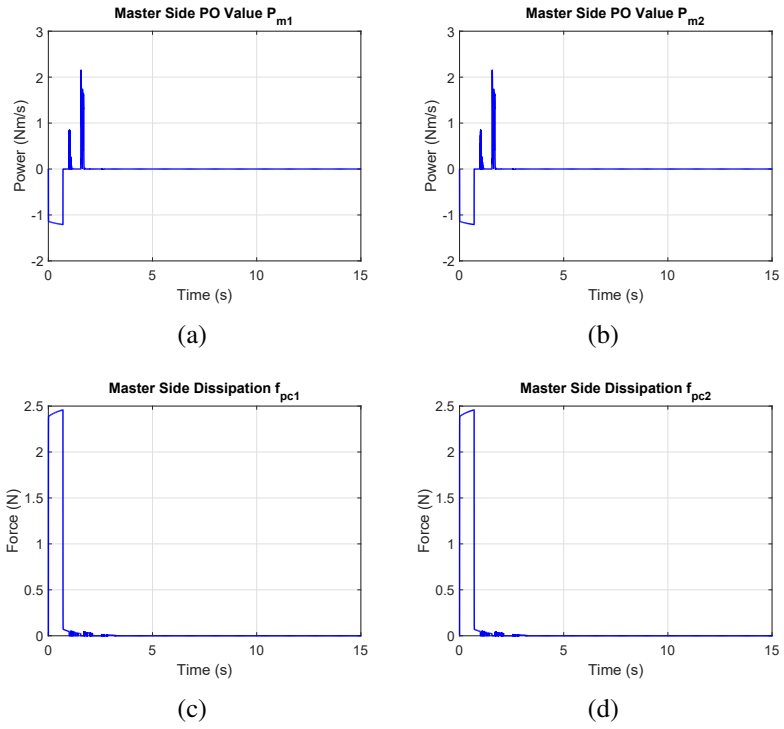

Figure 3.8: Case 1 - Masters side PO and dissipation values with $\alpha_i = 0.5$

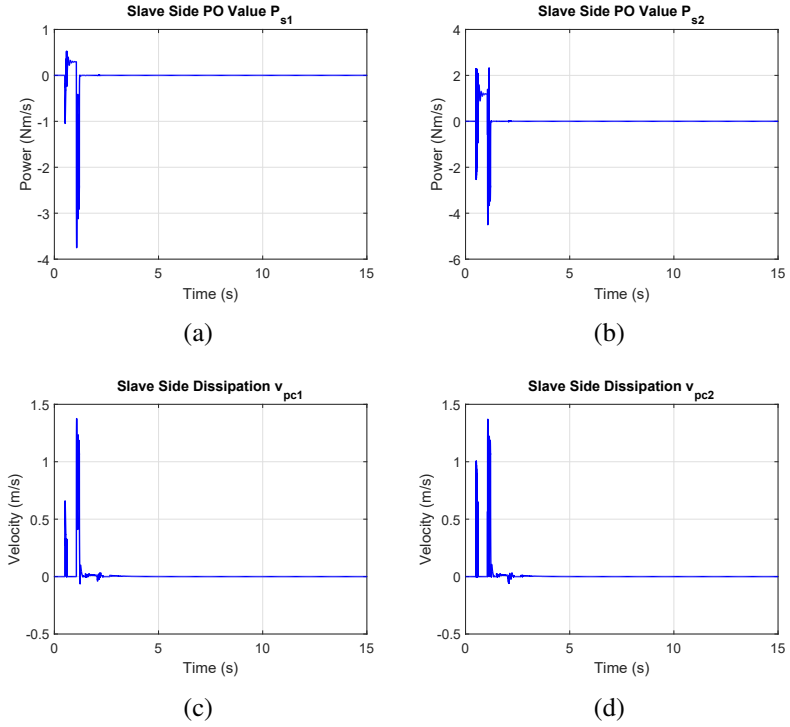

Figure 3.9: Case 1 - Slaves side PO and dissipation values with $\alpha_i = 0.5$

energy of the system with switching dissipation is shown in Fig.3.11 and the positive values of the energy confirm the stable operation of switching TDPC.

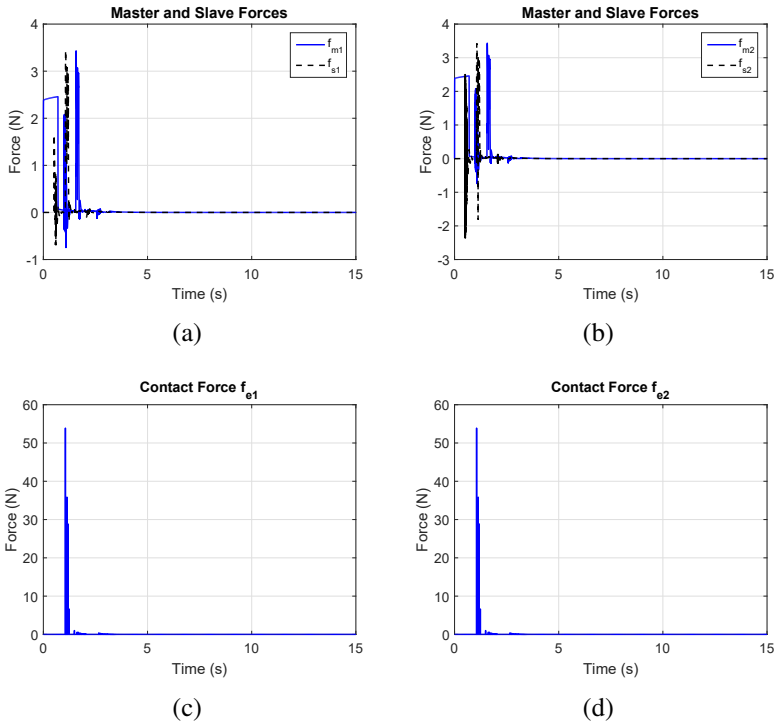

Figure 3.10: Case 1 - M/S: Forces and contact force values with $\alpha_i = 0.5$

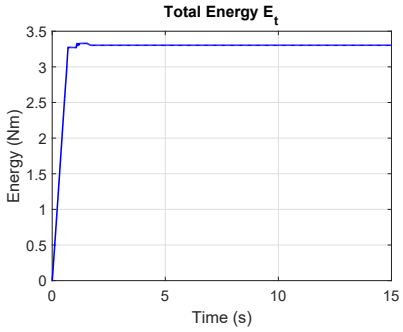

Figure 3.11: Case 1: Total energy with $\alpha_i = 0.5$

3.3.1.3 With Switching Action - Case 2

In this case, we simulated the multilateral teleoperation system with two masters and two slaves in the presence of a delay of $1s$ with a human input as a sinusoid. The sinusoidal input is simulated as $sin(t)$ which is then fed to a PD controller as discussed earlier. The

weighting coefficients are chosen to obey (3.12).

$$\alpha_{v11} = \alpha_{f11} = \alpha_{v22} = \alpha_{f22} = 0.7$$

$$\alpha_{v21} = \alpha_{f12} = \alpha_{v12} = \alpha_{f21} = 0.1.$$

Figs.3.12(a) and 3.12(b) show the positions of both the masters and slaves. It can be seen that the position tracking is satisfactory even in the presence of a large delay. Environmental forces for both the slaves are presented in Figs.3.12(c) and 3.12(d) which are almost the same for both the slaves except the first significant spike as they move in a similar manner. Passivity observer values for the masters and their corresponding dissipation values are shown in Figs.3.13(a), 3.13(b), 3.13(c) and 3.13(d) respectively. It is evident from the

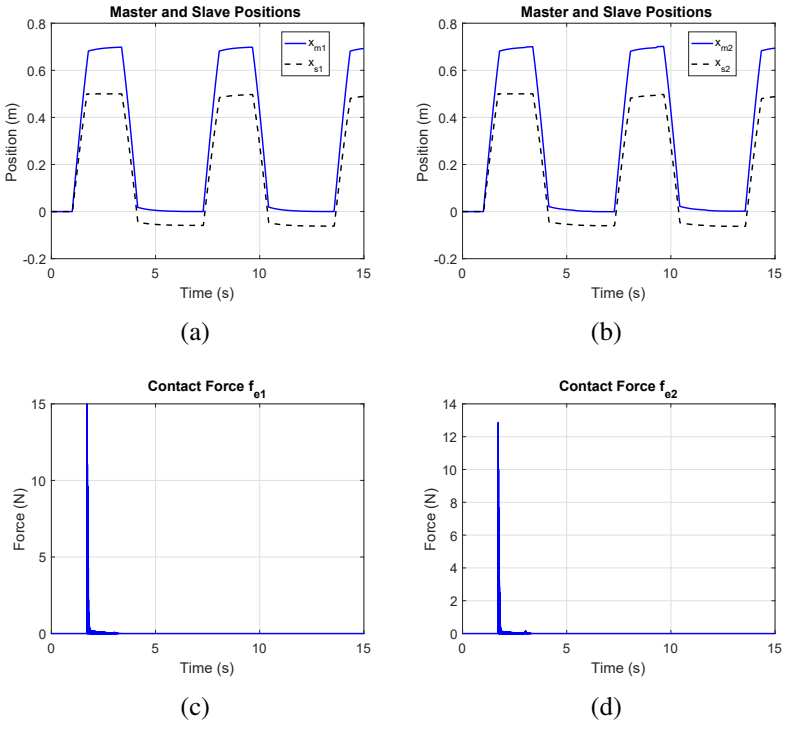

Figure 3.12: Case 2: M/S positions and contact forces with delay of 1s

results that whenever the passivity observers at master side observe a negative value, the switches and dampers come into action to maintain the passivity of the system. Similarly, the passivity observer values for the slaves and their corresponding dissipation values are given in Figs.3.14(a), 3.14(b), 3.14(c) and 3.14(d) respectively. It is clear that the switching dissipation scheme is working perfectly as the passivity is guaranteed by the use of damping injection as needed. Force and velocity signals for both the masters and slaves transmitted

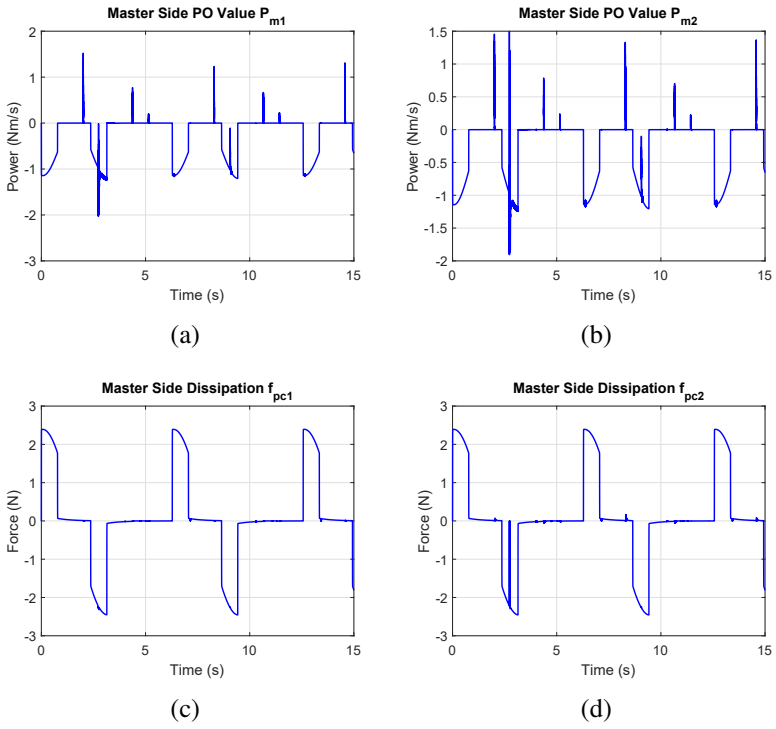

Figure 3.13: Case 2: Masters side PO and dissipation values with delay of 1s

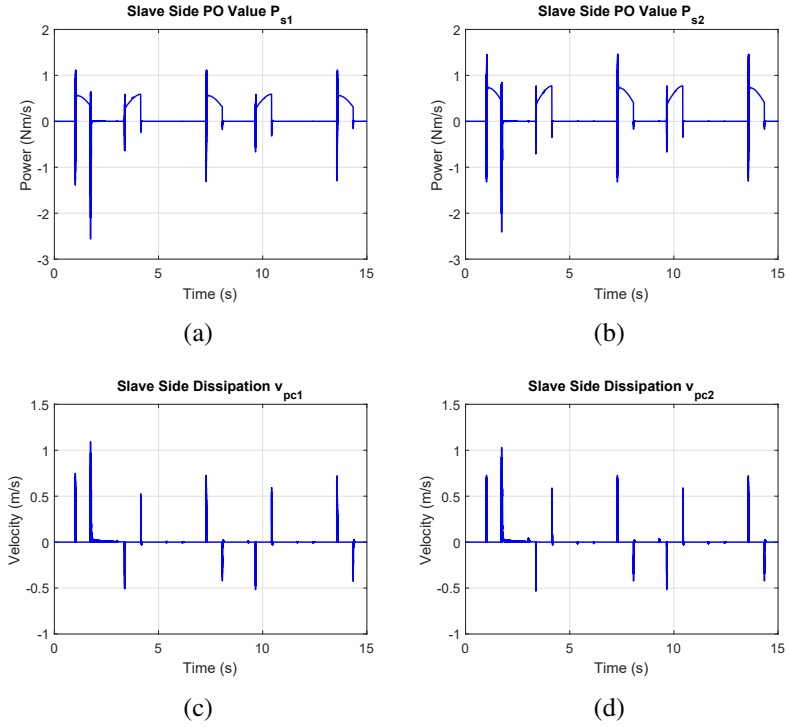

Figure 3.14: Case 2: Salves side PO and dissipation values with delay of 1s

in communication channel are shown in Figs.3.15(a), 3.15(b), 3.15(c) and 3.15(d). The total energy of the system is given in Fig.3.16 which is positive all the time affirming the stability of the system.

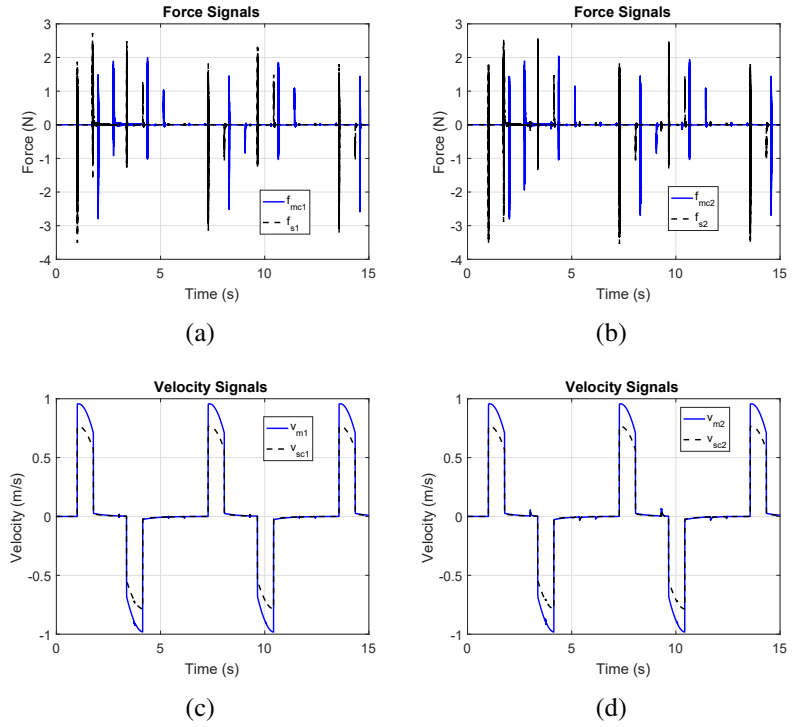

Figure 3.15: Case 2: Force and velocity signals with delay of 1s

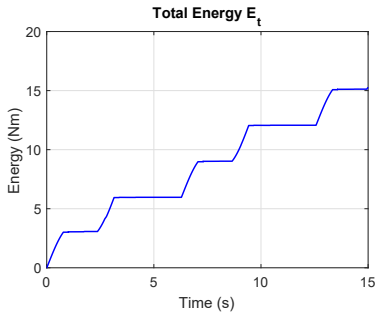

Figure 3.16: Case 2: Total energy with delay of 1s and different α_i

A summary of the simulation results presented above is given in Table 3.2.

3.3.2 Experimental Results

This section presents the experimental results to verify the effective and stable operation of the proposed scheme. The experiment is carried out using two Phantom Omni devices as

Table 3.2: Summary of Simulation Results

Case No.	Weighting coefficients	Time delay	Human input	No. of M/S
0	0.5	0.5 s	Ramp	2/2
1	0.5	0.5 s	Ramp	2/2
2	0.7 and 0.1	1 s	Sinusoid	2/2

the masters and two Novint Falcon as the slaves of the teleoperation system. The implementation is set up using Quanser's Real Time Control (QUARC) software which fully support both Phantom Omni and Novint Falcon as the target hardware. TCP/IP protocol is used in QUARC communications block to establish the connection between the two desktops for the signal transmission. In order to properly analyze all the signals in real time, a delay of $0.001s$ is added as needed and this delay was determined by a simple test of communication. As the Novint Falcon does not have any built in force sensor so we can not measure the environmental forces directly. Two FUTEK LLB-130 force sensors are mounted on the slaves to capture the effect of interaction of slaves with the environment. A combination of an instrumentation amplifier and a low pass filter is used for the smooth amplification of the environmental forces and this data is being pulled in Simulink using a Q8 Data Acquisition Card by Quanser. Data Acquisition Card specifications are same as in [142]. The experimental setup is shown in Fig.3.17. The Phantom Omni and Novint Falcon are set

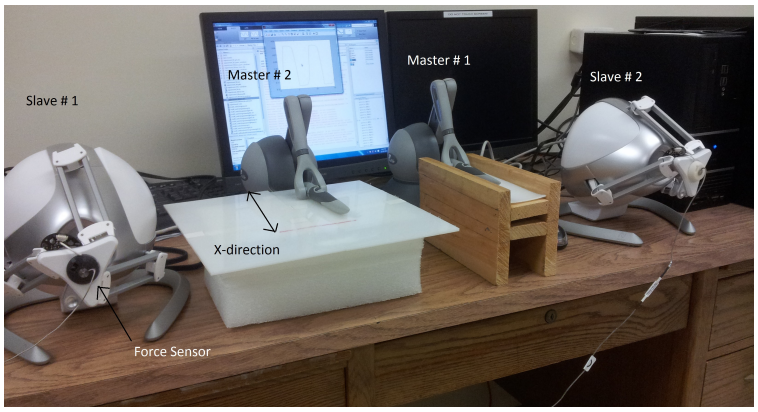

Figure 3.17: Experimental setup

up as to move only in X-direction. As discussed earlier, a human operator applies a force to both the masters and the position signals of Phantom Omni are measured directly. The velocity signals of the masters and the slaves are obtained by taking the derivative and applying a single pole filter $(\frac{1}{s+3})$, to avoid discontinuities, on the position signals. The value

of parameter b_i and gains of the slave controllers are same as in simulations.

3.3.2.1 Set 1: 2 Masters and 2 Slaves with no delay

In this scenario, weighting coefficients for both the masters and both the slaves are equal which means that each slave will take the average force effect on both the masters and each master will take the average velocity effect on both the slaves.

$$\alpha_{v11} = \alpha_{v12} = \alpha_{v21} = \alpha_{v22} = 0.5$$

$$\alpha_{f11} = \alpha_{f12} = \alpha_{f21} = \alpha_{f22} = 0.5.$$

In this situation, a foam is used as an environment with which the slaves interact as shown in Fig.3.18 [142]. Positions of both the masters and the slaves are shown in Figs.3.19(a)

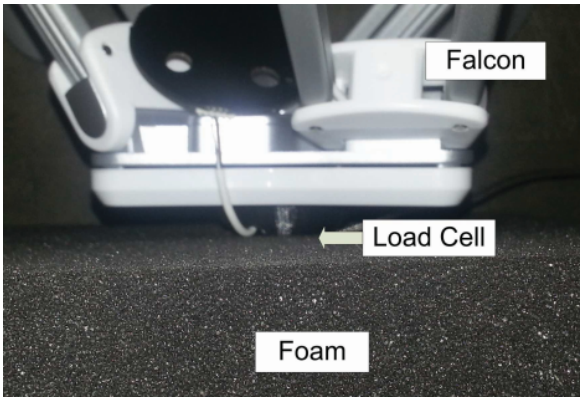

Figure 3.18: Direct contact with the foam

and 3.19(b) respectively. It is very clear from the results that the slaves try to follow the positions of masters with some delay and the position drift has been compensated by *r-passivity* [143]. Forces for the masters and the slaves side are presented in Figs.3.19(c) and 3.19(d). Master side passivity observer values and corresponding dissipation values are shown in Figs.3.20(a), 3.20(b), 3.20(c) and 3.20(d) respectively. It can be seen that the power values for both the masters are positive all the time and the switch at master side remain in an inactive state and there is no dissipation. As there is not a single interval in which PO values are negative, so there is no need for damping injection in the system.

Similarly, the passivity observer values for the slave side and corresponding dissipation values are shown in Figs.3.21(a), 3.21(b), 3.21(c) and 3.21(d) respectively. Passivity observer values are positive for most of the time so there is no need for switching action but

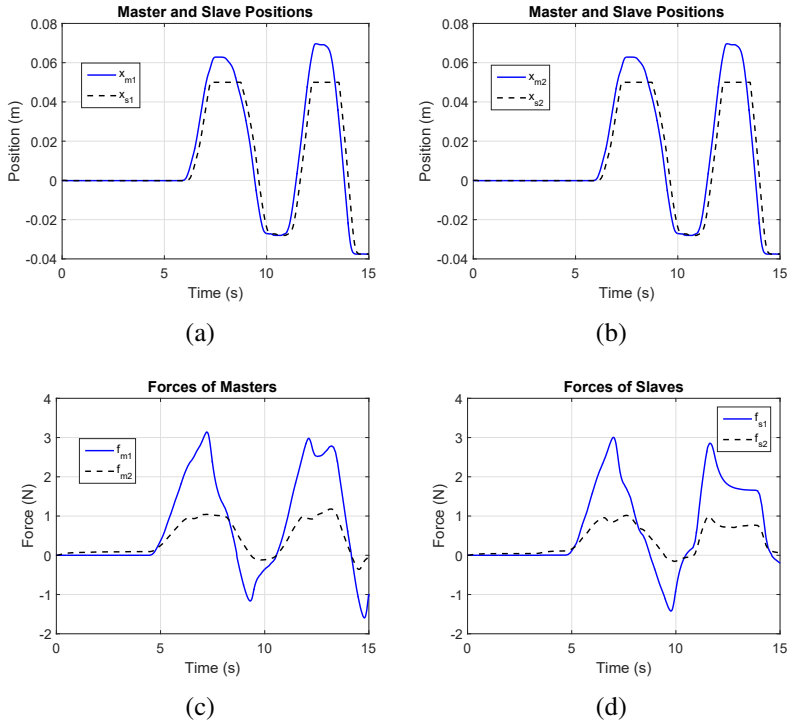

Figure 3.19: Set 1: M/S positions and forces with $\alpha_i = 0.5$

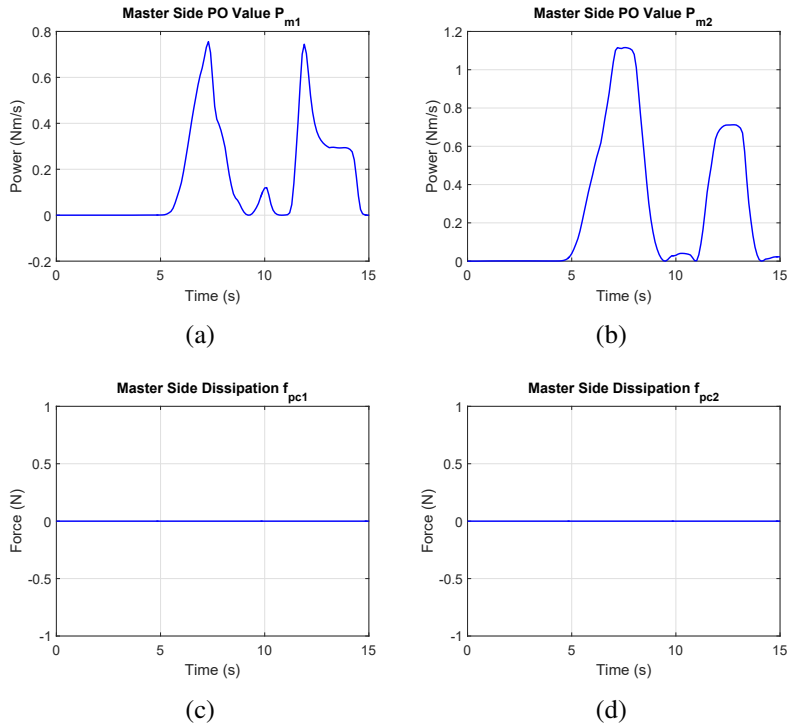

Figure 3.20: Set 1: Passivity observer and dissipation values for the masters with $\alpha_i = 0.5$

it is observed that at two different instants switches at slave side go in an active state for a very small interval.

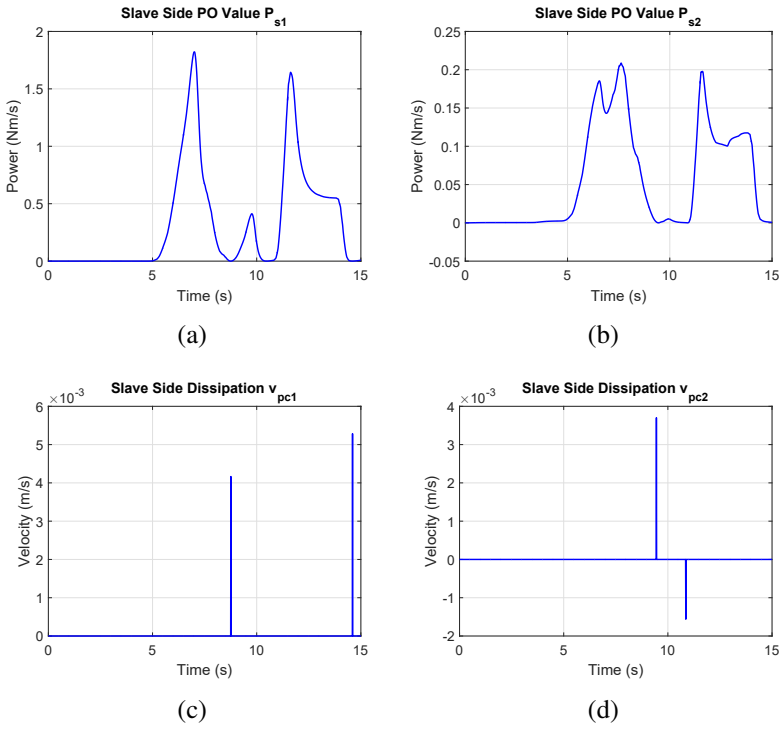

Figure 3.21: Set 1: Passivity observer and dissipation values for the slaves with $\alpha_i = 0.5$

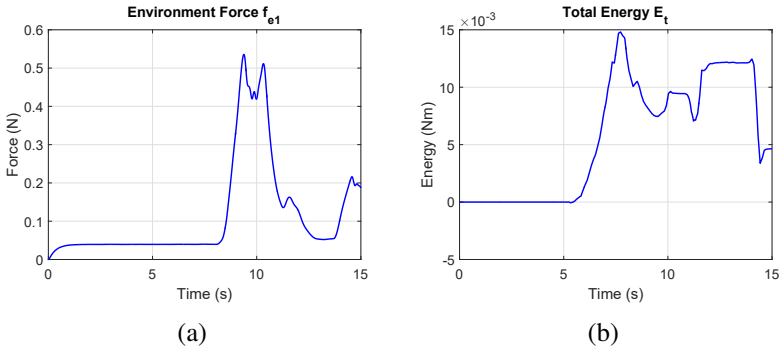

Figure 3.22: Set 1: Environment force and total energy with $\alpha_i = 0.5$

The interaction forces for both the slaves are same so only the forces of first slave are shown in Fig.3.22(a). It is evident from the results of the interaction forces that when the slaves move to and fro in X-direction, the slaves interact with the environment and the force sensors capture these forces. The total energy of the system is depicted in Fig.3.22(b),

positive values of which affirm the stable operation of multilateral teleoperation system under switching TDPC.

3.3.2.2 Set 2: 2 Masters and 2 Slaves with delay of $0.2s$

For this case, the weighting coefficients of the communication architecture are assigned such that the first master gives more weights to the first slave and the second master gives more weights to the second slave and same is the case with slaves assigning weights to the masters. The values of the weighting coefficients are given below.

$$\alpha_{v11} = \alpha_{v22} = \alpha_{f11} = \alpha_{f22} = 0.7$$

$$\alpha_{v12} = \alpha_{v21} = \alpha_{f12} = \alpha_{f21} = 0.1.$$

In this situation, an Aluminum plate is used as an environment with which the slaves interact as shown in Fig.3.23 [142]. The delay value of $0.2s$ is added to the system to verify

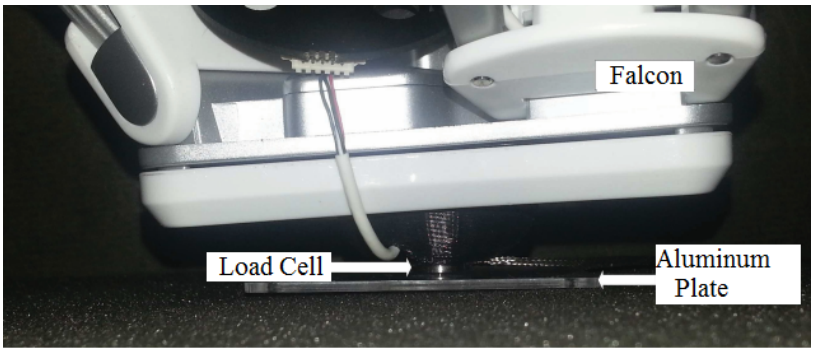

Figure 3.23: Direct contact with the Aluminum plate

the effectiveness of the switching TDPC under large delays. Positions of both the masters and slaves are shown in Figs.3.24(a) and 3.24(b). It can be observed that the position tracking is good under proposed scheme. The slaves follow the masters in presence of some delay. Feedback forces for both the masters and forces generated by the slave controllers are shown in Figs.3.24(c) and 3.24(d). The passivity observer values for both the masters and their corresponding dissipation values are presented in Figs.3.25(a), 3.25(b), 3.25(c) and 3.25(d) respectively. It can be seen that the power values at the master side are positive for all time so the dissipation values stay at zero confirming that no switching action is required. Similarly, the passivity observer values for both the slaves and their corresponding dissipation values are shown in Figs.3.26(a), 3.26(b), 3.26(c) and 3.26(d) respectively.

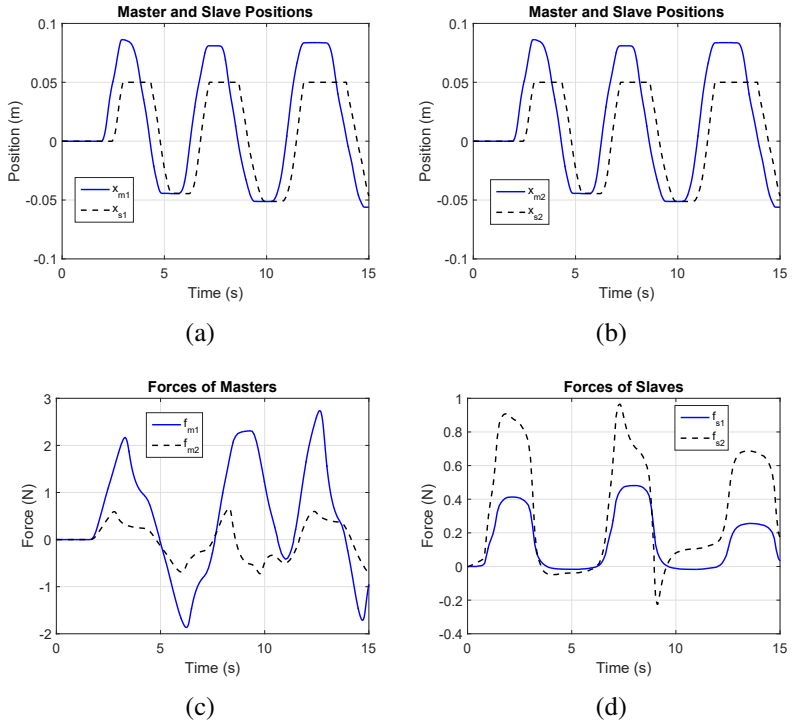

Figure 3.24: Set 2: M/S positions and forces with different α_i

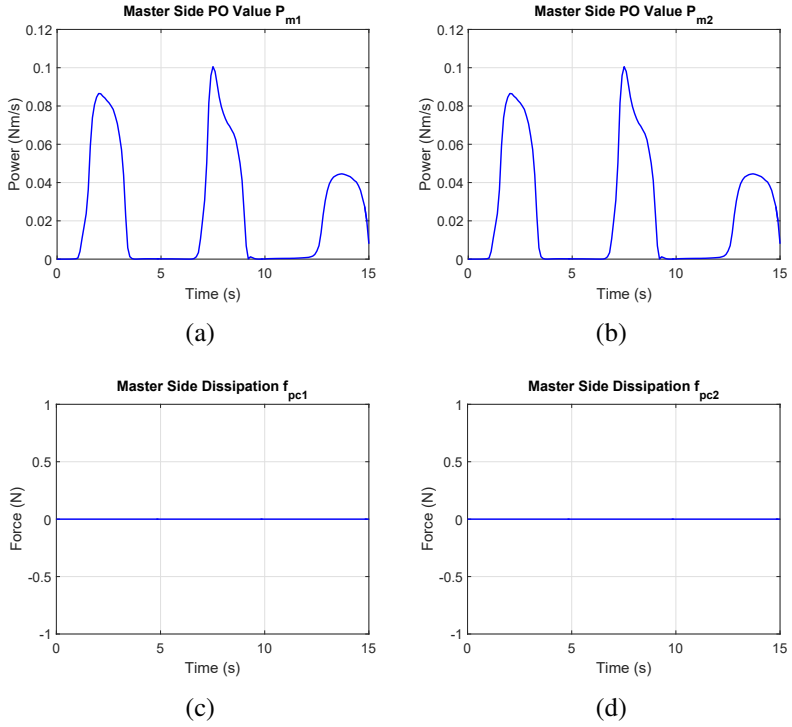

Figure 3.25: Set 2: PO and dissipation values for the masters with different α_i

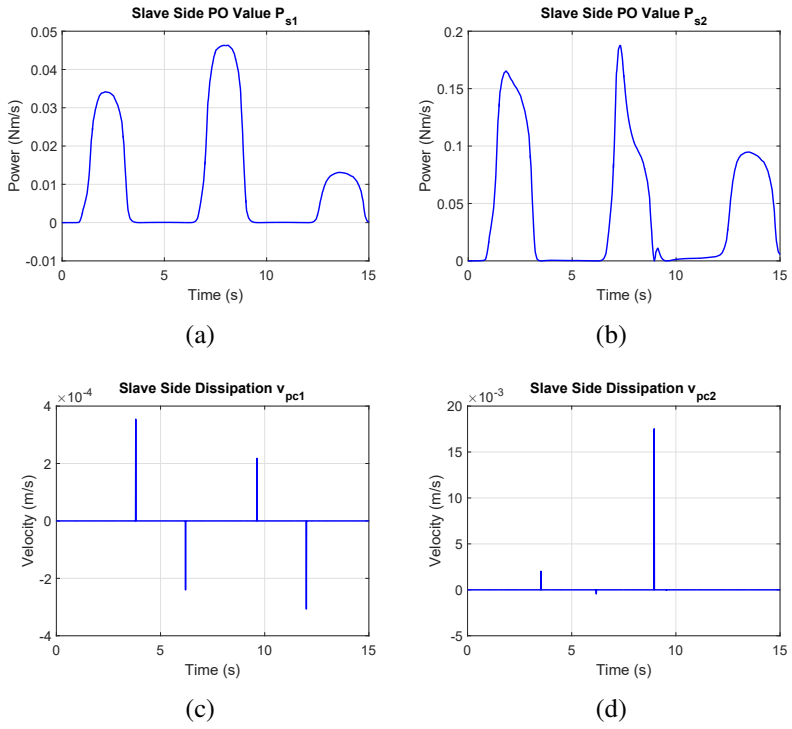

Figure 3.26: Set 2: PO and dissipation values for the slaves with different α_i

As the power values for the salves are positive for most of the time so the dissipation at

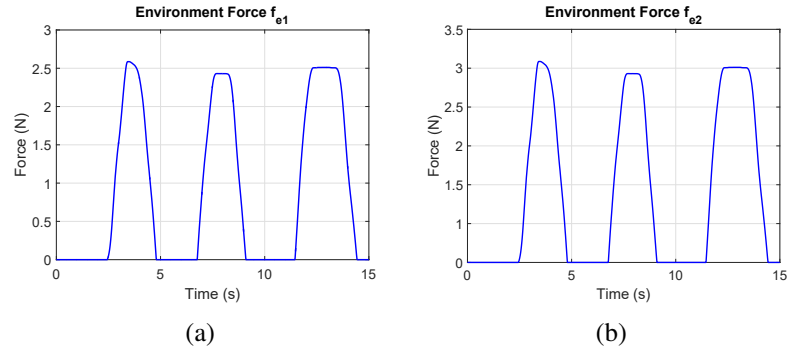

Figure 3.27: Set 2: Environment forces with different α_i

slave side is not required except the instants where the POs observe a negative value. The interaction forces of both the slaves with the environment are shown in Figs.3.27(a) and 3.27(b) and the effect of different weighting coefficients can be observed from the results. The total energy of the system is shown in Fig.3.28. As the energy is positive for all the time, it confirms that the passivity of the system is maintained thereby confirming the stable operation under the proposed scheme.

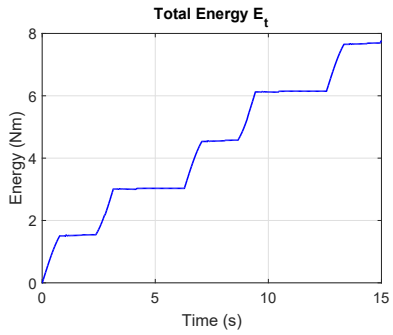

Figure 3.28: Set 2: Total energy with different α_i

3.4 Switching TDPC with Varying Time Delay

This case of switching TDPC considers the time varying delays in the communication channel instead of constant delays and will be valid for different number of masters and slaves in teleoperation. In Fig.3.2, signals $v_{mi}(t)$ and $f_{si}(t)$ are sent with delays T_{mi} and T_{si},

$$v_{sci}(t) = \sum_{j=1}^{n_m} v_{scij}(t),\ v_{scij}(t) = \alpha_{vij} v_{mj}(t - T_{mij}), \tag{3.30}$$

$$f_{mci}(t) = \sum_{j=1}^{n_s} f_{mcij}(t),\ f_{mcij}(t) = \alpha_{fij} f_{sj}(t - T_{sij}), \tag{3.31}$$

where n_m, n_s, α_{vij}, α_{fij}, T_{mij} and T_{sij} are same as before. The power of the multilateral communication is,

$$P = \sum_{i=1}^{n_m} [v_{mi}(t) f_{mci}(t)] - \sum_{i=1}^{n_s} [v_{sci}(t) f_{si}(t)]. \tag{3.32}$$

A positive constant b_i is introduced as in [139], and (3.32) can be expressed as

$$\begin{aligned} P &= \sum_{i=1}^{n_m} [\frac{1}{2b_i} f_{mci}^2(t) + \frac{b_i}{2} v_{mi}^2(t) - \frac{1}{2b_i}(f_{mci} - b_i v_{mi})^2(t)] \\ &\quad + \sum_{i=1}^{n_s} [\frac{1}{2b_i} f_{si}^2(t) + \frac{b_i}{2} v_{sci}^2(t) - \frac{1}{2b_i}(f_{si} + b_i v_{sci})^2(t)] \\ &= \sum_{i=1}^{n_m} [\frac{1}{b_i} f_{mci}^2(t) - \frac{1}{2b_i}(f_{mci} - b_i v_{mi})^2(t) + \frac{b_i}{2} v_{mi}^2(t) \\ &\quad - \frac{1}{2b_i} f_{mci}^2(t)] + \sum_{i=1}^{n_s} [b_i v_{sci}^2(t) - \frac{1}{2b_i}(f_{si} + b_i v_{sci})^2(t) \\ &\quad + \frac{1}{2b_i} f_{si}^2(t) - \frac{b_i}{2} v_{sci}^2(t)]. \end{aligned} \tag{3.33}$$

Using (3.30) and (3.31), the four terms in (3.33) become,

$$\begin{aligned}
\sum_{i=1}^{n_s}[\frac{1}{2b_i}f_{si}^2(t)]-\sum_{i=1}^{n_m}[\frac{1}{2b_i}f_{mci}^2(t)] &= \sum_{i=1}^{n_s}[\frac{1}{2b_i}f_{si}^2(t)]-\sum_{i=1}^{n_m}[\frac{1}{2b_i}(\sum_{j=1}^{n_s}\alpha_{fij}f_{sj}(t-T_{sij}))^2] \\
&\geq \sum_{i=1}^{n_s}[\frac{1}{2b_i}f_{si}^2(t)]-\sum_{i=1}^{n_m}[\frac{1}{2b_i}n_s\sum_{j=1}^{n_s}\alpha_{fij}^2 f_{sj}^2(t-T_{sij})] \\
&= \sum_{i=1}^{n_s}\sum_{j=1}^{n_s}[\frac{d}{dt}\int_{t-T_{sji}}^{t} n_s\sum_{i=1}^{n_m}\frac{1}{2b_j}\alpha_{fji}^2 f_{si}^2(\tau)d\tau] \\
&\quad -\sum_{i=1}^{n_m}\sum_{j=1}^{n_s}[\frac{1}{2b_i}\dot{T}_{sij}(t)\alpha_{fij}^2 f_{sj}^2(t-T_{sij}(t))], \qquad (3.34)
\end{aligned}$$

$$\begin{aligned}
\sum_{i=1}^{n_m}[\frac{b_i}{2}v_{mi}^2(t)]-\sum_{i=1}^{n_s}[\frac{b_i}{2}v_{sci}^2(t)] &= \sum_{i=1}^{n_m}[\frac{b_i}{2}v_{mi}^2(t)]-\sum_{i=1}^{n_s}[\frac{b_i}{2}(\sum_{j=1}^{n_m}\alpha_{vij}v_{mj}(t-T_{mij}))^2] \\
&\geq \sum_{i=1}^{n_m}[\frac{b_i}{2}[v_{mi}^2(t)]-\sum_{i=1}^{n_s}[\frac{b_i}{2}n_m\sum_{j=1}^{n_m}\alpha_{vij}^2 v_{mj}^2(t-T_{mij})] \\
&= \sum_{i=1}^{n_m}\sum_{j=1}^{n_m}[\frac{d}{dt}\int_{t-T_{mji}}^{t} n_m\sum_{i=1}^{n_s}\frac{b_j}{2}\alpha_{vji}^2 v_{mi}^2(\tau)d\tau] \\
&\quad -\sum_{i=1}^{n_s}\sum_{j=1}^{n_m}[\frac{b_i}{2}\dot{T}_{mij}(t)\alpha_{vij}^2 v_{mj}^2(t-T_{mij}(t))], \qquad (3.35)
\end{aligned}$$

where $\dot{T}_{sij}$ and $\dot{T}_{mij}$ are the changing rates of T_{sij} and T_{mij}. In this work, the weighting coefficients in (3.30) and (3.31) are selected such that they satisfy,

$$\sum_{i=1}^{n_s}\frac{1}{2b_i}=\sum_{i=1}^{n_s}[n_s\sum_{j=1}^{n_m}\frac{1}{2b_j}\alpha_{fji}^2],\ \sum_{i=1}^{n_m}\frac{b_i}{2}=\sum_{i=1}^{n_m}[n_m\sum_{j=1}^{n_s}\frac{b_j}{2}\alpha_{vji}^2] \qquad (3.36)$$

A more simplified form of (3.36) can be obtained when the number of masters and slaves and all the damping coefficients are equal.

$$n_s\sum_{j=1}^{n_s}\alpha_{fji}^2=1 \quad and \quad n_m\sum_{j=1}^{n_m}\alpha_{vji}^2=1$$

The examples of these weighting coefficients can be found in applications where multiple humans are collaborating over a task with different authority factors. For example, in medical training environments a trainee can work with an expert surgeon for different medical procedures by shifting the weights from low to high as the skills of the trainee improve with time. [35] lists different factors for the selection of the weighting coefficients for medical applications.

The first terms on the right hand side of the inequalities (3.34) and (3.35) can be viewed as the differential of the stored energy. Substituting (3.34) and (3.35) in (3.33) and noting the differential of the stored energy, the power of the communication channel can be expressed as,

$$\begin{aligned} P \;\geq\; & \sum_{i=1}^{n_m}[\frac{1}{b_i}f_{mci}^2(t) - \sum_{j=1}^{n_s}\frac{1}{2b_i}\dot{T}_{sij}(t)\alpha_{fij}^2 f_{sj}^2(t-T_{sij}(t)) \\ & -\frac{1}{2b_i}(f_{mci}-b_i v_{mi})^2(t)] + \sum_{i=1}^{n_s}[b_i v_{sci}^2(t) \\ & -\sum_{j=1}^{n_m}\frac{b_i}{2}\dot{T}_{mij}(t)\alpha_{vij}^2 v_{mj}^2(t-T_{mij}(t)) \\ & -\frac{1}{2b_i}(f_{si}+b_i v_{sci})^2(t)] + \frac{dE}{dt}. \end{aligned} \tag{3.37}$$

The comparison of (3.1) and (3.37) gives us the total power dissipation of the multilateral teleoperation as

$$\begin{aligned} P_{diss} \;\geq\; & \sum_{i=1}^{n_m}[\frac{1}{b_i}f_{mci}^2(t) - \frac{1}{2b_i}(f_{mci}-bv_{mi})^2(t) \\ & -\frac{1}{2b_i}\dot{T}_{sij}(t)f_{mci}^2(t)] \\ & +\sum_{i=1}^{n_s}[b_i v_{sci}^2(t) - \frac{1}{2b_i}(f_{si}+b_i v_{sci})^2(t) \\ & -\frac{b_i}{2}\dot{T}_{mij}(t)v_{sci}^2(t)]. \end{aligned} \tag{3.38}$$

$P_{diss} < 0$ indicates the activeness of the system, a clear sign of activating the passivity controller to maintain the passivity. For real-time checking, (3.38)$\geq$0 is divided in two sufficient conditions,

$$\begin{aligned} \frac{1}{b_i}f_{mci}^2(t) - \frac{1}{2b_i}(f_{mci}-b_i v_{mi})^2(t) - \frac{1}{2b_i}\dot{T}_{sij}(t)f_{mci}^2(t) \geq 0, \\ b_i v_{sci}^2(t) - \frac{1}{2b_i}(f_{si}+b_i v_{sci})^2(t) - \frac{b_i}{2}\dot{T}_{mij}(t)v_{sci}^2(t) \geq 0. \end{aligned}$$

The passivity observers on both master and the slave sides are designed exactly in same manner as in [129] and an upper bound of $\dot{T}_{mji,sji}$ can be imposed as ε as in [144].

$$P_{obsv}^{mi} = \frac{1}{b_i}f_{mci}^2(t) - \frac{1}{2b_i}(f_{mci}-b_i v_{mi})^2(t) - \frac{\varepsilon}{2b_i}f_{mci}^2(t), \tag{3.39}$$

$$P_{obsv}^{si} = b_i v_{sci}^2(t) - \frac{1}{2b_i}(f_{si}+b_i v_{sci})^2(t) - \frac{b_i\varepsilon}{2}v_{sci}^2(t). \tag{3.40}$$

Clearly, if $\varepsilon \geq 2$, P^{mi}_{obsv} and P^{si}_{obsv} are both negative which is not desirable as this will keep the passivity controllers active all the time. Thus, the power of the communication channel (3.37) can be rewritten as,

$$P \geq \sum_{i=1}^{n_m} [P^{mi}_{obs}] + \sum_{i=1}^{n_s} [P^{si}_{obs}] + \frac{dE}{dt}. \tag{3.41}$$

Again, in [17, 129, 131] the passivity controllers (PCs) at each port are designed in such a way that there is a risk of control crash during the operation. It can be seen that the control can crash when $v_m(t)$ or $f_s(t)$ is close to zero. In this work, the control laws for PC_{mi} and PC_{si} are designed as,

$$f_{pci} = \begin{cases} v_{mi} b_i & P^{mi}_{obs} < 0, \\ 0 & P^{mi}_{obs} \geq 0, \end{cases} \tag{3.42}$$

and

$$v_{pci} = \begin{cases} \dfrac{f_{si}}{b_i} & P^{si}_{obs} < 0, \\ 0 & P^{si}_{obs} \geq 0. \end{cases} \tag{3.43}$$

It is observed that the zero division is not an issue in our proposed control laws so the motivation of this work is clear. Again, the proposed switching TDPC approach clearly shows that when P^{mi}_{obsv} is negative, the dampers b_i are activated; when P^{mi}_{obsv} is positive, the dampers b_i are deactivated. When P^{si}_{obsv} is negative, the dampers $\frac{1}{b_i}$ are activated; when P^{si}_{obsv} is positive, the dampers $\frac{1}{b_i}$ are deactivated. Switching TDPC not only provides the guaranteed stability but also simplifies the design of the passivity controllers. Zero division is avoided in control laws which ensures the stability of the system for safe operation under time varying delays.

In general, passivity based control can ensure the stability but not necessarily the performance. Although the transparency is one of the performance metric in teleoperation, we do not emphasize on the transparency in this work but it is stated that the transparency is degraded in this approach. In ideal situation, without the passivity controllers the impedance of the master side and slave side is expressed as,

$$\frac{F_{mc}(s)}{V_m(s)} \quad and \quad \frac{F_s(s)}{V_{sc}(s)}$$

where the upper case letters are the Laplace transform of f_{mc}, v_m, f_s and v_{sc}. However, with the passivity controllers the impedance are,

$$\frac{F_{mc}(s) + F_{pc}(s)}{V_m(s)} \quad and \quad \frac{F_s(s)}{V_{sc}(s) - V_{pc}(s)}.$$

and here,

$$\frac{F_{mc}(s)+F_{pc}(s)}{V_m(s)} \neq \frac{F_s(s)}{V_{sc}(s)-V_{pc}(s)}.$$

thus, the transparency is degraded by the output of the passivity controllers [129].

3.4.1 Simulation Results

This section presents the simulation results with the proposed control scheme and the simulation parameters are given in Table 3.3. The parameter b_i is for damping injection. The damping of the system can be increased by increasing the value of b_i and it can be decreased by decreasing the value of b_i. The value selection of b_i varies according to the application but for proper impedance matching it is suggested to have this value exactly equal to the D gain of the proportional derivative controller of the slave [140]. We choose the values of b_i and D to be equal in our simulations. The varying time delays in our

Table 3.3: Simulation Parameters

	Value		Value
Human input	$sin(t)$	Endpoint mass m	0.1, 0.5 Kg
Ratio b_i	2.5 Ns/m	Slave D gain	2.5 Ns/m
Slave P gain	370 N/m	Sampling rate	1 KHz

simulations are selected as $T_{mij}(t) = 0.15 + 0.02sin(8t) + 0.06sin(7t) + 0.07sin(5t)$ and $T_{sij} = 0.2 + 0.01sin(10t) + 0.1sin(6t) + 0.05sin(3t)$ [145]. Figs.3.29(a) and 3.29(b) show the $T_{mij}(t)$ and T_{sij} delays and the changing rate of the delays are shown in Figs.3.29(c) and 3.29(d) respectively. It can be seen that the changing rates of the delays are upper bounded by 1. The human operator model is taken from [146], which is a sinusoidal input with proportional derivative control gains of 75 N/m and 50 Ns/m respectively. The environment with which the slaves interact is chosen to be a hard wall of stiffness K_1=30 kN/m which is located at a distance of $x = 0.04$ m and 0.01 m from the slaves for different scenarios. Asymmetric masters and slaves are considered in the simulations represented by the endpoint mass of 0.1 kg and 0.5 kg respectively. The environment contact force model is chosen to satisfy,

$$f_e = \begin{cases} f_e & if \quad x_{si} - x > 0 \\ 0 & if \quad x_{si} - x \leq 0. \end{cases} \tag{3.44}$$

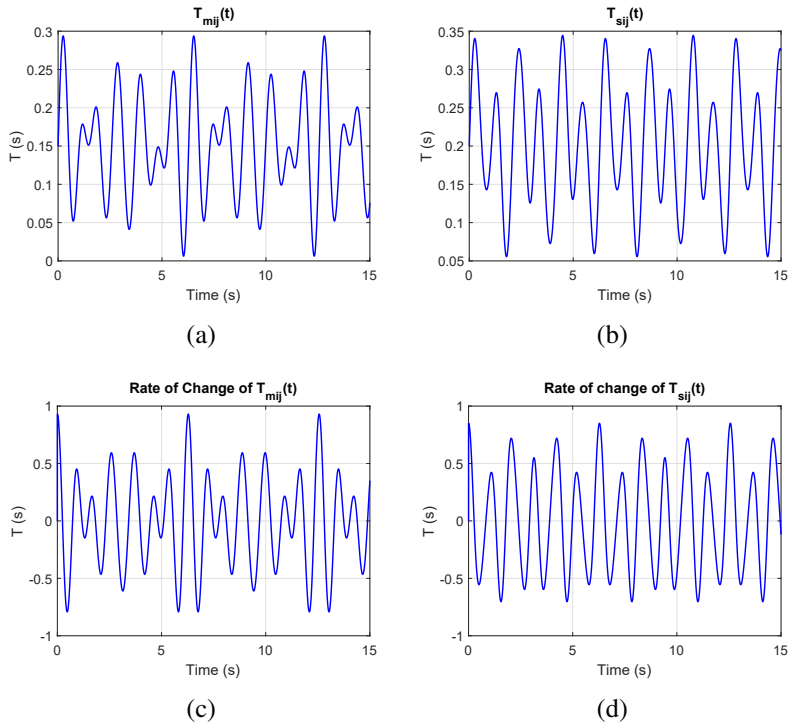

Figure 3.29: $T_{mij}(t)$, $T_{sij}(t)$ and their rates of change

3.4.1.1 Without Switching Action - Case 0

In this case, simulations are run for a system with 2 masters and 2 slaves with a sinusoid input to the masters and the weighting coefficients are chosen to be equal as given below. We do not implement the passivity controllers in this case.

$$\alpha_{v11} = \alpha_{v21} = \alpha_{v12} = \alpha_{v22} = 0.5$$

$$\alpha_{f11} = \alpha_{f21} = \alpha_{f12} = \alpha_{f22} = 0.5.$$

The system is unstable without switching actions when a contact is made. Figs.3.30(a) and 3.30(b) clearly show that without the switching action oscillations are produced in the positions of both the masters and slaves. The contact forces of both the slaves with the wall are depicted in Figs.3.30(c) and 3.30(d). Such oscillations in contact forces are not suitable for teleoperation systems where it is desired that the force feedback to the human operator must be smooth. Energy of the communication channel, numerical integral of (3.32), is clearly negative as shown Fig.3.31 which means that there is some activeness in the system which causes the instability. Stability of the system can be ensured by making this energy value positive.

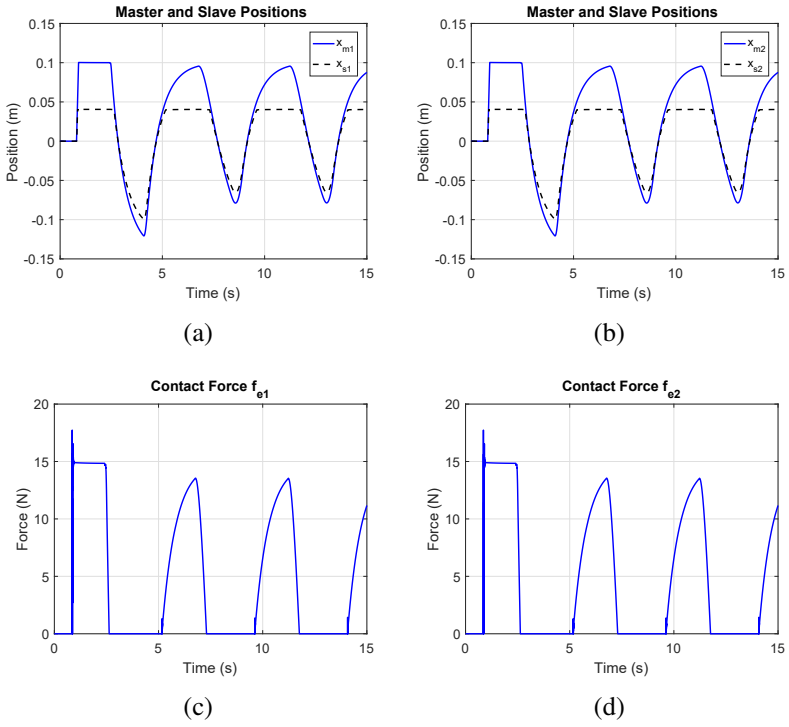

Figure 3.30: M/S Positions and contact forces

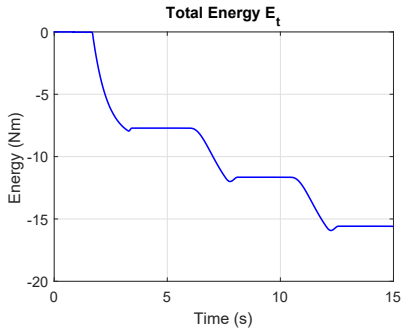

Figure 3.31: Total energy

3.4.1.2 With Switching Action - Case 1

In this case, we have 2 masters and 2 slaves with equal weighting coefficients as in the previous case and with a sinusoidal human input. When all the coefficients are 0.5, the slaves exhibit a stable response when they interact with the wall. The positions of the masters and slaves are presented in Figs.3.32(a) and 3.32(b). TDPC control inherits the position drift which is not desirable in teleoperation. Figs.3.32(a) and 3.32(b) demonstrate this position drift in the slaves but again this can be compensated by the use of $r-$ *passivity*

technique [143]. Velocity of the masters and slaves is shown in Figs.3.32(c) and 3.32(d). It is clear from the velocity results that the weight selection is of importance in the proposed structure. The slaves show same velocity responses when the weighting coefficients are of equal value. Passivity observers values for the first master and the corresponding

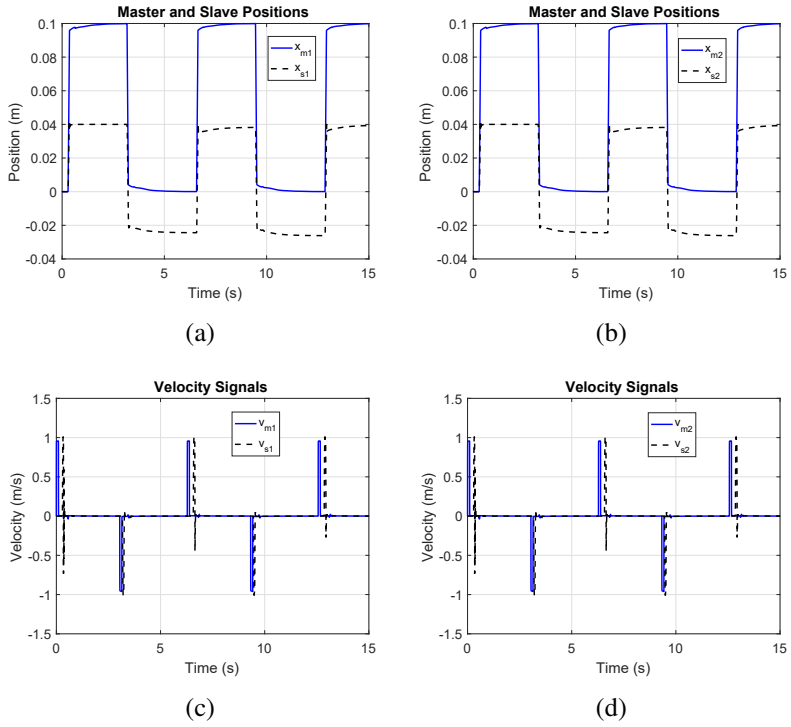

Figure 3.32: Case 1: M/S positions and velocities with $\alpha_i = 0.5$

dissipation values are shown in Figs.3.33(a) and 3.33(c). It is evident from the results of the passivity observers and the dissipation that the proposed control scheme is effectively maintaining the passivity of the system. Control law activates the damper at the master side whenever the POs observe a non-positive power and as soon as the POs observe a non-negative value, the control law deactivates the damper as there is no need of damping injection at that moment. Similarly, passivity observer values for the first salve and the corresponding dissipation values are shown in Figs.3.33(b) and 3.33(d). It is very clear that the control scheme is working perfectly for the stability of the system. Passivity observers values for the second master and the corresponding dissipation values are shown in Figs.3.34(a) and 3.34(c). Similarly, passivity observer values for the second salve and the corresponding dissipation values are shown in Figs.3.34(b) and 3.34(d).

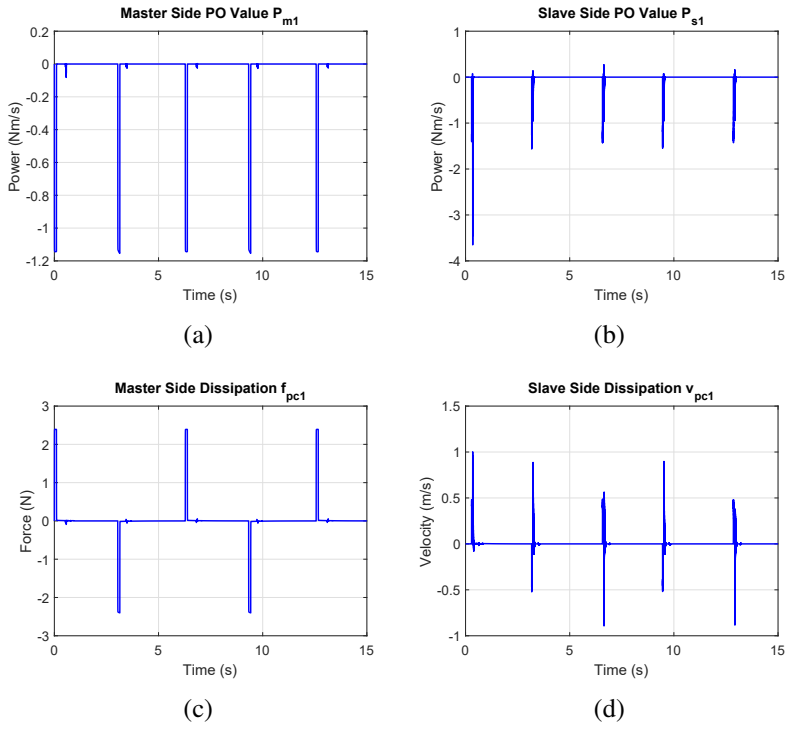

Figure 3.33: Case 1: M/S PO and dissipation values with $\alpha_i = 0.5$

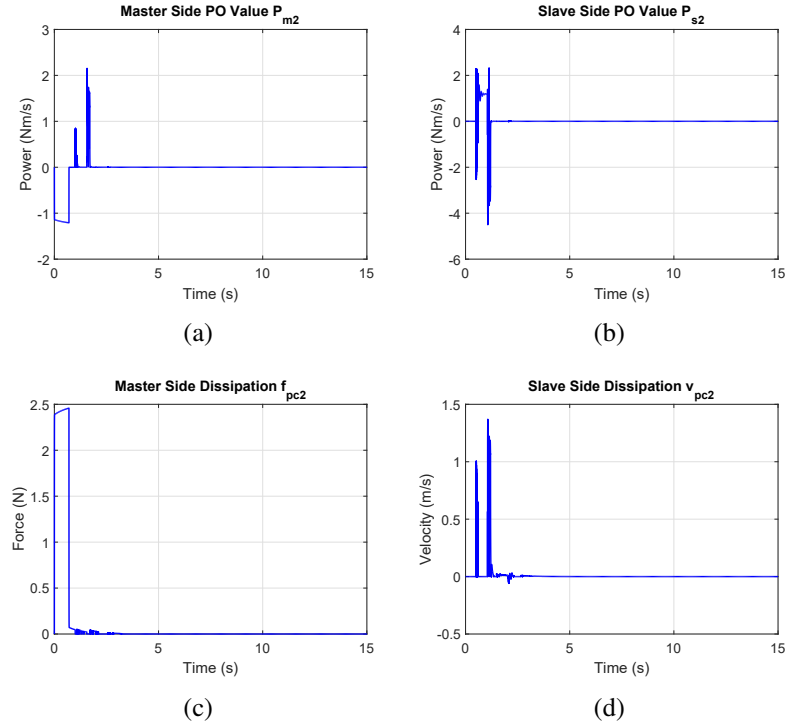

Figure 3.34: Case 1: M/S PO and dissipation values with $\alpha_i = 0.5$

Forces for the first pair of master and slave are presented in Fig.3.35(a). The environment contact force values for the first slave are shown in Fig.3.35(b). It can be seen that the values of the environment contact force satisfy (3.44) and the force spikes appear exactly the same time when the slave interacts with the wall. Similarly, the forces for the second pair of master and slave are depicted in Fig.3.35(c). The environment contact force values for the second slave are shown in Fig.3.35(d). It is observed that the interaction forces of the slaves with the wall are exactly the same due to the fact that the weighting coefficients chosen in the simulations are of equal value. The total energy is shown in Fig.3.36.

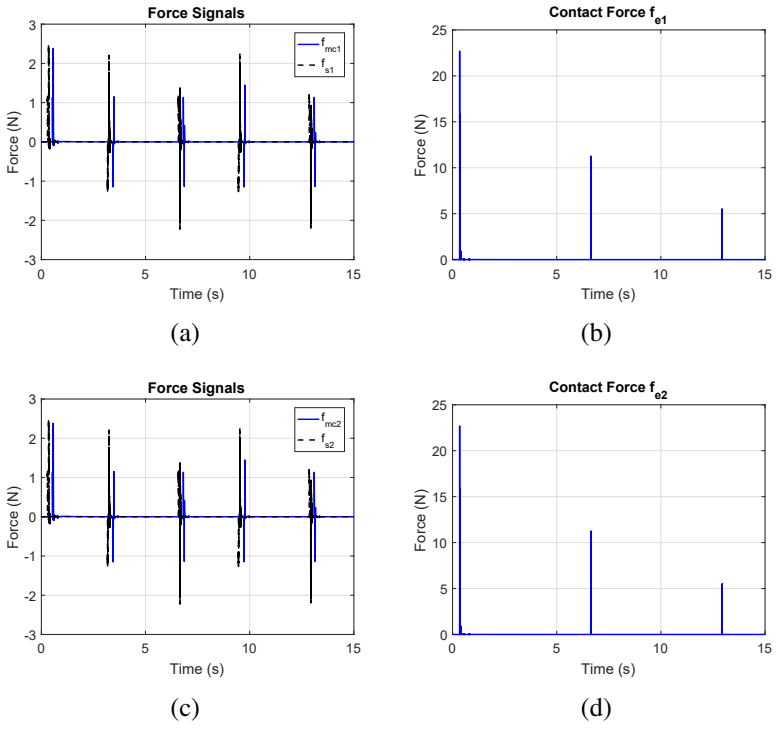

Figure 3.35: Case 1 - Force feedback and contact force with $\alpha_i = 0.5$

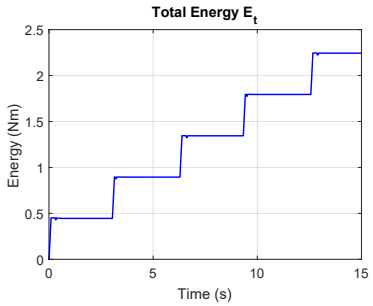

Figure 3.36: Case 1 - Total energy with $\alpha_i = 0.5$

3.4.1.3 With Switching Action - Case 2

In this case, we simulated the multilateral teleoperation system with 2 masters and 3 slaves in the presence of a time varying delay with a human input as a sinusoid. Different number of masters and slaves is chosen to validate the effectiveness of the proposed scheme for practical applications where number of masters and slaves could be different. The weighting coefficients are chosen to obey (3.36) as,

$$\alpha_{v11} = \alpha_{f11} = \alpha_{v12} = \alpha_{f12} = 0.3$$

$$\alpha_{v21} = \alpha_{f13} = \alpha_{v22} = \alpha_{f21} = 0.4$$

$$\alpha_{v31} = \alpha_{f22} = \alpha_{v32} = \alpha_{f23} = 0.5.$$

The slaves are required to make contact with a wall at x= 0.04 m. Figs.3.37(a), 3.37(b) and 3.37(c) show the positions of the masters and slaves. It can be seen that the position tracking is satisfactory even in the presence of a time varying delay and the effect of weighting coefficients is also evident. The slaves track the positions of the masters. Velocity signals of the masters and slaves are given in Figs.3.37(d), 3.37(e) and 3.37(f). The environmental contact forces are presented in Figs.3.37(g), 3.37(h) and 3.37(i). It can be noted that the weight selection affects the velocity of the masters and the force feedback from the slaves. The selection of the weighting coefficients can be varied depending upon the application, the performance of the task or the authority adjustment of the human operators. The total energy is given in Fig.3.37(j) positive values of which confirms the stability of the system. The transient responses of the forces for first and second slave are shown in Figs.3.37(k) and 3.37(l).

The passivity observer values for all the three slaves are shown in Figs.3.38(a), 3.38(b) and 3.38(c) and their corresponding dissipation values are shown in Figs.3.38(d), 3.38(e) and 3.38(f) respectively. It is clear from the results that whenever there is some activeness in the system, passivity controllers inject damping in the system to maintain the stability for safety. The passivity observer values for both the masters are presented in Figs.3.38(g) and 3.38(h) and their corresponding dissipation values are shown in Figs.3.38(j) and 3.38(k). Forces, f_{mc1}, f_{s1} and f_{mc2}, f_{s2} are shown in Figs.3.38(i) and 3.38(l). These results verify the effectiveness of our proposed approach for multilateral teleoperation system even in the presence of varying time delays.

A summary of the simulation results presented above is given in Table 3.4.

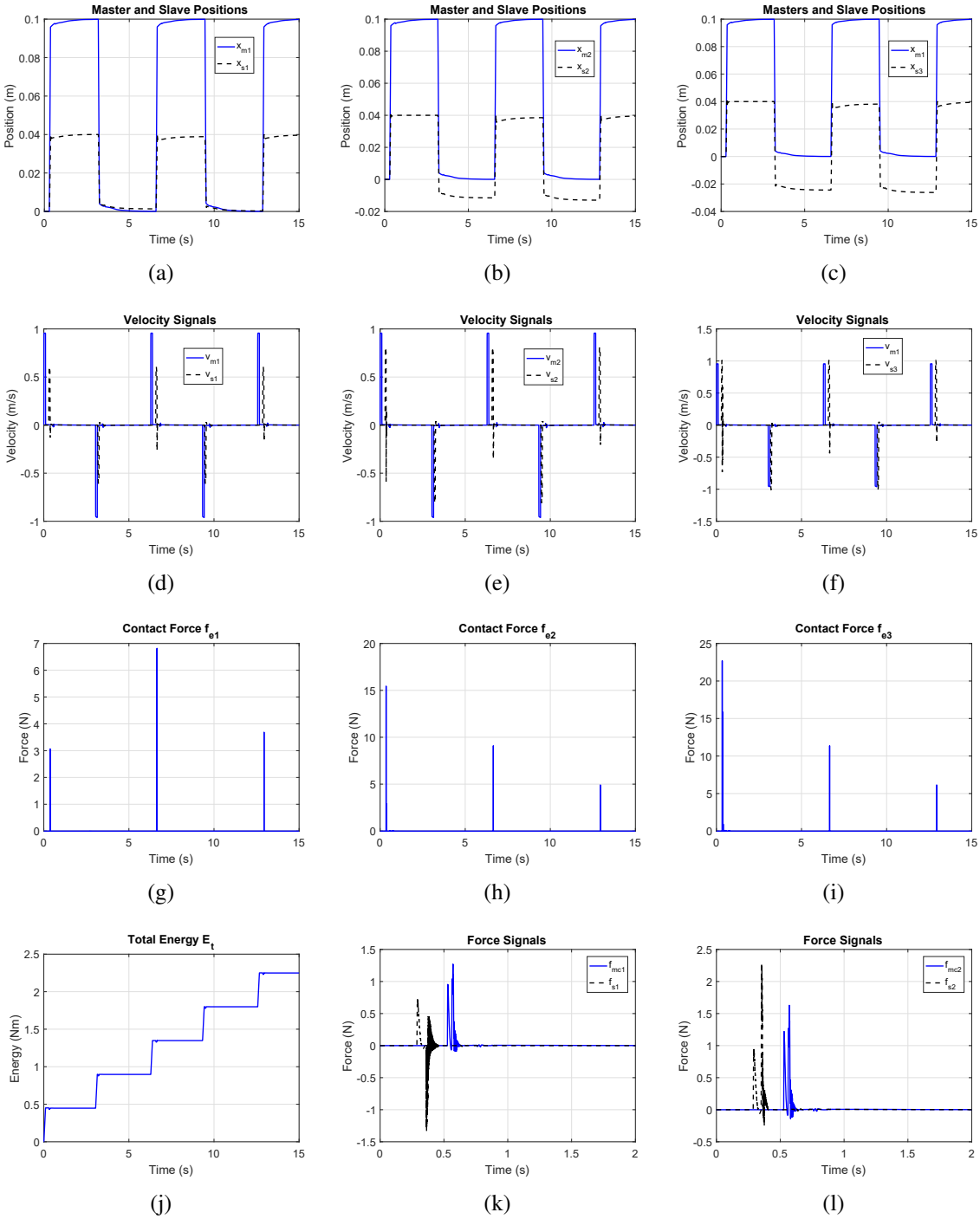

Figure 3.37: Case 2: M/S positions,velocities, contact forces, energy, masters and slaves forces with different α_i

3.4.2 Experimental Results

This section presents the experimental results to verify the effective and stable operation of the proposed scheme under varying time delays now. The experimental setup is exactly

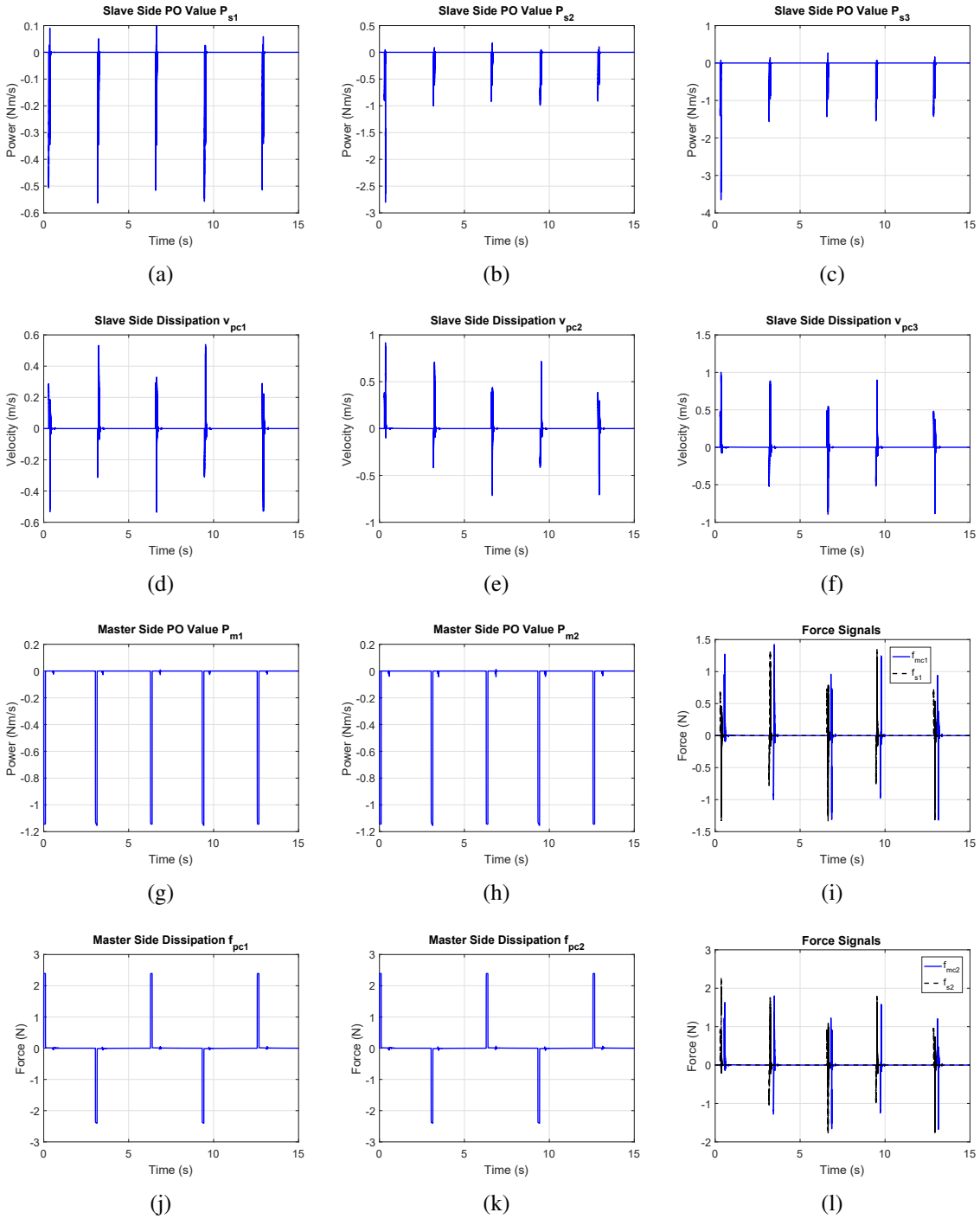

Figure 3.38: Case 2: PO and dissipation values for slaves, PO and dissipation values for masters, forces of masters and slaves with different α_i

the same as in previous section and Fig.3.17. The artificial delay is same as in [129]. This section not only repeats the second set of the experimental results of switching TDPC with

Table 3.4: Summary of Simulation Results

Case No.	Weighting coefficients	Time delay	Human input	No. of M/S
0	0.5	Fig.3.29	Sinusoid	2/2
1	0.5	Fig.3.29	Sinusoid	2/2
2	0.3, 0.4 and 0.5	Fig.3.29	Sinusoid	2/3

variable delays but also provides positions results without switching TDPC.

3.4.2.1 Without Switching Dissipation

This case is being presented just to verify the results of the simulation results section where the passivity controllers were not implemented thus showing the unstable results. This section only shows the position results of the experiment in Fig.3.39. It is obvious from the

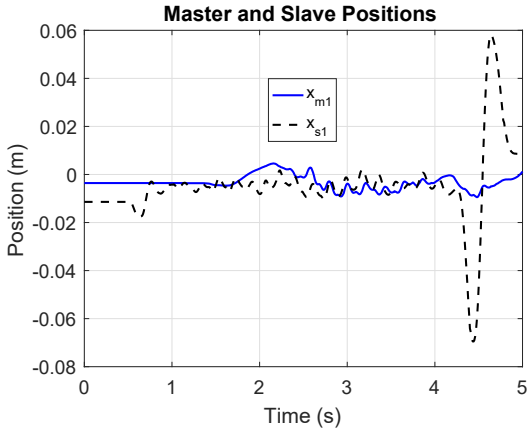

Figure 3.39: M/S positions

position results of a pair of a master and slave that the oscillations are produced in the system when a small input is applied on the master. As shown in Fig.3.39 the operator applies the input around $2s$ which produces small oscillations initially but after $4s$ the slave goes unstable.

3.4.2.2 With Switching Dissipation

For this case, with 2 masters and 2 slaves the weighting coefficients of the communication architecture are assigned as given below.

$$\alpha_{v11} = \alpha_{v22} = \alpha_{f11} = \alpha_{f22} = 0.7$$

$$\alpha_{v12} = \alpha_{v21} = \alpha_{f12} = \alpha_{f21} = 0.1.$$

In this experiment, an Aluminum plate is used as an environment with which the slaves interact as shown in Fig.3.23. Positions of both the masters and slaves are shown in Figs.3.40(a) and 3.40(b). The position difference in the start of the experiment is created intentionally to test the proposed approach and it is clear that the position tracking is satisfactory. The slaves follow the masters in presence of some delay. Feedback forces for both the masters and forces generated by the slave controllers are shown in Figs.3.40(c) and 3.40(d). The

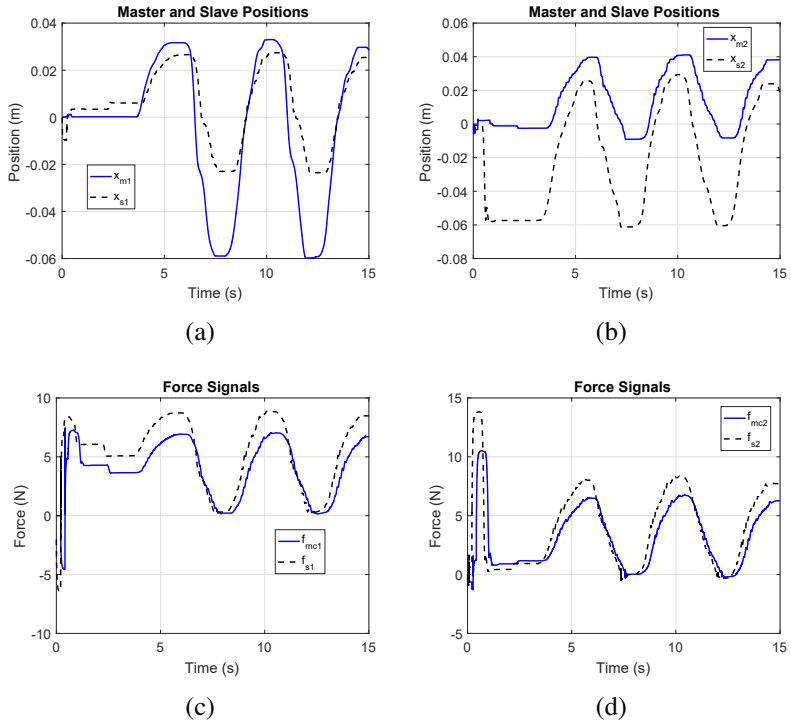

Figure 3.40: M/S positions and forces

passivity observer values for both the masters and their corresponding dissipation values are presented in Figs.3.41(a), 3.41(b), 3.41(c) and 3.41(d) respectively. It can be seen that the power values at the master side are positive for almost all time except in the start so the dissipation values stay at zero confirming that no switching action is required. Similarly, the passivity observer values for both the slaves and their corresponding dissipation values are shown in Figs.3.42(a), 3.42(b), 3.42(c) and 3.42(d) respectively. The interaction forces of both the slaves with the environment are shown in Figs.3.43(a) and 3.43(b).

The simulation and experimental results, for constant and varying time delay cases, presented above confirm the stable and safe teleoperation. It is observed that switching

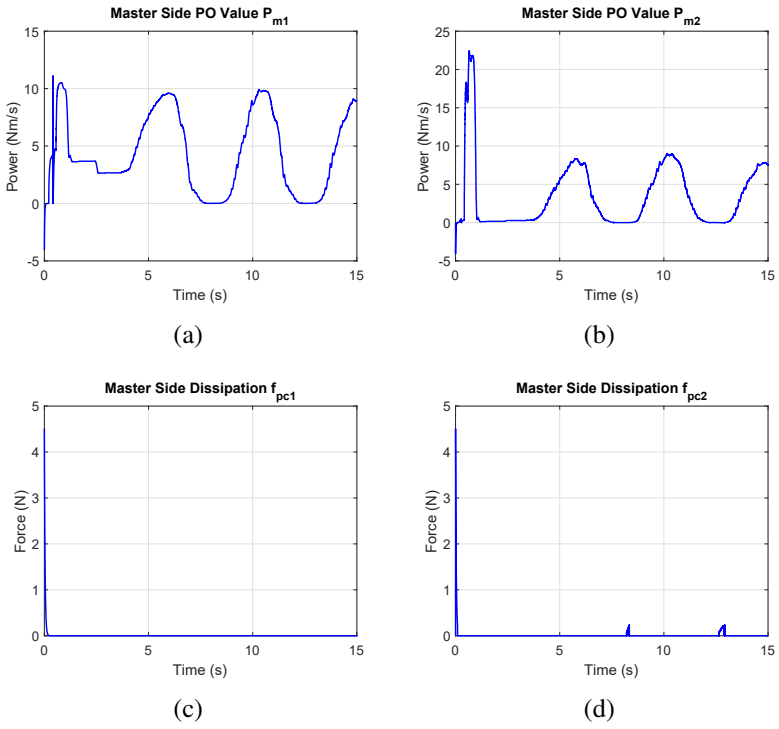

Figure 3.41: PO and dissipation values for the masters

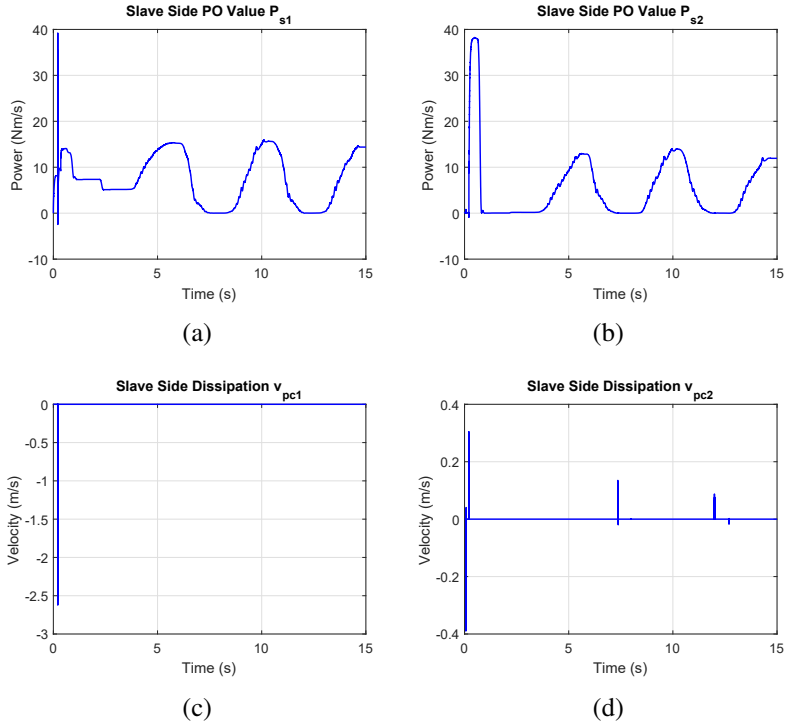

Figure 3.42: PO and dissipation values for the slaves

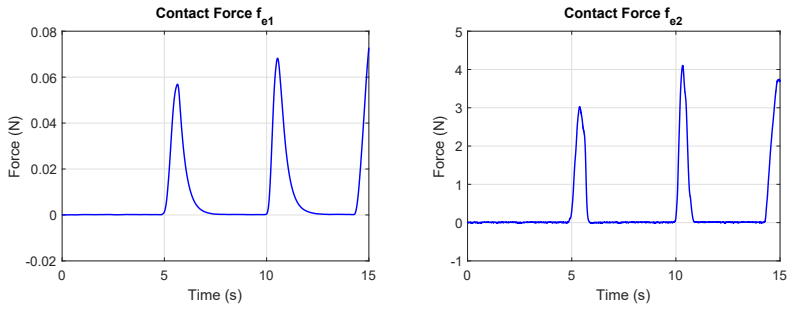

(a) (b)

Figure 3.43: Environmental contact forces

TDPC is not only capable of dealing with constant time delays in communication channel but it works equally well under varying time delays. The effect of weighting coefficients on the velocities of the masters and the forces of the slaves is clearly observable under the proposed communication architecture. The results provide good position tracking of the masters by the slaves as well as the force feedback for the human operator.

3.5 Summary

TDPC is a passivity based approach which has shown effective results for the stability of the teleoperation systems but has only disadvantage of zero division. A novel control design was proposed in this work which bypassed the zero division naturally and ensured the stable operation of multilateral teleoperation system, making control simpler and better. The communication structure proposed here allowed the assignment of different weights to the masters and slaves by the use of weighting coefficients. Stability of the system was maintained at every time instant by a switching action which injected damping in the system whenever it was needed. Extensive numerical simulation and experimental results validated the usefulness of the proposed scheme under constant and varying time delays.

Chapter 4

Modeling of Mobile Manipulators

Efficient model based control of any dynamical system relies on its accurate mathematical model. This chapter is focused on the mathematical modeling of the mobile manipulator system. Unlike fixed-base manipulators, the mathematical model of a mobile manipulator is a little bit complex due to the coupling of the robotic arm and the mobile base. Followed from [64, 147], this work derives the mathematical model of the mobile manipulator starting from the kinematic constraints then developing the Jacobian of the system and finally deriving the dynamics. This mathematical model, kinematics and dynamics, of the mobile manipulators will be used in subsequent chapters for cooperative/coordination control and teleoperation control design of multiple mobile manipulators.

4.1 System Description

Consider the $n+m$ DOF mobile manipulator system as shown in Fig.4.1 [64] where n and m are the degrees of freedom of the manipulator arm and the mobile base respectively. The mobile platform consists of a filled rectangular or circular plate and several wheels system. The manipulator arm consists of n numbers of links which are connected together with the rotation joints. The first link of the manipulator can rotate around z axis and the other links can rotate up and down. The platform of the mobile manipulator is a 2 wheeled differential drive mobile robot. The manipulator is assumed to be mounted on the center of the platform and on the midpoint of the wheel axle.

4.2 Kinematics of Mobile Manipulator

Kinematics of a mobile manipulator are always affected by some kinematical constraints. These constraints are normally classified into two categories of holonomic and nonholonomic constraints. These constraints must be considered in the mathematical modeling of the mobile manipulators to effectively design a controller for specific task requirements as

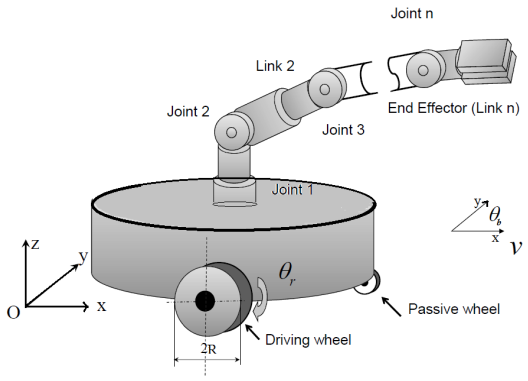

Figure 4.1: $n+m$ DOF mobile manipulator [64]

these constraints govern the overall motion of the system.

4.2.1 Holonomic Constraints

By definition, a holonomic constraint is a type of constraints which can be expressed by a mathematical expressions having only the joint position variables. A common way to express holonomic constraints is given below.

$$f(q,t) = 0 \tag{4.1}$$

where q denotes the generalized coordinates of the system. Holonomic constraints normally reduce the degrees of freedom of the system thus heavily affecting the equations of motion of that system.

4.2.2 Nonholonomic Constraints

In contrast to holonomic constraints, nonholonomic constraints can not be expressed by a mathematical expression depending only on the position variables. The mathematical expressions for such constraints usually include the time derivative of one or more position variables and these expressions can not be integrated to attain a relationship between the joint variables. Conventionally, a nonholonomic constraint is expressed as,

$$f(q,\dot{q},t) = 0 \tag{4.2}$$

4.2.3 Assumptions on Kinematic Structure

There are several assumptions made for the wheeled mobile platform.

- Wheel movement is limited to horizontal plane only. This means that the mobile base can only move in the $X-Y$ plane. Also, it cannot move sideways (in the direction of the axle of the wheels).
- Only point contact of the wheel to the horizontal plane is assumed. Also, it is subjected to pure rolling condition.
- The friction between axle and wheel, the friction between the wheel and the contact surface are completely ignored.
- The steering axis of mobile platform is orthogonal to the horizontal plane.
- It is assumed that the platform of the mobile manipulator is driven by two motors independently.

4.2.4 Derivation of Kinematics of Mobile Manipulator

Consider the mobile manipulator of Fig.4.1 assuming that it has two links of the robotic arm and is mounted on a differential drive platform [64, 147]. It is assumed that the lengths of the links are represented by l_1 and l_2 and the joint angles are represented by θ_1 and θ_2. Considering x, y as the position and θ_b as the orientation of the mobile base, the end-effector coordinates can be written as,

$$\begin{aligned} x_{EE} &= x - l_2 \sin\theta_2 \cos(\theta_b + \theta_1) \\ y_{EE} &= y - l_2 \sin\theta_2 \sin(\theta_b + \theta_1) \\ z_{EE} &= l_1 - l_2 \cos\theta_2. \end{aligned} \tag{4.3}$$

Differentiating (4.3) results in,

$$\begin{aligned} \dot{x}_{EE} &= \dot{x} + l_2 \sin\theta_2 \sin(\theta_b + \theta_1)\dot{\theta}_b + l_2 \sin\theta_2 \sin(\theta_b + \theta_1)\dot{\theta}_1 - l_2 \cos\theta_2 \cos(\theta_b + \theta_1)\dot{\theta}_2 \\ \dot{y}_{EE} &= \dot{y} - l_2 \sin\theta_2 \cos(\theta_b + \theta_1)\dot{\theta}_b - l_2 \sin\theta_2 \cos(\theta_b + \theta_1)\dot{\theta}_1 - l_2 \cos\theta_2 \sin(\theta_b + \theta_1)\dot{\theta}_2 \\ \dot{z}_{EE} &= l_2 \sin\theta_2 \dot{\theta}_2. \end{aligned} \tag{4.4}$$

An alternative form of (4.4) is,

$$\begin{aligned}
\dot{x}_{EE} &= v\cos\theta_b + l_2\sin\theta_2\sin(\theta_b+\theta_1)\omega + l_2\sin\theta_2\sin(\theta_b+\theta_1)\dot{\theta}_1 - l_2\cos\theta_2\cos(\theta_b+\theta_1)\dot{\theta}_2 \\
\dot{y}_{EE} &= v\sin\theta_b - l_2\sin\theta_2\cos(\theta_b+\theta_1)\omega - l_2\sin\theta_2\cos(\theta_b+\theta_1)\dot{\theta}_1 - l_2\cos\theta_2\sin(\theta_b+\theta_1)\dot{\theta}_2 \\
\dot{z}_{EE} &= l_2\sin\theta_2\dot{\theta}_2.
\end{aligned} \tag{4.5}$$

The velocity of the end-effector of the robotic arm and the velocity of the mobile base can be represented as,

$$\begin{aligned}
\dot{X} &= \begin{bmatrix} \dot{x} & \dot{y} & \dot{x}_{EE} & \dot{y}_{EE} & \dot{z}_{EE} \end{bmatrix}^T \\
\eta &= \begin{bmatrix} v & \omega & \dot{\theta}_1 & \dot{\theta}_2 \end{bmatrix}^T.
\end{aligned} \tag{4.6}$$

Now the relationship of $\dot{X}$ and η can be expressed with the help of the Jacobian J as,

$$\dot{X} = J\eta \tag{4.7}$$

The details of the J are given in Appendix A.1.

4.3 Dynamics of Mobile Manipulator

The *Langrangian* of the mobile manipulator system can be expressed as,

$$\mathcal{L}(\mathbf{q},\dot{\mathbf{q}}) = K(\mathbf{q},\dot{\mathbf{q}}) - P(\mathbf{q}), \tag{4.8}$$

The Euler Langrange (EL) equations of motion of an n-link manipulator can be written in the form [148],

$$\frac{du}{dt}\frac{\partial\mathcal{L}}{\partial\dot{\mathbf{q}}} - \frac{\partial\mathcal{L}}{\partial\mathbf{q}} = \tau, \tag{4.9}$$

where τ is the corresponding torque of the ith joint and $i = 1,2...,n$. A conventional way to express (4.9) is [65] given below and the detailed calculation of (4.10) is given in Appendix A.2,

$$M(\mathbf{q})\ddot{\mathbf{q}} + C(\mathbf{q},\dot{\mathbf{q}})\dot{\mathbf{q}} + G(\mathbf{q}) + \mathbf{f} = B(\mathbf{q})\tau, \tag{4.10}$$

where $M(\mathbf{q}) \in \mathcal{R}^{n\times n}$ is the inertia matrix which is a symmetric bounded positive definite matrix; $C(\mathbf{q},\dot{\mathbf{q}}) \in \mathcal{R}^{n\times n}$ is the Centripetal and Coriolis matrix; $G(\mathbf{q}) \in \mathcal{R}^n$ is the gravitational force vector; $\mathbf{f} = \begin{bmatrix} \mathbf{f}_n^T & \mathbf{f}_h^T \end{bmatrix}^T = \begin{bmatrix} (A^T(\mathbf{q}_b)\lambda)^T & 0 \end{bmatrix}^T \in \mathcal{R}^n$ is the generalized constraint force

or torque, where $\lambda = \begin{bmatrix} \lambda_n & \lambda_h \end{bmatrix}^T$ is the Lagrangian multiplier, λ_n considers the nonholonomic constraint and λ_h considers the holonomic constraints and $A(\mathbf{q}_b)$ is the kinematic constraint matrix. $B(\mathbf{q}) \in \mathcal{R}^{n \times m}$ is a full rank input transformation matrix and also assumed to be known; $\tau \in \mathcal{R}^m$ is the control input to the system. $\mathbf{q} = \begin{bmatrix} \mathbf{q}_b^T & \mathbf{q}_a^T \end{bmatrix}^T \in \mathcal{R}^n$ is the vector of generalized coordinates. $\mathbf{q}_b$ denotes the generalized coordinates of the wheeled mobile base and $\mathbf{q}_a$ denotes the generalized coordinates of the manipulator arm. The terms can be further represented as (4.11),

$$M(\mathbf{q}) = \begin{bmatrix} M_b & M_{ba} \\ M_{ab} & M_a \end{bmatrix}, \quad C(\mathbf{q}, \dot{\mathbf{q}}) = \begin{bmatrix} C_b & C_{ba} \\ C_{ab} & C_a \end{bmatrix},$$
$$G(\mathbf{q}) = \begin{bmatrix} G_b \\ G_a \end{bmatrix}, \quad B(\mathbf{q}) = \begin{bmatrix} B_b & 0 \\ 0 & B_a \end{bmatrix}, \quad \tau = \begin{bmatrix} \tau_b \\ \tau_a \end{bmatrix}, \tag{4.11}$$

where M_b and M_a describe the inertia matrices for the mobile base and the manipulator arm respectively. M_{ba} and M_{ab} describe the coupling inertia matrices of the mobile base and manipulator arm. C_b and C_a are Centripetal and Coriolis torques for the mobile base and the manipulator arm respectively. C_{ba} and C_{ab} are the coupling Centripetal and Coriolis torques of the mobile base and the manipulator arm. G_b and G_a are the gravitational forces of the mobile base and the manipulator arm respectively. B_b and B_a denote the input transformation matrices of the mobile platform and the manipulator arm respectively. τ_b and τ_a are the control input of the mobile base and the robotic arm.

4.3.1 Nonholonomic Constraint and Reduced Dynamics

Let $\mathbf{q}_b \in \mathcal{R}^m$ and $\mathbf{q}_a \in \mathcal{R}^n$ describe the coordinates of the mobile base and the manipulator arm respectively where m and n are the DOF of the mobile base and the manipulator arm respectively. The coordinates of the mobile base can be described as,

$$\mathbf{q}_b = \begin{bmatrix} x \\ y \\ \theta_b \end{bmatrix}, \tag{4.12}$$

where x, y are the coordinates of the center of the mobile base and θ_b is the orientation or the heading angle of the mobile base. According to the assumptions made for the wheels of the mobile base, the nonholonomic kinematic constraint for the mid point of the wheel

axle where the manipulator arm is mounted can be expressed as,

$$\dot{x}\sin\theta_b - \dot{y}\cos\theta_b = 0. \tag{4.13}$$

The constraint in (4.13) can also be written in the following form,

$$A(\mathbf{q}_b)\dot{\mathbf{q}}_b = 0, \tag{4.14}$$

where,

$$A(q_b) = [\sin\theta_b \quad -\cos\theta_b \quad 0]. \tag{4.15}$$

Suppose there are l numbers of non-integrable and independent velocity constraints and it is assumed to have the full rank l. The mobile platform here is assumed to be completely nonholonomic and we can write $A(\mathbf{q}_b)$ matrix of (4.14) as,

$$A(\mathbf{q}_b) = \begin{bmatrix} A_1^T(\mathbf{q}_b) & A_2^T(\mathbf{q}_b) & A_3^T(\mathbf{q}_b) & \dots & A_l^T(\mathbf{q}_b) \end{bmatrix}^T. \tag{4.16}$$

The nonholonomic generalized constraint forces can be given as,

$$\mathbf{f}_n = (A^T(\mathbf{q}_b)\lambda_n)^T. \tag{4.17}$$

$H(\mathbf{q}_b) \in \mathcal{R}^{n\times m}$ is a matrix with rank being m formed by a set of smooth and linearly independent vectors spanning the null space of matrix $A(\mathbf{q}_b)$, like,

$$H^T(\mathbf{q}_b)A^T(\mathbf{q}_b) = 0, \tag{4.18}$$

where $H(\mathbf{q}_b) = [H_1(\mathbf{q}_b)\ H_2(\mathbf{q}_b)\ \dots\ H_{n_b-l}(\mathbf{q}_b)]$. Note that here $H^T H$ is full rank. According to (4.14) and (4.18), the first order velocity kinematic model of a nonholonomic mobile platform which is also called the *steering system* can be written in the following form,

$$\dot{\mathbf{q}}_b = H(\mathbf{q}_b)\alpha, \tag{4.19}$$

where α is an auxiliary function $\alpha \in \mathcal{R}^2$ and called the *steering velocity* of the kinematic system. α_1 and α_2 are the linear and angular velocities of the wheeled mobile platform and can be written as (4.20) or α_1 and α_2 are the left wheel velocity and the right wheel velocity of the mobile base and can be written as (4.21),

$$\alpha = \begin{bmatrix} v & \omega \end{bmatrix}^T, \tag{4.20}$$

$$\alpha = \begin{bmatrix} \theta_R & \theta_L \end{bmatrix}^T. \tag{4.21}$$

We can rewrite (4.19) in the specific kinematic form, in terms of linear and angular velocities of the wheeled mobile platform or in terms of right and left wheel velocities.

$$\dot{\mathbf{q}}_b = \begin{bmatrix} \cos\theta_b & 0 \\ \sin\theta_b & 0 \\ 0 & 1 \end{bmatrix} \begin{bmatrix} v \\ \omega \end{bmatrix}, \tag{4.22}$$

$$\dot{\mathbf{q}}_b = \begin{bmatrix} \frac{R}{2}\cos\theta_b & \frac{R}{2}\cos\theta_b \\ \frac{R}{2}\sin\theta_b & \frac{R}{2}\sin\theta_b \\ \frac{R}{2D} & -\frac{R}{2D} \end{bmatrix} \begin{bmatrix} \theta_R \\ \theta_L \end{bmatrix}, \tag{4.23}$$

where R is the radius of the wheels and D is the distance of the two wheels of the mobile platform. Let $\eta = \begin{bmatrix} \alpha^T & \dot{\mathbf{q}}_a^T \end{bmatrix}^T$. Due to the nonholonomic constraint defined in (4.14) and (4.19), there exists a vector $\dot{\eta}$, such that,

$$\dot{\mathbf{q}} = H(\mathbf{q})\eta, \quad \ddot{\mathbf{q}} = H(\mathbf{q})\dot{\eta} + \dot{H}(\mathbf{q})\eta. \tag{4.24}$$

Considering (4.24), the dynamics of the mobile manipulator can be expressed as in (4.25) by substituting (4.24) into (4.10) as,

$$\bar{M}(\mathbf{q})\dot{\eta} + \bar{C}(\mathbf{q},\dot{\mathbf{q}})\eta + \bar{G}(\mathbf{q}) = \bar{\tau}, \tag{4.25}$$

which is the reduced dynamic model of the robotic system.

$$\begin{cases} \bar{M}(\mathbf{q}) = H_i^T(\mathbf{q})M(\mathbf{q})H(\mathbf{q}), \\ \bar{C}(\mathbf{q},\dot{\mathbf{q}}) = H^T(\mathbf{q})[M(\mathbf{q})\dot{H}(\mathbf{q}) + C(\mathbf{q},\dot{\mathbf{q}})H(\mathbf{q})], \\ \bar{G}(\mathbf{q}) = H^T(\mathbf{q})G(\mathbf{q}), \\ \bar{\tau} = H^T(\mathbf{q})B(\mathbf{q})\tau. \end{cases} \tag{4.26}$$

A more specific dynamic model can be described as [64],

$$\begin{bmatrix} H^T B_b \tau_b \\ B_a \tau_a \end{bmatrix} = \begin{bmatrix} H^T M_b H & H^T M_{ba} \\ M_{ab} H & M_a \end{bmatrix} \begin{bmatrix} \ddot{\alpha} \\ \ddot{\mathbf{q}}_a \end{bmatrix} + \begin{bmatrix} H^T M_b \dot{H} + H^T C_b H & H^T C_{ba} \\ M_{ab} \dot{H} + C_{ab} H & C_a \end{bmatrix} \begin{bmatrix} \dot{\alpha} \\ \dot{\mathbf{q}}_a \end{bmatrix} + \begin{bmatrix} H^T G_b \\ G_a \end{bmatrix}. \tag{4.27}$$

4.3.2 Dynamic Properties

The dynamic model of the mobile manipulator (4.25) has following properties [6].
Property 1: The inertia matrix $\bar{M}(q)$ is the symmetric positive definite matrix which follows the following inequality:

$$\lambda_{min}\bar{M}(\mathbf{q})I \leq \bar{M}(\mathbf{q}) \leq \lambda_{max}\bar{M}(\mathbf{q})I, \tag{4.28}$$

where $\lambda_{min}\bar{M}(\mathbf{q})$ and $\lambda_{max}\bar{M}(\mathbf{q})$ are the minimum and maximum eigenvalues of the $\bar{M}(\mathbf{q})$.
Property 2: There exists a skew-symmetric relationship between the inertia matrix $\bar{M}(\mathbf{q})$ and Centripetal and Coriolis matrix $\bar{C}(\mathbf{q},\dot{\mathbf{q}})$ as follow:

$$X^T[\dot{\bar{M}}(\mathbf{q}) - 2\bar{C}(\mathbf{q},\dot{\mathbf{q}})]X = 0. \tag{4.29}$$

Property 3: The left hand side of (4.25) is linearly parameterized in terms of system parameters as shown below:

$$\bar{M}(\mathbf{q})\dot{\eta} + \bar{C}(\mathbf{q},\dot{\mathbf{q}})\eta + \bar{G}(\mathbf{q}) = Y(\mathbf{q},\dot{\mathbf{q}},\eta,\dot{\eta})\mathbf{p}, \tag{4.30}$$

where $\mathbf{p}$ is the vector of uncertain or unknown parameters and Y is a *regressor matrix* which contains unknown parameters.

4.4 Summary

In this chapter, we developed the mathematical model of an $n+m$ DOF mobile manipulator system. The kinematic constraints were discussed first and then depending on the kinematic constraints of the system, the EL dynamic model was presented. This model will be used in the subsequent chapters to test the control algorithms for different applications.

Chapter 5

Cooperative Adaptive Backstepping Control of Two Mobile Manipulators

This chapter is focused on the development of a new adaptive backstepping control scheme for the cooperative control of two mobile manipulators to transport a common object which is rigidly attached to their end-effectors. The key idea is to provide simultaneous control of the mobile base and the end-effector. A two-stage controller is proposed where kinematic backstepping is applied to control the velocity of the mobile platform and the motion of the end-effector and an adaptive torque control is designed for trajectory tracking of the mobile manipulator system. Model parameters are assumed to be completely unknown and are estimated using an adaptive law. Damped Least Squares (DLS) method is used to update the model parameters. The simulation results for two mobile manipulators validate the effectiveness of the proposed controller.

As an extension of our previous work [149] which only deals with the trajectory tracking of a single mobile manipulator, this research work presents a novel backstepping adaptive control of two nonholonomic mobile manipulators to guarantee the perfect trajectory tracking of the end-effectors while carrying a load. The main contribution of this work is to propose an approach to simultaneously control the mobile platform and the robotic arm for proper trajectory tracking of the end-effectors for motion coordination. The object model is chosen such that the only force to deal with is the internal force of the object. The simulation results verify the effectiveness of the proposed control approach.

5.1 System Description

Consider two cooperating $n+m$ DOF mobile manipulator system as shown in Fig.5.1 [64]. The mobile platform consists of a solid rectangular or circular plate and two wheel system. The manipulator arm consists of n number of links which are connected together with the rotation joints. The first link of the manipulator can rotate around the z axis, and the

other links can rotate up and down. The platform of the mobile manipulator is a two-wheeled differential drive mobile robot. The manipulator is assumed to be mounted on the center of the platform and on the midpoint of the wheel axle. An object is attached to the end-effectors of the mobile manipulators. The dynamic model of the ith n-link mobile

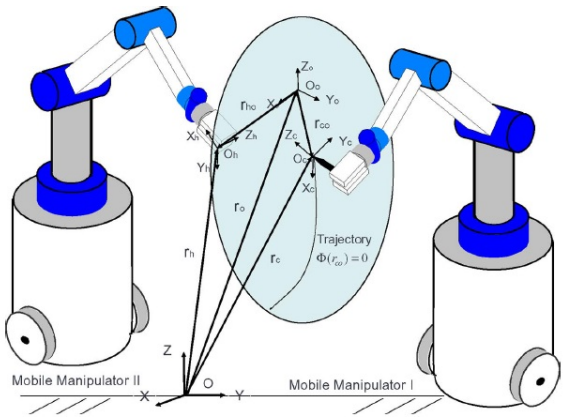

Figure 5.1: Two $n+m$ DOF mobile manipulators [64]

manipulator can be represented as [65],

$$M_i(\mathbf{q}_i)\ddot{\mathbf{q}}_i + C_i(\mathbf{q}_i,\dot{\mathbf{q}}_i)\dot{\mathbf{q}}_i + G_i(\mathbf{q}_i) + \mathbf{f}_i = B_i(\mathbf{q}_i)\tau_i, \tag{5.1}$$

where $M_i(\mathbf{q}_i) \in \mathcal{R}^{n\times n}$ is the inertia matrix which is a symmetric bounded positive definite matrix; $C_i(\mathbf{q}_i,\dot{\mathbf{q}}_i) \in \mathcal{R}^{n\times n}$ is the Centripetal and Coriolis matrix; $G_i(\mathbf{q}_i) \in \mathcal{R}^n$ is the gravitational force vector; $\mathbf{f}_i = \begin{bmatrix}\mathbf{f}_{in}^T & \mathbf{f}_{ih}^T\end{bmatrix}^T = \begin{bmatrix}(A_i^T(\mathbf{q}_{ib})\lambda)^T & 0\end{bmatrix}^T \in \mathcal{R}^n$ is the generalized constraint force or torque, where $\lambda_i = \begin{bmatrix}\lambda_{in} & \lambda_{ih}\end{bmatrix}^T$ is the Lagrangian multiplier, λ_{in} considers the nonholonomic constraint and λ_{ih} considers the holonomic constraints and $A_i(\mathbf{q}_{ib})$ is the kinematic constraint matrix. $B_i(\mathbf{q}_i) \in \mathcal{R}^{n\times m}$ is a full rank input transformation matrix and also assumed to be known; $\tau_i \in \mathcal{R}^m$ is the control input to the system. $\mathbf{q}_i = \begin{bmatrix}\mathbf{q}_{ib}^T & \mathbf{q}_{ia}^T\end{bmatrix}^T \in \mathcal{R}^n$ is the vector of generalized coordinates. $\mathbf{q}_{ib}$ denotes the generalized coordinates of the wheeled mobile base and $\mathbf{q}_{ia}$ denotes the generalized coordinates of the manipulator arm. Following (4.25), we have,

$$\bar{M}_i(\mathbf{q}_i)\dot{\eta}_i + \bar{C}_i(\mathbf{q}_i,\dot{\mathbf{q}}_i)\eta_i + \bar{G}_i(\mathbf{q}_i) = \bar{\tau}_i, \tag{5.2}$$

which is the reduced dynamic model of the robotic system.

$$\begin{cases} \bar{M}_i(\mathbf{q}_i) = H_i^T(\mathbf{q}_i) M_i(\mathbf{q}_i) H_i(\mathbf{q}_i), \\ \bar{C}_i(\mathbf{q}_i, \dot{\mathbf{q}}_i) = H_i^T(\mathbf{q}_i)[M_i(\mathbf{q}_i)\dot{H}_i(\mathbf{q}_i) + C_i(\mathbf{q}_i, \dot{\mathbf{q}}_i) H_i(\mathbf{q}_i)], \\ \bar{G}_i(\mathbf{q}_i) = H_i^T(\mathbf{q}_i) G_i(\mathbf{q}_i), \\ \bar{\tau}_i = H_i^T(\mathbf{q}_i) B_i(\mathbf{q}_i) \tau_i. \end{cases} \tag{5.3}$$

The model in (5.2) has the same dynamic properties as in section 4.3.2.

5.1.1 Object Model

The model of the object can be given by,

$$M_o(\mathbf{x}_o)\ddot{\mathbf{x}}_o + C_o(\mathbf{x}_o, \dot{\mathbf{x}}_o)\dot{\mathbf{x}}_o + G_o(\mathbf{x}_o) = \sum_{i=1}^{2} F_i, \tag{5.4}$$

where $x_o \in R^n$ is the position of the grasped object. $M_o(\mathbf{x}_o)\ddot{\mathbf{x}}_o, C_o(\mathbf{x}_o, \dot{\mathbf{x}}_o)\dot{\mathbf{x}}_o$ and $G_o(\mathbf{x}_o)$ are similar as in (5.1), which represent the inertia matrix, the centripetal and Coriolis force and the gravitational force in the object dynamics. F_i is the equivalent force exerted on the object from the ith manipulator. The kinematic chain between the object frame and the end-effector frame of the ith manipulator is given by [33].

$$x_o = \Phi_{oi}(x_i), \quad \dot{x}_o = L_i(x_i)\dot{x}_i, \quad f_i = L_i^T F_i,$$

where L_i is the nonsingular transformation matrix. The constraints imposed by the kinematic chain are,

$$\mathbf{x}_o = \mathbf{x}_o(x_i) = \mathbf{x}_o(x_i(\mathbf{q}_i)), \quad \dot{\mathbf{x}}_o = A_i(\mathbf{q}_i)\mathbf{q}_i$$

$$\ddot{\mathbf{x}}_o = A_i\ddot{\mathbf{q}}_i + \dot{A}_i\dot{\mathbf{q}}_i, \quad A_i = L_i J_i$$

It is assumed that there is no rotation of the object involved in the manipulation task and the end-effectors are rigidly attached to the object so there is no relative motion between the object and the end-effectors. Also, the object is not fragile so it does not get deformed with the applied forces.

5.2 Coordinated Control Design

This section develops the decentralized controllers for the coordinated control of the mobile manipulators, described by (5.2), to cooperatively transport an object given the desired

trajectories. The movements of the mobile base and the end-effectors are controlled simultaneously to attain synchronized motion. The mobile base is required to track the desired trajectory Φ_{di}. Similarly, the end-effector is required to track a desired trajectory Ψ_{di}. The subsections of this section address the design of control laws for the mobile manipulator system assuming that the desired trajectories are well defined according to the kinematic constraints of the system.

We address the modelling and control problem of the nonholonomic mobile manipulators for the $n+m$ DOF manipulator mounted on the differential drive wheeled mobile base. This section aims to design a two-stage controller with the objective to track the desired position and velocity of the end-effector. In the first step of the controller design, a kinematic velocity control law is considered using the backstepping control method to control the motion of the end-effector. In the second step, an adaptive torque controller is designed which estimates the unknown parameters of the mobile manipulator system and controls the torque in order to achieve the asymptotic trajectory tracking.

5.2.1 Control Objective

The trajectory tracking problem for two mobile manipulators can be described as follows. Let there are two mobile manipulators consisting of n-links connected together with joints mounted on the nonholonomic wheeled mobile vehicle. The system can be described by (5.2) which is subjected to nonholonomic constraints as in (4.24).

$$\begin{aligned} \dot{\mathbf{q}}_i &= H_i(\mathbf{q}_i)\eta_i \\ \dot{\eta}_i &= \bar{M}_i^{-1}(\mathbf{q}_i)[\bar{\tau}_i - \bar{C}_i(\mathbf{q}_i,\dot{\mathbf{q}}_i)\eta_i - \bar{G}_i(\mathbf{q}_i)]. \end{aligned} \tag{5.5}$$

η_i is assumed to be,

$$\eta_i = \begin{bmatrix} \alpha_i^T & \dot{\mathbf{q}}_{ia}^T \end{bmatrix}^T, \tag{5.6}$$

where α_i is the vector of steering velocity of the mobile platform and $\dot{q}_{ia}$ is the vector of joint velocities of the manipulator arm mounted on the mobile base. The controller is designed in two steps. First, motion/velocity tracking control of the end-effector of the mobile manipulator is designed assuming that the desired trajectory is generated by the kinematic equations and then using that control as a virtual input to (5.2) and by calculating the torque control $\bar{\tau}_i$ that accomplishes the asymptotic trajectory tracking of the mobile manipulator for any desired trajectory $\Psi_{di} = \begin{bmatrix} \dot{x}_{di} & \dot{y}_{di} & x_{EEdi} & y_{EEdi} & z_{EEdi} \end{bmatrix}^T = \begin{bmatrix} \dot{\Psi}_{bdi}(t) & \Psi_{adi}(t) \end{bmatrix}^T$,

where $\dot{x}_{di}$ and $\dot{y}_{di}$ are the derivative of the x_{di} and y_{di} components of the mobile platform, and x_{EEdi}, y_{EEdi}, z_{EEdi} are the desired end-effector position coordinates in respective directions. The object is attached rigidly to the end-effectors such that there is no relative motion between the object and the end-effector.

5.2.2 Assumptions

The following assumptions are made in control design.

1. The nonholonomic constraints and the kinematics of the platform are considered for the velocity control of the mobile platform and no external forces act on the robotic system.

2. It is assumed that the final position of the object is achieved just by reaching the final point of desired end-effector trajectory.

3. It is assumed that $\Psi_{di}(t)$ is computable with $\dot{\Psi}_{bdi}(t)$. In other words mobile manipulator is able to track the Ψ_{di} and $\dot{\Psi}_{bdi}$ simultaneously and Ψ_{di} and $\dot{\Psi}_{bdi}$ are in the range of the workspace of the mobile manipulator.

4. The desired trajectory of the end-effector $\Psi_{di}(t)$ and the desired velocity trajectory $\dot{\Psi}_{bdi}(t)$ are assumed to be bounded and uniformly continuous and also assumed that their derivatives up to the second order exist and are uniformly bounded and continuous however, Z_{EEdi} is assumed constant here.

5. It is assumed that the mass of the platform, mass of the links, length of the links and the inertia parameters are unknown for the mobile manipulator system.

Barbalat's Lemma [150]

If $f : R^{+} \rightarrow R$ is uniformly continuous and positive function for all $t \geq 0$, and if the limit of integral,

$$\lim_{t\rightarrow\infty} \int_{0}^{\infty} f(\tau) d\tau \tag{5.7}$$

exists and is finite, then

$$\lim_{t\rightarrow\infty} f(t) = 0 \tag{5.8}$$

Definition:

The L_s norm of a function $f : R^+ \rightarrow R$ is defined as:

$$||f(t)||_s = \Big(\int_0^\infty |f(\tau)|^s d\tau \Big)^{\frac{1}{s}}, \tag{5.9}$$

for all $s = [1, \infty)$, while

$$||f(t)||_\infty = max|f(t)| \qquad t \geq 0, \tag{5.10}$$

denotes the L_∞ norm of function f. $f \in L_s$ if $||f(t)||_s$ exists and is finite.

5.2.3 Velocity Tracking Problem

This section focuses on developing a control law $\eta_{ci}(t)$ such that all the state variables of the kinematics (4.24) for any $(\Psi_i(0), \dot{\Psi}_i(0)) \in \Phi_i$, Ψ_i and $\dot{\Psi}_i$ converge to a manifold specified as Φ_{di}.

$$\begin{aligned} &\Phi_{di} = \{(\Psi_i, \dot{\Psi}_i) \mid \Psi_i = \Psi_{di}, \dot{\Psi}_i = \dot{\Psi}_{di}\}, \\ &\Psi_i = \begin{bmatrix} \dot{x}_i & \dot{y}_i & x_{EEi} & y_{EEi} & z_{EEi} \end{bmatrix}^T. \end{aligned} \tag{5.11}$$

To simplify the control objective, assume the tracking error of the desired trajectory is $\mathbf{e}_i(t)$ and it can be written in the form of (5.12) where $\Psi_i(t)$ is denoting the configuration of the mobile platform velocity and the position of the end-effector and $\Psi_{di}(t)$ denotes the desired configuration of mobile platform velocity and the position of the end-effector.

$$\mathbf{e}_i(t) = \Psi_{di}(t) - \Psi_i(t). \tag{5.12}$$

The control objective can be formulated as,

$$\lim_{t \to \infty} \mathbf{e}_i(t) = 0 \quad \text{and} \quad \lim_{t \to \infty} \dot{\mathbf{e}}_i(t) = 0. \tag{5.13}$$

5.2.3.1 Kinematic Controller

We will use the backstepping approach to design a kinematic or velocity controller. To design a motion tracking controller, we only consider (4.24) which is the kinematic equation of the mobile manipulator.

$$\dot{\mathbf{q}}_i = H_i(q_i)\eta_i. \tag{5.14}$$

First, define an output of the system as,

$$\Psi_i = f_i(q_i), \tag{5.15}$$

The error and its derivative can be written as,

$$\begin{aligned} \mathbf{e}_i &= \Psi_{di} - \Psi_i \\ \dot{\mathbf{e}}_i &= \dot{\Psi}_{di} - \dot{\Psi}_i \end{aligned} \tag{5.16}$$

where $\mathbf{e}_i$ is the velocity error of the mobile platform and the position error of the end-effector. Taking the time derivative of (5.15),

$$\dot{\Psi}_i = \frac{\partial f_i(q_i)}{\partial q_i}\dot{\mathbf{q}}_i = \frac{\partial f_i(q_i)}{\partial q_i}H_i(\mathbf{q}_i)\eta_i = \Delta_i\eta_i, \tag{5.17}$$

where Δ_i is a decoupling matrix or extended Jacobian matrix and can be represented as

$$\Delta_i = \frac{\partial f_i(q_i)}{\partial q_i}H_i(\mathbf{q}_i). \tag{5.18}$$

From (5.16) and (5.17),

$$\dot{\mathbf{e}}_i = \dot{\Psi}_{di} - \Delta_i\eta_i. \tag{5.19}$$

Let $\eta_i = \eta_{ci}$ be the virtual velocity control, (5.19) can be written as,

$$\dot{\mathbf{e}}_i = \dot{\Psi}_{di} - \Delta_i\eta_{ci}. \tag{5.20}$$

Choosing a Lyapunov function as,

$$V_1 = \frac{1}{2}\mathbf{e}_i^T\mathbf{e}_i. \tag{5.21}$$

Taking the derivative of (5.21),

$$\dot{V}_1 = \mathbf{e}_i^T\dot{\mathbf{e}}_i = \mathbf{e}_i^T(\dot{\Psi}_{di} - \Delta_i\eta_{ci}). \tag{5.22}$$

We design the kinematic control law η_{ci} as

$$\eta_{ci} = \Delta_i^{-1}[\dot{\Psi}_{di} + K_i\mathbf{e}_i], \tag{5.23}$$

where $K_i > 0$ is the positive constant control gain. (5.23) is the velocity tracking kinematic controller. From (5.20) and (5.23),

$$\dot{\mathbf{e}}_i = \dot{\Psi}_{di} - \Delta_i[\Delta_i^{-1}(\dot{\Psi}_{di} + K_i\mathbf{e}_i)] = -K_i\mathbf{e}_i. \tag{5.24}$$

When $K_i > 0, \lim_{t\to\infty}\mathbf{e}_i(t) = 0$,

$$\dot{V}_1 \leq -K_i||\mathbf{e}_i||^2.$$

If Δ is a full rank square matrix, then Δ^{-1} can be obtained via simple inversion. If Δ is not a full rank matrix or the mobile manipulator is at a singular configuration, the system given in (5.14) contains linearly dependent equations. In this case, Δ^{-1} cannot be derived from the simple inversion of Δ. An alternative solution to invert the Δ at the sinuglar point or in the neighbourhood of a singularity is provided by the Damped Least Squares (DLS) inverse method [151, 152]. In the DLS inverse method, the inverse can be written as,

$$\Delta^{-1} = \Delta^T \left(\Delta\Delta^T + k^2 I\right)^{-1}, \tag{5.25}$$

where k is a damping factor.

5.2.4 Cooperative Torque Control Problem

Using a property of the dynamic system given in (4.30), design a control law such that all the state variables of the mobile manipulator dynamics converge to a desired trajectory $\Psi_{di}(t)$ so that the cooperative transportation of an object is achieved. In other words, design a controller $\bar{\tau}_i$ such that,

$$\lim_{t\to\infty} \eta_i(t) - \eta_{ci}(t) = 0 \quad or \quad \lim_{t\to\infty} \eta_{ei}(t) = 0, \tag{5.26}$$

where $\eta_{ci}(t)$ is the velocity controller designed in the first step and $\eta_{ei}(t)$ is the joint velocity error between actual and controlled joint velocities.

5.2.4.1 Adaptive Torque Control

In the first part of the controller design, a kinematic velocity controller is designed to track the desired trajectory of the mobile manipulator system. Using the controller η_{ci}, the adaptive torque controller is designed. The dynamics given in (5.2) are considered to design the controller. Using the properties of the dynamic system given in (4.28), (4.29) and (4.30), the adaptive torque controller is designed as follows.

Consider a Lyapunov function V_2 as,

$$V_2 = \frac{1}{2}\eta_{ei}^T \bar{M}_i \eta_{ei}, \tag{5.27}$$

where η_{ei} is defined as the state error of the kinematically controlled system and can be written as (5.28). Note that it is not an independent Lyapunov function for the adaptive torque control as η_{ei} given in the (5.28) depends on the kinematic control.

$$\eta_{ei} = \eta_i - \eta_{ci}. \tag{5.28}$$

Taking the time derivative of the Lyapunov function V_2 as,

$$\dot{V}_2 = \frac{1}{2}\eta_{ei}^T\Big[\dot{\bar{M}}_i\eta_{ei} + 2\bar{M}_i\dot{\eta}_{ei}\Big]. \tag{5.29}$$

From (5.28),

$$\dot{V}_2 = \eta_{ei}^T\Big[\frac{1}{2}\dot{\bar{M}}_i\Big(\eta_i - \eta_{ci}\Big) + \bar{M}_i\Big(\dot{\eta}_i - \dot{\eta}_{ci}\Big)\Big]. \tag{5.30}$$

From (5.5) we have,

$$\begin{aligned}
\dot{V}_2 &= \eta_{ei}^T\Big[\frac{1}{2}\dot{\bar{M}}_i\Big(\eta_i - \eta_{ci}\Big) + \bar{M}_i\Big[\bar{M}_i^{-1}\Big(\bar{\tau}_i - \bar{C}_i\eta_i - \bar{G}_i\Big) - \dot{\eta}_{ci}\Big]\Big] \\
&= \eta_{ei}^T\Big[\frac{1}{2}\dot{\bar{M}}_i\Big(\eta_i - \eta_{ci}\Big) + \bar{\tau}_i - \bar{C}_i\eta_i - \bar{G}_i - \bar{M}_i\dot{\eta}_{ci}\Big] \\
&= \eta_{ei}^T\Big[\frac{1}{2}\dot{\bar{M}}_i\eta_i - \frac{1}{2}\dot{\bar{M}}_i\eta_{ci} + \bar{\tau}_i - \bar{C}_i\eta_i - \bar{G}_i - \bar{M}_i\dot{\eta}_{ci}\Big].
\end{aligned} \tag{5.31}$$

Adding and subtracting $\bar{C}_i\eta_{ci}$ in (5.31) and re-arranging the terms, we obtain,

$$\begin{aligned}
\dot{V}_2 = \eta_{ei}^T\Big[&\Big(\frac{1}{2}\dot{\bar{M}}_i\eta_i - \bar{C}_i\eta_i\Big) - \Big(\frac{1}{2}\dot{\bar{M}}_i\eta_{ci} - \bar{C}_i\eta_{ci}\Big) - \bar{C}_i\eta_{ci} \\
&+ \bar{\tau}_i - \bar{G}_i - \bar{M}_i\dot{\eta}_{ci}\Big],
\end{aligned} \tag{5.32}$$

Using the dynamic property of the mobile manipulator system from (4.29), we can simplify (5.32) as follows.

$$\dot{V}_2 = \eta_{ei}^T\Big[\bar{\tau}_i - \bar{M}_i\dot{\eta}_{ci} - \bar{C}_i\eta_{ci} - \bar{G}_i\Big]. \tag{5.33}$$

Using the dynamic property in (4.30), the derivative of the Lyapunov function can be written as,

$$\dot{V}_2 = \eta_{ei}^T\Big[\bar{\tau}_i - Y_i\Big(\mathbf{q}_i, \dot{\mathbf{q}}_i, \eta_{ci}, \dot{\eta}_{ci}\Big)\mathbf{p}_i\Big]. \tag{5.34}$$

Therefore, the control law for the unknown parameters $\mathbf{p}_i$ can be chosen as,

$$\bar{\tau}_i = Y_i\Big(\mathbf{q}_i, \dot{\mathbf{q}}_i, \eta_{ci}, \dot{\eta}_{ci}\Big)\mathbf{p}_i - K_{1i}\eta_{ei}, \tag{5.35}$$

where K_{1i} is a constant control gain positive definite matrix.
With K_{1i} being positive definite matrix,

$$\dot{V}_2 = -\eta_{ei}^T K_{1i}\eta_{ei} \leq -\lambda_{imin}(K_{1i})||\eta_{ei}||^2. \tag{5.36}$$

However, here in (5.35), $\mathbf{p}_i$ is the vector of uncertain or unknown parameters so we need to add the adaptive controller to estimate the constant value of the vector $\mathbf{p}_i$. Define the

estimated parameter vector as $\hat{\mathbf{p}}_i$ and then define the error between the actual and estimated parameters as,

$$\mathbf{e}_{pi} = \mathbf{p}_i - \hat{\mathbf{p}}_i. \tag{5.37}$$

Choosing the control law $\bar{\tau}_i$, and parameter update law $\dot{\hat{\mathbf{p}}}_i$ as,

$$\begin{aligned}
\bar{\tau}_i &= Y_i(\mathbf{q}_i, \dot{\mathbf{q}}_i, \eta_{ci}, \dot{\eta}_{ci})\hat{\mathbf{p}}_i - K_{1i}\eta_{ei} \\
\dot{\hat{\mathbf{p}}}_i &= -(\Gamma_i^{-1})^T Y_i(\mathbf{q}_i, \dot{\mathbf{q}}_i, \eta_{ci}, \dot{\eta}_{ci})^T \eta_{ei} \\
&= -\Gamma_i^{-1} Y_i(\mathbf{q}_i, \dot{\mathbf{q}}_i, \eta_{ci}, \dot{\eta}_{ci})^T \eta_{ei},
\end{aligned} \tag{5.38}$$

where Γ_i is the symmetric positive definite gain matrix which ensures that (5.39) is positive definite.

Consider the Lyapunov function V_3 as,

$$V_3 = V_2 + \frac{1}{2}\mathbf{e}_{pi}^T \Gamma_i \mathbf{e}_{pi}. \tag{5.39}$$

Taking the time derivative of the Lyapunov function,

$$\begin{aligned}
\dot{V}_3 &= \eta_{ei}^T \Big[\bar{\tau}_i - Y_i(\mathbf{q}_i, \dot{\mathbf{q}}_i, \eta_{ci}, \dot{\eta}_{ci})\mathbf{p}_i \Big] + \dot{\mathbf{e}}_{pi}^T \Gamma_i \mathbf{e}_{pi} \\
&= \eta_{ei}^T \Big[\bar{\tau}_i - Y_i \mathbf{p}_i \Big] + (-\dot{\hat{\mathbf{p}}})_i^T \Gamma_i (\mathbf{p}_i - \hat{\mathbf{p}}_i),
\end{aligned} \tag{5.40}$$

Using the parameter update law from (5.38),

$$\begin{aligned}
\dot{V}_3 &= \eta_{ei}^T \Big[\bar{\tau}_i - Y_i \mathbf{p}_i \Big] + (\eta_{ei}^T) Y_i (\Gamma_i^{-1} \Gamma_i)(\mathbf{p}_i - \hat{\mathbf{p}}_i) \\
&= \eta_{ei}^T \Big[\bar{\tau}_i - Y_i \mathbf{p}_i + Y_i \mathbf{p}_i - Y_i \hat{\mathbf{p}}_i \Big] \\
&= \eta_{ei}^T \Big[\bar{\tau}_i - Y_i \hat{\mathbf{p}}_i \Big] \\
&\leq \eta_{ei}^T K_{1i} \eta_{ei} \\
&\leq -\lambda_{imin}(K_{1i}) ||\eta_{ei}||^2.
\end{aligned} \tag{5.41}$$

From the Lyapunov stability theorem and Barbalat's Lemma [150], $\eta_{ei} \in L_\infty$. Integrating (5.41) we get,

$$V_2(t) \leq V_2(0) - \lambda_{imin} K_{1i} \int_0^t ||\eta_{ei}||^2 dt.$$

Rearranging the above equation,

$$\int_0^t ||\eta_{ei}||^2 dt \leq \frac{V_2(0) - V_2(t)}{\lambda_{imin} K_{1i}},$$

Since $V_2(0)$ is finite and $V_2(t) \in L_\infty$, we can write, $\eta_{ei} \in L_2$. Also, because $\dot{\eta}_{ei}$ is a function of η_{ei}. In (5.36) and (5.41), $\lambda_{imin}(K_{1i})$ is the minimum eigenvalue of the control gain K_{1i}. Thus, from the Barbalat's lemma [150], we can write,

$$\lim_{t\to\infty} \eta_{ei} = 0 \Longrightarrow \lim_{t\to\infty} \eta_i = \eta_{ci}. \tag{5.42}$$

Hence the system tracking error tends to be zero asymptotically and the system in (5.38) is stable. As for the cooperative transportation of the object, there is no interaction with the environment we can deal with the internal forces of the object the same way as in [33]. We simply make the internal force component zero which does not affect the motion of the object. Another way to control the internal forces of the object is to use a virtual linkage model and grasp matrix as in [68].

5.3 Simulation Results

This section presents the simulation results of two 2-DOF mobile manipulators for the desired trajectory tracking based on the controller designed in the previous section. The simulation parameters are given in Table 5.1.

Table 5.1: Simulation Parameters

	Value		Value
Mass of platform	32 kg	Mass of link 1	3 kg
Mass of link 2	3 kg	Inertia of platform	1 kgm^2
Inertia of link 1	1 kgm^2	Inertia of link 2	1 kgm^2
Radius of wheel	0.5 m	Length of link 1	1 m
Length of link 2	1 m	Gravitational force	9.8 ms^{-2}

Consider the given mobile manipulator system of (5.2) for which the time dependent desired trajectory $\Psi_{di} = \left[\dot{x}_{di}, \dot{y}_{di}, x_{EE_{di}}, y_{EE_{di}}, z_{EE_{di}}\right]^T$ is selected as,

$$\begin{cases} \dot{x}_{di} & = 0.1 + 0.05\sin t \\ \dot{y}_{di} & = 0.1 + 0.05\cos t \\ x_{EEdi} & = 0.1t - 0.05\cos t + 0.05 + 1 \\ y_{EEdi} & = 0.1t + 0.05\sin t + 1 \\ z_{EEdi} & = 1. \end{cases}$$

The initial conditions for both mobile manipulators are $\Psi_i = \left[\dot{x}_i, \dot{y}_i, x_{EEi}, y_{EEi}, z_{EEi}\right]^T = [0\ 0\ 0\ 0\ 1], [0\ 0\ 0\ 1\ 1]$. The controller gains are chosen to be $k_i = 1.01, K_i = 250, K_{1i} = 80I_4 \times I_4, \Gamma_i = 10I_6 \times I_6$. The parameters of the object are $M_o = \text{diag}\{5,1\}$, $C_o = \text{diag}\{0,0\}$, $G_o = \text{diag}\{0,5 * 9.8\}^T$ and $f_d^{int} = 0$. The kinematic chain between the object and the manipulators is given by $x_o = x_1 = diag(-1,1) \times x_2$.

Figs.5.2(a), 5.2(b), 5.2(c) and 5.2(d) describe the desired and the actual end-effector position and the errors of the mobile manipulators. The actual position of the end-effector converges to the desired trajectory quickly with some error. Although, the end-effectors do not follow the desired trajectory accurately, the main objective of transporting the object is accomplished. The convergence time of the actual trajectory to the desired trajectory is around 20 seconds. It proves that the designed controller is efficient for the trajectory tracking of the non-zero velocity mobile manipulator's end-effector position control.

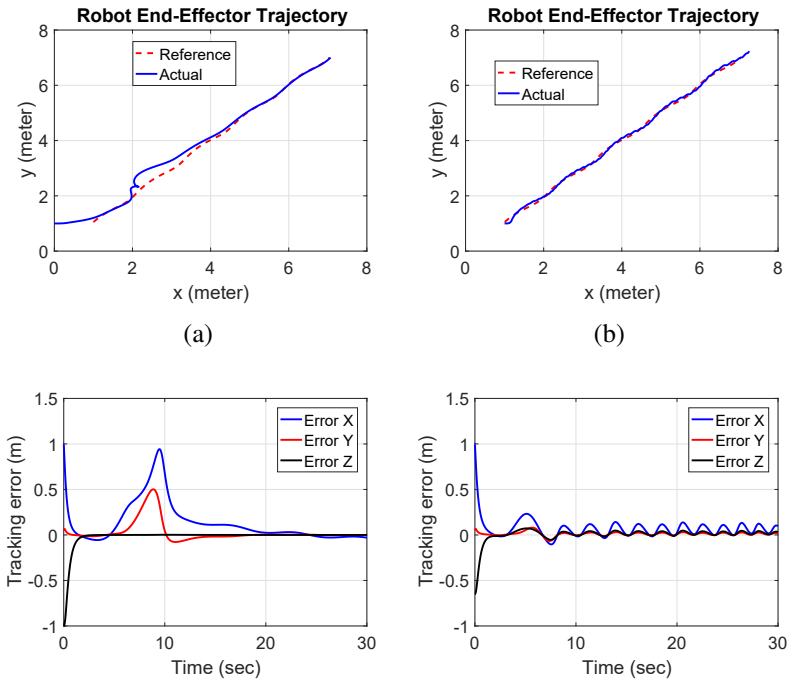

Figure 5.2: End-effector positions and errors

The desired and actual velocities of the mobile base for the first mobile manipulator in x and y directions are shown in Figs.5.3(a) and 5.3(b). The velocities converge to the desired velocities after around 15 seconds. The velocities for the second mobile manipulator are shown in Figs.5.3(c) and 5.3(d).

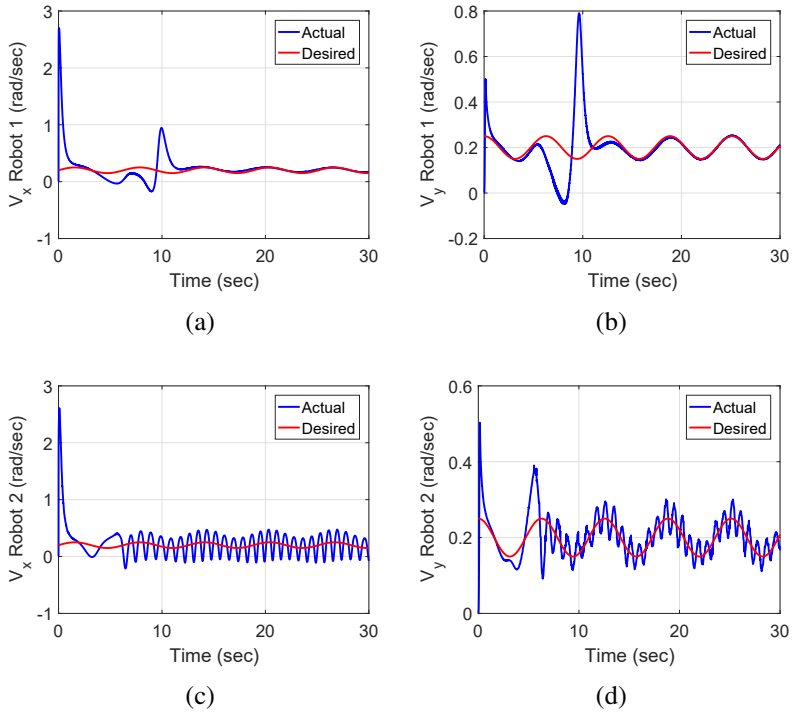

Figure 5.3: Velocity of mobile base in x and y direction

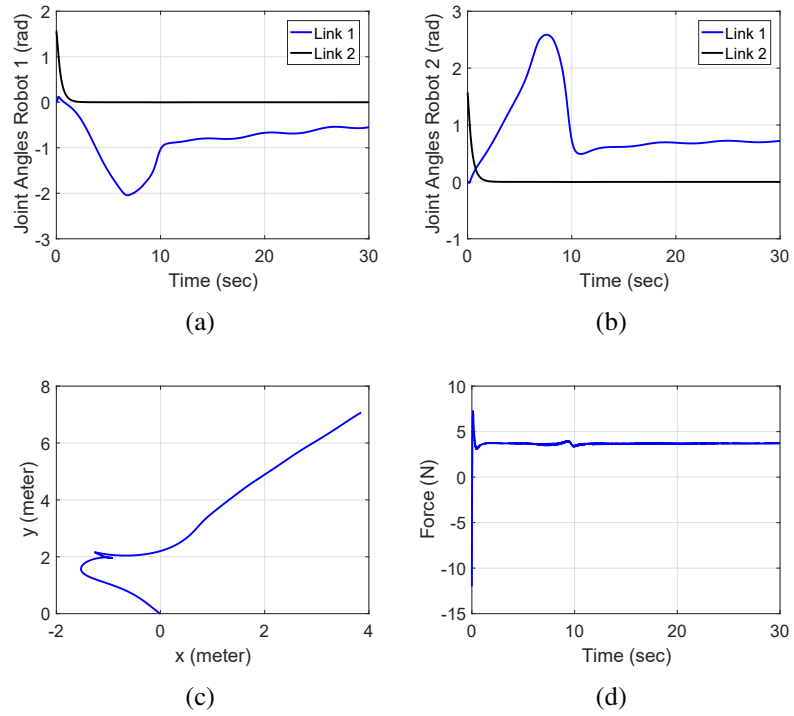

Figure 5.4: Joint angles, object trajectory and internal force

Fig.5.4(a) represents the joint angles of the links of the first manipulator and Fig.5.4(b) represents the joint angles of the links of the second manipulator. Fig.5.4(c) shows the trajectory of the object which is being transported. The effect of the tracking errors on the end-effector position and mobile base velocity of second mobile manipulator is evident from the object's trajectory. The object slightly oscillates when the mobile manipulators move while carrying the object. The internal force of the object is depicted in Fig.5.4(d). As this internal force is greater than zero when the mobile manipulators start moving, we see that the two mobile manipulators are always in contact with the object during the task accomplishment.

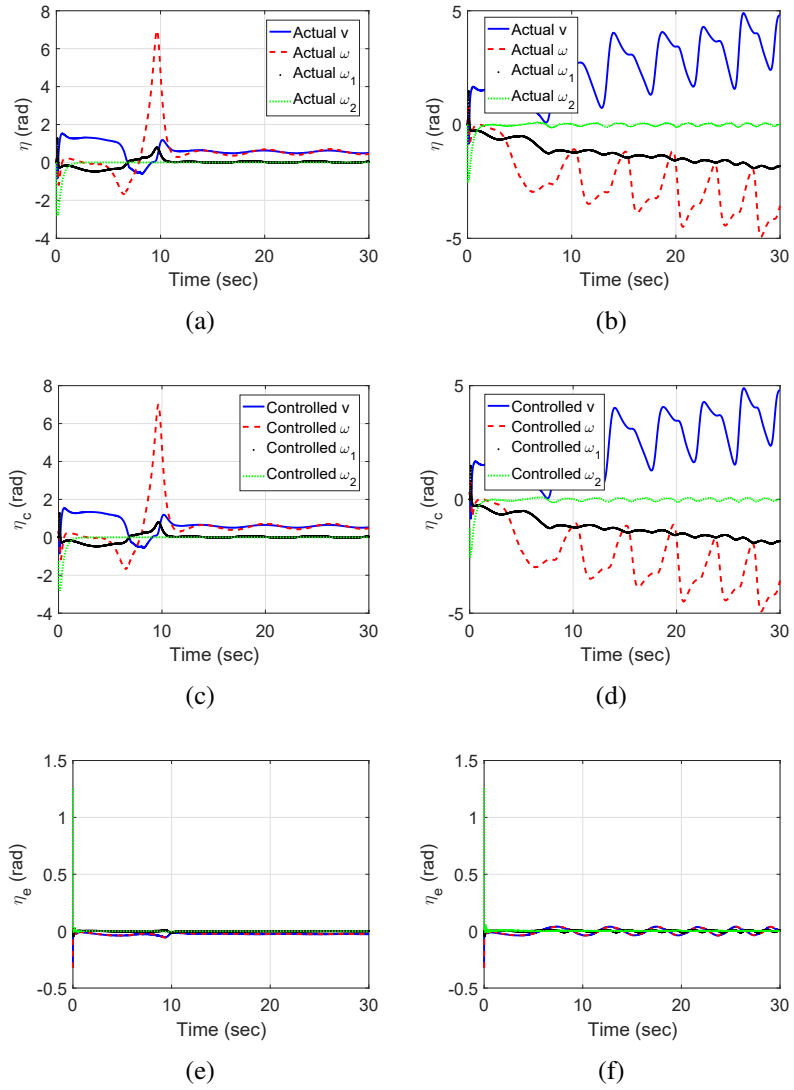

Figure 5.5: Actual velocities, controlled velocities and error

Figs.5.5(a) and 5.5(b) show the actual joint velocities of the the mobile base and the first and second joint of the manipulator arm for both mobile manipulators. Similarly, Figs.5.5(c) and 5.5(d) give the plot of the controlled joint velocities of the mobile base and both joints. From these results, it can be seen that the controlled velocities η_c are the same as that of the actual velocities η. The ultimate goal is to control the joint velocities and it can be clearly identified from both figures that both velocities are same. The errors of these velocities are almost zero as shown in Figs.5.5(e) and 5.5(f).

5.4 Summary

In this chapter, we proposed a novel adaptive control design for the trajectory tracking of the end-effectors of the mobile manipulators to manipulate an object. A two stage controller design approach was adopted where the first step was focused on a kinematic velocity controller for the mobile base/end-effector and the second step provided the torque control for the manipulator joints. Simulations were carried out for a nonholonomic mobile manipulators system with the proposed control design and the results not only verified the guaranteed stability of the system but also provided substantial evidence of the satisfactory trajectory tracking.

Chapter 6

Cooperative Control of Networked Mobile Manipulators

Transportation or manipulation of objects with a team of mobile manipulators is extremely invaluable when the objects are heavy or difficult to manipulate by a single mobile manipulator. This chapter develops a cooperative and coordination control scheme for networked mobile manipulators jointly connected in a graph topology under communication delays for object transportation. The synchronization of the mobile manipulators is achieved with the tracking control and the cooperation control is implemented using decoupled dynamics of the mobile manipulators. An integration of the force control with the synchronization control is adapted to achieve the cooperative transportation of the object which is rigidly attached to the end-effectors of the mobile manipulators. The null space control provides the tracking of the mobile base to follow a desired trajectory. Numerical simulations are carried out to prove the efficacy of the proposed scheme.

The mobility of a robotic manipulator not only maximizes the task generality of the system but also provides an increased task space in structured or unstructured environments. This increase in the manipulation task capabilities of the mobile manipulators outclasses the conventional fixed base robotic manipulators however, this comes at the cost of additional control design challenges. The control algorithms for the mobile manipulators not only have to achieve a task specific criteria but also have to deal with other issues like redundancy resolution and simultaneous or decoupled control of the robotic arm and the mobile base. As we leverage the increased task space and dexterity of the mobile manipulator system, we face the challenges of high dimensionality and complexity in the control design [2, 64, 103].

It must be noted that the performance of a control scheme heavily depends on one's knowledge of the system dynamics including any uncertainty like parametric uncertainties, time delays or payloads. In the aforementioned works, some of the proposed control design do not take into account either time delays or payload. Although adaptation of uncertain or unknown parameters has been well addressed but there is a lack of control schemes

which not only manage to deal with parametric uncertainties but also with time delays and payloads. Only a few control designs have been proposed recently which deal with the force allocation or the load distribution while cooperatively manipulating or transporting the objects with the help of mobile manipulators. Followed from [68, 126, 127, 153–157], we propose a decoupled null space and operational space control for the synchronization of the mobile manipulators transporting an object to a desired position. An adaptive control design is developed to deal with the uncertain parameters of the system. A synchronizing controller is used to achieve the synchronization of the agents communicating over a strongly connected graph while dealing with the time delays. Decoupling of null and operational space provides the decentralized control of the mobile platform and the manipulator arm. A predefined object trajectory is provided to the agents to control the mobile platforms to achieve the main objective of the transportation of the object. The main contributions of this chapter are:

- To propose a cooperative and coordinated control scheme for multiple mobile manipulators communicating over a strongly connected graph.
- To deal with the time delays in the graph topology where the agents seek information from each other to achieve a common goal.
- To implement a sophisticated internal force control methodology satisfying the kinematic constraints of the system.
- To transport the object in a distributed manner where the end-effectors are controlled using dynamic decoupling.

6.1 System Description

The dynamics of a networked system of N mobile manipulators with $i = 1, \ldots N$ can be described in Euler Lagrange (EL) form as follows [65, 86, 112].

$$M_i(q_i)\ddot{q}_i + C_i(q_i,\dot{q}_i)\dot{q}_i + G_i(q_i) + f_i(q_i) = B_i(q_i)\tau_i, \tag{6.1}$$

where $M_i(q_i) \in \mathcal{R}^{n\times n}$ is the inertia matrix which is a symmetric bounded positive definite matrix; $C_i(q_i,\dot{q}_i) \in \mathcal{R}^{n\times n}$ is the Centripetal and Coriolis matrix; $G_i(q_i) \in \mathcal{R}^n$ is the

gravitational force vector; $f_i(q_i) = \begin{bmatrix} f_{in}^T & f_{ih}^T \end{bmatrix}^T = \begin{bmatrix} (A_i^T(q_{ip})\lambda)^T & 0 \end{bmatrix}^T \in \mathcal{R}^n$ is the generalized constraint force or torque, where $\lambda_i = \begin{bmatrix} \lambda_{in} & \lambda_{ih} \end{bmatrix}^T$ is the Lagrangian multiplier, λ_{in} considers the nonholonomic constraint and λ_{ih} considers the holonomic constraints and $A_i(q_{ip})$ is the kinematic constraint matrix. $B_i(q_i) \in \mathcal{R}^{n\times m}$ is a full rank input transformation matrix and also assumed to be known, $\tau_i \in \mathcal{R}^m$ is the control input to the system. $q_i = \begin{bmatrix} q_{ip}^T & q_{ia}^T \end{bmatrix}^T \in \mathcal{R}^n$ is the vector of generalized coordinates. q_{ip} denotes the generalized coordinates of the wheeled mobile platform and q_{ia} denotes the generalized coordinates of the manipulator arm [64]. The terms can be further represented as,

$$M_i(q_i) = \begin{bmatrix} M_{ip} & M_{ipa} \\ M_{iap} & M_{ia} \end{bmatrix}, C_i(q_i,\dot{q}) = \begin{bmatrix} C_{ip} & C_{ipa} \\ C_{iap} & C_{ia} \end{bmatrix}$$
$$G_i(q_i) = \begin{bmatrix} G_{ip} \\ G_{ia} \end{bmatrix},\ B_i(q_i) = \begin{bmatrix} B_{ip} & 0 \\ 0 & B_{ia} \end{bmatrix}, \tau_i = \begin{bmatrix} \tau_{ip} \\ \tau_{ia} \end{bmatrix},$$

where M_{ip} and M_{ia} describe the inertia matrices for the mobile platform and the manipulator arm respectively. M_{ipa} and M_{iap} describe the coupling inertia matrices of the mobile platform and the manipulator arm. C_{ip} and C_{ia} are Centripetal and Coriolis torques for the mobile platform and the manipulator arm respectively. C_{ipa} and C_{iap} are the coupling Centripetal and Coriolis torques of the mobile platform and the manipulator arm. G_{ip} and G_{ia} are the gravitational forces of the mobile platform and the manipulator arm respectively. B_{ip} and B_{ia} denote the input transformation matrices of the mobile platform and the manipulator arm respectively. τ_{ip} and τ_{ia} are the control input of the mobile platform and the robotic arm. Fig.6.1 depicts a general schematic of a mobile manipulator with 2 planar links [153, 154].

$$q_{ip} = \begin{bmatrix} x_i \\ y_i \\ \theta_{ip} \end{bmatrix}, \tag{6.2}$$

where x_i, y_i are the coordinates of the center of the mobile platform and θ_{ip} is the orientation or the heading angle of the mobile platform. The nonholonomic kinematic constraint for the mid point of the wheel axle where the manipulator arm is mounted can be expressed as,

$$\dot{x}_i \sin\theta_{ip} - \dot{y}_i \cos\theta_{ip} = 0. \tag{6.3}$$

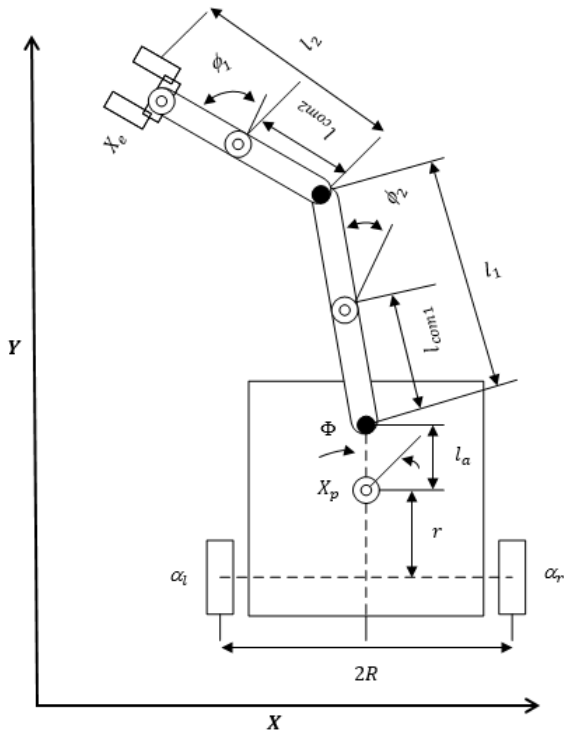

Figure 6.1: A nonholonomic mobile manipulator [153, 154]

The constraint in (6.3) can also be written in the following form,

$$A_i(q_{ip})\dot{q}_{ip} = 0, \tag{6.4}$$

where

$$A_i(q_{ip}) = [\sin\theta_{ip} \quad -\cos\theta_{ip} \quad 0]. \tag{6.5}$$

Suppose there are l numbers of non-integrable and independent velocity constraints and it is assumed to have the full rank l. The mobile platform here is assumed to be completely nonholonomic and we can write $A_i(q_{ip})$ matrix of (6.4) as,

$$A_i(q_{ip}) = \begin{bmatrix} A_1^T(q_{ip}) & A_2^T(q_{ip}) & A_3^T(q_{ip}) & \ldots & A_l^T(q_{ip}) \end{bmatrix}^T.$$

The nonholonomic generalized constraint forces can be given as

$$f_{in} = (A_i^T(q_{ip})\lambda_{in})^T. \tag{6.6}$$

$H_i(q_{ip}) \in \mathcal{R}^{n\times m}$ is a matrix with rank being m formed by a set of smooth and linearly independent vectors spanning the null space of matrix $A_i(q_{ip})$, i.e.

$$H_i^T(q_{ip})A_i^T(q_{ip}) = 0, \tag{6.7}$$

where $H_i(q_{ip}) = [H_1(q_{ip}) \;\; H_2(q_{ip}) \;\; \ldots \;\; H_{n_p-l}(q_{ip})]$. Note that here $H_i^T H_i$ is of full rank. According to (6.4) and (6.7), the first order velocity kinematic model of a nonholonomic mobile platform which is also called the *steering system* can be written in the following form,

$$\dot{q}_{ip} = H_i(q_{ip})\alpha_i, \tag{6.8}$$

where α_i is an auxiliary function $\alpha_i \in \mathcal{R}^2$ and called the *steering velocity* of the kinematic system. α_1 and α_2 are the linear and angular velocities of the wheeled mobile platform and can be written as (6.9) or α_1 and α_2 are the left wheel velocity and the right wheel velocity of the mobile platform and can be written as (6.10),

$$\alpha_i = \begin{bmatrix} v_i & \omega_i \end{bmatrix}^T, \tag{6.9}$$

$$\alpha_i = \begin{bmatrix} \theta_{iR} & \theta_{iL} \end{bmatrix}^T. \tag{6.10}$$

We can rewrite (6.8) in the specific kinematic form, in terms of linear and angular velocities of the wheeled mobile platform and in terms of right and left wheel velocities.

$$\dot{q}_{ip} = \begin{bmatrix} \cos\theta_{ip} & 0 \\ \sin\theta_{ip} & 0 \\ 0 & 1 \end{bmatrix} \begin{bmatrix} v_i \\ \omega_i \end{bmatrix}, \tag{6.11}$$

$$\dot{q}_{ip} = \begin{bmatrix} \frac{R}{2}\cos\theta_{ip} & \frac{R}{2}\cos\theta_{ip} \\ \frac{R}{2}\sin\theta_{ip} & \frac{R}{2}\sin\theta_{ip} \\ \frac{R}{2D} & -\frac{R}{2D} \end{bmatrix} \begin{bmatrix} \theta_{iR} \\ \theta_{iL} \end{bmatrix}, \tag{6.12}$$

where in this work R is the radius of the wheels and D is the distance of the two wheels of the mobile platform.

Let $\eta_i = \begin{bmatrix} \alpha_i^T & \dot{q}_{ia}^T \end{bmatrix}^T$. Due to the nonholonomic constraint defined in (6.4) and (6.8), there exists a vector $\dot{\eta}_i$, such that [65],

$$\dot{q}_i = H_i(q_i)\dot{\eta}_i. \tag{6.13}$$

A reduced dynamic model now can be obtained by substituting (6.13) and its derivative in (6.1) and pre-multiplying $H_i(q_i)^T$,

$$M_{\eta_i}(q_i)\ddot{\eta}_i + C_{\eta_i}(q_i,\dot{q}_i)\dot{\eta}_i + G_{\eta_i}(q_i) = \tau_{\eta_i}, \tag{6.14}$$

where,

$$\begin{cases} M_{\eta_i}(q_i) = H_i^T(q_i)M_i(q_i)H_i(q_i), \\ C_{\eta_i}(q_i,\dot{q}_i) = H_i^T(q_i)[M_i(q_i)\dot{H}_i(q_i) + C_i(q_i,\dot{q}_i)H_i(q_i)], \\ G_{\eta_i}(q_i) = H_i^T(q_i)G_i(q_i), \\ \tau_{\eta_i} = H_i^T(q_i)B_i(q_i)\tau_i. \end{cases}$$

A more specific dynamic model can be described by [64].

$$\begin{bmatrix} H_i^T B_{ip}\tau_{ip} \\ B_{ia}\tau_{ia} \end{bmatrix} = \begin{bmatrix} H_i^T M_{ip}H_i & H_i^T M_{ipa} \\ M_{iap}H_i & M_{ia} \end{bmatrix} \begin{bmatrix} \ddot{\alpha}_i \\ \ddot{q}_{ia} \end{bmatrix}$$

$$+ \begin{bmatrix} H_i^T M_{ip}\dot{H}_i + H_i^T C_{ip}H_i & H_i^T C_{ipa} \\ M_{iap}\dot{H}_i + C_{iap}H & C_{ia} \end{bmatrix} \begin{bmatrix} \dot{\alpha}_i \\ \dot{q}_{ia} \end{bmatrix} + \begin{bmatrix} H_i^T G_{ip} \\ G_{ia} \end{bmatrix}$$

In this work, the mobile manipulators are subjected to the following assumptions.

Assumption 1: The mobile platform is driven with two wheels operated by two independent motors or actuators and the manipulator arm is fixed on this platform.

Assumption 2: The mobile manipulator is considered to be redundant and operating away from singularity.

Assumption 3: It is considered that $\dot{\eta}_i = [\dot{\theta}_{iR} \;\; \dot{\theta}_{iL} \;\; \dot{\theta}_1 \;\ldots\; \dot{\theta}_k]^T$ where $\dot{\theta}_j$ is the angular velocity of the manipulator joints and $j = 1,\ldots k$.

In most of the mobile manipulation applications, the desired trajectory is defined in the task space or operational space. Let X_i contains all the variables which are required to define the task of the end-effector of the mobile manipulator then the kinematic equation of the end-effector can be written as,

$$X_{ma} = f_i(\eta_i), \tag{6.15}$$

where $f_i(.)$ being a nonlinear transformation describes the relation between the joint space of the system and the operational space of the end-effector [65]. The velocity of the end-effector can be derived by differentiating (6.15),

$$\dot{X}_{ma} = J_{ma}(\eta_i)\dot{\eta}_i,$$

where $J_{ma}(\eta_i) = \frac{\partial f_i(\eta_i)}{\partial \eta_i}$ is the non-square Jacobian matrix of the end-effector and is non-invertible due to the redundancy of the system. The redundancy of the system can be utilized to achieve additional tasks. A user defined kinematic function for the motion of the mobile platform can be defined as,

$$X_{mp} = g_i(\eta_i), \tag{6.16}$$

By differentiating (6.16), we have,

$$\dot{X}_{mp} = J_{mp}(\eta_i)\dot{\eta}_i,$$

where the Jacobian matrix is $J_{mp}(\eta_i) = \frac{\partial g_i(\eta_i)}{\partial \eta_i}$. We can use the extended position $X_i = [X_{ma}^T \; X_{mp}^T]^T$ to accomplish the secondary task while simultaneously achieving the primary task. Now the mobile manipulator system has an extended differential kinematic model as given by,

$$\dot{X}_i = \begin{bmatrix} J_{ma}(\eta_i) \\ J_{mp}(\eta_i) \end{bmatrix} \dot{\eta}_i = J(\eta_i)\dot{\eta}_i. \tag{6.17}$$

where $J(\eta_i)$ is the extended square Jacobian matrix of the whole system and for the sake of brevity, we will use J as $J(\eta_i)$. From (6.17), we can have,

$$\dot{\eta}_i = J^{-1}\dot{X}_i, \quad \ddot{\eta}_i = J^{-1}\ddot{X}_i - J^{-1}\dot{J}J^{-1}\dot{X}_i \tag{6.18}$$

We get the extended operational space dynamic equation of the system by substituting (6.18) in (6.14) and premultiplying J^{-T} as follows,

$$M_{x_i}(q_i)\ddot{X}_i + C_{x_i}(q_i,\dot{q}_i)\dot{X}_i + G_{x_i}(q_i) = \tau_{x_i}, \tag{6.19}$$

where,

$$\begin{cases} M_{x_i}(q_i) = J^{-T}M_{\eta_i}(q_i)J^{-1}, \\ C_{x_i}(q_i,\dot{q}_i) = J^{-T}[-M_{\eta_i}(q_i)J^{-1}\dot{J} + C_{\eta_i}(q_i,\dot{q}_i)]J^{-1}, \\ G_{x_i}(q_i) = J^{-T}G_{\eta_i}(q_i), \\ \tau_{x_i} = J^{-T}\tau_{\eta_i}. \end{cases}$$

The extended operational space dynamic model of the mobile manipulator has the following properties which will be used in the controller design and stability analysis [155].

Property 1: The matrix $M_{x_i}(q_i)$ is symmetric positive definite and there exist positive

constants λ_{Mi} and $\bar{\lambda}_{Mi}$ such that $\lambda_{Mi} I_n \leq M_{x_i}(q_i) \leq \bar{\lambda}_{Mi} I_n$, where I_n is an $n \times n$ identity matrix.

Property 2: The nonlinear system dynamics depend linearly on a dynamic parameter vector Θ_i such that $M_{x_i}(q_i)\dot{\xi}_i + C_{x_i}(q_i,\dot{q}_i)\xi_i + G_{x_i}(q_i) = Y_i(q_i,\dot{q}_i,\xi_i,\dot{\xi}_i)\Theta_i$ where $Y_i(q_i,\dot{q}_i,\xi_i,\dot{\xi}_i)$ is called the regressor matrix containing the known functions and $\xi_i \in \mathcal{R}^n$ is a differentiable vector.

Property 3: Under a proper definition of the matrix $C_{x_i}(q_i,\dot{q}_i)$, the matrix $\dot{M}_{x_i}(q_i) - 2C_{x_i}(q_i,\dot{q}_i)$ is skew symmetric such that $\xi_i^T(\dot{M}_{x_i}(q_i) - 2C_{x_i}(q_i,\dot{q}_i))\xi_i = 0$ for all $\xi_i \in \mathcal{R}^n$.

6.2 Coordination Control Design

This section focuses on the development of a synchronization controller for networked mobile manipulators, modelled by (6.14), connected over a communication topology. The synchronized motion is achieved by simultaneously controlling the position of the end-effector X_{ma} and the position of the mobile platform X_{mp}. In this work, the problem of trajectory tracking is considered in the operational space so the desired objective is to design a control law to track a given desired trajectory for the mobile manipulators. A desired trajectory, $X_d = [X_{da}, X_{dp}] \in \mathcal{R}^n$, is considered to be tracked by each mobile manipulator. It is considered that X_d is kinematically well defined and is twice differentiable such that $\dot{X}_d, \ddot{X}_d \in \mathcal{L}_\infty$.

The formation control of the mobile manipulators is also considered here as part of the control design. We assume, $X_{dr} = X_d + \sigma_i$, where $\sigma_i \in \mathcal{R}^n$ is defined as a constant vector for the formation. The reference velocity is defined as $\dot{X}_{ri} = \dot{X}_{dr} - \gamma(X_i - X_{dr})$ and the sliding vector in the operational space is defined as the difference of the extended and reference velocity, $e_{xi} = \dot{X}_i - \dot{X}_{ri}$, where $e_{xi} \in \mathcal{R}^n$. The control torque to each individual system is given by,

$$\begin{aligned} \tau_{xi} &= \hat{M}_{xi}(q_i)\ddot{X}_{ri} + \hat{C}_{xi}(q_i,\dot{q}_i)\dot{X}_{ri} + \hat{G}_{xi}(q_i) - K_i e_{xi} + \tau_{sm} \\ &= Y_i(q_i,\dot{q}_i,\dot{X}_{ri},\ddot{X}_{ri})\hat{\Theta}_i - K_i e_{xi} + \tau_{sm}, \end{aligned} \tag{6.20}$$

where $\hat{M}_{xi}(q_i), \hat{C}_{xi}(q_i,\dot{q}_i)$ and $\hat{G}_{xi}(q_i)$ are the estimates of $M_{xi}(q_i), C_{xi}(q_i,\dot{q}_i)$ and $G_{xi}(q_i)$, K_i is a positive constant gain and τ_{sm} is the control input for synchronous motion and will be defined later. Property 2 is used to obtain the second equality in (6.20). Now the closed

loop system for the ith system can be obtained by substituting (6.20) into (6.19) as,

$$M_{xi}(q_i)\dot{e}_{xi} + C_{xi}(q_i,\dot{q}_i)e_{xi} = Y_i\tilde{\Theta}_i - K_i e_{xi} + \tau_{sm}, \tag{6.21}$$

where $\tilde{\Theta}_i = \hat{\Theta}_i - \Theta_i$ is the error of the dynamic parameter estimation. The adaptive law to update the unknown parameters $\dot{\hat{\Theta}}_i$ is given as,

$$\dot{\hat{\Theta}}_i = -\Gamma_i^{-1} Y_i^T e_{xi}, \tag{6.22}$$

where Γ_i is a constant positive definite matrix.

In the proposed framework, the mobile manipulators are assumed to be sharing the information, the signal e_{xi}, to their neighbours. As the system is considered to be connected over a strongly connected graph which is fixed, the synchronous motion control input is designed as,

$$\tau_{sm} = \sum_{j\in\mathcal{N}_i} \frac{w_{ij}}{d_i}[e_{xj}(t-T_d) - e_{xi}(t)], \tag{6.23}$$

where $\mathcal{N}_i$ is a set of all the agents, d_i is the in-degree of the ith mobile manipulator and T_d is the positive bounded time delay for signal communication among the agents. The assumptions which are made for this part of the controller design are as follows.

Assumption 4: The constant communication delay T_d is not known to the controllers and is same for all the links.

Assumption 5: The weights w_{ij} for the exchanged signals are considered to be the same. Now we address the first result of the coordinated control of the mobile manipulators.

Theorem 1: Consider a network of multiple nonholonomic mobile manipulators modelled by (6.19) *with the control laws* (6.20) *and* (6.22)*. Under a strongly connected graph and synchronous motion control* (6.23)*, all the mobile manipulators achieve the synchronous motion and follow a desired trajectory.*

Proof: Consider the Lyapunov Krasovskii functional candidate as,

$$V = \sum_{i\in N_j,N_n} [\frac{1}{2}e_{xi}^T M_{xi} e_{xi} + \frac{1}{2}\tilde{\Theta}_i\Gamma_i\tilde{\Theta}_i + \frac{1}{2}w_{ij}\int_{t-T_d}^{t} e_{xi}^T(\sigma)e_{xi}(\sigma)d\sigma]. \tag{6.24}$$

Let $V_i = \frac{1}{2}e_{xi}^T M_{xi} e_{xi} + \frac{1}{2}\tilde{\Theta}_i\Gamma_i\tilde{\Theta}_i$ and N_j, N_n are the sets of the connected and disconnected agents in the communication topology. Taking the time derivative of V along the trajectories of (6.20), (6.22) and (6.23), we get,

$$\dot{V} = \sum_{i\in N_j,N_n} [-K_i e_{xi}^T e_{xi} + e_{xi}^T\tau_{sm} + \frac{1}{2}w_{ij}(e_{xi}^T(t)e_{xi}(t) - e_{xi}^T(t-T_d)e_{xi}(t-T_d))] \tag{6.25}$$

As in the strongly connected graph we only have the set of connected agents as N_j, then

$$\begin{aligned}\dot{V}_{N_j} &= \sum_{i\in N_j}[-K_i e_{xi}^T e_{xi} - \sum_{i\in\mathcal{N}_i}\frac{w_{ij}}{d_i}e_{xi}^T(e_{xi}(t)-e_{xj}(t-T_d)) + \frac{w_{ij}}{2}e_{xi}^T(t)e_{xi}(t) \\ &\quad -e_{xi}^T(t-T_d)e_{xi}(t-T_d)]. \end{aligned} \tag{6.26}$$

Let $w_{ij}=\lambda_s$, then

$$\begin{aligned}\dot{V}_{N_j} &= -\sum_{i\in N_j}K_i e_{xi}^T e_{xi} + \sum_{i\in N_j}\sum_{j\in\mathcal{N}_i}(\frac{\lambda_s}{d_i}e_{xi}^T(e_{xj}(t-T_d)-e_{xi}(t))) + \frac{\lambda_s}{2}\sum_{i\in N_j}(e_{xi}^T(t)e_{xi}(t) \\ &\quad -e_{xi}^T(t-T_d)e_{xi}(t-T_d)). \end{aligned} \tag{6.27}$$

As the communication delay is same for all the robots, the last term in (6.27) can be written as, $\sum_{i\in N_j}(e_{xi}^T(t)e_{xi}(t)-e_{xi}^T(t-T_d)e_{xi}(t-T_d)) = \sum_{i\in N_j}\sum_{i\in\mathcal{N}_i}(e_{xi}^T(t)e_{xi}(t)-e_{xj}^T(t-T_d)e_{xj}(t-T_d))/d_i$.

Hence, (6.27) can be written as,

$$\dot{V}_{N_j} = -\sum_{i\in N_j}(K_i\|e_{xi}\|^2 - \sum_{i\in\mathcal{N}_i}\frac{\lambda_s}{2d_i}\|e_{xi}(t)-e_{xj}(t-T_d)\|^2 \leq 0. \tag{6.28}$$

Finally, $\dot{V}=\dot{V}_{N_j}\leq 0$ then $V(t)\leq V(0)$ for $t\geq 0$. So we can conclude that $e_{xi},\hat{\Theta}_i\in\mathcal{L}_\infty$ and $e_{xi}, e_{xi}(t)-e_{xi}(t-T_d), e_{xj}(t)-e_{xj}(t-T_d)\in\mathcal{L}_2$. Using, $e_{xi}=\dot{X}_i-\dot{X}_{ri}=(\dot{X}_i-\dot{X}_{dr})+\gamma(X_i-X_{dr})$ and $e_{xi}\in\mathcal{L}_2$, which means that $X_i-X_{dr}\in\mathcal{L}_2\cap\mathcal{L}_\infty, \dot{X}_i-\dot{X}_{dr}\in\mathcal{L}_2$ and $lim_{t\to\infty}X_i(t)-X_{dr}(t)=0$ [40]. This concludes that all the agents keep a formation while following a desired trajectory in the operational space. By the definition of $\dot{X}_{ri}$, we have $\dot{X}_{ri},\ddot{X}_{ri}\in\mathcal{L}_\infty$. As $\dot{X}_{ri},\ddot{X}_{ri},e_{xi},\dot{e}_{xi}\in\mathcal{L}_2$ with the definition of e_{xi}, we obtain that $\dot{X}_i,\ddot{X}_i\in\mathcal{L}_\infty$. Again, as $e_{xi}\in\mathcal{L}_\infty$, it is achieved that $\tau_{sm}\in\mathcal{L}_\infty$. Now from (6.21), Property 1 and above mentioned bounded signals, we can obtain $\dot{e}_{xi}\in\mathcal{L}_\infty$. From $\dot{V}$, we have $\ddot{V}\in\mathcal{L}_\infty$ as $\dot{e}_{xi}$ is bounded and the delays are constant. Therefore, using Lemma 2 [155], we get that $\dot{V}\to 0$ as $t\to\infty$, which leads to the result that $e_{xi}, e_{xi}(t)-e_{xi}(t-T_d), e_{xj}(t)-e_{xj}(t-T_d)\to 0$ as $t\to\infty$ for $i\in\mathcal{V}, j\in\mathcal{N}_i$. With the results mentioned above, we have $x_i(t)-x_j(t)\to 0, \dot{x}_i(t)-\dot{x}_j(t)\to 0$ as $t\to\infty$ for all $i\in\mathcal{V}, j\in\mathcal{N}_i$. Therefore, all the agents in the network achieve synchronized motion while keeping a formation in the operational space given a desired trajectory.

6.3 Cooperation Control Design

The coordination control designed in the previous section provides the motion control of the mobile manipulators given a desired trajectory of the mobile platform and the end-effector. Although, the controller designed previously guarantees the stability and tracking

under time delays, we design a cooperative controller in this section to make the overall control of the systems more flexible. The main objective of the cooperative controller is to transport the object to a desired point cooperatively. We take advantage of the decoupling of the operational and null space of the mobile manipulators to design this controller [153]. The motion of the mobile manipulators is decoupled in the operational space (end-effector) and the null space (mobile platform). This decoupling of the operational and null space allows the prioritization of the tasks in the event of a disagreement between the operational and null space.

6.3.1 Decoupling of Null and Operational Space

Assuming that the operational space consists of the x-y coordinates of the end-effector, from (6.17), we have the general solution of the velocity as,

$$\dot{\eta}_i = J^{\star}(\eta_i)\dot{X}_{ma} + N_i\dot{\eta}_i, \tag{6.29}$$

where $J^{\star}(\eta_i)$ is the pseudo inverse of $J(\eta_i)$ and $N_i = I - J^{\star}(\eta_i)J(\eta_i)$ is the null space. Differentiating (6.29),

$$\ddot{\eta}_i = J^{\star}(\eta_i)\ddot{X}_{ma} + \dot{J}^{\star}(\eta_i)\dot{X}_{ma} + N_i\ddot{\eta}_i + \dot{N}_i\dot{\eta}_i. \tag{6.30}$$

A weighted pseudo inverse can be defined as,

$$J^{\circ} = M_{\eta_i}^{-1}J^T(JM_{\eta_i}^{-1}J^T)^{-1}. \tag{6.31}$$

Now, the input torque and the operational space force relation can be given as,

$$\tau_{\eta_i} = J^T f_{io} + N_i^T \tau_{j_i}, \tag{6.32}$$

where f_{io} is the operational space force and τ_{j_i} is the vector of joint torques. Under this decoupling, the acceleration in the operational space is not affected by the torque in the null space. Considering $J^{\star} = J^{\circ}$, the null space can be rewritten as $N_i^{\circ} = I - J^{\circ}J$.

Now by defining f_{ei} as the external forces acting on the mobile manipulator, (6.14) can be rewritten as,

$$M_{\eta_i}(q_i)\ddot{\eta}_i + C_{\eta_i}(q_i,\dot{q}_i)\dot{\eta}_i + G_{\eta_i}(q_i) = \tau_{\eta_i} + f_{ei}. \tag{6.33}$$

Using (6.29), (6.30) along with $I = J^T(\eta_i)J^{\star T}(\eta_i) + N_i$, (6.33) becomes,

$$J^T f_{io} + N_i^T \tau_{j_i} = T_1 + T_2 + T_3, \tag{6.34}$$

where T_1, T_2, T_3 are the terms defined as [153],

$$T_1 = J^T J^{\circ T}(M_{\eta_i}(q_i)J^{\circ}(\ddot{X}_{ma} - \dot{J}\dot{\eta}_i) + C_{\eta_i}(q_i,\dot{q}_i)\dot{\eta}_i + G_{\eta_i}(q_i) - f_{ei}),$$

T_1 is containing all the operational space forces.

$$T_2 = N_i^T(M_{\eta_i}(q_i)N_i\ddot{\eta}_i + (C_{\eta_i}(q_i,\dot{q}_i)\dot{\eta}_i + G_{\eta_i}(q_i)) - f_{ei}),$$

T_2 is containing all the null space torques and,

$$T_3 = (J^T J^{\circ T} M_{\eta_i}(q_i)N_i\ddot{\eta}_i + N_i^T M_{\eta_i}(q_i)J^{\circ}(\ddot{X} - \dot{J}\dot{\eta}_i)),$$

T_3 is containing all the coupling torques and forces.

The decoupling of the internal and end-effector motion can be obtained by letting $T_3 = 0$ so that $J^{\circ T} M_{\eta_i}(q_i)N_i\ddot{\eta}_i = 0$ and $N_i^T M_{\eta_i}(q_i)J^{\circ} = 0$ [158]. As J° in (6.31) is dynamically consistent so the above equations are always satisfied. The substitution of (6.29) and (6.30) into (6.33) with the premultiplication of $J^{\circ T}$ and using (6.31), the decoupling of (6.19) can be obtained as,

$$M_{x_i}^{\circ}(q_i)\ddot{X}_{ma} + C_{x_i}^{\circ}(q_i,\dot{q}_i)\dot{X}_{ma} + G_{x_i}^{\circ}(q_i) = F_i^{\circ} + F_e^{\circ}, \tag{6.35}$$

where,

$M_{x_i}^{\circ}(q_i) = J^{\circ T} M_{\eta_i}(q_i)J^{\circ}$, $C_{x_i}^{\circ}(q_i,\dot{q}_i)\dot{X} = J^{\circ T} C_{\eta_i}(q_i,\dot{q}_i)\dot{\eta}_i - M_{x_i}^{\circ}(q_i)\dot{J}\dot{\eta}_i$, $G_{x_i}^{\circ}(q_i) = J^{\circ T} G_{\eta_i}(q_i)$, $F_i^{\circ} = J^{\circ T}\tau_{\eta_i}$ and $F_e^{\circ} = J^{\circ T} f_{ei}$.

The control input to decouple the operational and null space now can be designed as,

$$\begin{aligned}\tau_{\eta_i} &= J^T M_{x_i}^{\circ}(q_i)(u_{Oi} - \dot{J}\dot{\eta}_i) + C_{\eta_i}(q_i,\dot{q}_i)\dot{\eta}_i + J^T F_e^{\circ} \\ &\quad + N_i^{\circ T} M_{\eta_i}(u_{Ni} + \dot{J}^{\circ}\dot{X}_{ma}) + G_{\eta_i}(q_i),\end{aligned} \tag{6.36}$$

where u_{Oi} and u_{Ni} are the operational and null space control inputs respectively. The substitution of (6.36) into (6.35) with the premultiplication of the controller with $JM_{\eta_i}^{-1}(q_i)$ gives the operational space closed loop dynamics as,

$$u_{Oi} = \ddot{X}_{ma}. \tag{6.37}$$

Now, by premultiplying (6.35) with $\bar{N}M_{\eta_i}^{-1}(q_i)$ for τ_{η_i}, the null space can be given as,

$$-\bar{N}\ddot{\eta}_i + \bar{N}u_{Ni} + \bar{N}\dot{J}^{\circ}\dot{X}_{ma} = -\bar{N}M_{\eta_i}^{-1}(q_i)\bar{N}^T f_{ei}. \tag{6.38}$$

From this we have that $\bar{N}^T f_{ei} = \bar{N}^T J^T F_e^\circ = (J\bar{N})F_e^\circ = 0$ [127]. Hence, (6.38) can be rewritten as,

$$\ddot{\eta}_i = \dot{J}^\circ \dot{X}_{ma} + u_{Ni}. \tag{6.39}$$

As we have achieved the decoupled dynamics in (6.37) and (6.39), the distributed coordination control can easily be designed in the null and operational space.

6.3.2 Null Space Control

The additional objective of keeping a formation of the mobile manipulators can be achieved in the null space by controlling the position of the mobile platform. The input command for the mobile platform wheels and the arm joints can be considered as the null space controller in (6.39),

$$u_{Ni} = [\tau_{pi} \quad \tau_{ai}]^T. \tag{6.40}$$

It should be noted that as the end-effector is being controlled by u_{Oi}, we make $\tau_{ai} = 0$. As in [154], the equations of motion of the mobile platform with the kinematic constraints take the form,

$$M_{\eta_{pi}} \ddot{\eta}_{pi} + C_{\eta_{pi}} \dot{\eta}_{pi} = B_{\eta_{pi}} \tau_{pi}, \tag{6.41}$$

where $M_{\eta_{pi}} = H_{pi}^T M_{pi} H_{pi}$, $C_{\eta_{pi}} = H_{pi}^T (C_{pi} H_{pi} + M_{pi} \dot{H}_{pi}$ and $B_{\eta_{pi}} = H_{pi}^T B_{pi}$. Now τ_{pi} can be designed as,

$$\tau_{pi} = B_{\eta_{pi}}^{-1} M_{\eta_{pi}} u_{\eta_{pi}} + B_{\eta_{pi}}^{-1} C_{\eta_{pi}} \dot{\eta}_{pi}, \tag{6.42}$$

where $u_{\eta_{pi}} = J_{pi}^{-1}(u_{pi} - \dot{J}_{pi}\dot{\eta}_i)$ is defined as the change in the control input for the mobile platform in the null space. It should be noted that the subscripts mp and pi are being used interchangeably in this work for the mobile platform. Now u_{pi} can be designed as,

$$u_{pi} = \ddot{X}_{pi}. \tag{6.43}$$

The mobile platform can be controlled to track a desired trajectory X_{pi}^d with the controller $u_{pi} = \ddot{X}_{pi}^d + k_{pv}(\dot{X}_{pi}^d - \dot{X}_{pi}) + k_{bp}(X_{pi}^d - X_{pi})$ where k_{pv} and k_{bp} are positive control gains. The error dynamics $\ddot{e}_{pi} = -k_{pv}\dot{e}_{pi} - k_{bp}e - pi$ when $e_{pi} = X_{pi} - X_{pi}^d$ are stable and the mobile base can track X_{pi}^d without any effect on the task space control. As we consider different scenarios for the formation control and consensus of mobile manipulators, one of the scenarios is to have the velocity consensus of the agents. For this case, the control input

can be defined as,

$$u_{pi} = \sum_{j \in \mathcal{N}_i} \frac{w_{ij}}{d_i} [\dot{X}_{pj}(t - T_d) - \dot{X}_{pi}] = u_{pi_v}. \tag{6.44}$$

The results of the null space coordination control are presented next.

Theorem 2: Consider the null space dynamics in (6.39) *and the mobile platform dynamics in* (6.41) *with the control inputs* (6.40) *and* (6.42)*. The controller* (6.44) *guarantees the velocity consensus of the mobile base of the agents.*

Proof: Consider a positive semi-definite functional candidate as,

$$V = \sum_{i \in N_j, N_n} [\frac{1}{2} \dot{X}_{pi}^T \dot{X}_{pi} + \frac{1}{2} w_{ij} \int_{t-T_d}^{t} \dot{X}_{pi}^T(\sigma) \dot{X}_{pi}(\sigma) d\sigma]. \tag{6.45}$$

Taking time derivative of V along (6.43) and (6.44), we get

$$\dot{V} = \sum_{i \in N_j, N_n} [\dot{X}_{pi}^T u_{pi_v} + \frac{1}{2} w_{ij} (\dot{X}_{pi}^T(t) \dot{X}_{pi}(t) - \dot{X}_{pi}(t - T_d)^T \dot{X}_{pi}(t - T_d)]. \tag{6.46}$$

By following the proof of *Theorem 1* and using (6.44), we get

$$\dot{V}_{N_j} = -\frac{\lambda_s}{2d_i} \sum_{i \in N_j} \sum_{j \in N_n} \|\dot{X}_{pj}(t - T_d) - \dot{X}_{pi}(t)\|^2 \leq 0.$$

Hence, $\dot{V} = \dot{V}_{N_j} \leq 0$. Again following *Theorem 1*, we conclude that all the mobile platform velocities match such that the $lim_{t \to \infty}(\dot{X}_{pi}(t - T_d) - \dot{X}_{pi}(t)) = 0$.

6.3.3 Operational Space Control

The cooperative transportation of an object can be achieved by the force and motion control in the operational space of the mobile manipulators.

Assumption 6: The end-effectors are rigidly connected to the object so there is no relative motion and the grasp pose of each manipulator remains constant during the manipulation task.

According to Assumption 6 mentioned above, the constraints description related to the coordinate frames is depicted in Fig.6.2 [157]. We consider the object model as in [156, 157, 159],

$$M_o \ddot{X}_o + C_o = h_o, \tag{6.47}$$

where X_o is the position of the object, h_o is the resultant wrench from the end-effector and is comprised of the corresponding forces and torques $h_o = [f_o^T, \tau_o^T]^T$ and M_o, C_o are given

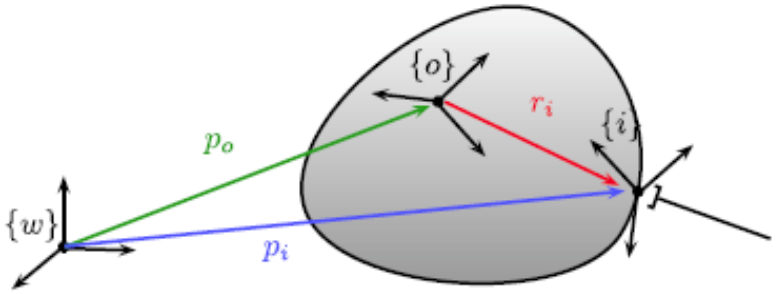

Figure 6.2: The coordinate system [157]

as,

$$M_o = \begin{bmatrix} m_o I_3 & 0_3 \\ 0_3 & I_o \end{bmatrix}, \quad C_o = \begin{bmatrix} -m_o g \\ w \times I_o w \end{bmatrix},$$

where m_o and I_o are the mass and inertia of the object respectively. I_3 is an identity matrix of dimensions 3×3 and 0_3 is the null matrix of dimension 3×3. The desired trajectory of the object is given by

$$M_o^d \ddot{X}_o^d + C_o^d = h_d + h_{env}, \tag{6.48}$$

where $\ddot{X}_o^d$ is the desired acceleration of the object, h_{env} is the environmental or external wrench and h_d is defined as,

$$h_d = a_d \ddot{X}_o^d - b_d(\dot{X}_o - \dot{X}_o^d) - c_d(X_o - X_o^d),$$

with a_d, b_d and c_d being the constant positive gains. From (6.48) we have,

$$\ddot{X}_o^d = M_o^{d^{-1}}(h_d + h_{env} - C_o^d).$$

Now the resultant wrench of the object can be written as,

$$h_o^d = C_o - h_{env} + M_o[M_o^{d^{-1}}(h_d + h_{env} - C_o^d)]. \tag{6.49}$$

For the internal force/torque control or load distribution, there have been some research presenting conflicting results on the allocation of unique or non-unique load distribution related to the internal wrencehs [160, 161]. In this work, the force control for the object is achieved by following the approach of [156] which suggests that there is no unique solution to the load distribution yielding no internal wrenches. The kinematic constraints have been taken into consideration to define the internal wrenches and the grasp transformation matrix. We only mention the relationship of the manipulator wrenches and the grasp

transformation matrix as,

$$h_o = G\left[h_1 \ ... \ h_N\right]^T, \tag{6.50}$$

where h_i is comprised of the corresponding forces and torques $h_i = [f_i^T, \tau_i^T]^T$ and G is the grasp matrix or grip transformation matrix which is explicitly dependent on the kinematic parameters. The vector which contains all the end-effector wrenches is given as $h = [h_1^T \ ... \ h_N^T]^T$.

Definition 1: The end-effector wrenches are considered internal wrenches which generate zero virtual work for any virtual displacement of the end-effector meeting the kinematic constraints.

From this definition, without any ambiguity, we conclude that the internal wrenches are those end-effector wrenches which do not contribute to the motion of the object. It should also be noted that the wrenches which belong to the null space of the grasp matrix G have a total virtual work equal to zero with any virtual displacement meeting the constraints. So, a set of potential end-effector wrenches can be found given a desired wrench h_o^d to be applied to the object. A generalized inverse of grip transformation matrix G^* can be expressed as,

$$\left[h_1^d \ ... \ h_N^d\right]^T = G^* h_o^d. \tag{6.51}$$

The desired motion of the end-effector $\dot{X}_{ma}^d$ can be determined if we have the desired motion of the object $\dot{X}_o^d$ by,

$$\dot{X}_{ma}^d = G^T \dot{X}_o^d, \tag{6.52}$$

where $\dot{X}_{ma}^d = [(\dot{X}_1^d)^T \ ... \ (\dot{X}_N^d)^T]$. It is clear that having $\dot{X}_{ma}^d$, individual manipulators will be able to do proper integration and derivation to calculate X_{ma}^d and $\ddot{X}_{ma}^d$.

Theorem 3: Consider the object dynamics in (6.47) *with the assumption that the grasp matrix G and the inertia of the object M_o are known. Then, from* (6.51) *and* (6.52) *we achieve the tracking for the cooperative manipulation as given in* (6.53) *without having internal wrenches.*

$$h_o(t) = h_o^d(t) \qquad \dot{X}_o(t) = \dot{X}_o^d(t) \tag{6.53}$$

Proof: From (6.52), we have $\forall i : X_{ma}(t) = X_{ma}^d(t)$ which means that $\dot{X}_{ma} = \dot{X}_{ma}^d$ and $\ddot{X}_{ma} = \ddot{X}_{ma}^d$ meet the kinematic constraints. Combining (6.50) and (6.51) gives an expression of the object wrench as,

$$h_o = GG^* h_o^d. \tag{6.54}$$

where GG^* is an identity matrix. If we substitute this result in object dynamics (6.47) and choose $h_o^d = M_o\ddot{X}_o^d + C_o\dot{X}_o^d$, then this gives us $\ddot{X}_o(t) = \ddot{X}_o^d$ which means that $X_o(t) = X_o^d(t)$ for $X_o^d(0) = X_o(0)$ and $\dot{X}_o^d(0) = \dot{X}_o(0)$. This concludes that the motion of the manipulators meets the kinematic constraints so no internal wrenches are applied to the object [157] [1]. Then, in order to have the cooperative force control, an operational space reference velocity is defined as,

$$\dot{v}_{ri} = \dot{X}_{ma}^d - k_a(X_{ma} - X_{ma}^d) - k_b(h_i - h_i^d). \tag{6.55}$$

where k_a, k_b are the positive constants, X_{ma}^d is the desired trajectory for the end-effectors, h_i is the wrench from the sensors and h_i^d is the desired wrench to be exerted by the end-effector. The desired trajectory X_{ma}^d is similar to X_{dr} as,

$$X_{ma}^d = X_o^d + \sigma_i.$$

An operational space sliding vector for the control design is defined as $\delta_i = \dot{X}_{ma} - \dot{v}_{ri}$ and now the control input can be designed as,

$$u_{Oi} = \ddot{v}_{ri} + u_{Oi_f} - p\delta_i, \tag{6.56}$$

where u_{Oi_f} is designed as,

$$u_{Oi_f} = \sum_{j \in \mathbb{N}_i} \frac{w_{ij}}{d_i}[\delta_j(t - T_d) - \delta_i(t)]. \tag{6.57}$$

The closed loop dynamics now can be obtained by substituting (6.56) into (6.37) as,

$$\dot{\delta}_i = u_{Oi_f} - p\delta_i. \tag{6.58}$$

The results of operational space cooperative control are presented next.

Theorem 4: Consider the operational space dynamics in (6.37)*, when the object is being manipulated by the desired force, the operational space control* (6.56) *achieves the desired position of the end-effector.*

Proof: Consider a Lyapunov Krasovskii functional candidate as,

$$V = \sum_{i \in N_j, N_n} [\frac{1}{2}\delta_i^T\delta_i + \frac{1}{2}w_{ji}\int_{t-T_d}^{t} \delta_i^T(\sigma)\delta_i(\sigma)d\sigma] \tag{6.59}$$

Following *Theorem 1*, we see that as $t \to \infty$, $\delta_i - \delta_i(t - T_d) \to 0$ and $\delta_i - \delta_j(t - T_d) \to 0$. Subsequently, as $t \to \infty$, $u_{Oi_f} \to 0$, which means that according to (6.58) if δ_i is bounded then $lim_{t\to\infty}\delta_i(t) = 0$, then $lim_{t\to\infty}(\dot{X}_{ma}(t) - \dot{v}_{ri}(t)) = 0$.

[1] For more details on the internal wrenches and grasp analysis, readers are referred to [156, 157].

6.4 Simulation Results

This section presents the simulation results of three mobile manipulators for the desired trajectory tracking based on the controller designed in the previous sections. Fig.6.3 shows the simulation scenario of the mobile manipulators manipulating a common object [153]. The simulation parameters are given in Table 6.1 [149]. Consider the given mobile manipulator system of (6.19) for which the time dependent desired trajectory for the mobile platform and the end-effector $\left[\dot{x}_{di}, \dot{y}_{di}, x_{EEdi}, y_{EEdi}, z_{EEdi}\right]^T$ is selected as,

$$\begin{cases} \dot{x}_{di} & = 0.1 + 0.05\sin t \\ \dot{y}_{di} & = 0.1 + 0.05\cos t \\ x_{EEdi} & = 0.1t - 0.05\cos t + 0.05 + 1 \\ y_{EEdi} & = 0.1t + 0.05\sin t + 1 \\ z_{EEdi} & = 0. \end{cases}$$

The initial conditions for the mobile manipulators are $[0\,0\,0\,0\,1]$, $[0\,0\,0\,0\,1]$ and $[0\,0\,0\,1\,1.05]$.

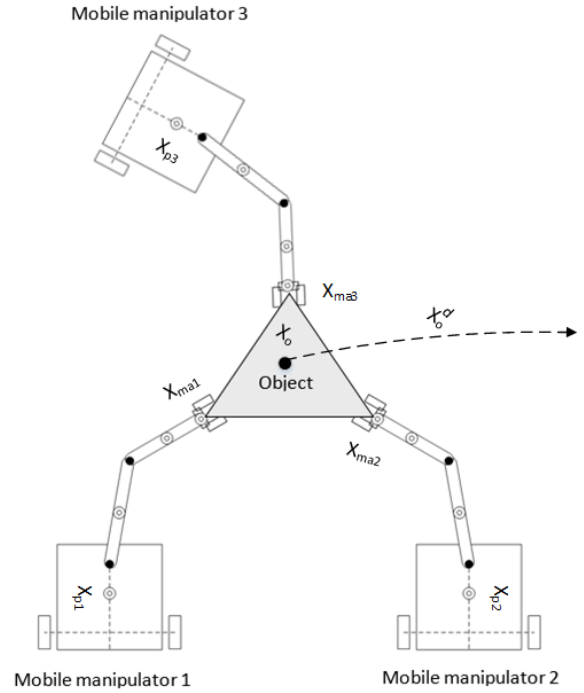

Figure 6.3: A general scenario of the mobile manipulators holding an object

The controller gains k_a and k_b are chosen to be 2 and 8 respectively. The parameters

of the object are $m_o = 20\ kg$ and $I_o = 4\ kgm^2$ where $M_o = diag[m_o, m_o, m_o, I_o]$, $C_o = diag[0,0,0,0]$ [86] and the desired object trajectory is with deviation of mobile platforms $\sigma_i = [1/2\sqrt{3}, 0.5], [-1/\sqrt{3}, 0], [1/2\sqrt{3}, 0.5]\ m$, for the end-effectors and similarly σ_i for all three mobile platforms is $[1/2\sqrt{3}, 1.1], [-1/\sqrt{3}+0.9, 0], [1/2\sqrt{3}, -1.1]\ m$. The control gains K_i and Γ_i are chosen to be 100 and $20I$.

Table 6.1: Simulation Parameters

	Value		Value
Mass of platform	32 kg	Mass of link 1	3 kg
Mass of link 2	3 kg	Inertia of platform	1 kgm^2
Inertia of link 1	1 kgm^2	Inertia of link 2	1 kgm^2
Radius of wheel	0.5 m	Length of link 1	1.5 m
Length of link 2	1.5 m	Gravitational force	9.8 ms^{-2}

6.4.1 Simulation Scenario 1

The simulation considers the communication topology $\mathcal{G}_1$ as in Fig.6.4 where the Laplacian matrix is given by $\mathcal{L} = [1\ 0\ -1; -1\ 1\ 0; 0\ -1\ 1]$. The in-degree d_i and the weights w_{ij} are

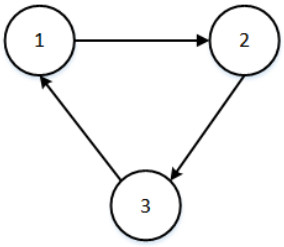

Figure 6.4: Graph topology $\mathcal{G}_1$.

chosen to be 1. The agents are strongly connected over a communication topology and the delay T_d is considered to be 0.5 s. The main objective is to transport the object to a desired position following a desired trajectory while the end-effectors grasp the object rigidly. As discussed in previous sections, a reference velocity is designed for the agents to accomplish the transportation task. Figs.6.5(a),6.5(c) and 6.5(e) represent the end-effector errors of the mobile manipulators. It is evident from these results that under the proposed control with time delays, the networked mobile manipulators are stable. The system achieves the primary goal of the transportation of the object over a predefined trajectory.

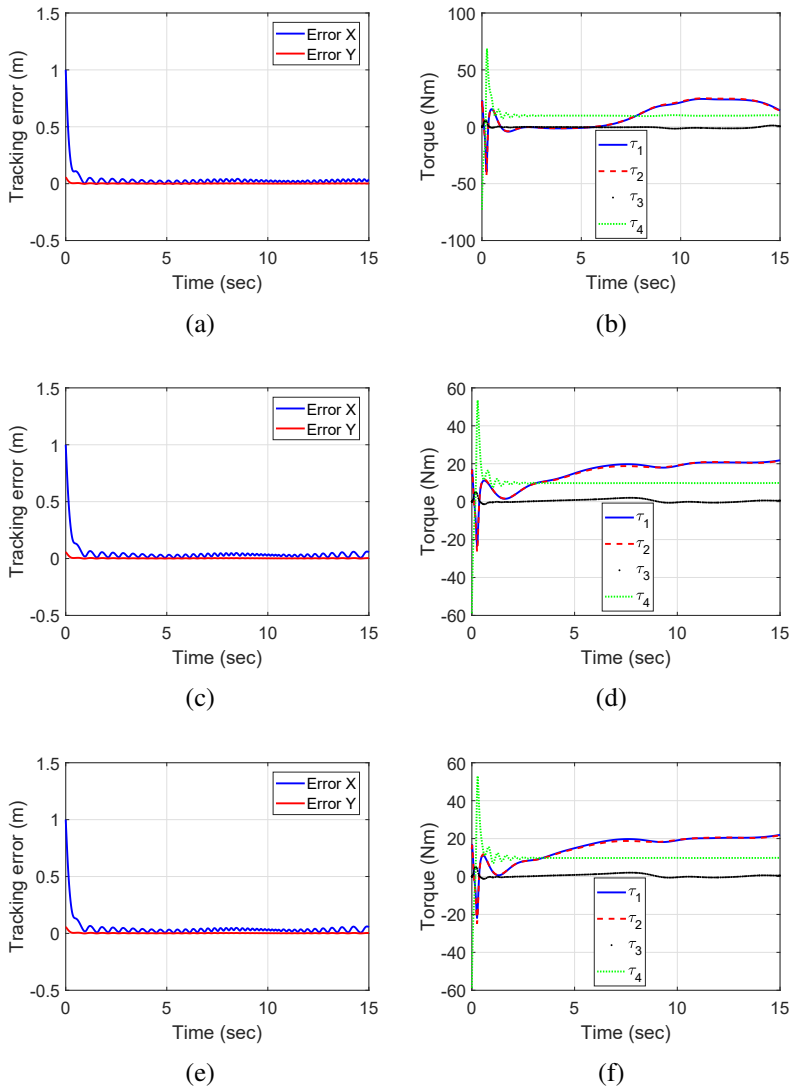

Figure 6.5: End-effector errors and actuator torques

Figs.6.5(b), 6.5(d) and 6.5(f) depict the actuator torques of the agents. Figs.6.6(a), 6.6(c) and 6.6(e) show the errors of the mobile platforms of the mobile manipulators while executing the task. As the priority is to deliver the object to a specified position, the platforms regulate or adjust their positions accordingly and thus exhibiting some errors in the position. Moreover, the controller for the mobile platforms is implemented only in the null space so the errors in the position are normal. Figs.6.6(b), 6.6(d) and 6.6(f) present the errors of the sliding vector and it is observed that the errors converge to almost zero as desired in the control design. The first 5 seconds simulation results for the sliding vector errors are shown in Figs.6.7(a), 6.7(b) and 6.7(c) for three mobile manipulators. It can be seen that

the errors are quite small although not exactly zero. For agent 1, the sliding error e_x is not greater than 0.02 and same is the case with agent 2 and agent 3. Fig.6.7(d) shows the object trajectory errors. The object closely follows the predefined trajectory and achieves the desired position. Figs.6.8 and 6.9 show the end-effector positions of all three agents at 4 s

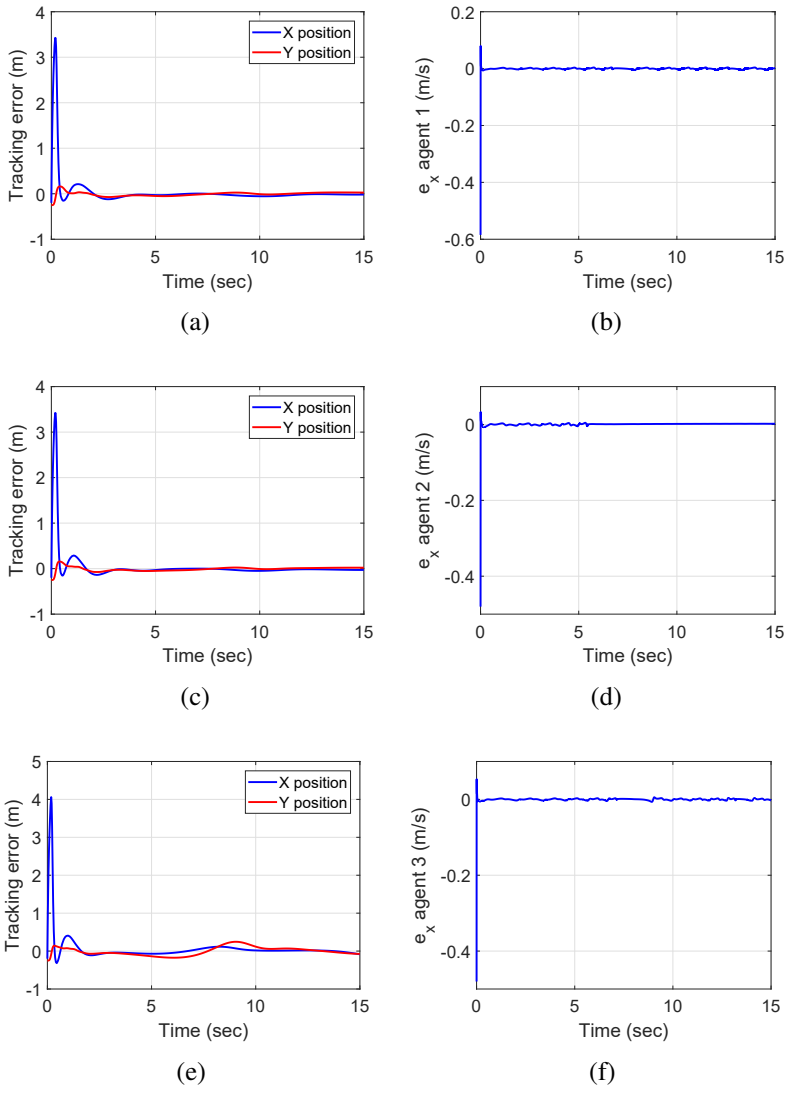

Figure 6.6: Mobile platform position and sliding vector errors

and 12 s. It is observed that the agents maintain a formation while transporting the object following a desired trajectory. The agents accomplish the required task of transportation of the object satisfactorily and move in synchrony for the required task.

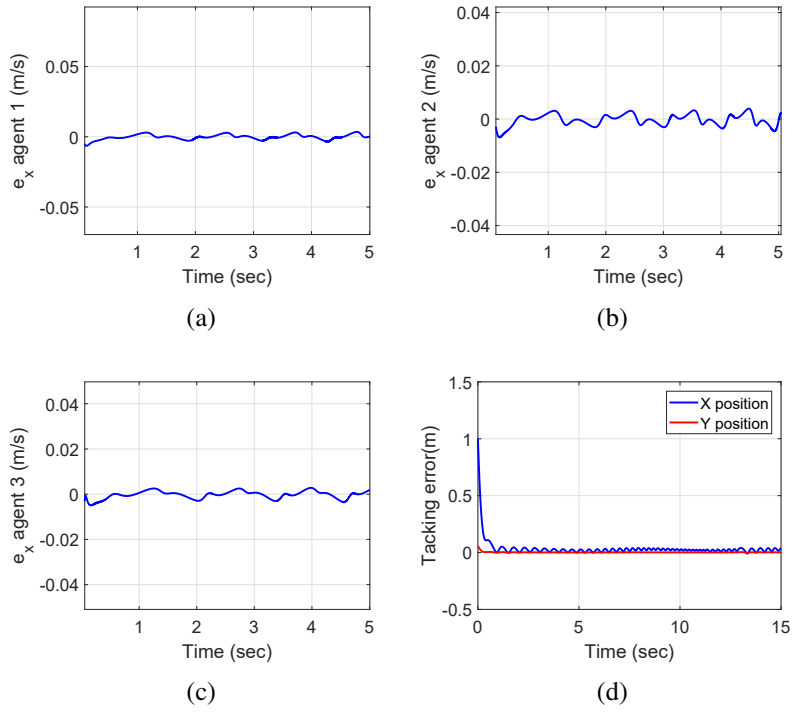

Figure 6.7: Sliding vector and object tracking errors

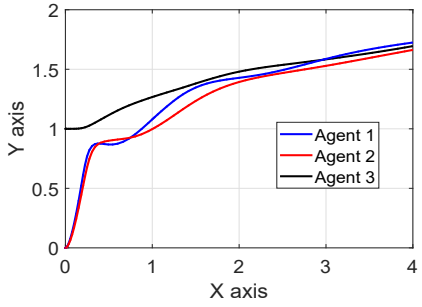

Figure 6.8: End-effector positions (m) of agents at 4 s

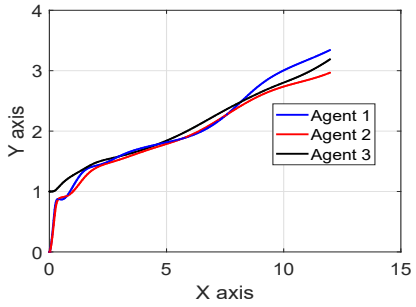

Figure 6.9: End-effector positions (m) of agents at 12 s

6.4.2 Simulation Scenario 2

The simulation again considers the communication topology $\mathcal{G}_1$ as given in Fig.6.4. The agents are strongly connected over a communication topology and the delay T_d is considered to be 1 s now. In this case, $\mathcal{L}$, d_i and w_{ij} are same as in the previous case. It is observed from the results in Figs.6.10(a), 6.10(c) and 6.10(e) that the increase in time delay does not significantly affect the tracking of the end-effector positions. The prioritized objective of the transportation of the object is still achieved with satisfactory trajectory tracking. The control torques for the actuators are shown in Figs.6.10(b), 6.10(d) and 6.10(f).

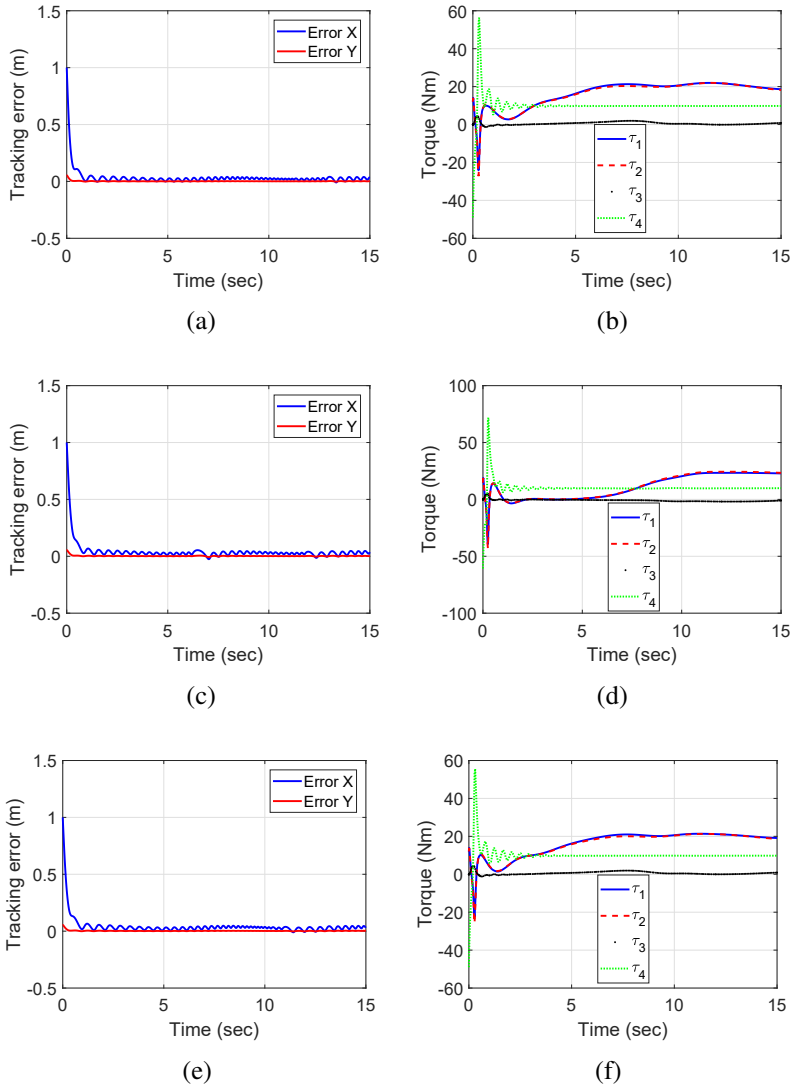

Figure 6.10: End-effector errors and actuator torques

The simulation results in Figs.6.11(a), 6.11(c) and 6.11(e) again show bounded errors in the tracking of the mobile platforms. Although the errors exist in the position tracking of the mobile platforms, the agents still manage to maintain the formation and successfully meet the task criteria. The reason again for these errors is the controller design in the null space. It can also be noted that the increase in T_d affects the positions of the mobile platforms and the errors slightly increase as compared to the previous case. The sliding errors in Figs.6.11(b), 6.11(d) and 6.11(f) converge to almost zero quickly thus meeting the proposed design analysis. Again during the first 5 seconds, simulation results for the sliding

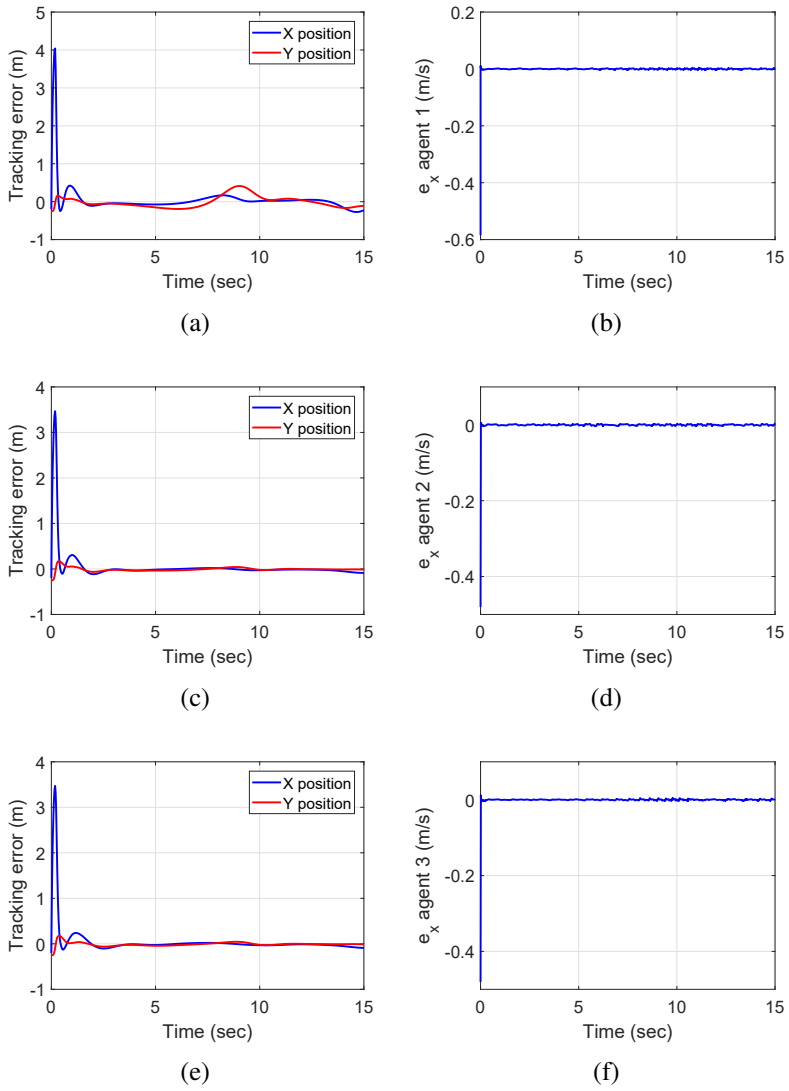

Figure 6.11: Mobile platform position and sliding vector errors

vector errors are shown in Figs.6.12(a), 6.12(b) and 6.12(c) for three mobile manipulators.

The object tracking errors are shown in Fig.6.12(d). It can be seen that although the errors do not precisely converge to zero but the object follows the desired trajectory closely thus meeting the task objective.

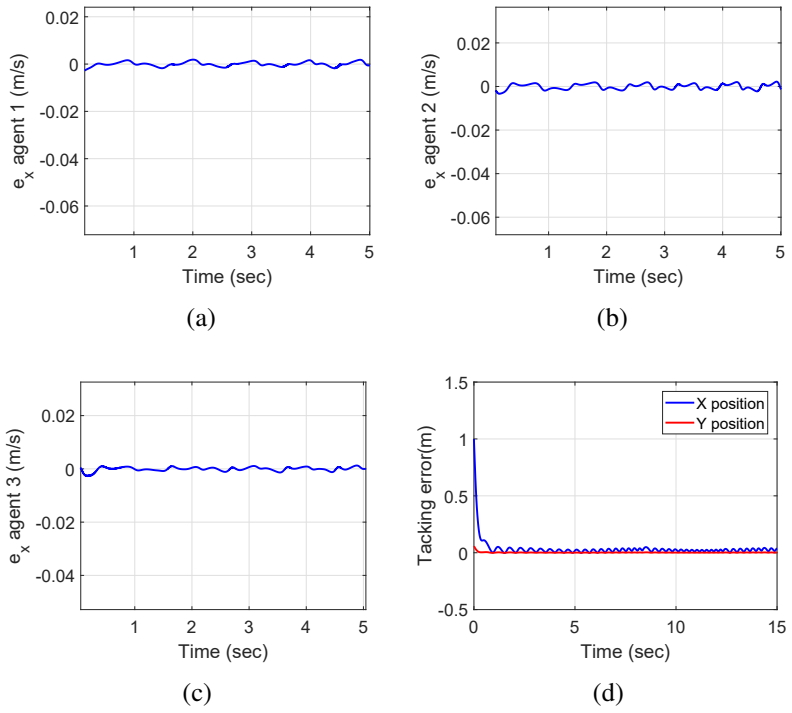

Figure 6.12: Sliding vector and object tracking errors

As in the previous case, Figs.6.13 and 6.14 show the end-effector positions of all three agents at 4 s and 12 s. It can be observed that the agents maintain a formation while transporting the object following a desired trajectory.

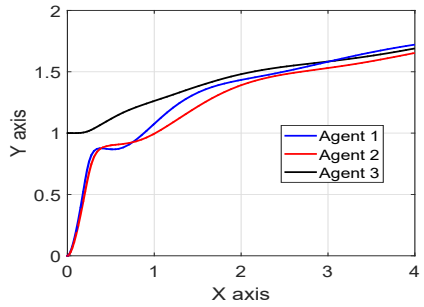

Figure 6.13: End-effector positions (m) of agents at 4 s

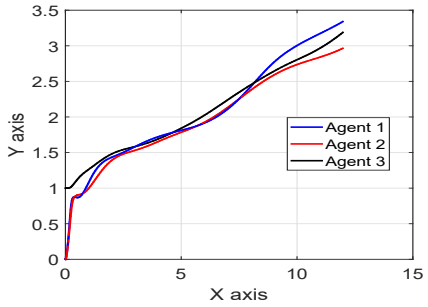

Figure 6.14: End-effector positions (m) of agents at 12 s

6.5 Summary

In this work, a systematic way of distributed operational space and null space control was presented where the controller for the synchronous motion of the mobile manipulators while maintaining a formation was designed. In null space control, the controllers for the mobile platforms to follow a predefined trajectory were designed. As the main objective of this work was to deal with transportation of an object to a desired position while the manipulators rigidly hold the object, we analysed the system both in the operational and null space. We designed the operational space controller to achieve consensus of the agents and the tracking of the end-effector positions. The parametric uncertainties were taken into account in the control design. One of the obvious benefit that we got in distributed nature of control was to allow the individual agent to deal with the disturbance issues on its own. The work also focused on the decoupled control of the null space and operational space. As mentioned earlier, the motion of the mobile manipulators was decoupled in the null space and operational space thus allowing the prioritization of the tasks. The null space controller was designed for the control of the mobile platforms and the operational space controller controlled the motion of the object and the force while the manipulators grasped the object at different points. Unlike previous researches in the existing literature, we followed a load distribution methodology based on the grasp matrix which not only met the kinematic constraints of the rigid connection between the object and the end-effectors but also dealt with the non-motion inducing wrenches or internal wrenches. The proposed controller not only provided the velocity synchronization in the presence of constrained end-effector motion but proved to be flexible and efficient in networked mobile manipulators. The additional DOFs can always be used for other missions such as obstacle avoidance. Although

the proposed control scheme provided satisfactory results as required by the application of the object manipulation, it did not take into consideration the communication uncertainties like switching graph topology or link failure. Moreover, there was no consideration of any assumptions on the structure of the mobile platforms of the mobile manipulators like the slippage or skidding of the wheels. These considerations might require extensive modelling of the system but would provide more robust control and flexibility in task execution.

Chapter 7

Adaptive Robust Control of Multilateral Teleoperation Systems

The ever increasing demand of industrial applications like heavy object manipulation, safe and stable operation and complex task performances require a well designed control system to achieve all these goals. Traditional bilateral teleoperation systems are sometime not suitable for such applications and there comes the need to extend these systems to multilateral teleoperation. Another disadvantage of bilateral teleoperation systems having fixed base manipulators is the limited workspace and dexterity. Teleoperation of mobile manipulators emerges as a decent solution to all these problems and provides enough flexibility of achieving task execution goals with guaranteed stability and safety of operation. Additionally, the mobility of a robotic manipulator not only maximizes the task generality of the system but also provides an increased task space in structured or unstructured environments. This increase in the manipulation task capabilities of the mobile manipulators outclasses the conventional fixed base robotic manipulators however, this comes at the cost of additional control design challenges.

Although multilateral teleoperation of mobile manipulators is a solution to the requirements of the industrial applications, the system becomes complicated due to increased number of human operators, master robots, slave robots and the transmission of signals over the communication channel. The multilateral teleoperation control design poses challenges in handling the time delay, dynamics of the master and slave robots, the realism of the teleoperation system and the internal forces of the target object. The control algorithms for the mobile manipulators not only have to achieve a task specific criteria but also have to deal with other issues like redundancy resolution and simultaneous or decoupled control of the robotic arm and the mobile base. As we leverage the increased task space and dexterity of the mobile manipulator system, we face the challenges of high dimensionality and complexity in the control design [2, 64, 103].

This chapter addresses a novel multilateral teleoperation control scheme for single master multiple slave system, which can be extended to n masters and n slaves without the loss

of generality, where the master is a n degrees of freedom manipulator arm and the slaves are n degrees of freedom mobile manipulators. The human operator operates the master robot to remotely control the slaves handling a target object. The master position signal is transmitted to the slave side to generate a desired object trajectory as well as the reference mobile base velocity. An adaptive robust controller is designed for the slaves to follow the desired trajectory which not only provides the excellent trajectory tracking but also optimize the internal force distribution of the object. A null space controller is designed for the mobile platforms of the mobile manipulators to achieve the velocity consensus while achieving the main task of object transportation. The novel control design replaces the transmission of environmental force signal over the communication channel by the estimated parameters of the environment to avoid the passivity problem of the traditional teleoperation. The environmental force is predicted on the master side based on the estimated environmental parameters. The proposed control design can simultaneously achieve the objectives of stability, synchronization and optimal internal force distribution. The simulation results of a single master and three slaves teleoperation system validate the efficacy of the proposed control algorithm. The main contributions of this chapter are:

- To propose a novel control design for a single master multiple slave teleoperation system, which can be easily extended to n masters and n slaves, to cooperatively handle a target object in a remote environment.

- To achieve the control objectives of stability, synchronization and force distribution while the end-effectors and the mobile platforms are controlled separately.

- To predict the undelayed environment reaction force on the master side in such a way that the communication channel passivity is naturally avoided.

- To deal with the arbitrary time delay in communication channel as well as in the graph topology over which the slaves are connected.

7.1 System Description

This section presents the dynamical equations of the master, object and the environment and the slaves including their properties and assumptions.

7.1.1 Master System

A non-redundant p-link fixed-base manipulator can be described in joint space as [33],

$$M(q_m)\ddot{q}_m + C(q_m,\dot{q}_m)\dot{q}_m + G(q_m) = u_m + J_m^T(q_m)F_h \tag{7.1}$$

where $q_m \in R^p$ represents the joint angle of the manipulator, $M(q_m) \in R^{p\times p}$ is the inertia matrix of the manipulator which is symmetric positive definite, $C(q_m,\dot{q}_m) \in R^p$ is the Centripetal and Coriolis torque, $G(q_m) \in R^p$ is the gravitational torque. The control input is represented as $u_m \in R^p$, the Jacobian matrix is $J_m(q_m) = \frac{\partial x_m}{\partial q_m} \in R^{p\times p}$ where $x_m = \Phi_m(q_m) \in R^p$ is representing the angle and the position of the end-effector of the manipulator. The force which is applied by the human operator to the end-effector of the master manipulator is represented by $F_h \in R^p$. The dynamics in (7.1) can be rewritten in Cartesian space as,

$$M_c(q_m)\ddot{x}_m + C_c(q_m,\dot{q}_m)\dot{x}_m + G_c(q_m) = u_{m_c} + F_{h_c}, \tag{7.2}$$

where,

$$\begin{cases} M_c = J_m^{-T} M J_m^{-1}, \\ C_c = J_m^{-T} C J_m^{-1} - J_m^{-T} M J_m^{-1} \dot{J}_m J_m^{-1}, \\ G_c = J_m^{-T} G, \\ u_{m_c} = J_m^{-T} u_m. \end{cases}$$

7.1.2 Object and Environment

The dynamics of the object can be expressed as,

$$M_o(x_o)\ddot{x}_o + C_o(x_o,\dot{x}_o)\dot{x}_o + G_o(x_o) = \sum_{i=1}^{n} F_i - F_e, \tag{7.3}$$

where $x_o \in R^p$ is describing the position of the object. The inertia matrix of the object is $M_o(x_o)$, $C_o(x_o,\dot{x}_o)$ is the Centripetal and Coriolis torque and G_o represents the gravitational torque. The force exerted on the object by the end-effector of the slaves is represented by F_i and F_e is the reaction force of the environment. The environment reaction force, under flexible contact model, can be written as [33],

$$F_e = B_e\dot{x}_o + K_e x_o + C_e = \theta_e^T \varphi_e(x_o,\dot{x}_o), \tag{7.4}$$

where $\theta_e = [B_e, K_e, C_e]^T$ are known parameters and $\varphi_e = [\dot{x}_o, x_o, 1]$ is the regressor signal for the object. This model can consider $\theta_e = 0$ which essentially means the free motion. There exists a kinematic chain between the object and the end-effectors of the slaves which can be expressed as [162],

$$x_o = \Phi_o(x_{si}), \quad \dot{x}_o = L_i(x_{si})\dot{x}_{si}, \quad f_i = L_i^T F_i, \tag{7.5}$$

where L_i is the transformation matrix and $L_i = \frac{\partial x_o(x_{si})}{\partial x_{si}}$. The constraints imposed on the movement of the object and the slaves due to the kinematic chain can be represented as,

$$\begin{aligned} x_o = x_o(x_{si}) = x_o(x_{si}(q_{si})) = \Psi(q_{si}), \quad A_i = L_i J_{si} \\ \ddot{x}_o = A_i \ddot{q}_{si} + \dot{A}_i \dot{q}_{si}, \quad \dot{x}_o = A_i(q_{si})\dot{q}_{si}. \end{aligned} \tag{7.6}$$

7.1.3 Slave System

The dynamics of a networked system of n-link N mobile manipulator slaves with $i = 1, \ldots N$ can be described in Euler Lagrange (EL) form as follows [65, 86, 112].

$$M_{si}(q_{si})\ddot{q}_{si} + C_{si}(q_{si}, \dot{q}_{si})\dot{q}_{si} + G_{si}(q_{si}) + f_i(q_{si}) = B_i(q_{si})\tau_{si}, \tag{7.7}$$

where $M_{si}(q_{si}) \in \mathcal{R}^{n\times n}$ is the inertia matrix which is a symmetric bounded positive definite matrix; $C_{si}(q_{si}, \dot{q}_i) \in \mathcal{R}^{n\times n}$ is the Centripetal and Coriolis matrix; $G_{si}(q_{si}) \in \mathcal{R}^n$ is the gravitational force vector; $f_i(q_{si}) = \begin{bmatrix} f_{in}^T & f_{ih}^T \end{bmatrix}^T = \begin{bmatrix} (A_i^T(q_{ip})\lambda)^T & 0 \end{bmatrix}^T \in \mathcal{R}^n$ is the generalized constraint force or torque, where $\lambda_i = \begin{bmatrix} \lambda_{in} & \lambda_{ih} \end{bmatrix}^T$ is the Lagrangian multiplier, λ_{in} considers the nonholonomic constraint and λ_{ih} considers the holonomic constraints and $A_i(q_{ip})$ is the kinematic constraint matrix. $B_i(q_i) \in \mathcal{R}^{n\times m}$ is a full rank input transformation matrix and also assumed to be known, $\tau_{si} \in \mathcal{R}^m$ is the control input to the system. $q_{si} = \begin{bmatrix} q_{ip}^T & q_{ia}^T \end{bmatrix}^T \in \mathcal{R}^n$ is the vector of generalized coordinates. q_{ip} denotes the generalized coordinates of the wheeled mobile platform and q_{ia} denotes the generalized coordinates of the manipulator arm [64]. The terms, for brevity dropping the subscript s, can be further represented as,

$$M_i(q_i) = \begin{bmatrix} M_{ip} & M_{ipa} \\ M_{iap} & M_{ia} \end{bmatrix}, C_i(q_i, \dot{q}_i) = \begin{bmatrix} C_{ip} & C_{ipa} \\ C_{iap} & C_{ia} \end{bmatrix}$$

$$G_i(q_i) = \begin{bmatrix} G_{ip} \\ G_{ia} \end{bmatrix}, \; B_i(q_i) = \begin{bmatrix} B_{ip} & 0 \\ 0 & B_{ia} \end{bmatrix}, \tau_i = \begin{bmatrix} \tau_{ip} \\ \tau_{ia} \end{bmatrix},$$

where M_{ip} and M_{ia} describe the inertia matrices for the mobile platform and the manipulator arm respectively. M_{ipa} and M_{iap} describe the coupling inertia matrices of the mobile platform and the manipulator arm. C_{ip} and C_{ia} are Centripetal and Coriolis torques for the mobile platform and the manipulator arm respectively. C_{ipa} and C_{iap} are the coupling Centripetal and Coriolis torques of the mobile platform and the manipulator arm. G_{ip} and G_{ia} are the gravitational forces of the mobile platform and the manipulator arm respectively. B_{ip} and B_{ia} denote the input transformation matrices of the mobile platform and the manipulator arm respectively. τ_{ip} and τ_{ia} are the control input of the mobile platform and the robotic arm. The coordinates of the mobile platform can be described as,

$$q_{ip} = \begin{bmatrix} x_i \\ y_i \\ \theta_{ip} \end{bmatrix}, \tag{7.8}$$

where x_i, y_i are the coordinates of the center of the mobile platform and θ_{ip} is the orientation or the heading angle of the mobile platform. The nonholonomic kinematic constraint for the mid point of the wheel axle where the manipulator arm is mounted can be expressed as,

$$\dot{x}_i \sin\theta_{ip} - \dot{y}_i \cos\theta_{ip} = 0. \tag{7.9}$$

The constraint in (7.9) can also be written in the following form,

$$A_i(q_{ip})\dot{q}_{ip} = 0, \tag{7.10}$$

where

$$A_i(q_{ip}) = [\sin\theta_{ip} \quad -\cos\theta_{ip} \quad 0]. \tag{7.11}$$

Suppose there are l numbers of non-integrable and independent velocity constraints and it is assumed to have the full rank l. The mobile platform here is assumed to be completely nonholonomic and we can write $A_i(q_{ip})$ matrix of (7.10) as,

$$A_i(q_{ip}) = \begin{bmatrix} A_1^T(q_{ip}) & A_2^T(q_{ip}) & A_3^T(q_{ip}) & \ldots & A_l^T(q_{ip}) \end{bmatrix}^T.$$

The nonholonomic generalized constraint forces can be given as

$$f_{in} = (A_i^T(q_{ip})\lambda_{in})^T. \tag{7.12}$$

$H_i(q_{ip}) \in \mathcal{R}^{n\times m}$ is a matrix with rank being m formed by a set of smooth and linearly independent vectors spanning the null space of matrix $A_i(q_{ip})$, i.e,

$$H_i^T(q_{ip})A_i^T(q_{ip}) = 0, \tag{7.13}$$

where $H_i(q_{ip}) = [H_1(q_{ip}) \;\; H_2(q_{ip}) \;\; \ldots \;\; H_{n_p-l}(q_{ip})]$. Note that here $H_i^T H_i$ is of full rank. According to (7.10) and (7.13), the first order velocity kinematic model of a nonholonomic mobile platform which is also called the *steering system* can be written in the following form,

$$\dot{q}_{ip} = H_i(q_{ip})\alpha_i, \tag{7.14}$$

where α_i is an auxiliary function $\alpha_i \in \mathcal{R}^2$ and called the *steering velocity* of the kinematic system. α_1 and α_2 are the linear and angular velocities of the wheeled mobile platform and can be written as (7.15) or α_1 and α_2 are the left wheel velocity and the right wheel velocity of the mobile platform and can be written as (7.16),

$$\alpha_i = \begin{bmatrix} v_i & \omega_i \end{bmatrix}^T, \tag{7.15}$$

$$\alpha_i = \begin{bmatrix} \theta_{iR} & \theta_{iL} \end{bmatrix}^T. \tag{7.16}$$

We can rewrite (7.14) in the specific kinematic form, in terms of linear and angular velocities of the wheeled mobile platform and in terms of right and left wheel velocities.

$$\dot{q}_{ip} = \begin{bmatrix} \cos\theta_{ip} & 0 \\ \sin\theta_{ip} & 0 \\ 0 & 1 \end{bmatrix} \begin{bmatrix} v_i \\ \omega_i \end{bmatrix}, \tag{7.17}$$

$$\dot{q}_{ip} = \begin{bmatrix} \frac{R}{2}\cos\theta_{ip} & \frac{R}{2}\cos\theta_{ip} \\ \frac{R}{2}\sin\theta_{ip} & \frac{R}{2}\sin\theta_{ip} \\ \frac{R}{2D} & -\frac{R}{2D} \end{bmatrix} \begin{bmatrix} \theta_{iR} \\ \theta_{iL} \end{bmatrix}, \tag{7.18}$$

where in this work R is the radius of the wheels and D is the distance of the two wheels of the mobile platform.

Let $\eta_i = \begin{bmatrix} \alpha_i^T & \dot{q}_{ia}^T \end{bmatrix}^T$. Due to the nonholonomic constraint defined in (7.10) and (7.14), there exists a vector $\dot{\eta}_i$, such that [65],

$$\dot{q}_i = H_i(q_i)\dot{\eta}_i. \tag{7.19}$$

A reduced dynamic model now can be obtained by substituting (7.19) and its derivative in (7.7) and pre-multiplying $H_i(q_i)^T$,

$$M_{\eta_i}(q_i)\ddot{\eta}_i + C_{\eta_i}(q_i,\dot{q}_i)\dot{\eta}_i + G_{\eta_i}(q_i) = \tau_{\eta_i}, \tag{7.20}$$

where,

$$\begin{cases} M_{\eta_i}(q_i) = H_i^T(q_i)M_i(q_i)H_i(q_i), \\ C_{\eta_i}(q_i,\dot{q}_i) = H_i^T(q_i)[M_i(q_i)\dot{H}_i(q_i) + C_i(q_i,\dot{q}_i)H_i(q_i)], \\ G_{\eta_i}(q_i) = H_i^T(q_i)G_i(q_i), \\ \tau_{\eta_i} = H_i^T(q_i)B_i(q_i)\tau_i. \end{cases}$$

A more specific dynamic model can be described by [64].

$$\begin{bmatrix} H_i^T B_{ip}\tau_{ip} \\ B_{ia}\tau_{ia} \end{bmatrix} = \begin{bmatrix} H_i^T M_{ip}H_i & H_i^T M_{ipa} \\ M_{iap}H_i & M_{ia} \end{bmatrix} \begin{bmatrix} \ddot{\alpha}_i \\ \ddot{q}_{ia} \end{bmatrix}$$

$$+ \begin{bmatrix} H_i^T M_{ip}\dot{H}_i + H_i^T C_{ip}H_i & H_i^T C_{ipa} \\ M_{iap}\dot{H}_i + C_{iap}H & C_{ia} \end{bmatrix} \begin{bmatrix} \dot{\alpha}_i \\ \dot{q}_{ia} \end{bmatrix} + \begin{bmatrix} H_i^T G_{ip} \\ G_{ia} \end{bmatrix}$$

In this work, the mobile manipulators are subjected to the following assumptions.

Assumption 1: The mobile platform is driven with two wheels operated by two independent motors or actuators and the manipulator arm is fixed on this platform.

Assumption 2: The mobile manipulator is considered to be redundant and operating away from singularity.

Assumption 3: It is considered that $\dot{\eta}_i = [\dot{\theta}_{iR} \;\; \dot{\theta}_{iL} \;\; \dot{\theta}_1 \;\ldots\; \dot{\theta}_k]^T$ where $\dot{\theta}_j$ is the angular velocity of the manipulator joints and $j = 1,\ldots k$.

In most of the mobile manipulation applications, the desired trajectory is defined in the task space or operational space. Let X_i contains all the variables which are required to define the task of the end-effector of the mobile manipulator then the kinematic equation of the end-effector can be written as,

$$X_{ma} = f_i(\eta_i), \tag{7.21}$$

where $f_i(.)$ being a nonlinear transformation describes the relation between the joint space of the system and the operational space of the end-effector [65]. The velocity of the end-effector can be derived by differentiating (7.21),

$$\dot{X}_{ma} = J_{ma}(\eta_i)\dot{\eta}_i,$$

where $J_{ma}(\eta_i) = \frac{\partial f_i(\eta_i)}{\partial \eta_i}$ is the non-square Jacobian matrix of the end-effector and is non-invertible due to the redundancy of the system. The redundancy of the system can be utilized to achieve additional tasks. A user defined kinematic function for the motion of the mobile platform can be defined as,

$$X_{mp} = g_i(\eta_i), \tag{7.22}$$

By differentiating (7.22), we have,

$$\dot{X}_{mp} = J_{mp}(\eta_i)\dot{\eta}_i,$$

where the Jacobian matrix is $J_{mp}(\eta_i) = \frac{\partial g_i(\eta_i)}{\partial \eta_i}$. We can use the extended position $X_i = [X_{ma}^T \; X_{mp}^T]^T$ to accomplish the secondary task while simultaneously achieving the primary task. Now the mobile manipulator system has an extended differential kinematic model as given by,

$$\dot{X}_i = \begin{bmatrix} J_{ma}(\eta_i) \\ J_{mp}(\eta_i) \end{bmatrix} \dot{\eta}_i = J(\eta_i)\dot{\eta}_i. \tag{7.23}$$

where $J(\eta_i)$ is the extended square Jacobian matrix of the whole system and for the sake of brevity, we will use J as $J(\eta_i)$. From (7.23), we can have,

$$\dot{\eta}_i = J^{-1}\dot{X}_i, \quad \ddot{\eta}_i = J^{-1}\ddot{X}_i - J^{-1}\dot{J}J^{-1}\dot{X}_i \tag{7.24}$$

We get the extended operational space dynamic equation of the system, similar to (7.2), by substituting (7.24) in (7.20) and premultiplying J^{-T} as follows,

$$M_{x_i}(q_i)\ddot{X}_i + C_{x_i}(q_i,\dot{q}_i)\dot{X}_i + G_{x_i}(q_i) = \tau_{x_i}, \tag{7.25}$$

where,

$$\begin{cases} M_{x_i}(q_i) = J^{-T}M_{\eta_i}(q_i)J^{-1}, \\ C_{x_i}(q_i,\dot{q}_i) = J^{-T}[-M_{\eta_i}(q_i)J^{-1}\dot{J} + C_{\eta_i}(q_i,\dot{q}_i)]J^{-1}, \\ G_{x_i}(q_i) = J^{-T}G_{\eta_i}(q_i), \\ \tau_{x_i} = J^{-T}\tau_{\eta_i}. \end{cases}$$

The combined dynamics of the slaves and the object can be written as,

$$M_S(x_o, q_{si})\ddot{x}_o + C_S(x_o, \dot{x}_o, q_{si}, \dot{q}_{si})\dot{x}_o + G_S(x_o, q_{si}) = u_S - F_e, \tag{7.26}$$

where,

$$\begin{cases} M_S = M_o + \sum_{i=1}^{n} A_i^{-T} M_{si} A_i^{-1}, \\ C_S = C_o + \sum_{i=1}^{n} (A_i^{-T} C_{si} A_i^{-1} - A_i^{-T} M_{si} A_i^{-1} \dot{A}_i A_i^{-1}), \\ G_S = G_o + \sum_{i=1}^{n} A_i^{-T} G_{si}, \\ u_S = \sum_{i=1}^{n} A_i^{-T} \tau_{si}. \end{cases}$$

The dynamic models in (7.2) and (7.26) have the following properties which will be used in the controller design and stability analysis.

Property 1: The matrices M_c and M_S are symmetric positive definite and there exist positive constants $\mu_{m1}, \mu_{m2}, \mu_{o1}$ and μ_{o2} such that $\mu_{m1} I \leq M_c \leq \mu_{m2} I$, and $\mu_{o1} I \leq M_S \leq \mu_{o2} I$, where I is an $n \times n$ identity matrix.

Property 2: A part of the nonlinear system dynamics depends linearly on dynamic parameter vectors φ_m and φ_o such that,

$$M_c(q_m)\ddot{x}_{m,r} + C_c(q_m, \dot{q}_m)\dot{x}_{m,r} + G_c(q_m) = \varphi_m(q_m, \dot{q}_m, \dot{x}_{m,r}, \ddot{x}_{m,r})^T \theta_m, \tag{7.27}$$

$$M_S(x_o, q_{si})\ddot{x}_{o,r} + C_S(x_o, \dot{x}_o, q_{si}, \dot{q}_{si})\dot{x}_{o,r} + G_S(x_o, q_{si}) = \varphi_o(x_o, \dot{x}_o, q_{si}, \dot{q}_{si}, \dot{x}_{o,r}, \ddot{x}_{o,r})^T \theta_o, \tag{7.28}$$

where θ_m and θ_o are the unknown parameters of the master, slaves and the object and φ_m and φ_o are the regressor matrices. The reference velocities and accelerations are represented by $\dot{x}_{m,r}, \ddot{x}_{m,r}, \dot{x}_{o,r}$ and $\ddot{x}_{o,r}$.

Property 3: Under a proper definition of the matrices, the matrices $\dot{M}_c - 2C_c$, $\dot{M}_S - 2C_S$ are skew symmetric.

Assumption 4: If we define the estimate and estimation error of the parameters as $\hat{\theta}$ and $\tilde{\theta}$ where $\tilde{\theta} = \hat{\theta} - \theta$, then we assume that the extent of the uncertainty in parameters is known such that,

$$\theta \in \Omega_\theta \triangleq \{\theta : \theta_{min} \leq \theta \leq \theta_{max}\} \tag{7.29}$$

where θ_{min} and θ_{max} are known constant vectors or scalars.

Assumption 5: The signals F_{hc} and F_e are measurable and the position and velocities of the master and slaves are also available.

7.2 Control Architecture

This work proposes a novel structure of the communication channel for teleoperation where the slave side receives the signal x_m and the master side receives the environment parameters θ_e which are estimated online. Unlike traditional teleoperation systems, the signal we receive at master side contain estimated values of the environmental parameters instead of the force signal F_e which naturally avoids the passivity problem of the communication channel. At master side, a force predictor $\hat{F}_e$ is designed to predict the environmental force using the estimated environmental parameters $\hat{\theta}_e$ and the signals x_m and $\dot{x}_m$. The human input signal F_h is used to generate the desired master trajectories x_m, $\dot{x}_m$ and $\ddot{x}_m$. The signal received at the slave side x_m is optimally processed to generate the desired object trajectory x_{od} for the end-effector of the slave control and a reference velocity signal is also generated for the mobile base of the slaves. An adaptive robust slave controller u_S is designed to minimize the tracking error $x_o - x_{od}$. Finally, the internal force control is implemented to obtain the slave control inputs. The control objectives of this work include:

Stability: To synthesize the input such that the robust stability is achieved in the presence of communication delays.

Synchronization: To make the object trajectory follow the desired trajectory precisely minimizing the tracking error.

Force Distribution: To control the internal force of the slaves to have an optimized distribution of the slave inputs.

A general schematic of the control architecture is shown in Fig.7.1.

7.2.1 Parameter Estimation

All the unknown parameters θ_e, θ_o and θ_m are estimated using a projection type adaptation law [163]. The parameter $\hat{\theta}$ is estimated as,

$$\dot{\hat{\theta}} = P_{\hat{\theta}}(\Gamma\gamma), \quad \hat{\theta} \in \Omega_\theta \tag{7.30}$$

where Γ is a positive definite matrix and γ is an adaptation parameter.

$$P_{\hat{\theta}}(\bullet) = \begin{cases} \bullet & if \;\; \hat{\theta} \in \mathring{\Omega} \;\; or \;\; n_{\hat{\theta}}^T \bullet \leq 0, \\ \left(I - \Gamma \dfrac{n_{\hat{\theta}} n_{\hat{\theta}}^T}{n_{\hat{\theta}}^T \Gamma n_{\hat{\theta}}^T}\right) \bullet & \hat{\theta} \in \delta\Omega_\theta \;\; and \;\; n_{\hat{\theta}}^T \bullet > 0, \end{cases} \tag{7.31}$$

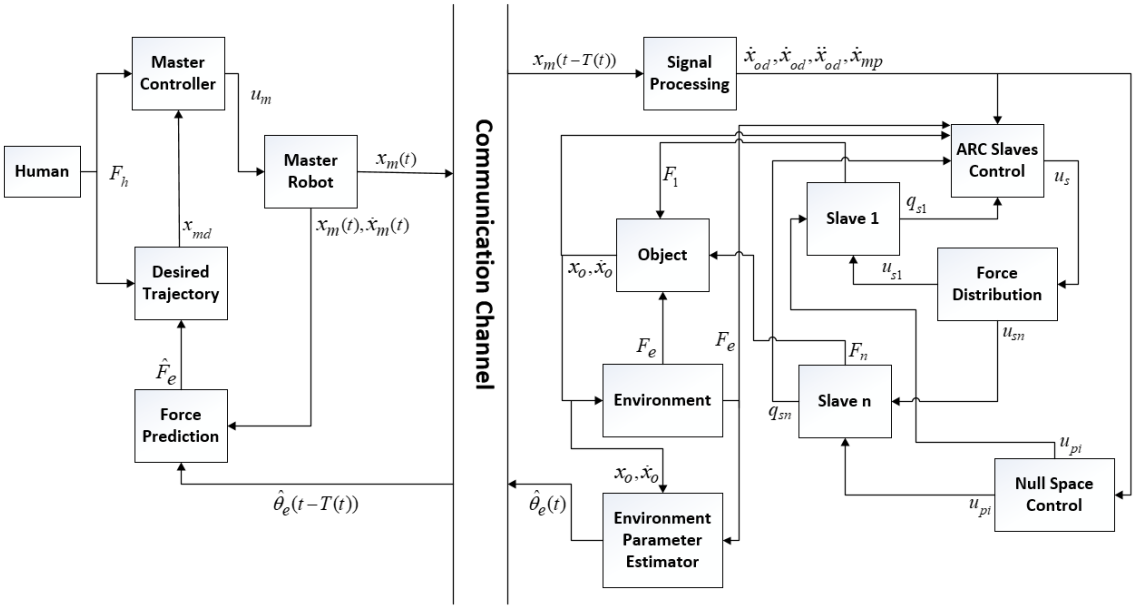

Figure 7.1: Control architecture of SMMS teleoperation system.

where $\mathring{\Omega}$ and $\delta\Omega_\theta$ are the interior and the boundary of Ω_θ and $n_{\hat{\theta}}^T$ denotes the unit normal vector at $\hat{\theta} \in \delta\Omega_\theta$. This projection type adaptation law has the following properties.

Property 4: The parameter estimates are always within the known bounded set $\bar{\Omega}_\theta$, that is, $\hat{\theta}(t) \in \bar{\Omega}_\theta,\ \forall t$. This means that from Assumption 4, $\theta_{min} \leq \hat{\theta}(t) \leq \theta_{max},\ \forall t$.

Property 5: It holds that,

$$\tilde{\theta}^T(\Gamma^{-1}P_{\hat{\theta}}(\Gamma\gamma) - \gamma) \leq 0,\ \forall\gamma, \tag{7.32}$$

For the estimation of θ_e, a filter $H_f(s) = \dfrac{1}{(\gamma_f s+1)^2}$ is used on both sides of (7.4).

$$F_{ef} = \varphi_{ef}^T\theta_e, \tag{7.33}$$

where F_{ef} and φ_{ef} are the filtered values of F_e and φ_e. If we define the prediction output $\hat{F}_{ef} = \varphi_{ef}^T\hat{\theta}_e$, then the prediction error can be defined as,

$$\varepsilon = \hat{F}_{ef} - F_{ef} = \varphi_{ef}^T\tilde{\theta}_e, \tag{7.34}$$

Now $\dot{\hat{\theta}}_e$ can be designed as,

$$\dot{\hat{\theta}}_e = P_{\hat{\theta}}(\Gamma_e\gamma_e), \tag{7.35}$$

$$\dot{\Gamma}_e = \begin{cases} \alpha\Gamma_e - \dfrac{\Gamma_e \varphi_{ef} \varphi_{ef}^T \Gamma_e}{1 + \nu \varphi_{ef}^T \Gamma_e \varphi_{ef}} & if \;\; \lambda_{max}(\Gamma_e(t)) \leq \zeta_M, \\ 0 & otherwise, \end{cases} \tag{7.36}$$

$$\gamma_e = \frac{\varphi_{ef}\varepsilon}{1 + \nu \varphi_{ef}^T \Gamma_e \varphi_{ef}}, \tag{7.37}$$

where α is the forgetting factor, $\nu \geq 0$ and ζ_M is the bound on $||\Gamma_e(t)||$.

Lemma 1: The parameter estimation $\hat{\theta}_e$ always stay within a known bound when the least square estimation algorithm (7.35) is used as $\theta_{e_{min}} \leq \hat{\theta}_e(t) \leq \theta_{e_{max}}, \forall t$. Additionally, when there are only uncertainties in the parameters of the systems, the persistent excitation (PE) condition given below is satisfied [163].

$$\int_t^{(t+T)} \varphi_{ef} \varphi_{ef}^T d\tau \geq \xi I, \forall t > t_0 \;\; \text{for some } T, \xi > 0 \tag{7.38}$$

then $\hat{\theta}_e$ converges to its true value θ_e.

7.2.2 Controller Design for the Master Side

This section presents a novel adaptive and robust controller design for the master manipulator. As the estimates of the environmental parameters are transmitted over the communication channel, the master side receives $\hat{\theta}_e(t-T)$ and predicts the force $\hat{F}_e$ as,

$$\hat{F}_e = \hat{\theta}_e^T(t - T(t)) \varphi_e \Big(k_m \Phi_o(x_m), k_m L_i \dot{x}_m \Big). \tag{7.39}$$

The master manipulator is required to follow a desired trajectory $x_{m_{dt}}$, which is designed as follows,

$$\begin{aligned} M_d(x_{md})\ddot{x}_{md} + C_d(x_{md}, \dot{x}_{md})\dot{x}_{md} + G_d(x_{md}) &= \varphi_m(x_{md}, \dot{x}_{md}, \ddot{x}_{md})^T \theta_d \\ &= L_i^{-T} F_{h_c} - k_f \hat{\theta}_e(t - T(t)) \varphi_e(k_m x_{md}, k_m \dot{x}_{md}), \end{aligned} \tag{7.40}$$

$$x_{m_{dt}} = \Phi_o^{-1}(x_{md}), \tag{7.41}$$

where x_{md} is the virtual object trajectory, $k_f > 0$ is the force scaling factor, and θ_d is the target parameter vector of the impedance behavior which is chosen to satisfy x_{md}. The objective to design the controller is to ensure that x_m tracks the desired trajectory $x_{m_{dt}}$

precisely.

Define s_m as follows:

$$s_m = \dot{e}_m + k_{m1} e_m, \quad e_m = x_m - x_{m_{dt}}, \tag{7.42}$$

where $k_{m1} > 0$ is a diagonal matrix. Differentiate (7.42) and note (7.2),

$$M_c \dot{s}_m + C_c s_m = u_{m_c} + F_{h_c} - \varphi_m(q_m, \dot{q}_m, \dot{x}_{m,r}, \ddot{x}_{m,r})^T \theta_m, \tag{7.43}$$

The controller is designed as follows:

$$\begin{aligned} u_{m_c} &= \varphi_m(q_m, \dot{q}_m, \dot{x}_{m,r}, \ddot{x}_{m,r})^T \hat{\theta}_m - F_{h_c} + u_f - K_p s_m, \\ \dot{\hat{\theta}}_m &= P_{\hat{\theta}_m}(\Gamma_m \gamma_m), \quad \gamma_m = \varphi_m(q_m, \dot{q}_m, \dot{x}_{m,r}, \ddot{x}_{m,r}) s_m, \end{aligned} \tag{7.44}$$

where $u_f - K_p s_m$ is the robust control law, the term $\varphi_m(q_m, \dot{q}_m, \dot{x}_{m,r}, \ddot{x}_{m,r})^T \hat{\theta}_m - F_{h_c}$ is the model compensation for tracking, K_p is chosen to be a symmetric positive definite matrix and u_f will be designed later. Substituting (7.44) into (7.43) and rearranging the terms,

$$M_c \dot{s}_m + C_c s_m = -K_p s_m + u_f + \varphi_m(q_m, \dot{q}_m, \dot{x}_{m,r}, \ddot{x}_{m,r})^T \tilde{\theta}_m, \tag{7.45}$$

where u_f can be designed to satisfy the conditions below:

$$\begin{aligned} &(a) \quad s_m^T \left(u_f + \varphi_m(q_m, \dot{q}_m, \dot{x}_{m,r}, \ddot{x}_{m,r})^T \tilde{\theta}_m \right) \leq \sigma_m, \\ &(b) \quad s_m^T u_f \leq 0, \end{aligned} \tag{7.46}$$

where $\sigma_m > 0$ is a small design parameter.

Theorem 1: For a desired trajectory, the controller in (7.44) guarantees that all the signals of the master side are bounded.

Proof: Choose a Lyapunov function,

$$V_m = \frac{1}{2} s_m^T M_c s_m \tag{7.47}$$

The derivative of V_m is:

$$\begin{aligned} \dot{V}_m &= s_m^T M_c \dot{s}_m + \frac{1}{2} s_m^T \dot{M}_c s_m \\ &= s_m^T (M_c \dot{s}_m + C_c s_m) \\ &= -s_m^T K_p s_m + s_m^T (u_f + \varphi_m^T \tilde{\theta}_m) \leq -\lambda_m V_m + \sigma_m \end{aligned} \tag{7.48}$$

Then it follows that,

$$V_m \leq e^{-\lambda_m t} V_m(0) + \frac{\sigma_m}{\lambda_m}[1 - e^{-\lambda_m t}] \tag{7.49}$$

V_m will be bounded when,

$$V_m \leq e^{-\lambda_m t} V_m(0) + \frac{\sigma_m}{\lambda_m}[1 - e^{-\lambda_m t}] \tag{7.50}$$

where $\lambda_m = 2\sigma_{min}(K_p)/\mu_{m2}$ and $\sigma_{min}(\bullet)$ is the minimum eigenvalue of a matrix.
Thus, s_m is bounded and e_m and $\dot{e}_m$ are also bounded from (7.42). Using the adaptation law (7.30), $\hat{\theta}_m$ is bounded thus the control input u_{m_c} is bounded. As $x_{m_{dt}}$, $\dot{x}_{m_{dt}}$ and $\ddot{x}_{m_{dt}}$ are bounded, x_m and $\dot{x}_m$ are also bounded.

7.2.3 Controller Design for the Slave Side

The controller design for the slaves can be divided into two parts where the first controller deals with the control of the mobile platform and the second one deals with the trajectory tracking of the end-effectors. We take advantage of the decoupling of the operational and null space of the mobile manipulators to design the controllers [153]. The motion of the mobile manipulators is decoupled in the operational space (end-effector) and the null space (mobile platform). This decoupling of the operational and null space allows the prioritization of the tasks in the event of a disagreement between the operational and null space. The decoupling of null space and operational space and the null space control of the mobile manipulators system has already been presented in sections 6.3.1 and 6.3.2. The desired trajectory X_{mp} is generated from the signal $x_m(t - T(t))$ by applying a similar filter which is used to generate x_{od} as discussed below. Once the null space controller is designed, an adaptive robust controller (ARC) will be designed for the end-effectors of the slaves for trajectory tracking.

7.2.3.1 ARC for Slaves

According to the proposed control architecture, the slave side receives the delayed position signal $x_m(t - T(t))$ of the master. The desired object trajectory x_{od} can be obtained by an optimal processing on the master position signal. A filter, $H_r(s) = \dfrac{1}{(\tau_r s + 1)^2}$ can be used with $x_{od} = H_r(s)[k_m \Phi_o(x_m(t - T(t)))]$, which can simultaneously provide the desired velocity and acceleration of the object.

Define s_s as follows:

$$s_s = \dot{e}_s + k_{s1} e_s, \quad e_s = x_o - x_{od} \tag{7.51}$$

where $k_{s1} > 0$ is a diagonal matrix. Now differentiating (7.51) and noting (7.26),

$$M_S \dot{s}_s + C_S s_s = u_S - F_e - \varphi_o(x_o, \dot{x}_o, q_{si}, \dot{q}_{si}, \dot{x}_{o,r}, \ddot{x}_{o,r})^T \theta_o \tag{7.52}$$

where $\dot{x}_{o,r} = \dot{x}_{od} - k_{s1} e_s$ and $\ddot{x}_{o,r} = \ddot{x}_{od} - k_{s1} \dot{e}_s$.
Now the slave controller is designed as follows:

$$\begin{aligned} u_S &= -K_d s_s + u_r + \varphi_o(x_o, \dot{x}_o, q_{si}, \dot{q}_{si}, \dot{x}_{o,r}, \ddot{x}_{o,r})^T \hat{\theta}_o + F_e \\ \dot{\hat{\theta}}_o &= P_{\hat{\theta}_o}(\Gamma_o \gamma_o), \quad \gamma_o = -\varphi_o(x_o, \dot{x}_o, q_{si}, \dot{q}_{si}, \dot{x}_{o,r}, \ddot{x}_{o,r}) s_s \end{aligned} \tag{7.53}$$

where $-K_d s_s + u_r$ is the robust control law, the term $\varphi_o(x_o, \dot{x}_o, q_{si}, \dot{q}_{si}, \dot{x}_{o,r}, \ddot{x}_{o,r})^T \hat{\theta}_o + F_e$ is the model compensation for tracking, K_d is chosen to be a symmetric positive definite matrix and u_r will be designed later. Substituting (7.53) into (7.52) and rearranging the terms,

$$M_S \dot{s}_s + C_S s_s = -K_d s_s + u_r + \varphi_o(x_o, \dot{x}_o, q_{si}, \dot{q}_{si}, \dot{x}_{o,r}, \ddot{x}_{o,r})^T \tilde{\theta}_o \tag{7.54}$$

Now, u_r can be designed to satisfy the conditions below.

$$\begin{aligned} &(a) \quad s_s^T \left(u_r + \varphi_o(x_o, \dot{x}_o, q_{si}, \dot{q}_{si}, \dot{x}_{o,r}, \ddot{x}_{o,r})^T \tilde{\theta}_o \right) \leq \sigma_s \\ &(b) \quad s_s^T u_r \leq 0 \end{aligned} \tag{7.55}$$

where $\sigma_s > 0$ is a small design parameter.

Theorem 3: The controller (7.53) can guarantee that all the slave side signals are bounded if the received signal $x_m(t - T(t))$ is bounded.

Proof: Choose a Lyapunov function,

$$V_s = \frac{1}{2} s_s^T M_S s_s \tag{7.56}$$

V_s will be bounded when,

$$V_s \leq e^{-\lambda_s t} V_s(0) + \frac{\sigma_s}{\lambda_s} [1 - e^{-\lambda_s t}] \tag{7.57}$$

where $\lambda_s = 2\sigma_{min}(K_d)/\mu_{o2}$ and $\sigma_{min}(\bullet)$ is the minimum eigenvalue of a matrix.
The derivative of V_s is:

$$\begin{aligned} \dot{V}_s &= s_s^T M_S \dot{s}_s + \frac{1}{2} s_s^T \dot{M}_S s_s \\ &= s_s^T (M_S \dot{s}_s + C_S s_s) \\ &= -s_s^T K_d s_s + s_s^T (u_r + \varphi_o^T \tilde{\theta}_o) \leq -\lambda_s V_s + \sigma_s \end{aligned} \tag{7.58}$$

Then it follows that,

$$V_s \leq e^{-\lambda_s t} V_s(0) + \frac{\sigma_s}{\lambda_s}[1 - e^{-\lambda_s t}] \tag{7.59}$$

Thus, s_s is bounded and e_s and $\dot{e}_s$ are also bounded from (7.51). Using the adaptation law (7.30), $\hat{\theta}_o$ is bounded thus the control input u_S is bounded. As $x_m(t - T(t))$ is bounded and the filter $H_r(s)$ is stable then the trajectories x_{od}, $\dot{x}_{od}$ and $\ddot{x}_{od}$ are bounded, x_o and $\dot{x}_o$ are also bounded.

There exists the redundancy of the slave controller (7.53) with $u_S = \sum_{i=1}^{n} A_i^{-T} u_{si}$ where u_{si} are the input to the slaves. The inputs u_{si} with the internal force distribution are designed as follows [162]:

$$[u_{s1} \cdots u_{sn}] = A_s^{\ddagger} u_S + F_{int} \tag{7.60}$$

where $A_s^{\ddagger} = Q^{-1} A_s^T [A_s Q^{-1} A_s^T]$, $A_s = [A_1^{-T} \ldots A_n^{-T}]$ and Q is a weighting matrix which is used to optimize the norm of the control inputs. The internal force F_{int} is chosen as $A_s F_{int} = 0$ so that it has no effect on the motion of the object. Another possible selection of F_{int} can be as follows:

$$F_{int} = [A_1^T \quad -A_2^T \quad A_3^T \cdots A_{n-1}^T \quad -A_n^T] f_d \tag{7.61}$$

where f_d is an arbitrary predefined force vector.

Remark 1: Theorem 1 guarantees the stability of the master side without being dependent on the stability of the slave side. Theorem 2 and Theorem 3 guarantee the stability of the slave side when the signal transmitted from the master side is bounded.

Remark 2: Unlike conventional teleoperation, the master side receives the estimated values of the environmental parameters and environmental force is predicted. When we have $\hat{\theta}_e \longrightarrow \theta_e$ in *Lemma 1* and tracking performance of $x_o(t) \longrightarrow [k_m \Phi_o(x_m(t - T(t)))]$ then we achieve $\hat{F}_e \longleftrightarrow F_e(t + T(t))$ which provides the human operator the feeling of operation without any delay.

Remark 3: Theorem 2 guarantees that given a reference velocity, the mobile platforms of the manipulators achieve the velocity consensus.

Remark 4: Theorem 3 guarantees that $e_s = x_o - x_{od}$ will be converging to the known bound when the parameters are unknown.

Remark 5: An optimized distribution of the control input for slaves can be achievable when internal force control (7.60) is used.

7.3 Simulation Results

In the simulation, a 2-DOF master robotic arm is operated by the human operator. The parameters of the 2-DOF mobile manipulators are given in Table 6.1. The parameter values of the master manipulator are $m_1 = 1\ kg, m_2 = 1\ kg, I_1 = 0.2\ kgm^2, I_2 = 0.2\ kgm^2, l_{c1} = 0.05\ m, l_{c2} = 0.05\ m, L_1 = 0.1\ m, L_2 = 0.1\ m$. The parameters of the object are $M_o = diag\{5,1\}, C_o = \{0\}, G_o = \{0, 5*9.8\}$. The kinematic chain between the object and the slave manipulators is given by $x_o = x_1 = diag(-1,1) \times x_2$. The parameters in (7.4) are chosen to be $B_e = [50,-30]^T, K_e = [50,10]^T$ and $C_e = [0,0]^T$. For the control design, the projection type estimation algorithm parameters are $\alpha = 0.02, \zeta_m = 5000$ and $\nu = 0.1$. The initial estimates and the lower and upper bounds of the parameter variations are chosen to be $\theta_e(0) = [80,0,80,3,0,0]^T, \theta_{e_{min}} = [0,-40,0,0,0,0]^T$ and $\theta_{e_{max}} = [100,100,80,80,0,0]^T$. The filter $H_f(s)$ is chosen to have $\gamma_f = 0.005$. The scaling gains are $k_m = 10$ and $k_f = 0.1$ respectively. The weighting matrix for internal force control is $Q = diag\{1,1\}$ and $f_d = 0$. The slave gains are $k_{s1} = diag\{50,150\}$ and $K_d = diag\{250,375\}$. The filter $H_r(s)$ is chosen to have $\tau_r = 0.005$ in order to generate the desired object trajectory. The target parameter of the master side is chosen as $\theta_d = [2,0.4]^T$ this means that $M_d = diag\{2,2\}, C_d = \{0\}$ and $G_d = [0, 2*9.8]^T$. The master parameters are $\Gamma_m = diag\{2,2,4,4\}, k_{m1} = diag\{150,150\}$ and $K_p = diag\{75,37.5\}$. The gains for the mobile base are $k_{pv} = 10$ and $k_{bp} = 14$. The time delays in the simulation can be upto 1 s.

7.3.1 Simulation Scenario:

The simulation considers the teleoperation of a single master multiple slave system (SMMS) where the slaves are connected with a communication topology $\mathcal{G}_1$ as in Fig.6.4 where the Laplacian matrix is given by $\mathcal{L} = [1\ 0\ -1; -1\ 1\ 0; 0\ -1\ 1]$. The in-degree d_i and the weights w_{ij} are chosen to be 1. The agents are strongly connected over a communication topology and the delay T_d is considered to be 0.2 s. The main objective is to transport the object to a desired position following a desired trajectory while the end-effectors grasp the object rigidly. The communication delay between the master and slaves is set to be 0.5 s. The human inputs are simulated as $F_h(1) = 0.5sin(\pi t)$ and $F_h(2) = sin(\pi t)$ as shown in Figs.7.2(a) and 7.2(b). The desired and actual master trajectories are shown in Figs.7.3(a), 7.3(b), 7.3(c) and 7.3(d) and their corresponding errors are shown in Figs.7.3(e) and 7.3(f).

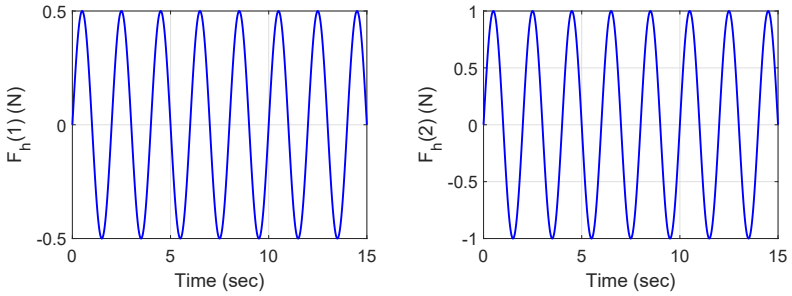

(a) (b)

Figure 7.2: The human inputs

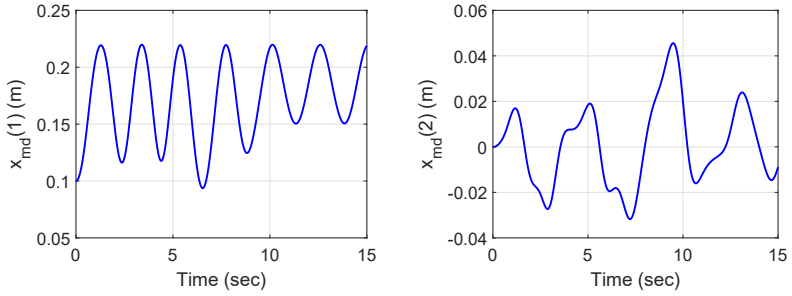

(a) (b)

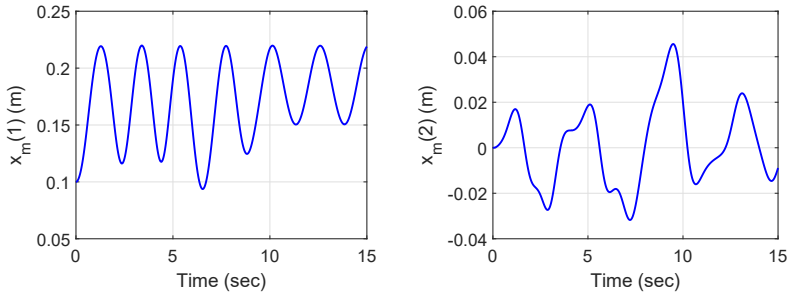

(c) (d)

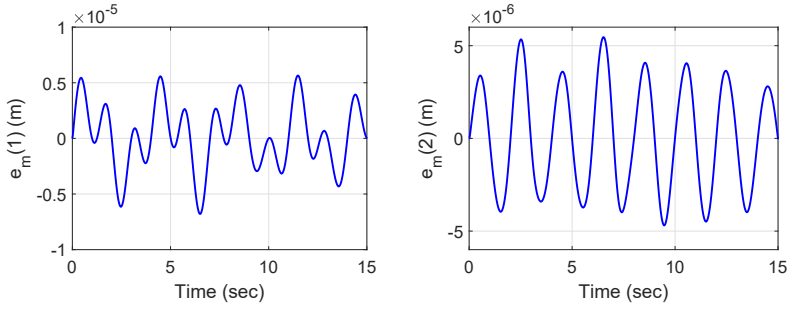

(e) (f)

Figure 7.3: Master trajectories: desired, actual and their error

In the master side, the environmental force is predicted based on the estimated environmental parameters. The actual and predicted environmental forces are presented in Figs.7.4(a), 7.4(b), 7.4(c) and 7.4(d). It should be noted that although the actual environmental forces are delayed due to communication channel delay but the human operator is still able to feel the environmental force without any delays. This means that the proposed controller design not only ensures the stability of the system but also provides good realism in the teleoperation system.

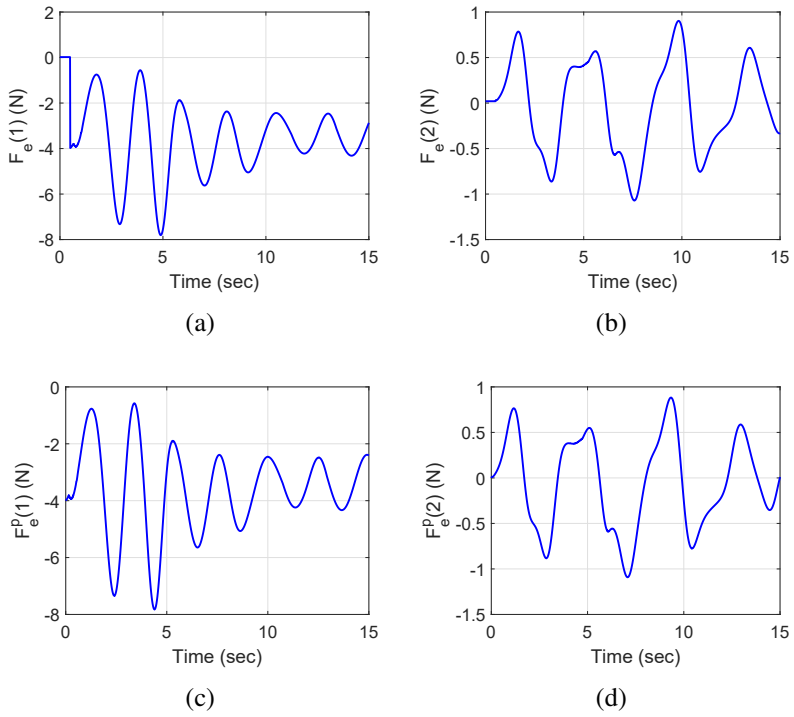

Figure 7.4: The contact force F_e and its prediction $\hat{F}_e$

The estimated environmental parameters of (7.4) are shown in Figs.7.5(a), 7.5(b), 7.5(c), 7.5(d), 7.5(e) and 7.5(f) respectively. It can be observed that the estimation starts with the initial estimates and converges to the true values of the parameters. This also ensures that the adaptation laws are working perfectly and the environmental force can be predicted with precision. The forces exerted on the object by the slave end-effectors are presented in Figs.7.6(a), 7.6(b), 7.6(c), 7.6(d), 7.6(e) and 7.6(f) respectively. It can be observed from the object trajectory that the slaves stay still for few seconds in the start of the simulation and then start moving the object to follow the desired trajectory. This affects the forces exerted on the object by the slaves. As the object starts moving, the forces are being exerted on the

object by the end-effectors. It should also be noted that the practical internal force of the object can essentially be just the difference of all the forces exerted on the object.

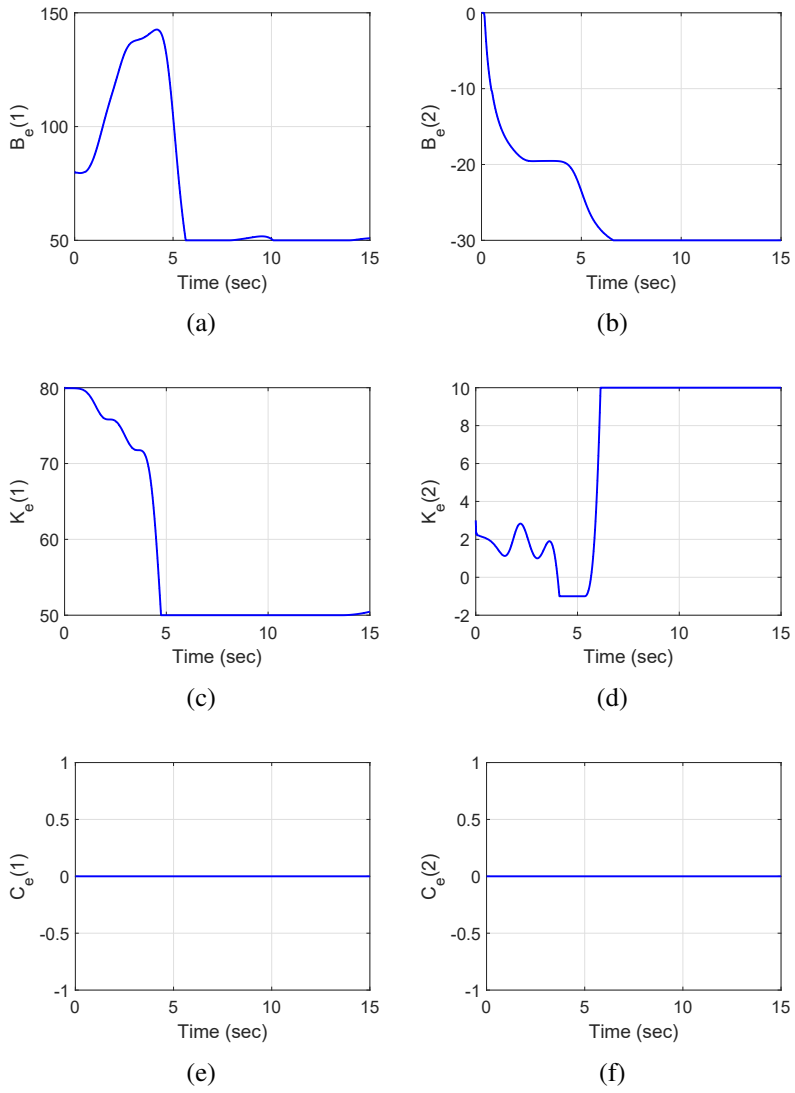

Figure 7.5: The estimates of environmental parameters $\hat{\theta}_e$

The desired object trajectory and its errors are shown in Figs.7.7(a), 7.7(b), 7.7(c) and 7.7(d). It is clear from the results that the object closely follows the desired trajectory and the task accomplishment of the transportation of the object can be achieved as desired. The tracking errors of the positions of the mobile platforms of the slaves are shown in Figs.7.8(a), 7.8(b) and 7.8(c). The mobile platforms regulate their position during the task accomplishment to achieve the prioritized mission of the object transportation. The results of mobile platforms show some errors but as the platforms are only controlled in the null

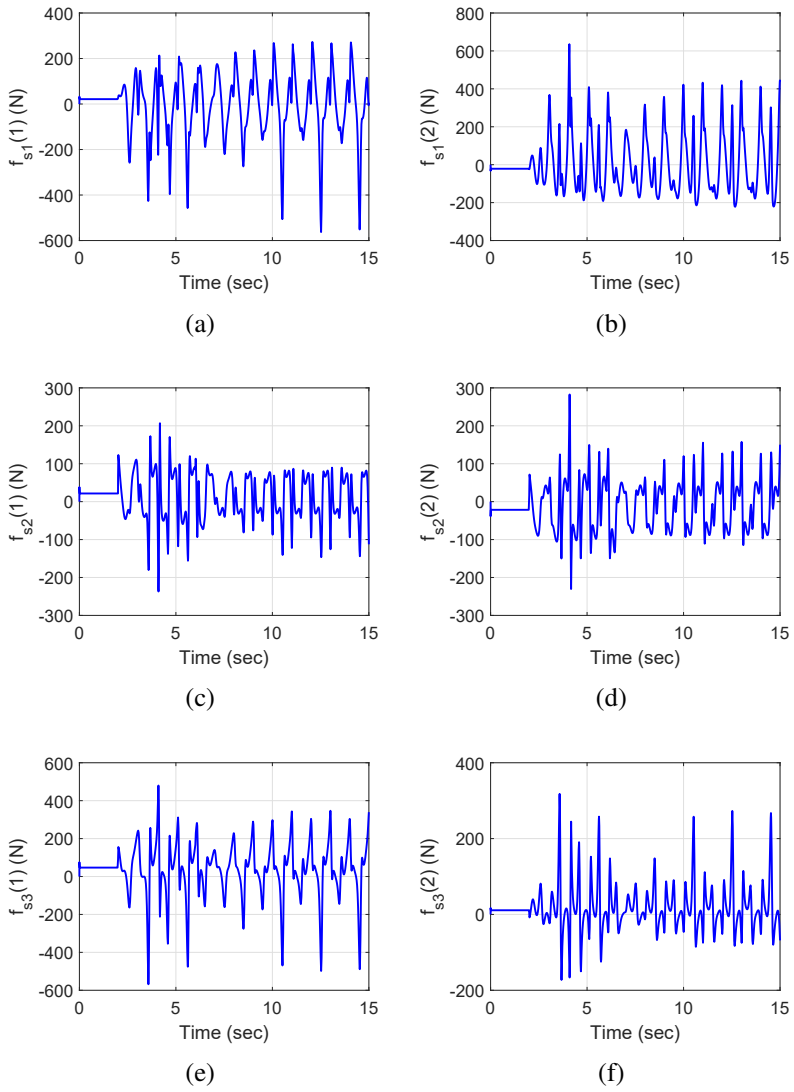

Figure 7.6: The forces exerted on the object

space only so these errors are acceptable as we achieve the main task.

From the results presented here, we can conclude that the teleoperation control structure for SMMS is efficient under communication delays. In contrast to traditional teleoperation schemes where the environment force signals are sent over the communication channel to the master side, our proposed control design is working perfectly when we transmit the estimated environmental parameters to the master side. The desired object trajectory is tracked with very small errors and the mobile platforms of the slaves adjust their positions to achieve the prioritized task of object transportation.

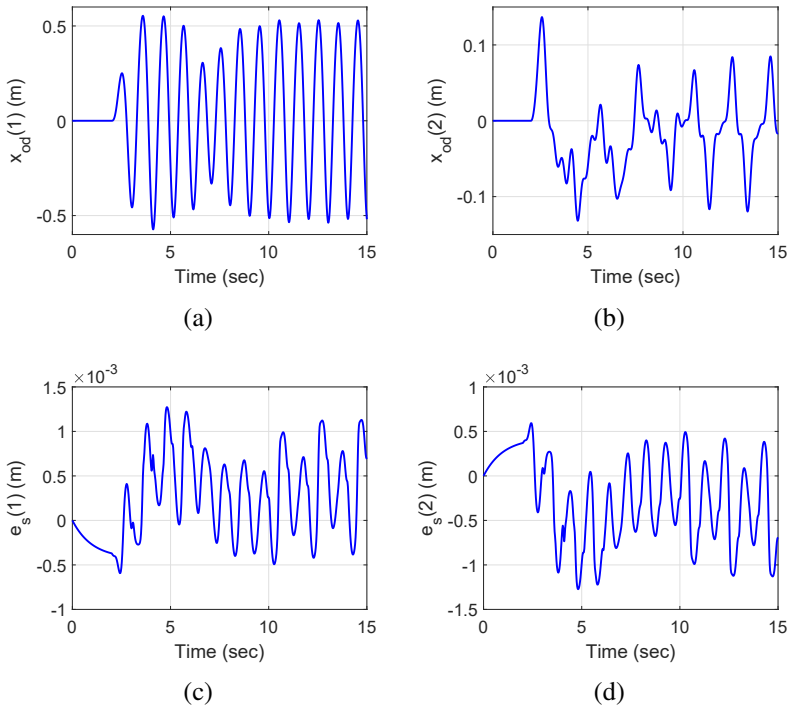

Figure 7.7: The desired object trajectory x_{od} and its tracking error

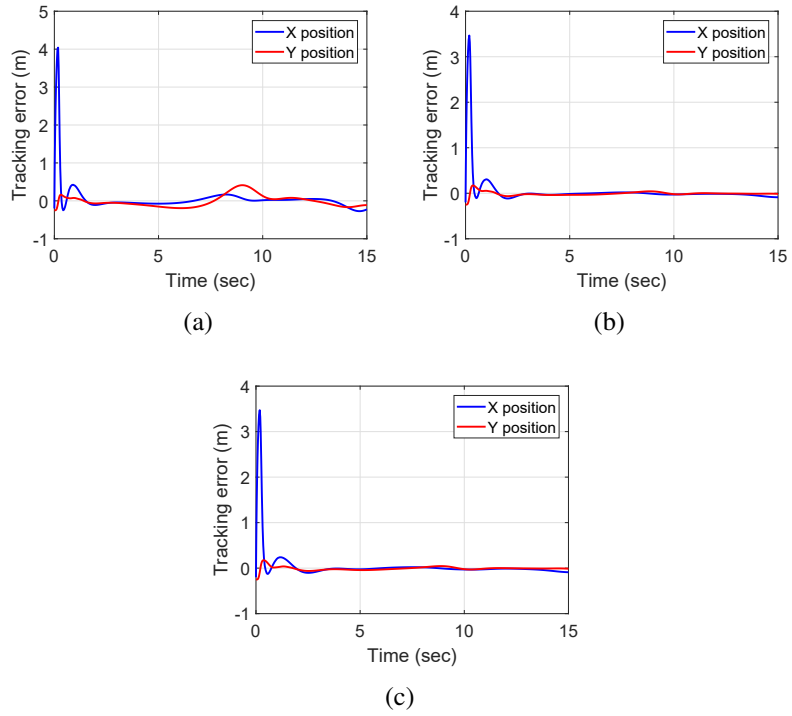

Figure 7.8: Mobile platform position errors

7.4 Summary

In this chapter, we proposed a novel control scheme for the teleoperation of single master multiple slave system where the master was considered to be a robotic manipulator whereas the slaves were the mobile manipulators. A human operator operated the master robot to remotely control the slaves to handle a target object. A desired master trajectory was generated at the master side so the master tracked that trajectory and the master position signal was transmitted to the slave side over the communication channel. An optimal processing was carried out on the position signal of the master to generate the desired object trajectory and the reference velocity signal for the mobile platforms. A robust adaptive controller and a null space controller were designed for the slaves and an internal force distribution was implemented. The slaves interacted with the target object and exerted forces on it. The force feedback signal of traditional teleoperation was replaced by the estimated environmental parameters to avoid the passivity problem of the communication channel. The environment force was effectively predicted using the estimated environmental parameters. The control design achieved the control objectives of stability, synchronization and force distribution. The simulation results of one master and three slaves teleoperation system validated the effectiveness of the proposed control scheme.

Chapter 8

Conclusions and Future Work

This chapter first summarizes the contribution of this research work and then provides some future directions to extend the proposed control designs for the teleoperation and cooperative control of multiple manipulators.

8.1 Conclusions

In this thesis, novel control design schemes have been proposed for the teleoperation and cooperative control of robotic manipulators. For the multilateral teleoperation control of fixed-base robotic manipulators several control schemes have been proposed in recent years and one of the widely used control scheme is Time Domain Passivity Control. Although, TDPC has provided efficient results in the bilateral and multilateral teleoperation of manipulators, its conventional control laws experience singular points or zero division. This zero division is not desirable in teleoperation control as it crashes the control law leading the whole system to be unstable. This instability can be dangerous not only for the hardware but the safety of the human operator is also compromised. To avoid zero division, this work has proposed an improved control design of TDPC for multilateral teleoperation of fixed-base manipulators which not only ensures the stability of the system but also provides the flexibility of assigning weights to the master and slaves during the operation. The weights can be assigned to to influence the velocity of the masters or the forces of the slaves depending on the nature of the application. The proposed control design has been tested in extensive simulations and experiments under constant and time varying delays and the results validate the efficacy of the proposed control design.

A couple of control designs have also been proposed for the cooperative/coordinated control of the mobile manipulators handling a target object which is rigidly attached to their end-effectors. One of the proposed controller is based on the adaptive backstepping for cooperative manipulation of the object under parametric uncertainties simultaneously controlling the end-effectors and the mobile bases. The controller was designed in two

stages where the first stage dealt with the velocity control of the mobile base/end-effectors and the second stage dealt with the torque control of the mobile manipulators. The simulation results of the proposed controller for two mobile manipulators system validated the effectiveness of the control design in transportation of the object following desired trajectories. Another control architecture has also been proposed for cooperative manipulation of an object and the controller design is divided in the operational and null space of the mobile manipulators. An adaptive synchronous motion controller is designed first then the redundancy resolution of the mobile manipulators has been achieved by decoupling the system into operational and null space. The operational space controller controls the end-effectors to follow a given trajectory and the null space controller controls the mobile platforms. The decoupling of the mobile manipulator system is done in such a way that the control of operational space and null space do not affect each other meaning that the torques of the null space do not affect the motion of the end-effectors. The controller design assumed that the agents are strongly connected over a fixed communication topology. The simulation was carried out for three mobile manipulators carrying a common object. The results validated the stability of the system while transporting the object to a desired position.

Finally, a novel adaptive robust control design has been proposed for the teleoperation of single master multiple slaves system. The teleoperation framework involves one fixed-base manipulator as the master and three mobile manipulators as the slaves. Unlike traditional teleoperation structure, the proposed framework predicts the environment reaction force on the master side instead of directly transmitting the force from the slave side. Although the signal transmission from the master is same like other teleoperation schemes as it transmits the velocity signal of the master to the slave side however, on the slave side the environmental parameters are estimated and then transmitted to the master side for force prediction. The advantage of this transmission of the estimated parameters of the environment to the master side is the undelayed force which the human operator feels. The adaptive robust control not only provided good tracking of the slaves but also improved the transparency of the system. An optimal internal force distribution was implemented to manipulate the target object attached to the end-effectors of the mobile manipulators. The null space control is applied to control the mobile platforms of the mobile manipulator system. The simulation results of SMMS system proved the efficacy of the proposed scheme.

8.2 Future Work

In terms of the transparency of the teleoperation systems, the proposed TDPC in Chapter 3 is comparatively conservative with the output of the passivity controllers. Transparency is one of the main performance metric in teleoperation systems and to provide the human operator the real feel of the operation in the remote environment, it is important to have better realism in teleoperation control. One possible future direction can be the improvement of the proposed TDPC to ensure the better transparency of the system.

For the cooperative/coordinated control or teleoperation of mobile manipulators in Chapter 5, 6 and 7, there is a possibility to test different control mechanism to control the internal force of the object which is being manipulated. The possible options can be the virtual linkage model or the use of grasp matrix for object manipulation. The integration of the proposed cooperative control with different internal force control methods may provide interesting results. Additionally, in Chapter 6 and 7 the proposed control did not consider the cases where the agents are not connected over a strong communication topology. Future directions may focus on testing the proposed control considering the switching graph topologies or the link failure scenarios to add to the robustness of the control. In chapter 7, the control design of mobile manipulator teleoperation assumes that the signals F_{hc} and F_e are measurable. In reality, sometimes the hardware is not equipped with the required sensors so it is necessary to realize a control design which can deal with the system when some of the signals are not measurable.

Moreover, the assumptions on the kinematic modeling of the mobile manipulator system may need consideration of the slippage or skidding of the wheels. These considerations would definitely need extensive mathematical modeling but will result in better flexible control schemes. The control schemes which have only been tested in simulations need real time testing too. Real time control of teleoperaion systems is highly desirable to test the proposed schemes under the constraint of time delays.

Bibliography

[1] Peter F. Hokayem and Mark W. Spong. Bilateral teleoperation: An historical survey. *Automatica*, 42(12):2035–2057, December 2006.

[2] Bruno Siciliano and Oussama Khatib. *Springer Handbook of Robotics*. Springer, 2016.

[3] Manuel Ferre, Martin Buss, Rafael Aracil, Claudio Melchiorri, and Carlos Balaguer. *Advances in telerobotics*, volume 31. Springer, 2007.

[4] Jong-Hwan Kim, Shuzhi Sam Ge, Prahlad Vadakkepat, Norbert Jesse, Abdullah Al Manum, Sadasivan Puthusserypady K, Ulrich Rückert, Joaquin Sitte, Ulf Witkowski, Ryohei Nakatsu, et al. Advances in robotics. *Lecture Notes in Computer Science*, 5744, 2009.

[5] John J Craig. *Introduction to robotics: mechanics and control*, volume 3. Pearson Prentice Hall Upper Saddle River, 2005.

[6] Mark W Spong and Mathukumalli Vidyasagar. *Robot dynamics and control*. John Wiley & Sons, 2008.

[7] Peyman Setoodeh, Shahin Sirouspour, and Ali Shahdi. Discrete-time multi-model control for cooperative teleoperation under time delay. In *Robotics and Automation, 2006. ICRA 2006. Proceedings 2006 IEEE International Conference on*, pages 2921–2926. IEEE, 2006.

[8] Ramtin Rakhsha and Daniela Constantinescu. Passive shared virtual environment for distributed haptic cooperation. In *Haptics Symposium (HAPTICS), 2014 IEEE*, pages 221–226. IEEE, 2014.

[9] Takahiro Kanno and Yasuyoshi Yokokohji. Multilateral teleoperation control over time-delayed computer networks using wave variables. In *Haptics Symposium (HAPTICS), 2012 IEEE*, pages 125–131. IEEE, 2012.

[10] Ilia G Polushin, Sergey N Dashkovskiy, Amir Takhmar, and Rajni V Patel. A small gain framework for networked cooperative force-reflecting teleoperation. *Automatica*, 49(2):338–348, 2013.

[11] Shahin Sirouspour. Modeling and control of cooperative teleoperation systems. *Robotics, IEEE Transactions on*, 21(6):1220–1225, 2005.

[12] Robert J. Anderson and Mark W. Spong. Bilateral control of teleoperators with time delay. *IEEE Transactions on Automatic Control*, 34(5):494–501, May 1989.

[13] Robert J. Anderson and Mark W. Spong. Asymptotic stability of force reflecting teleoperators with time delay. *The International Journal of Robotics Research*, 11(2):135–149, April 1992.

[14] John E. Speich, Kevin Fite, and Michael Goldfarb. A method for simultaneously increasing transparency and stability robustness in bilateral telemanipulation. In *Proceedings of the IEEE International Conference on Robotics and Automation ICRA 2000*, pages 2671–2676, San Francisco, CA, April 2000.

[15] Wei Zhang, Michael S. Branicky, and Stephen M. Phillips. Stability of networked control systems. *IEEE Control Systems Magazine*, 21:84–99, February 2001.

[16] Yongqiang Ye, Ya-Jun Pan, and Yash Gupta. A power based time domain passivity control for haptic interfaces. In *the Proceedings of the 48th IEEE Conference on Decision and Control*, pages 7521–7526, Shanghai, China, 2009.

[17] Yonqiang Ye, Ya-Jun Pan, Yash Gupta, and Julian Ware. A power based time domain passivity control for haptic interfaces. *IEEE Transactions on Control Systems Technology*, 19(4):874–883, July 2011.

[18] H WP Maurice Heemels, Andrew R Teel, Nathan van de Wouw, and Dragan Nesic. Networked control systems with communication constraints: Tradeoffs between transmission intervals, delays and performance. *Automatic Control, IEEE Transactions on*, 55(8):1781–1796, 2010.

[19] Sekhar Tatikonda and Sanjoy Mitter. Control under communication constraints. *Automatic Control, IEEE Transactions on*, 49(7):1056–1068, 2004.

[20] Joao P Hespanha, Payam Naghshtabrizi, and Yonggang Xu. A survey of recent results in networked control systems. *PROCEEDINGS-IEEE*, 95(1):138, 2007.

[21] Yodyium Tipsuwan and Mo-Yuen Chow. Control methodologies in networked control systems. *Control engineering practice*, 11(10):1099–1111, 2003.

[22] Tai C Yang. Networked control system: a brief survey. *IEE Proceedings-Control Theory and Applications*, 153(4):403–412, 2006.

[23] Wei Zhang, Michael S Branicky, and Stephen M Phillips. Stability of networked control systems. *Control Systems, IEEE*, 21(1):84–99, 2001.

[24] Alberto Bemporad, Maurice Heemels, and Mikael Johansson. *Networked control systems*, volume 406. Springer, 2010.

[25] Fei-Yue Wang and Derong Liu. *Networked control systems*. Springer, 2008.

[26] Johan Nilsson et al. *Real-time control systems with delays*. PhD thesis, Lund institute of Technology Lund, Sweden, 1998.

[27] Mahya Shahbazi, S Farokh Atashzar, and Rajni Patel. A systematic review of multilateral teleoperation systems. *IEEE Transactions on Haptics*, 2018.

[28] Shahin Sirouspour and Peyman Setoodeh. Adaptive nonlinear teleoperation control in multi-master/multi-slave environments. In *Control Applications, 2005. CCA 2005. Proceedings of 2005 IEEE Conference on*, pages 1263–1268. IEEE, 2005.

[29] Pawel Malysz and Shahin Sirouspour. Cooperative teleoperation control with projective force mappings. In *Haptics Symposium, 2010 IEEE*, pages 301–308. IEEE, 2010.

[30] Pawel Malysz and Shahin Sirouspour. Trilateral teleoperation control of kinematically redundant robotic manipulators. *The International Journal of Robotics Research*, 30(13):1643–1664, 2011.

[31] Mahya Shahbazi, Heidar Ali Talebi, Seyed Farokh Atashzar, Farzad Towhidkhah, Rajni V Patel, and Siamak Shojaei. A novel shared structure for dual user systems with unknown time-delay utilizing adaptive impedance control. In *Robotics and Automation (ICRA), 2011 IEEE International Conference on*, pages 2124–2129. IEEE, 2011.

[32] H Amini, V Dabbagh, SM Rezaei, M Zareinejad, NA Mardi, and Ahmed AD Sarhan. Robust control-based linear bilateral teleoperation system without force sensor. *Journal of the Brazilian Society of Mechanical Sciences and Engineering*, 37(2):579–587, 2015.

[33] Zheng Chen, Ya-Jun Pan, and Jason Gu. Integrated adaptive robust control for multilateral teleoperation systems under arbitrary time delays. *International Journal of Robust and Nonlinear Control*, 26(12):2708–2728, 2016.

[34] Behzad Khademian and Keyvan Hashtrudi-Zaad. A robust multilateral shared controller for dual-user teleoperation systems. In *Electrical and Computer Engineering, 2008. CCECE 2008. Canadian Conference on*, pages 001871–001876. IEEE, 2008.

[35] Moein Shahbazi, S Farokh Atashzar, and Rajni V Patel. A dual-user teleoperated system with virtual fixtures for robotic surgical training. In *Robotics and Automation (ICRA), 2013 IEEE International Conference on*, pages 3639–3644. IEEE, 2013.

[36] Mahya Shahbazi, Seyed Farokh Atashzar, Heidar A Talebi, and Rajni V Patel. Novel cooperative teleoperation framework: Multi-master/single-slave system. *IEEE/ASME Transactions on Mechatronics*, 20(4):1668–1679, 2015.

[37] Peter F Hokayem and Mark W Spong. Bilateral teleoperation: An historical survey. *Automatica*, 42(12):2035–2057, 2006.

[38] Gunter Niemeyer and J-JE Slotine. Using wave variables for system analysis and robot control. In *Robotics and Automation, 1997 IEEE International Conference on*, volume 2, pages 1619–1625. IEEE, 1997.

[39] Günter Niemeyer and Jean-Jacques E Slotine. Telemanipulation with time delays. *The International Journal of Robotics Research*, 23(9):873–890, 2004.

[40] Charles A Desoer and Mathukumalli Vidyasagar. *Feedback systems: input-output properties*, volume 55. Siam, 1975.

[41] Da Sun, Fazel Naghdy, and Haiping Du. Stability control of force-reflected nonlinear multilateral teleoperation system under time-varying delays. *Journal of Sensors*, 2016, 2015.

[42] Takahiro Kanno and Yasuyoshi Yokokohji. Avoiding conflicts of operators in multi-user teleoperation systems. In *World Haptics Conference (WHC), 2013*, pages 401–406. IEEE, 2013.

[43] Yasunori Kawai and Tokio Yoshino2 Takanori Miyoshi. An experiments on improving tracking performance in multilateral teleoperation using wave filter. In *Proc. of SICE Annual Conference*, pages 1859–1862, 2014.

[44] Mahya Shahbazi, H Ali Talebi, and Rajni V Patel. Networked dual-user teleoperation with time-varying authority adjustment: A wave variable approach. In *2014 IEEE/ASME International Conference on Advanced Intelligent Mechatronics*, pages 415–420. IEEE, 2014.

[45] Naser Yasrebi and Daniela Constantinescu. Centralized multi-user multi-rate haptic cooperation using wave transformation. In *Mechatronics and Automation, 2009. ICMA 2009. International Conference on*, pages 3816–3821. IEEE, 2009.

[46] Ildar Farkhatdinov, Jee-Hwan Ryu, and Jury Poduraev. A feasibility study of time-domain passivity approach for bilateral teleoperation of mobile manipulator. In *Control, Automation and Systems, 2008. ICCAS 2008. International Conference on*, pages 272–277. IEEE, 2008.

[47] Jee-Hwan Ryu, Dong-Soo Kwon, and Blake Hannaford. Stable teleoperation with time-domain passivity control. *Robotics and Automation, IEEE Transactions on*, 20(2):365–373, 2004.

[48] Julian Ware, Ya-Jun Pan, and Trent Hilliard. A new bilaterally teleoperated robotic vehicle platform with passivity control. In *American Control Conference (ACC), 2011*, pages 2837–2842. IEEE, 2011.

[49] J Ware and Y-J Pan. Realisation of a bilaterally teleoperated robotic vehicle platform with passivity control. *IET control theory & applications*, 5(8):952–962, 2011.

[50] Yongqiang Ye, Ya-Jun Pan, Yash Gupta, and Julian Ware. A power-based time domain passivity control for haptic interfaces. *Control Systems Technology, IEEE Transactions on*, 19(4):874–883, 2011.

[51] Yongqiang Ye, Ya-Jun Pan, and Trent Hilliard. Bilateral teleoperation with time-varying delay: A communication channel passification approach. *IEEE/ASME Transactions on Mechatronics*, 18(4):1431–1434, 2013.

[52] Michael Panzirsch, Thomas Hulin, Jordi Artigas, Christian Ott, and Manuel Ferre. Integrating measured force feedback in passive multilateral teleoperation. In *International Conference on Human Haptic Sensing and Touch Enabled Computer Applications*, pages 316–326. Springer, 2016.

[53] Zheng Chen, Ya-Jun Pan, Jason Gu, and Shane Forbrigger. A novel multilateral teleoperation scheme with power-based time-domain passivity control. *Transactions of the Institute of Measurement and Control*, 40(11):3252–3262, 2018.

[54] Ken Goldberg, Billy Chen, Rory Solomon, Steve Bui, Bobak Farzin, Jacob Heitler, Derek Poon, and Gordon Smith. Collaborative teleoperation via the internet. In *Robotics and Automation, 2000. Proceedings. ICRA'00. IEEE International Conference on*, volume 2, pages 2019–2024. IEEE, 2000.

[55] Zhijun Li, Yuanqing Xia, Dehong Wang, Di-Hua Zhai, Chun-Yi Su, and Xingang Zhao. Neural network-based control of networked trilateral teleoperation with geometrically unknown constraints. *IEEE transactions on cybernetics*, 46(5):1051–1064, 2016.

[56] Zhijun Li, Chenguang Yang, Chun-Yi Su, Shuming Deng, Fuchun Sun, and Weidong Zhang. Decentralized fuzzy control of multiple cooperating robotic manipulators with impedance interaction. *IEEE Transactions on Fuzzy Systems*, 23(4):1044–1056, 2015.

[57] Zhijun Li, Yuanqing Xia, and Fuchun Sun. Adaptive fuzzy control for multilateral cooperative teleoperation of multiple robotic manipulators under random network-induced delays. *IEEE Transactions on Fuzzy Systems*, 22(2):437–450, 2014.

[58] Zhijun Li, Liang Ding, Haibo Gao, Guangren Duan, and Chun-Yi Su. Trilateral teleoperation of adaptive fuzzy force/motion control for nonlinear teleoperators with communication random delays. *IEEE transactions on Fuzzy Systems*, 21(4):610–624, 2013.

[59] Umar Farooq, Jason Gu, Mohamed El-Hawary, Muhammad Usman Asad, and Jun Luo. An extended state convergence architecture for multilateral teleoperation systems. *IEEE Access*, 5:2063–2079, 2017.

[60] Umar Farooq, Jason Gu, Mohamed El-Hawary, Valentina E Balas, Marius M Balas, Ghulam Abbas, Muhammad Usman Asad, and Jun Luo. State convergence-based control of a multi-master-single-slave non-linear teleoperation system. *Acta Polytechnica Hungarica*, 15(4), 2018.

[61] M Shahbazi, HA Talebi, and MJ Yazdanpanah. A control architecture for dual user teleoperation with unknown time delays: A sliding mode approach. In *2010 IEEE/ASME International Conference on Advanced Intelligent Mechatronics*, pages 1221–1226. IEEE, 2010.

[62] Mahya Shahbazi, S Farokh Atashzar, Heidar A Talebi, Farzad Towhidkhah, and MJ Yazdanpanah. A sliding-mode controller for dual-user teleoperation with unknown constant time delays. *Robotica*, 31(04):589–598, 2013.

[63] M Shahbazi, SF Atashzar, HA Talebi, and RV Patel. A multi-master/single-slave teleoperation system. In *ASME 2012 5th Annual Dynamic Systems and Control Conference joint with the JSME 2012 11th Motion and Vibration Conference*, pages 107–112. American Society of Mechanical Engineers, 2012.

[64] Zhijun Li and Shuzhi Sam Ge. *Fundamentals in Modeling and Control of Mobile Manipulators*, volume 49. CRC Press, 2013.

[65] Mohamed Boukattaya, Mohamed Jallouli, and Tarak Damak. On trajectory tracking control for nonholonomic mobile manipulators with dynamic uncertainties and external torque disturbances. *Robotics and autonomous systems*, 60(12):1640–1647, 2012.

[66] Glenn White. *Simultaneous motion and interaction force control of a nonholonomic mobile manipulator*. State University of New York at Buffalo, 2006.

[67] Mohamed Boukattaya, Tarak Damak, and Mohamed Jallouli. Robust adaptive control for mobile manipulators. *International Journal of Automation and Computing*, 8(1):8–13, 2011.

[68] Gong-Bo Dai and Yen-Chen Liu. Distributed coordination and cooperation control for networked mobile manipulators. *IEEE Transactions on Industrial Electronics*, 64(6):5065–5074, 2017.

[69] Antonio Petitti, Antonio Franchi, Donato Di Paola, and Alessandro Rizzo. Decentralized motion control for cooperative manipulation with a team of networked mobile manipulators. In *Robotics and Automation (ICRA), 2016 IEEE International Conference on*, pages 441–446. IEEE, 2016.

[70] Victor H Andaluz, Jessica S Ortiz, María Pérez, Flavio Roberti, and Ricardo Carelli. Adaptive cooperative control of multi-mobile manipulators. In *Industrial Electronics Society, IECON 2014-40th Annual Conference of the IEEE*, pages 2669–2675. IEEE, 2014.

[71] Taher Hekmatfar, Ellips Masehian, and Seyed Javad Mousavi. Cooperative object transportation by multiple mobile manipulators through a hierarchical planning architecture. In *Robotics and Mechatronics (ICRoM), 2014 Second RSI/ISM International Conference on*, pages 503–508. IEEE, 2014.

[72] Víctor H Andaluz, Paúl A Canseco, Andrés Rosales, Flavio Roberti, and Ricardo Carelli. Multilayer scheme for the adaptive cooperative coordinated control of mobile manipulators. In *IECON 2012-38th Annual Conference on IEEE Industrial Electronics Society*, pages 2737–2743. IEEE, 2012.

[73] Hyunsoo Yang and Dongjun Lee. Cooperative grasping control of multiple mobile manipulators with obstacle avoidance. In *Robotics and Automation (ICRA), 2013 IEEE International Conference on*, pages 836–841. IEEE, 2013.

[74] A-N Ponce-Hinestroza, J-A Castro-Castro, H-I Guerrero-Reyes, Vicente Parra-Vega, and E Olguín-Díaz. Cooperative redundant omnidirectional mobile manipulators: Model-free decentralized integral sliding modes and passive velocity fields. In *Robotics and Automation (ICRA), 2016 IEEE International Conference on*, pages 2375–2380. IEEE, 2016.

[75] Markus Giftthaler, Farbod Farshidian, Timothy Sandy, Lukas Stadelmann, and Jonas Buchli. Efficient kinematic planning for mobile manipulators with non-holonomic constraints using optimal control. *arXiv preprint arXiv:1701.08051*, 2017.

[76] Mahdi Souzanchi-K, Aliasghar Arab, Mohammad-R Akbarzadeh-T, and Mohammad Mehdi Fateh. Robust impedance control of uncertain mobile manipulators using time-delay compensation. *IEEE Transactions on Control Systems Technology*, 2017.

[77] Zijian Wang and Mac Schwager. Kinematic multi-robot manipulation with no communication using force feedback. In *Robotics and Automation (ICRA), 2016 IEEE International Conference on*, pages 427–432. IEEE, 2016.

[78] Chao Tang, Chunquan Xu, Aiguo Ming, and Makoto Shimojo. Cooperative control of two mobile manipulators transporting objects on the slope. In *Mechatronics and Automation, 2009. ICMA 2009. International Conference on*, pages 2805–2810. IEEE, 2009.

[79] Rafael Fierro and Frank L Lewis. Control of a nonholonomic mobile robot: backstepping kinematics into dynamics. In *Decision and Control, 1995., Proceedings of the 34th IEEE Conference on*, volume 4, pages 3805–3810, 1995.

[80] Jindong Tan, Ning Xi, and Yuechao Wang. Integrated task planning and control for mobile manipulators. *The International Journal of Robotics Research*, 22(5):337–354, 2003.

[81] Miroslav Krstic, Ioannis Kanellakopoulos, and Peter V Kokotovic. *Nonlinear and adaptive control design*. Wiley, 1995.

[82] Chiman Kwan and Frank L Lewis. Robust backstepping control of nonlinear systems using neural networks. *IEEE Transactions on Systems, Man, and Cybernetics-Part A: Systems and Humans*, 30(6):753–766, 2000.

[83] Randy Freeman and Petar V Kokotovic. *Robust nonlinear control design: state-space and Lyapunov techniques*. Springer Science & Business Media, 2008.

[84] Alpaslan Yufka and Metin Ozkan. Formation-based control scheme for cooperative transportation by multiple mobile robots. *International Journal of Advanced Robotic Systems*, 12(9):120, 2015.

[85] Joel M Esposito. Decentralized cooperative manipulation with a swarm of mobile robots: The approach problem. In *American Control Conference (ACC), 2010*, pages 4762–4767. IEEE, 2010.

[86] Zhijun Li, Jianxun Li, and Yu Kang. Adaptive robust coordinated control of multiple mobile manipulators interacting with rigid environments. *Automatica*, 46(12):2028–2034, 2010.

[87] Zhijun Li, Shuzhi Sam Ge, and Aiguo Ming. Adaptive robust motion/force control of holonomic-constrained nonholonomic mobile manipulators. *IEEE Transactions on Systems, Man, and Cybernetics, Part B (Cybernetics)*, 37(3):607–616, 2007.

[88] Sebastian Erhart, Dominik Sieber, and Sandra Hirche. An impedance-based control architecture for multi-robot cooperative dual-arm mobile manipulation. In *Intelligent Robots and Systems (IROS), 2013 IEEE/RSJ International Conference on*, pages 315–322. IEEE, 2013.

[89] Johan Markdahl, Yiannis Karayiannidis, and Xiaoming Hu. Cooperative object path following control by means of mobile manipulators: a switched systems approach. *IFAC Proceedings Volumes*, 45(22):773–778, 2012.

[90] Antonio Franchi, Antonio Petitti, and Alessandro Rizzo. Decentralized parameter estimation and observation for cooperative mobile manipulation of an unknown load using noisy measurements. In *Robotics and Automation (ICRA), 2015 IEEE International Conference on*, pages 5517–5522. IEEE, 2015.

[91] Caio Igor Gonçalves Chinelato and Luiz de Siqueira Martins-Filho. Control of cooperative mobile manipulators transporting a payload. In *Mechanical Engineering (COBEM), International Congress of*, pages 9943–9954, 2013.

[92] Min Wu, Yanhao He, and Steven Liu. Collaboration of multiple mobile manipulators with compliance based leader/follower approach. In *Industrial Technology (ICIT), 2016 IEEE International Conference on*, pages 48–53. IEEE, 2016.

[93] Zijian Wang and Mac Schwager. Force-amplifying n-robot transport system (force-ants) for cooperative planar manipulation without communication. *The International Journal of Robotics Research*, 35(13):1564–1586, 2016.

[94] Michael A Neumann, Matthew H Chin, and Christopher A Kitts. Object manipulation through explicit force control using cooperative mobile multi-robot systems. In *Proceedings of the World Congress on Engineering and Computer Science*, volume 1, 2014.

[95] Víctor Andaluz, VTL Rampinelli, Flavio Roberti, and Ricardo Carelli. Coordinated cooperative control of mobile manipulators. In *Industrial Technology (ICIT), 2011 IEEE International Conference on*, pages 300–305. IEEE, 2011.

[96] Hossein Bolandi and Amir Farhad Ehyaei. Trajectory planning of two cooperative mobile manipulators under closed-chain and differential constraints. *International Journal of Innovative Computing, Information and Control*, 8(2):1077–1102, 2012.

[97] Javier Alonso-Mora, Ross Knepper, Roland Siegwart, and Daniela Rus. Local motion planning for collaborative multi-robot manipulation of deformable objects. In *Robotics and Automation (ICRA), 2015 IEEE International Conference on*, pages 5495–5502. IEEE, 2015.

[98] Alexandres Nikou, Christos Verginis, Shahab Heshmati-Alamdari, and Dimos V Dimarogonas. A nonlinear model predictive control scheme for cooperative manipulation with singularity and collision avoidance. In *Control and Automation (MED), 2017 25th Mediterranean Conference on*, pages 707–712. IEEE, 2017.

[99] Andres Mora, Dylan F Glas, Takayuki Kanda, and Norihiro Hagita. A teleoperation approach for mobile social robots incorporating automatic gaze control and three-dimensional spatial visualization. *IEEE Transactions on Systems, Man, and Cybernetics: Systems*, 43(3):630–642, 2013.

[100] Zhijun Li, Jun Deng, Renquan Lu, Yong Xu, Jianjun Bai, and Chun-Yi Su. Trajectory-tracking control of mobile robot systems incorporating neural-dynamic optimized model predictive approach. *IEEE Transactions on Systems, Man, and Cybernetics: Systems*, 46(6):740–749, 2016.

[101] Zhijun Li, Hanzhen Xiao, Chenguang Yang, and Yiwen Zhao. Model predictive control of nonholonomic chained systems using general projection neural networks optimization. *IEEE Transactions on Systems, Man, and Cybernetics: Systems*, 45(10):1313–1321, 2015.

[102] Shao-Cheng Tong and Yong-Ming Li. Adaptive backstepping output feedback control for siso nonlinear system using fuzzy neural networks. *International Journal of Automation and Computing*, 6(2):145–153, 2009.

[103] Zhijun Li, Pey Yuen Tao, Shuzhi Sam Ge, Martin Adams, and Wijerupage Sardha Wijesoma. Robust adaptive control of cooperating mobile manipulators with relative motion. *IEEE Transactions on Systems, Man, and Cybernetics, Part B (Cybernetics)*, 39(1):103–116, 2009.

[104] Dongjun Lee and Mark W Spong. Bilateral teleoperation of multiple cooperative robots over delayed communication networks: Theory. In *Robotics and Automation, 2005. ICRA 2005. Proceedings of the 2005 IEEE International Conference on*, pages 360–365. IEEE, 2005.

[105] Oscar M Palafox and Mark W Spong. Bilateral teleoperation of a formation of nonholonomic mobile robots under constant time delay. In *Intelligent Robots and Systems, 2009. IROS 2009. IEEE/RSJ International Conference on*, pages 2821–2826. IEEE, 2009.

[106] Suna Zhao, Zhijun Li, Rongxin Cui, Yu Kang, Fuchun Sun, and Rong Song. Brain–machine interfacing-based teleoperation of multiple coordinated mobile robots. *IEEE Transactions on Industrial Electronics*, 64(6):5161–5170, 2017.

[107] Suna Zhao, Peng Xu, Zhijun Li, and Chun-Yi Su. Brain-actuated teleoperation control of a mobile robot. In *Robotics and Biomimetics (ROBIO), 2015 IEEE International Conference on*, pages 464–469. IEEE, 2015.

[108] Carlos Escolano, Javier Mauricio Antelis, and Javier Minguez. A telepresence mobile robot controlled with a noninvasive brain–computer interface. *IEEE Transactions on Systems, Man, and Cybernetics, Part B (Cybernetics)*, 42(3):793–804, 2012.

[109] Baocheng Wang, Zhijun Li, Wenjun Ye, and Qing Xie. Development of human-machine interface for teleoperation of a mobile manipulator. *International Journal of Control, Automation and Systems*, 10(6):1225–1231, 2012.

[110] Baocheng Wang, Zhijun Li, and Nan Ding. Speech control of a teleoperated mobile humanoid robot. In *Automation and Logistics (ICAL), 2011 IEEE International Conference on*, pages 339–344. IEEE, 2011.

[111] Tonatiuh Hernandez, Emmanuel Nuño, and Alma Y Alanis. Teleoperation of mobile manipulators with non-holonomic restrictions. In *Networking, Sensing, and Control (ICNSC), 2016 IEEE 13th International Conference on*, pages 1–6. IEEE, 2016.

[112] Zhijun Li and Chun-Yi Su. Neural-adaptive control of single-master–multiple-slaves teleoperation for coordinated multiple mobile manipulators with time-varying communication delays and input uncertainties. *IEEE transactions on neural networks and learning systems*, 24(9):1400–1413, 2013.

[113] Ildar Farkhatdinov and Jee-Hwan Ryu. Switching of control signals in teleoperation systems: Formalization and application. In *Advanced Intelligent Mechatronics, 2008. AIM 2008. IEEE/ASME International Conference on*, pages 353–358. IEEE, 2008.

[114] Víctor H Andaluz, Lucio Salinas, Flavio Roberti, Juan M Toibero, and Ricardo Carelli. Switching control signal for bilateral tele-operation of a mobile manipulator. In *Control and Automation (ICCA), 2011 9th IEEE International Conference on*, pages 778–783. IEEE, 2011.

[115] Antoine Lasnier and Toshiyuki Murakami. Hybrid sensorless bilateral teleoperation of two-wheel mobile manipulator with underactuated joint. In *Advanced Intelligent Mechatronics (AIM), 2010 IEEE/ASME International Conference on*, pages 347–352. IEEE, 2010.

[116] Diego D Santiago, Emanuel Slawiñski, and Vicente A Mut. Stable delayed bilateral teleoperation of mobile manipulators. *Asian Journal of Control*, 19(3):1140–1152, 2017.

[117] Emanuel Slawiñski, Vicente A Mut, Paolo Fiorini, and Lucio R Salinas. Quantitative absolute transparency for bilateral teleoperation of mobile robots. *IEEE Transactions on Systems, Man, and Cybernetics-Part A: Systems and Humans*, 42(2):430–442, 2012.

[118] Y Uny Cao, Alex S Fukunaga, and Andrew Kahng. Cooperative mobile robotics: Antecedents and directions. *Autonomous robots*, 4(1):7–27, 1997.

[119] Masafumi Hashimoto, Fuminori Oba, and Toru Eguchi. Dynamic control approach for motion coordination of multiple wheeled mobile robots transporting a single object. In *Intelligent Robots and Systems' 93, IROS'93. Proceedings of the 1993 IEEE/RSJ International Conference on*, volume 3, pages 1944–1951. IEEE, 1993.

[120] Dieter Fox, Wolfram Burgard, Hannes Kruppa, and Sebastian Thrun. A probabilistic approach to collaborative multi-robot localization. *Autonomous robots*, 8(3):325–344, 2000.

[121] Yasuhisa Hirata, Kazuhiro Kosuge, Hajime Asama, Hayato Kaetsu, and Kuniaki Kawabata. Coordinated transportation of a single object by multiple mobile robots without position information of each robot. In *Intelligent Robots and Systems, 2000.(IROS 2000). Proceedings. 2000 IEEE/RSJ International Conference on*, volume 3, pages 2024–2029. IEEE, 2000.

[122] Carlo Ferrari, Enrico Pagello, Jun Ota, and Tamio Arai. Multirobot motion coordination in space and time. *Robotics and autonomous systems*, 25(3):219–229, 1998.

[123] Reza Olfati-Saber and Richard M Murray. Consensus problems in networks of agents with switching topology and time-delays. *IEEE Transactions on automatic control*, 49(9):1520–1533, 2004.

[124] Reza Olfati-Saber. Flocking for multi-agent dynamic systems: Algorithms and theory. *IEEE Transactions on automatic control*, 51(3):401–420, 2006.

[125] Chris Godsil and Gordon F Royle. *Algebraic Graph Theory*, volume 207. Springer Science & Business Media, 2013.

[126] Yen-Chen Liu and Nikhil Chopra. Synchronization of networked mechanical systems with communication delays and human input. *Journal of Dynamic Systems, Measurement, and Control*, 135(4):041004, 2013.

[127] Yen-Chen Liu and Nikhil Chopra. Controlled synchronization of heterogeneous robotic manipulators in the task space. *IEEE Transactions on Robotics*, 28(1):268–275, 2012.

[128] Blake Hannaford and Jee-Hwan Ryu. Time-domain passivity control of haptic interfaces. *IEEE Transactions on Robotics and Automation*, 18(1):426–434, February 2002.

[129] Yongqiang Ye, Ya-Jun Pan, and Trent Hilliard. Bilateral teleoperation with time-varying delay: A communication channel passification approach. *IEEE/ASME Transactions on Mechatronics*, 18(4):1431–1434, August 2013.

[130] Jee-Hwan Ryu, Carsten Preusche, Blake Hannaford, and Gerd Hirzinger. Time domain passivity control with reference energy following. *IEEE Transactions on Control Systems Technology*, 13(5):737–742, 2005.

[131] Yongqiang Ye, Ya-Jun Pan, and Yash Gupta. Time domain passivity control of teleoperation systems with random asymmetric time delays. In *Decision and Control, 2009 held jointly with the 2009 28th Chinese Control Conference. CDC/CCC 2009. Proceedings of the 48th IEEE Conference on*, pages 7533–7538. IEEE, 2009.

[132] Jee-Hwan Ryu, Blake Hannaford, Dong-Soo Kwon, and Jong-Hwan Kim. A simulation/experimental study of the noisy behavior of the time-domain passivity controller. *IEEE transactions on robotics*, 21:733–741, 2005.

[133] Michael Panzirsch, Jordi Artigas, Jee-Hwan Ryu, and Manuel Ferre. Multilateral control for delayed teleoperation. In *Advanced Robotics (ICAR), 2013 16th International Conference on*, pages 1–6. IEEE, 2013.

[134] Mahyar Fotoohi, Shahin Sirouspour, and David Capson. Stability and performance analysis of centralized and distributed multi-rate control architectures for multi-user haptic interaction. *The International Journal of Robotics Research*, 26(9):977–994, 2007.

[135] Ke Huang and Dongjun Lee. Consensus-based peer-to-peer control architecture for multiuser haptic interaction over the internet. *Robotics, IEEE Transactions on*, 29(2):417–431, 2013.

[136] Ha Van Quang and Jee-Hwan Ryu. Stable multilateral teleoperation with time domain passivity approach. In *Intelligent Robots and Systems (IROS), 2013 IEEE/RSJ International Conference on*, pages 5890–5895. IEEE, 2013.

[137] Victor Mendez, Mahdi Tavakoli, and Jian Li. A method for passivity analysis of multilateral haptic systems. *Advanced Robotics*, 28(18):1205–1219, 2014.

[138] Jinmei Cheng, Yongqiang Ye, and Danwei Wang. Avoiding zero division by switching dissipation in time domain passivity control. In *the Proceedings of the IASTED International Conference on Modelling, Identification, and Control*, pages 251–258, Phuket, Thailand, 2010.

[139] Günter Niemeyer and J-JE Slotine. Stable adaptive teleoperation. *IEEE Journal of oceanic engineering*, 16(1):152–162, 1991.

[140] Günter Niemeyer and Jean-Jacques E. Slotine. Telemanipulation with time delays. *International Journal of Robotics Research*, 23(9):873–890, September 2004.

[141] Dongjun Lee and Mark W Spong. Passive bilateral teleoperation with constant time delay. *IEEE transactions on robotics*, 22(2):269–281, 2006.

[142] Trent Hilliard. Stabilization of asymmetric bilateral teleoperation systems with time-varying delays. Master's thesis, 2012.

[143] Vinay Chawda and Marcia K OMalley. Position synchronization in bilateral teleoperation under time-varying communication delays. *Ieee/asme transactions on mechatronics*, 20(1):245–253, 2015.

[144] Regelio Lozano, Nikhil Chopra, and Mark W Spong. Passivation of force reflecting bilateral teleoperators with time varying delay. In *Proceedings of the 8. Mechatronics Forum*, pages 954–962. Citeseer, 2002.

[145] Yen-Chen Liu. Task-space bilateral teleoperation systems for heterogeneous robots with time-varying delays. *Robotica*, 33(10):2065–2082, 2015.

[146] Dongjun Lee and Mark W Spong. Passive bilateral control of teleoperators under constant time-delay. *IFAC Proceedings Volumes*, 38(1):109–114, 2005.

[147] Bhavik Patel. Backstepping-adaptive control of mobile manipulators for trajectory tracking. Master's thesis, 2016.

[148] Lorenzo Sciavicco and Bruno Siciliano. Modelling and control of robot manipulators, 1996.

[149] Bhavik Patel, Ya-Jun Pan, and Usman Ahmad. Adaptive backstepping control approach for the trajectory tracking of mobile manipulators. In *Robotics and Biomimetics (ROBIO), 2017 IEEE International Conference on*, pages 1769–1774. IEEE, 2017.

[150] Fanglai Zhu. Full-order and reduced-order observer-based synchronization for chaotic systems with unknown disturbances and parameters. *Physics letters A*, 372(3):223–232, 2008.

[151] Samuel R Buss. Introduction to inverse kinematics with jacobian transpose, pseudoinverse and damped least squares methods. *IEEE Journal of Robotics and Automation*, 17(1-19):16, 2004.

[152] Stefano Chiaverini, Bruno Siciliano, and Olav Egeland. Review of the damped least-squares inverse kinematics with experiments on an industrial robot manipulator. *IEEE Transactions on control systems technology*, 2(2):123–134, 1994.

[153] Glenn D White, Rajankumar M Bhatt, and Venkat N Krovi. Dynamic redundancy resolution in a nonholonomic wheeled mobile manipulator. *Robotica*, 25(2):147–156, 2007.

[154] Glenn D White, Rajankumar M Bhatt, Chin Pei Tang, and Venkat N Krovi. Experimental evaluation of dynamic redundancy resolution in a nonholonomic wheeled mobile manipulator. *IEEE/ASME Transactions on Mechatronics*, 14(3):349–357, 2009.

[155] Yen-Chen Liu. Distributed synchronization for heterogeneous robots with uncertain kinematics and dynamics under switching topologies. *Journal of the Franklin Institute*, 352(9):3808–3826, 2015.

[156] Sebastian Erhart and Sandra Hirche. Internal force analysis and load distribution for cooperative multi-robot manipulation. *IEEE Transactions on Robotics*, 31(5):1238–1243, 2015.

[157] Sebastian Erhart and Sandra Hirche. Model and analysis of the interaction dynamics in cooperative manipulation tasks. *IEEE Transactions on Robotics*, 32(3):672–683, 2016.

[158] Bojan Nemec and Leon Zlajpah. Force control of redundant robots in unstructured environment. *IEEE transactions on industrial electronics*, 49(1):233–240, 2002.

[159] Sebastian Erhart. *Cooperative multi-robot manipulation under uncertain kinematic grasp parameters*. PhD thesis, Universitätsbibliothek der TU München, 2016.

[160] Ian D Walker, Robert A Freeman, and Steven I Marcus. Analysis of motion and internal loading of objects grasped by multiple cooperating manipulators. *The International journal of robotics research*, 10(4):396–409, 1991.

[161] Jae Heon Chung, Byung-Ju Yi, and Whee Kuk Kim. Analysis of internal loading at multiple robotic systems. *Journal of mechanical science and technology*, 19(8):1554–1567, 2005.

[162] Shahin Sirouspour and Peyman Setoodeh. Multi-operator/multi-robot teleoperation: an adaptive nonlinear control approach. In *Intelligent Robots and Systems, 2005.(IROS 2005). 2005 IEEE/RSJ International Conference on*, pages 1576–1581. IEEE, 2005.

[163] Bin Yao. Integrated direct/indirect adaptive robust control of siso nonlinear systems in semi-strict feedback form. In *American Control Conference, 2003. Proceedings of the 2003*, volume 4, pages 3020–3025. IEEE, 2003.

Appendix A

Mathematical Equations

The mathematical formulation of the mobile manipulator system is taken from [64, 147].

A.1 The Jacobian

Jacobian of the mobile manipulator is given in terms of linear and angular velocities of the wheeled platform and also in terms of right and left wheel velocities of the platform.

$$J = \begin{bmatrix} J_{11} & J_{12} & J_{13} & J_{14} \\ J_{21} & J_{22} & J_{23} & J_{24} \\ J_{31} & J_{32} & J_{33} & J_{34} \\ J_{41} & J_{42} & J_{43} & J_{44} \\ J_{51} & J_{52} & J_{53} & J_{54} \end{bmatrix} \tag{A.1}$$

where,

$$\begin{aligned}
&J_{11} = \cos\theta_b, \quad J_{12} = 0, \quad J_{13} = 0, \quad J_{14} = 0, \\
&J_{21} = \sin\theta_b, \quad J_{22} = 0, \quad J_{23} = 0, \quad J_{24} = 0, \\
&J_{31} = \cos\theta_b, \\
&J_{32} = l_2 \sin\theta_2 \sin(\theta_b + \theta_1), \\
&J_{33} = l_2 \sin\theta_2 \sin(\theta_b + \theta_1), \\
&J_{34} = -l_2 \cos\theta_2 \cos(\theta_b + \theta_1), \\
&J_{41} = \sin\theta_b, \\
&J_{42} = -l_2 \sin\theta_2 \cos(\theta_b + \theta_1), \\
&J_{43} = -l_2 \sin\theta_2 \cos(\theta_b + \theta_1), \\
&J_{44} = -l_2 \cos\theta_2 \sin(\theta_b + \theta_1), \\
&J_{51} = 0, \quad J_{52} = 0, \quad J_{53} = 0, \quad J_{54} = L_2 \cos\theta_2.
\end{aligned}$$

OR

$$J_{11} = \frac{R}{2}\cos\theta_b, \quad J_{12} = \frac{R}{2}\cos\theta_b, \quad J_{13} = 0, \quad J_{14} = 0,$$
$$J_{21} = \frac{R}{2}\sin\theta_b,$$
$$J_{22} = \frac{R}{2}\sin\theta_b,$$
$$J_{23} = 0,$$
$$J_{24} = 0,$$
$$J_{31} = \frac{R}{2}\cos\theta_b - \left[L_2\cos\theta_2\sin(\theta_b+\theta_1\right]\frac{R}{2D},$$
$$J_{32} = \frac{R}{2}\cos\theta_b + \left[L_2\cos\theta_2\sin(\theta_b+\theta_1\right]\frac{R}{2D},$$
$$J_{33} = -L_2\cos\theta_2\sin(\theta_b+\theta_1), J_{34} = -L_2\sin\theta_2\cos(\theta_b+\theta_1),$$
$$J_{41} = \frac{R}{2}\sin\theta_b + \left[L_2\cos\theta_2\cos(\theta_b+\theta_1\right]\frac{R}{2D},$$
$$J_{42} = \frac{R}{2}\sin\theta_b - \left[L_2\cos\theta_2\cos(\theta_b+\theta_1\right]\frac{R}{2D},$$
$$J_{43} = L_2\cos\theta_2\cos(\theta_b+\theta_1, J_{44} = -L_2\sin\theta_2\sin(\theta_b+\theta_1),$$
$$J_{51} = 0, \quad J_{52} = 0, \quad J_{53} = 0, \quad J_{54} = L_2\cos\theta_2.$$

A.2 The Dynamic Model

Let L_1 and L_2 denote the distance between the joints and the center of mass of the links. The coordinates of the center of mass of Link 1 can be written as,

$$\begin{aligned} x_1 &= x, \\ y_1 &= y, \\ z_1 &= L_2. \end{aligned} \tag{A.2}$$

The coordinates of the center of mass of link z can be written as,

$$\begin{aligned} x_2 &= x_1 + L_2 \cos\theta_2 \cos(\theta_b + \theta_1), \\ y_2 &= y_1 + L_2 \cos\theta_2 \sin(\theta_b + \theta_1), \\ z_2 &= l_1 + L_2 sin\theta_2. \end{aligned} \tag{A.3}$$

The total kinetic energy can be written as follow,

$$\begin{aligned} K(q,\dot{q}) = &\frac{1}{2}m_b(\dot{x}^2+\dot{y}^2) + \frac{1}{2}I_b\dot{\theta}_b^2 + \frac{1}{2}m_1(\dot{x}^2+\dot{y}^2) + \frac{1}{2}I_1(\dot{\theta}_b+\dot{\theta}_1)^2 \\ &+ \frac{1}{2}m_2(\dot{x}^2+\dot{y}^2) + \frac{1}{2}I_2[(\dot{\theta}_b+\dot{\theta}_1)^2+\dot{\theta}_2)^2]^2. \end{aligned} \tag{A.4}$$

The total potential energy is given by,

$$P(q) = m_1 g l_1 + m_2 g l_1 + L_2 \sin\theta_2. \tag{A.5}$$

The velocity constraints of the system is,

$$\dot{x}\sin(\psi) - \dot{y}\cos(\psi) = 0. \tag{A.6}$$

From Routh equation, we obtain,

$$\frac{\partial}{\partial t}\Big(\frac{\partial L}{\partial \dot{q}}\Big) - \frac{\partial L}{\partial q} = Q + A(q)^T\lambda, \tag{A.7}$$

where, $L = K - P$

$Q =$ The forces or torques acted on the platform and links

$\lambda =$ Langrangian multiplier

Substituting (A.4) and (A.5) into (A.7), we get (A.8).

$$M(q)\ddot{q} + C(q,\dot{q})\dot{q} + G(q) + f = B(q)\tau, \tag{A.8}$$

where,

$$M(q) = \begin{bmatrix} M_{11} & M_{12} & M_{13} & M_{14} & M_{15} \\ M_{21} & M_{22} & M_{23} & M_{24} & M_{25} \\ M_{31} & M_{32} & M_{33} & M_{34} & M_{35} \\ M_{41} & M_{42} & M_{43} & M_{44} & M_{45} \\ M_{51} & M_{52} & M_{53} & M_{54} & M_{55} \end{bmatrix},$$

$$C(q,\dot{q}) = \begin{bmatrix} C_{11} & C_{12} & C_{13} & C_{14} & C_{15} \\ C_{21} & C_{22} & C_{23} & C_{24} & C_{25} \\ C_{31} & C_{32} & C_{33} & C_{34} & C_{35} \\ C_{41} & C_{42} & C_{43} & C_{44} & C_{45} \\ C_{51} & C_{52} & C_{53} & C_{54} & C_{55} \end{bmatrix},$$

$$\begin{aligned}
M_{11} &= M_{22} = m_b + m_1 + m_2, \\
M_{33} &= I_b + I_1 + I_2 + m_2 L_2^2 \cos^2\theta_2, \\
M_{44} &= I_1 + I_2 + m_2 L_2^2 \cos^2\theta_2, \\
M_{55} &= I_2 + m_2 L_2^2 \cos^2\theta_2, \\
M_{12} &= M_{21} = M_{35} = M_{53} = M_{45} = M_{54} = 0, \\
M_{13} &= M_{31} = M_{41} = M_{14} = -m_2 L_2 \cos\theta_2 \sin(\theta_b + \theta_1), \\
M_{15} &= M_{51} = -m_2 L_2 \sin\theta_2 \cos(\theta_b + \theta_1) \\
M_{23} &= M_{32} = M_{24} = M_{42} = m_2 L_2 \cos(\theta_2) \cos(\theta_b + \theta_1), \\
M_{25} &= M_{52} = -m_2 L_2 \sin(\theta_b + \theta_1), \\
M_{34} &= M_{43} = I_1 + I_2 + m_2 L_2^2 \cos^2\theta_2, \\
C_{ij} &= 0, \quad i = 1,2,3,4,5,\ j = 1,2 \\
C_{13} &= C_{14} = -m_2 L_2 \cos\theta_2 \cos(\theta_b + \theta_1)(\dot{\theta}_b + \dot{\theta}_1) + m_2 L_2 \sin\theta_2 \sin(\theta_b + \theta_1)\dot{\theta}_2, \\
C_{15} &= -m_2 L_2 \cos\theta_2 \cos(\theta_b + \theta_1)\dot{\theta}_2 + m_2 L_2 \sin\theta_2 \sin(\theta_b + \theta_1)(\dot{\theta}_b + \dot{\theta}_2), \\
C_{23} &= C_{24} = -m_2 L_2 \cos\theta_2 \sin(\theta_b + \theta_1)(\dot{\theta}_b + \dot{\theta}_1) + m_3 L_2 \sin\theta_2 \cos(\theta_b + \theta_1)\dot{\theta}_2, \\
C_{25} &= -m_2 L_2 \sin\theta_2 \cos(\theta_b + \theta_1)(\dot{\theta}_b + \dot{\theta}_1) - m_2 L_2 \cos\theta_2 \sin(\theta_b + \theta_1)\dot{\theta}_2, \\
C_{35} &= C_{45} = m_2 L_2^2 \cos\theta_2 \sin\theta_2 (\dot{\theta}_b + \dot{\theta}_1),
\end{aligned}$$

$$
\begin{aligned}
C_{33} &= C_{34} = C_{43} = C_{44} = -m_2 L_2^2 \cos\theta_2 \sin\theta_2 \dot{\theta}_2, \\
C_{53} &= C_{54} = m_2 L_2^2 \cos\theta_2 \sin\theta_2 (\dot{\theta}_b + \dot{\theta}_1), \\
C_{55} &= m_2 L_2^2 \cos\theta_2 \sin\theta_2 \dot{\theta}_2, \\
G &= [0\ 0\ 0\ 0\ m_2 g L_2 \cos\theta_2]^T.
\end{aligned}
$$

A.3 Regressor Matrix

$$Y = \begin{bmatrix} Y_{11} & Y_{12} & Y_{13} & Y_{14} & Y_{15} & Y_{16} \\ Y_{21} & Y_{22} & Y_{23} & Y_{24} & Y_{25} & Y_{26} \\ Y_{31} & Y_{32} & Y_{33} & Y_{34} & Y_{35} & Y_{36} \\ Y_{41} & Y_{42} & Y_{43} & Y_{44} & Y_{45} & Y_{46} \end{bmatrix}, \tag{A.9}$$

$$p = \begin{bmatrix} m_t & m_2 L_2 & m_2 L_2^2 & I_b & I_1 & I_2 \end{bmatrix}^T, \tag{A.10}$$

$$\begin{aligned}
Y_{11} =& \frac{R^2}{4}(\dot{v}+\dot{\omega}) + \frac{R^2}{4}(\sin^2\theta_b - \cos^2\theta_b)\omega, \\
Y_{12} =& 2\cos\theta_2 \frac{R^2}{4D}(\cos(\theta_b+\theta_1) - \sin(\theta_b+\theta_1)\cos\theta_b)\dot{v} + \frac{R}{2}\cos\theta_2(\cos(\theta_b+\theta_1)\sin\theta_b - \\
& \sin(\theta_b+\theta_1)\cos\theta_b))\ddot{\theta}_1 - \frac{R}{2}\sin\theta_2(\cos(\theta_b+\theta_1)\cos\theta_b + \sin(\theta_b+\theta_1)\sin\theta_b)\ddot{\theta}_2 + \frac{R^2}{4D} \\
& \cos\theta_2(\cos(\theta_b+\theta_1)\cos\theta_b + \sin(\theta_b+\theta_1)\sin\theta_b)v - \frac{R^2}{4D}\cos\theta_b(\cos\theta_2\cos(\theta_b+\theta_1) \\
& (\dot{\theta}_b+\dot{\theta}_1) - \cos\theta_2\cos(\theta_b+\theta_1)\dot{\theta}_2)v - \frac{R^2}{4D}\sin\theta_b(\cos\theta_2\sin(\theta_b+\theta_1)(\dot{\theta}_b+\dot{\theta}_1) - \sin\theta_2 \\
& \cos(\theta_b+\theta_1)\dot{\theta}_2)v + \frac{R^2}{4D}\cos\theta_2(\cos\theta_b\sin(\theta_b+\theta_1) + \sin\theta_b\cos(\theta_b+\theta_1))\omega + \frac{R^2}{4D}\cos\theta_b \\
& (\cos\theta_2\cos(\theta_b+\theta_1)(\dot{\theta}_b+\dot{\theta}_1) - \sin\theta_2\sin(\theta_b+\theta_1)\dot{\theta}_2)\omega + \frac{R^2}{4D}\sin\theta_b(\cos\theta_2\sin(\theta_b+\theta_1) \\
& (\dot{\theta}_b+\dot{\theta}_1) - \sin\theta_2\cos(\theta_b+\theta_1)\dot{\theta}_2)\omega - \frac{R}{2}\cos\theta_b(\cos\theta_2\cos(\theta_b+\theta_1)(\dot{\theta}_b+\dot{\theta}_1) - \sin\theta_2 \\
& \sin(\theta_b+\theta_1)\dot{\theta}_2)\dot{\theta}_1 - \frac{R}{2}\sin\theta_b(\cos\theta_2\sin(\theta_b+\theta_1)(\dot{\theta}_b+\dot{\theta}_1) - \sin\theta_2\cos(\theta_b+\theta_1)\dot{\theta}_2)\dot{\theta}_1 + \\
& \frac{R}{2}\cos\theta_b(\sin\theta_2\sin(\theta_b+\theta_1)(\dot{\theta}_b+\dot{\theta}_1) - \cos\theta_2\cos(\theta_b+\theta_1)\dot{\theta}_2)\dot{\theta}_2 - \frac{R}{2}\sin\theta_b \\
& (\sin\theta_2\cos(\theta_b+\theta_1)(\dot{\theta}_b+\dot{\theta}_1) - \cos\theta_2\sin(\theta_b+\theta_1)\dot{\theta}_2)\dot{\theta}_2 \\
Y_{13} =& \frac{R^2}{4D^2}\cos^2\theta_2\dot{v} - \frac{R^2}{4D^2}\cos^2\theta_2\dot{\omega} + \frac{R}{2D}\cos^2\theta_2\ddot{\theta}_1 - \frac{R^2}{4D^2}\cos\theta_2\sin\theta_2\dot{\theta}_2 v + \frac{R^2}{4D^2}\cos\theta_2 \\
& \sin\theta_2\dot{\theta}_2\omega - \frac{R}{2D}\cos\theta_2\sin\theta_2\dot{\theta}_2\dot{\theta}_1 - \frac{R}{2D}\cos\theta_2\sin\theta_2(\dot{\theta}_b+\dot{\theta}_1)\dot{\theta}_2, \\
Y_{14} =& \frac{R^2}{4D^2}\dot{v} - \frac{R^2}{4D^2}\dot{\omega}, \\
Y_{15} =& \frac{R^2}{4D^2}\dot{v} - \frac{R^2}{4D^2}\dot{\omega} + \frac{R}{2D}\dot{\theta}_1, \\
Y_{16} =& \frac{R^2}{4D^2}\dot{v} - \frac{R^2}{4D^2}\dot{\omega} + \frac{R}{2D}\dot{\theta}_1,
\end{aligned}$$

$$
\begin{aligned}
Y_{21} =& \frac{R^2}{4}\dot{v} + \frac{R^2}{4}\dot{\omega} + \frac{R^2}{4}(\sin^2\theta_b - \cos^2\theta_b)\omega, \\
Y_{22} =& 2\cos\theta_2 \sin(\theta_b+\theta_1)\frac{R^2}{4D}\cos\theta_b\dot{\omega} - 2\cos\theta_2\cos(\theta_b+\theta_1)\frac{R^2}{4D}\sin\theta_b\dot{\omega} \\
& - \cos\theta_2\sin(\theta_b+\theta_1)\frac{R}{2}\cos\theta_b\ddot{\theta}_1 + \cos\theta_2\cos(\theta_b+\theta_1)\frac{R}{2}\sin\theta_b\ddot{\theta}_1 \\
& - \sin\theta_2\cos(\theta_b+\theta_1)\frac{R}{2}\cos\theta_b\ddot{\theta}_2 + \sin\theta_2\sin(\theta_b+\theta_1)\frac{R}{2}\sin\theta_b\ddot{\theta}_2 \\
& - \cos\theta_2\sin(\theta_b+\theta_1)\frac{R^2}{4D}\sin\theta_b v - \cos\theta_2\cos(\theta_b+\theta_1)\frac{R^2}{4D}\cos\theta_b v \\
& - \cos\theta_2\cos(\theta_b+\theta_1)(\dot{\theta}_b+\dot{\theta}_1)\frac{R^2}{4D}\cos\theta_b v + \sin\theta_2\sin(\theta_b+\theta_1)\dot{\theta}_2\frac{R^2}{4D}\cos\theta_b v \\
& - \cos\theta_2\sin(\theta_b+\theta_1)(\dot{\theta}_b+\dot{\theta}_1)\frac{R^2}{4D}\sin\theta_b v + \sin\theta_2\cos(\theta_b+\theta_1)\dot{\theta}_2\frac{R^2}{4D}\sin\theta_b v \\
& - \cos\theta_2\sin(\theta_b+\theta_1)\frac{R^2}{4D}\cos\theta_b\omega - \cos\theta_2\cos(\theta_b+\theta_1)\frac{R^2}{4D}\sin\theta_b\omega \\
& + \cos\theta_2\cos(\theta_b+\theta_1)(\dot{\theta}_b+\dot{\theta}_1)\frac{R^2}{4D}\cos\theta_b\omega - \sin\theta_2\sin(\theta_b+\theta_1)\dot{\theta}_2\frac{R^2}{4D}\cos\theta_b\omega \\
& + \cos\theta_2\sin(\theta_b+\theta_1)(\dot{\theta}_b+\dot{\theta}_1)\frac{R^2}{4D}\sin\theta_b\omega - \sin\theta_2\cos(\theta_b+\theta_1)\dot{\theta}_2\frac{R^2}{4D}\sin\theta_b\omega \\
& - \cos\theta_2\cos(\theta_b+\theta_1)(\dot{\theta}_b+\dot{\theta}_1)\frac{R}{2}\cos\theta_b\dot{\theta}_1 + \sin\theta_2\sin(\theta_b+\theta_1)\dot{\theta}_2\frac{R}{2}\cos\theta_b\dot{\theta}_1 \\
& - \cos\theta_2\sin(\theta_b+\theta_1)(\dot{\theta}_b+\dot{\theta}_1)\frac{R}{2}\sin\theta_b\dot{\theta}_1 + \sin\theta_2\cos(\theta_b+\theta_1)\dot{\theta}_2\frac{R}{2}\sin\theta_b\dot{\theta}_1 \\
& + \sin\theta_2\sin(\theta_b+\theta_1)(\dot{\theta}_b+\dot{\theta}_1)\frac{R}{2}\cos\theta_b\dot{\theta}_2 - \cos\theta_2\cos(\theta_b+\theta_1)\dot{\theta}_2\frac{R}{2}\cos\theta_b\dot{\theta}_2 \\
& - \sin\theta_2\cos(\theta_b+\theta_1)(\dot{\theta}_b+\dot{\theta}_1)\frac{R}{2}\sin\theta_b\dot{\theta}_2 - \cos\theta_2\sin(\theta_b+\theta_1)\dot{\theta}_2\frac{R}{2}\sin\theta_b\dot{\theta}_2, \\
Y_{23} =& -\frac{R^2}{4D^2}\cos^2\theta_2\dot{v} + \frac{R^2}{4D^2}\cos^2\theta_2\dot{\omega} - \frac{R^2}{4D^2}\cos^2\theta_2\ddot{\theta}_1 + \cos\theta_2\sin\theta_2\dot{\theta}_2\frac{R^2}{4D^2}v \\
& - \cos\theta_2\sin\theta_2\dot{\theta}_2\frac{R^2}{4D^2}\omega + \cos\theta_2\sin\theta_2\dot{\theta}_2\frac{R}{2D}\dot{\theta}_1 + \cos\theta_2\sin\theta_2(\dot{\theta}_b+\dot{\theta}_1)\frac{R}{2D}\dot{\theta}_2, \\
Y_{24} =& -\frac{R^2}{4D^2}\cos^2\theta_2\dot{v} + \frac{R^2}{4D^2}\cos^2\theta_2\dot{\omega}, \\
Y_{25} =& -\frac{R^2}{4D^2}\cos^2\theta_2\dot{v} + \frac{R^2}{4D^2}\cos^2\theta_2\dot{\omega} + \frac{R}{2D}\ddot{\theta}_1, \\
Y_{26} =& -\frac{R^2}{4D^2}\cos^2\theta_2\dot{v} + \frac{R^2}{4D^2}\cos^2\theta_2\dot{\omega} + \frac{R}{2D}\ddot{\theta}_1, \\
Y_{31} =& 0, \\
Y_{32} =& -\cos\theta_2\sin(\theta_b+\theta_1)\frac{R}{2}\cos\theta_b\dot{v} + \cos\theta_2\cos(\theta_b+\theta_1)\frac{R}{2}\sin\theta_b\dot{v} - \cos\theta_2 \\
& \sin(\theta_b+\theta_1)\frac{R}{2}\cos\theta_b\dot{\omega} + \cos\theta_2\cos(\theta_b+\theta_1)\frac{R}{2}\sin\theta_b\dot{\omega} + \cos\theta_2\sin(\theta_b+\theta_1)
\end{aligned}
$$

$$\frac{R}{2}\sin\theta_b v+\cos\theta_2\cos(\theta_b+\theta_1)\frac{R}{2}\cos\theta_b v+\cos\theta_2\sin(\theta_b+\theta_1)\frac{R}{2}\cos\theta_b\omega$$
$$+\cos\theta_2\cos(\theta_b+\theta_1)\frac{R}{2}\sin\theta_b\omega,$$

$$Y_{33}=\frac{R}{2D}\cos^2\theta_2\dot{v}-\frac{R}{2D}\cos^2\theta_2\dot{\omega}+\cos^2\theta_2\ddot{\theta}_1-\cos\theta_2\sin\theta_2\dot{\theta}_2\frac{R}{2D}v+\cos\theta_2$$
$$\sin\theta_2\dot{\theta}_2\frac{R}{2D}\omega-\cos\theta_2\sin\theta_2\dot{\theta}_2\dot{\theta}_1+\cos\theta_2\sin\theta_2(\dot{\theta}_b+\dot{\theta}_1)\dot{\theta}_2,$$

$$Y_{34}=0,$$

$$Y_{35}=\frac{R}{2D}\dot{v}-\frac{R}{2D}\dot{\omega}+\ddot{\theta}_1,$$

$$Y_{36}=\frac{R}{2D}\dot{v}-\frac{R}{2D}\dot{\omega}+\ddot{\theta}_1,$$

$$Y_{41}=0,$$

$$Y_{42}=\sin\theta_2\cos(\theta_b+\theta_1)\frac{R}{2}\cos\theta_b\dot{v}-\sin\theta_2\sin(\theta_b+\theta_1)\frac{R}{2}\sin\theta_b\dot{v}-\sin\theta_2$$
$$\cos(\theta_b+\theta_1)\frac{R}{2}\cos\theta_b\dot{\omega}-\sin\theta_2\sin(\theta_b+\theta_1)\frac{R}{2}\sin\theta_b\dot{\omega}+\sin\theta_2\cos(\theta_b+\theta_1)$$
$$\frac{R}{2}\sin\theta_b v+\sin\theta_2\sin(\theta_b+\theta_1)\frac{R}{2}\cos\theta_b v+\sin\theta_2\cos(\theta_b+\theta_1)\frac{R}{2}\cos\theta_b\omega$$
$$+\sin\theta_2\sin(\theta_b+\theta_1)\frac{R}{2}\sin\theta_b\omega,$$

$$Y_{43}=\cos\theta_2\sin\theta_2(\dot{\theta}_b+\dot{\theta}_1)\frac{R}{2D}v-\cos\theta_2\sin\theta_2(\dot{\theta}_b+\dot{\theta}_1)\frac{R}{2D}\omega+\cos\theta_2\sin\theta_2$$
$$(\dot{\theta}_b+\dot{\theta}_1)\dot{\theta}_1+\cos\theta_2\sin\theta_2\dot{\theta}_2\dot{\theta}_2,$$

$$Y_{44}=0,$$

$$Y_{45}=0,$$

$$Y_{46}=0.$$

A.3.1 Regressor Matrix in Terms of Linear and Angular Velocities

$$Y = \begin{bmatrix} Y_{11} & Y_{12} & Y_{13} & Y_{14} & Y_{15} & Y_{16} & Y_{17} & Y_{18} \\ Y_{21} & Y_{22} & Y_{23} & Y_{24} & Y_{25} & Y_{26} & Y_{27} & Y_{28} \\ Y_{31} & Y_{32} & Y_{33} & Y_{34} & Y_{35} & Y_{36} & Y_{37} & Y_{38} \\ Y_{41} & Y_{42} & Y_{43} & Y_{44} & Y_{45} & Y_{46} & Y_{47} & Y_{48} \end{bmatrix}, \tag{A.11}$$

$$p = \begin{bmatrix} m_b & m_1 & m_2 & m_2 L_2 & m_2 L_2^2 & I_b & I_1 & I_2 \end{bmatrix}^T, \tag{A.12}$$

$$\begin{aligned}
Y_{11} =& Y_{12} = Y_{13} = \dot{\eta}_1, \\
Y_{14} =& \cos\theta_2(\cos(\theta_b+\theta_1)\sin\theta_b - \sin(\theta_b+\theta_1)\cos\theta_b)\dot{\eta}_2 + \cos\theta_2\sin(\theta_b+\theta_1) \\
& (\sin\theta_b - \cos\theta_b)\dot{\eta}_3 - \sin\theta_2(\cos(\theta_b+\theta_1)\cos\theta_b + \sin(\theta_b+\theta_1)\sin\theta_b)\dot{\eta}_4 + \cos\theta_b \\
& (\sin(\theta_b+\theta_1)\sin\theta_2\dot{\theta}_2 - \cos(\theta_b+\theta_1)\cos\theta_2(\dot{\theta}_b+\dot{\theta}_1))(\eta_2+\eta_3) + \sin\theta_b(\cos(\theta_b+\theta_1) \\
& \sin\theta_2\dot{\theta}_2 - \cos\theta_2\cos(\theta_b+\theta_1)(\dot{\theta}_b+\dot{\theta}_1))(\eta_2+\eta_3) + \cos\theta_b(\sin(\theta_b+\theta_1)\sin\theta_2 \\
& (\dot{\theta}_b+\dot{\theta}_1) - \cos\theta_2\cos(\theta_b+\theta_1)\dot{\theta}_2)\eta_4 + \sin\theta_b(\cos(\theta_b+\theta_1)\sin\theta_2(\dot{\theta}_b+\dot{\theta}_1) - \sin\theta_2 \\
& \cos(\theta_b+\theta_1)\dot{\theta}_2)\eta_4, \\
Y_{15} =& Y_{16} = Y_{17} = Y_{18} = 0, \\
Y_{21} =& Y_{22} = Y_{23} = 0, \\
Y_{24} =& \cos\theta_2(\cos(\theta_b+\theta_1)\sin\theta_b - \sin(\theta_b+\theta_1)\cos\theta_b)\dot{\eta}_1 + \cos\theta_2(\sin(\theta_b+\theta_1)\sin\theta_b + \cos(\theta_b \\
& + \theta_1)\cos\theta_b)\dot{\theta}_b\eta_1, \\
Y_{25} =& \cos^2\theta_2\dot{\eta}_2 + \cos^2\theta_2\dot{\eta}_3 + \cos\theta_2\sin\theta_2\dot{\theta}_2(\dot{\eta}_2+\dot{\eta}_3) + \cos\theta_2\sin\theta_2(\dot{\theta}_b+\dot{\theta}_1)\dot{\eta}_4, \\
Y_{26} =& \eta_2, \\
Y_{27} =& Y_{28} = \dot{\eta}_2 + \dot{\eta}_3, \\
Y_{31} =& Y_{32} = Y_{33} = Y_{36} = 0, \\
Y_{34} =& \cos\theta_2\sin(\theta_b+\theta_1)(\sin\theta_b - \cos\theta_b)\dot{v} + \cos\theta_2\sin(\theta_b+\theta_1)(\sin\theta_b + \cos\theta_b)\dot{\theta}_2 v, \\
Y_{35} =& \cos^2\theta_2\dot{\eta}_2 + \cos^2\theta_2\dot{\eta}_3 - \cos\theta_2\sin\theta_2\dot{\theta}_2(\dot{\eta}_2+\dot{\eta}_3) - \cos\theta_2\sin\theta_2(\dot{\theta}_b+\dot{\theta}_1)\dot{\eta}_4, \\
Y_{36} =& 0, \\
Y_{37} =& Y_{38} = \dot{\eta}_2 + \dot{\eta}_3,
\end{aligned}$$

$$
\begin{aligned}
Y_{41} =& Y_{42} = Y_{43} = 0, \\
Y_{44} =& -\sin\theta_2 \cos(\theta_b + \theta_1)(\cos\theta_b - \sin\theta_b)\dot{v} + \sin\theta_2 \cos(\theta_b + \theta_1)(\sin\theta_b + \cos\theta_b)\dot{\theta}_b v, \\
Y_{45} =& \cos^2\theta_2 \dot{\eta}_2 + \cos^2\theta_2 \dot{\eta}_3 + \cos\theta_2 \sin\theta_2 \dot{\theta}_2(\dot{\eta}_2 + \dot{\eta}_3) + \cos\theta_2 \sin\theta_2(\dot{\theta}_b + \dot{\theta}_1)\dot{\eta}_4, \\
Y_{46} =& Y_{47} = 0, \\
Y_{48} =& \dot{\eta}_4.
\end{aligned}
$$

Appendix B

Author's Publications

1. **Ahmad, U.**, Pan, Y. J., Shen, H., Adaptive Robust Control for Teleoperation of Single Master Multiple Slave Manipulators under Time Delays, *IET Control Theory and Applications, November 2018* (In-preparation).

2. **Ahmad, U.**, Pan, Y. J., Shen, H., Null Space and Operational Space Control of Mobile Manipulators for Object Transportation, *International Journal of Robust and Nonlinear Control, November 2018* (In-preparation).

3. Shen, H., Pan, Y. J., **Ahmad, U.**, Bingwei, W., Pose Synchronization of Multiple Networked Manipulators Using Non-singular Terminal Sliding Mode Control, *IEEE Transactions on Automation Science and Engineering, October 2018* (Submitted).

4. Sheng, L., **Ahmad, U.**, Ye, Y., Pan, Y., J., Time Domain Passivity Control Scheme for Bilateral Teleoperation, *International Journal of Robotics and Automation, June 2018* (Submitted).

5. **Ahmad, U.**, and Pan, Y. J. (2018). A Time Domain Passivity Approach for Asymmetric Multilateral Teleoperation System. *IEEE Access, 6, 519-531*.

6. Shen, H., Pan, Y. J., **Ahmad, U.**, Liu, S., Wu, Min., He, Y., Tracking Performance Evaluations on the Robust Teleoperative Control of Multiple Manipulators, 2019 *American Control Conference, July 2019* (Submitted).

7. **Ahmad, U.**, Pan, Y. J., Shen, H., Liu, S., Cooperative Control of Mobile Manipulators Transporting an Object based on an Adaptive Backstepping Approach, In *2018 IEEE 14th International Conference on Control and Automation (ICCA) (pp. 198-203), IEEE*.

8. Patel, B., Pan, Y. J., **Ahmad, U.** (2017, December). Adaptive Backstepping Control Approach for the Trajectory Tracking of Mobile Manipulators, In *Robotics and*

Biomimetics (ROBIO), 2017 IEEE International Conference on (pp. 1769-1774). IEEE.

9. **Ahmad, U.**, Pan, Y. J. (2016, December). Switching Time Domain Passivity Control for Multilateral Teleoperation Systems under Time Varying Delays, In *Decision and Control (CDC), 2016 IEEE 55th Conference on (pp. 1429-1434). IEEE*.

10. **Ahmad, U.**, Pan, Y. J., ul Husnain, A. (2016, November). Switching Time Domain Passivity Control for Multilateral Teleoperation Systems, In *Robotics and Artificial Intelligence (ICRAI), 2016 2nd International Conference on (pp. 69-74). IEEE*.

11. Zou, M., Pan, Y. J., Forbrigger, S. **Ahmad, U.** (2016, November). Adaptive Robust Control for Bilateral Teleoperated Robotic Manipulators with Arbitrary Time Delays, In *Robotics and Artificial Intelligence (ICRAI), 2016 2nd International Conference on (pp. 69-74). IEEE*.